



**HAL**  
open science

# Contactless detection of cardiopulmonary activity for a person in different scenarios

Sarah Samad

► **To cite this version:**

Sarah Samad. Contactless detection of cardiopulmonary activity for a person in different scenarios. Electronics. INSA de Rennes; Université Libanaise, 2017. English. NNT: 2017ISAR0030 . tel-01943726

**HAL Id: tel-01943726**

**<https://theses.hal.science/tel-01943726>**

Submitted on 4 Dec 2018

**HAL** is a multi-disciplinary open access archive for the deposit and dissemination of scientific research documents, whether they are published or not. The documents may come from teaching and research institutions in France or abroad, or from public or private research centers.

L'archive ouverte pluridisciplinaire **HAL**, est destinée au dépôt et à la diffusion de documents scientifiques de niveau recherche, publiés ou non, émanant des établissements d'enseignement et de recherche français ou étrangers, des laboratoires publics ou privés.

UNIVERSITE  
BRETAGNE  
LOIRE

**THESE INSA Rennes**  
sous le sceau de l'Université Bretagne Loire  
pour obtenir le titre de  
DOCTEUR DE L'INSA RENNES  
Spécialité : Electronique et télécommunications

présentée par

**Sarah Samad**

ECOLE DOCTORALE : *MATISSE*

LABORATOIRE : *IETR*

## Contactless detection of cardiopulmonary activity for a person in different scenarios

**Thèse soutenue le 24.5.2017**  
devant le jury composé de :

**Rodolphe Vauzelle**

Professeur à l'Université de Poitiers / Président du jury

**Florence Sagnard**

Chargée de recherche HDR à IFSTTAR, COSYS, LEOST / Rapporteur

**Zaher Dawy**

Professeur à l'American University of Beirut / Rapporteur

**Friedman Tchoffo Talom**

Expert propagation, Phd à Thales / Examineur

**Dany Obeid**

Maître de Conférences à l'Université Libanaise / Co-encadrant

**Gheorghe Zaharia**

Maître de Conférences à l'INSA de Rennes / Co-encadrant

**Sawsan Sadek**

Professeur associé à l'Université Libanaise / Co-directeur de thèse

**Ghaïs El Zein**

Professeur à l'INSA de Rennes / Directeur de thèse

Intitulé de la thèse

Contactless detection of cardiopulmonary activity for a person in different scenarios

Détection sans contact de l'activité cardio-pulmonaire d'une personne dans différents scénarios

Sarah Samad



En partenariat avec





## **Acknowledgments**

I would first like to thank the director of my thesis, Prof. Ghais El Zein for the patient guidance and advice that he has provided. I could not have imagined having a better advisor and mentor for my PhD study.

I would also thank Prof. Sawsan Sadek who has guided me; encouraged me, her motivation and energy inspired me and helped me to achieve the work in a pleasant and comfortable atmosphere. I deeply thank her for her scientific and personal support.

I am grateful to thank my co-supervisor Dr. Gheorghe Zaharia who cared so much about my work, and who responded to my questions and queries so promptly. Indeed, his comments were all helpful in making a significant thesis.

My thanks go also to my co-supervisor Dr. Dany Obeid for his kindness and scientific advice, particularly when exploring new ideas. He is my primary resource for getting my questions answered.

I am grateful to thank Prof. Florence Sagnard, Prof. Zaher Dawy, Prof. Rodolphe Vauzelle and Dr. Friedman Tchoffo Talom for reading and evaluating my work and for participating in this jury.

I would thank everybody at the Lebanese University especially the dean of the EDST Prof. Fawaz El-Omar, and the director of center Azm Prof. Mohamad Khalil as well everybody at the French side especially the director of INSA Rennes Mhamad Drissi, the director of IETR laboratory Eric Pottier and the director of the doctoral school MATISSE Jean-Marie Lion for having welcomed me to these institutions.

I would thank the IETR laboratory as well the Azm center and the Lebanese university colleagues and staff especially Aurore Gouin, Pascal Richard, Katell Kervella, Jana El-Hajj and Zeinab Ibrahim for their help in administrative procedures and Guy Grunfelder and Yvan Kokar for their help in practical sides.

I would also thank Laser, Rennes metropole and INSA Rennes for funding this work.

I would thank my friends in Rennes for being by my side and helping me when I was pregnant especially Charlotte Jabr, Hala Abdulrahman, Nadine Khodr, Rida El-Chall and Ali Cheaito.

I warmly thank my parents my mother Nelly and my father Souheil who supported me during my life and scarifies their life in educating my brothers, sisters and me, and many thanks to my sisters Myriam and Sedra and my brothers Habib, Ahmad and Mhamad who supported me as well my husband's parents Assaad and Fatima and my little piece of cake my daughter Fatima who shined my life.

I warmly thank my soul mate and husband Ahmad for being a good supporter; he has been non-judgmental of me and instrumental in instilling confidence. Without him, it was impossible to complete my work.

Finally, I would thank God for all the blessings he made me who I am today. Without his will, I would have never found the right path.

# Contents

<b>Acknowledgments .....</b>	<b>4</b>
<b>List of Figures .....</b>	<b>9</b>
<b>List of Tables.....</b>	<b>15</b>
<b>List of Abbreviations .....</b>	<b>17</b>
<b>Résumé étendu .....</b>	<b>19</b>
<b>Chapter 1 Contactless cardiopulmonary monitoring ..</b>	<b>49</b>
<b>1.1. Introduction.....</b>	<b>49</b>
<b>1.2. Previous work.....</b>	<b>49</b>
<b>1.3. Chest motion.....</b>	<b>50</b>
<b>1.3.1. Chest motion due to heartbeat.....</b>	<b>51</b>
<b>1.3.2. Chest motion due to respiration .....</b>	<b>54</b>
<b>1.4. Doppler radar.....</b>	<b>55</b>
<b>1.4.1. Doppler effect .....</b>	<b>55</b>
<b>1.4.2. Bistatic and monostatic radar architectures .....</b>	<b>57</b>
<b>1.4.3. Radar families .....</b>	<b>57</b>
<b>1.5. Radar application for heartbeat detection.....</b>	<b>60</b>
<b>1.5.1. Comparison of radar types for vital detection.....</b>	<b>61</b>
<b>1.5.2. Vital sign detection using CW.....</b>	<b>62</b>
<b>1.5.3. Operating frequency .....</b>	<b>68</b>
<b>1.5.4. Power considerations .....</b>	<b>68</b>
<b>1.6. Conclusion .....</b>	<b>69</b>
<b>Chapter 2 Heartbeat detection of a person using filtering methods at different radiated powers.....</b>	<b>71</b>
<b>2.1. Introduction.....</b>	<b>71</b>

2.2. System description .....	72
2.3. System advantages .....	74
2.4. The measurement setup .....	74
2.5. Characteristics of the measured signal.....	78
2.6. Signal processing techniques .....	79
2.6.1. Review of processing techniques .....	79
2.6.2. Separation of respiration and heartbeat signals.....	84
2.7. Conclusion .....	96
<b>Chapter 3 Heartbeat detection from different sides and at several operating frequencies using wavelets .....</b>	<b>99</b>
3.1. Introduction.....	99
3.2. Choice of the operating frequency .....	100
3.3. Antennas .....	102
3.4. Measurement setup.....	102
3.5. Signal Processing techniques .....	108
3.5.1. Overview of the wavelet transform .....	108
3.5.2. Re-sampling method .....	113
3.5.3. Choice of the wavelet type.....	114
3.5.4. Application of wavelets.....	116
3.5.5. Application of smoothing .....	118
3.6. Results and discussion .....	126
3.7. $S_{DI8}$ pass band reducing .....	129
3.8. Conclusion .....	129
<b>Chapter 4 Heartbeat measurement based on several scenarios .....</b>	<b>132</b>



<b>4.1. Introduction.....</b>	<b>132</b>
<b>4.2. Measurements behind a wall .....</b>	<b>133</b>
4.2.1. Effect of barriers on wave propagation.....	134
4.2.2. Measurement setup.....	135
4.2.3. Signal processing and results.....	136
<b>4.3. Single antenna system .....</b>	<b>139</b>
4.3.1. Comparison between one and two antennas systems for a holding breath person .....	140
4.3.2. Results for a normally breathing person using single-antenna VNA system.....	149
<b>4.4. Models and processing of a moving person .....</b>	<b>151</b>
4.4.1. Modeling of a chest motion when moving forward .....	152
4.4.2. Phase variation of chest movement of a walking person at 20 GHz	161
4.4.3. Signal processing and results.....	162
<b>4.5. Conclusion .....</b>	<b>164</b>
<b>Future work .....</b>	<b>166</b>
<b>General conclusion .....</b>	<b>168</b>
<b>Research publications.....</b>	<b>171</b>
<b>Bibliography.....</b>	<b>173</b>

## List of Figures

Figure 1. Le signal ECG normalisé.....	24
Figure 2. Système de mesure sans contact.....	24
Figure 3. Module de la FFT de la variation de phase de $S_{21}$ d'une personne qui retient son souffle .....	26
Figure 4. Module de la FFT de la variation de phase de $S_{21}$ filtré d'une personne qui respire normalement.....	26
Figure 5. Détection des pics de la variation de phase de $S_{21}$ lissée pour une personne qui retient son souffle à 20 GHz et à $P_r = 3, -2, -7, -12$ and $-17$ dBm (Noir), signal ECG (Vert).....	27
Figure 6. Détection des pics après application d'un filtre passe bande sur la variation de phase de $S_{21}$ pour une personne qui respire normalement à 20 GHz et à $P_r = 3, -2, -7, -12$ and $-17$ dBm (Noir), signal ECG (Vert) .....	28
Figure 7. Détection des pics après application d'un filtre passe haut avec lissage de la variation de phase de $S_{21}$ pour une personne qui respire normalement à 20 GHz et à $P_r = 3, -2, -7, -12$ and $-17$ dBm (Noir), signal ECG (Vert) .....	28
Figure 8. Variation de la phase de $S_{21}$ pour les 4 côtés d'exposition ( $f_e = 5.8$ GHz) .....	32
Figure 9. Signal $S_{D18}$ pour les 4 côtés avec une fréquence opérationnelle 5.8 GHz .....	35
Figure 10. Signal $S_{D18}$ lissé pris de face à 5.8 GHz et 0 dBm (Noir), Signal ECG.....	36
Figure 11. Variation de phase de $S_{11}$ pour une personne qui retient son souffle à 20 GHz et $P_r = -2, -7, -12$ and $-17$ dBm .....	40
Figure 12. Variation de phase de $S_{21}$ pour une personne qui retient son souffle à 20 GHz et $P_r = -2, -7, -12$ and $-17$ dBm .....	41
Figure 1.1. Five events of the cardiac cycle [18].....	51
Figure 1.2. ECG output.....	53
Figure 1.3. Heart anatomy ( <a href="http://www.texasheart.org">http://www.texasheart.org</a> ).....	53
Figure 1.4. Doppler effect.....	56
Figure 1.5. Monostatic and bistatic radar [38].....	57
Figure 1.6. Radar types .....	58
Figure 1.7. Emitted and received frequencies of LFM .....	59
Figure 1.8. PSD of UWB radar [43] .....	59

Figure 1.9. Time evolution of a transmitted UWB signal [43].....	60
Figure 1.10. CW radar sensor [63].....	62
Figure 1.11. Homodyne quadrature receiver architecture [66].....	64
Figure 1.12. (a) Constellation graph I/Q data dc information preserved .....	65
Figure 1.13. Double side band radar architecture for vital sign detection [66] .....	66
Figure 1.14. Frequency tuning using double side band for the null point elimination [63] .....	66
Figure 1.15. Two radar transceivers for the body motion elimination [66].....	67
Figure 2.1. The measurement setup .....	72
Figure 2.2. Photo of the experiment.....	75
Figure 2.3. Normalized ECG .....	76
Figure 2.4. $S_{21}$ phase variation for a non-breathing person at 20 GHz and $P_r = 3, -2, -7, -12$ and $-17$ dBm.....	77
Figure 2.5. Phase variation of $S_{21}$ for a breathing person at 20 GHz and $P_r = 3, -2, -7, -12$ and $-17$ dBm.....	77
Figure 2.6. Realistic magnitude response of a filter .....	82
Figure 2.7. Flowchart of the processing techniques used in time and frequency domains for a person who holds his breath .....	84
Figure 2.8. Flowchart of the processing techniques used in frequency and time domains for a person who breaths .....	85
Figure 2.9. Positive part of absolute value of the FFT applied for the phase variation of $S_{21}$ when measured at 20 GHz and $P_r = 3, -2, -7, -12$ and $-17$ dBm for a person who is holding the breath. ....	86
Figure 2.10. Positive part of the absolute value of FFT applied for the phase variation of $S_{21}$ when measured at 20 GHz and $P_r = 3, -2, -7, -12$ and $-17$ dBm for a person who breathes .....	87
Figure 2.11. FFT applied for HP filtered $S_{21}$ phase variation when measured at 20 GHz and $P_r = 3, -2, -7, -12$ and $-17$ dBm for a person who breathes.....	88
Figure 2.12. ECG signal taken simultaneously with VNA system when taking measurements for a person who holds his breath at 20 GHz and $P_r = 3, -2, -7, -12$ and $-17$ dBm.....	89

Figure 2.13. ECG signal taken simultaneously with VNA system when taking measurements for a person who breathes normally at 20 GHz and at 20 GHz and $P_r = 3, -2, -7, -12$ and $-17$ dBm.....	90
Figure 2.14. PDM applied to $S_{21}$ phase variation for a non-breathing person after applying smoothing with $n = 199$ at 20 GHz and at 20 GHz and $P_r = 3, -2, -7, -12$ and $-17$ dBm (Black), ECG signal (Green).....	92
Figure 2.15. Peak detection applied to $S_{21}$ phase variation after applying BP filter for a breathing person for different radiated powers at 20 GHz and $P_r = 3, -2, -7, -12$ and $-17$ dBm (Black), ECG signal (Green).....	93
Figure 2.16. PDM applied to $S_{21}$ phase variation after applying HP filter and smoothing for a breathing person at 20 GHz and $P_r = 3, -2, -7, -12$ and $-17$ dBm (Black), ECG signal (Green).....	94
Figure 3.1. Measurement positions.....	103
Figure 3.2. Phase variation of $S_{21}$ due to the cardiopulmonary activities at different sides and at 2.4 GHz and 0 dBm.....	105
Figure 3.3. Phase variation of $S_{21}$ due to the cardiopulmonary activities at different sides and at 5.8 GHz and 0 dBm.....	106
Figure 3.4. Phase variation of $S_{21}$ due to the cardiopulmonary activities at different sides and at 10 GHz and 0 dBm.....	107
Figure 3.5. Wavelet decomposition.....	113
Figure 3.6. Flowchart of the proposed algorithm for finding the most suitable wavelet family.....	115
Figure 3.7. Wavelet decompositions using Bior 2.4.....	116
Figure 3.8. Addition of the decomposition 1 till 8.....	117
Figure 3.9. $S_{D18}$ signal at different sides at 5.8 GHz.....	118
Figure 3.10. $S_{D18}$ smoothing using $n = 199, 299$ and $399$ .....	119
Figure 3.11. Flowchart of the proposed algorithm for extracting the heartbeat rate and heartbeat rate error using wavelets decomposition.....	120
Figure 3.12. Smoothed $S_{D18}$ taken from the front side using several wavelets at 5.8 GHz and 0 dBm (Black), ECG signal (Green).....	121

Figure 3.13. Smoothed $S_{D18}$ taken from the back side using several wavelets at 5.8 GHz and 0 dBm (Black), ECG signal (Green) .....	122
Figure 3.14. Smoothed $S_{D18}$ taken from the left side using several wavelets at 5.8 GHz and 0 dBm (Black), ECG signal (Green) .....	123
Figure 3.15. Smoothed $S_{D18}$ taken from the right side using several wavelets at 5.8 GHz and 0 dBm (Black), ECG signal (Green) .....	124
Figure 3.16. Comparison between relative errors after applying classical filtering (blue) and wavelets (red) taking from 4 sides .....	128
Figure 4.1. Measurement system behind a wall.....	133
Figure 4.2. Phase variation of $S_{21}$ at $P_r = 0$ dBm and $f_e = 5.8$ and 10 GHz with and without wall.....	136
Figure 4.3. $S_{D18}$ signal obtained at $P_r = 0$ dBm and $f_e = 5.8$ and 10 GHz with and without wall.....	137
Figure 4.4. Peak detection of the smoothed $S_{D18}$ obtained at $P_r = 0$ dBm and $f_e = 5.8$ and 10 GHz with and without wall (Black), ECG signal (Green) .....	138
Figure 4.5. Measurement system with single antenna vs. electrocardiograph.....	141
Figure 4.6. Phase variation of $S_{11}$ of a person holding his breath at $P_r = -2, -7, -12$ and $-17$ dBm and $f_e = 20$ GHz.....	144
Figure 4.7. Phase variation of $S_{21}$ of a person holding his breath at $P_r = -2, -7, -12$ and $-17$ dBm and $f_e = 20$ GHz.....	145
Figure 4.8. Peak detection for the phase variation of $S_{11}$ after applying smoothing with $n = 199$ at $P_r = -2, -7, -12$ and $-17$ dBm and $f_e = 20$ GHz (Black), ECG signal (Green)...	146
Figure 4.9. Peak detection of phase variation of $S_{21}$ after applying smoothing with $n = 199$ at $P_r = -2, -7, -12$ and $-17$ dBm and $f_e = 20$ GHz (Black), ECG signal (Green)...	147
Figure 4.10. Phase variation of $S_{11}$ for a breathing person at $P_r = -2, -7, -12$ and $-17$ dBm and $f_e = 20$ GHz.....	149
Figure 4.11. Peak detection of the extracted heartbeat signal at $P_r = -2, -7, -12$ and $-17$ dBm and $f_e = 20$ GHz (Black), ECG signal (Green).....	150
Figure 4.12. Detection setup for a moving person ( $v$ is the velocity of the person) .....	152
Figure 4.13. (b) Model of the phase variation due to respiration at 20 GHz .....	154

Figure 4.14. Phase variation of $S_{21}$ at $P_e = -19, -24, -29, -34, -39$ and $-44$ dBm and $f_e = 20$ GHz .....	156
Figure 4.15. Phase noise at $P_e = -19, -24, -29, -34, -39$ and $-44$ dBm and $f_e = 20$ GHz. ....	157
Figure 4.16. Phase noise variance vs. emitted power at 20 GHz.....	159
Figure 4.17. Phase noise variation vs. signal power at VNA input at $d = 1$ and $f_e = 20$ GHz.....	159
Figure 4.18. Signal power at VNA input vs. distance at $P_e = -19$ dBm and $f_e = 20$ GHz.....	160
Figure 4.19. Phase noise model for a person moving toward the VNA system at $f_e = 20$ GHz and $P_e = -19$ dBm walking from $d = 3$ m to $d = 1$ m at a velocity $v = 0.25$ m/s....	160
Figure 4.20. Phase variation due to a person chest moving toward the VNA system at 20 GHz .....	161
Figure 4.21. Phase variation of a moving person at first 0.5 s with presence of respiration, heartbeat and noise at 20 GHz .....	161
Figure 4.22. Phase variation of a moving person at last 0.5 s with presence of respiration, heartbeat and noise at 20 GHz .....	162
Figure 4.23. $S_{D18}$ applied on model for heartbeat extraction at $P_e = -19$ dBm and $f_e = 20$ GHz.....	163
Figure 4.24. Peak detection of $S_{D18}$ signal and heartbeat model at $P_e = -19$ dBm and $f_e = 20$ GHz.....	163



## List of Tables

Tableau 1. Erreur relative entre le système VNA et ECG .....	30
Table 2.1. Antenna gain .....	73
Table 2.2. Measurement setup .....	76
Table 2.3. Frequencies and rates of respiration and heartbeat .....	79
Table 2.4. Relative error of HR using FFT .....	91
Table 2.5. Relative error for a non-breathing person.....	95
Table 2.6. Relative error for a breathing person .....	95
Table 3.1. Radar frequencies designation according to IEEE standard letter band nomenclature.....	100
Table 3.2. ISM bands .....	101
Table 3.3. Antenna characteristics .....	102
Table 3.4. Characteristics of the measurement setup.....	103
Table 3.5. Theoretical values of the phase variation .....	104
Table 3.6. Wavelet type description .....	109
Table 3.7. Mean $RMSE$ .....	115
Table 3.8. Relative error between $HR_{VNA}$ and $H_{RECG}$ .....	127
Table 4.1. Measurement setup .....	135
Table 4.2. $HR_{VNA}$ and $HR_{ECG}$ and their relative errors .....	139
Table 4.3. Measurement setup .....	142
Table 4.4. Heartbeat rate comparison between $HR_{VNA} - SA$ and $HR_{ECG}$ .....	148
Table 4.5. Heartbeat rate comparison between $HR_{VNA} - TA$ and $HR_{ECG}$ .....	148
Table 4.6. Heartbeat rate comparison between $HR_{VNA} - SA$ and $HR_{ECG}$ for a breathing person with different radiated powers.....	151
Table 4.7. Variance of the phase noise at $P_e = -19, -24, -29, -34, -39$ and $-44$ dBm and $f_e = 20$ GHz .....	158





## List of Abbreviations

<b>ALC</b>	Automatic Leveling Control
<b>BPF</b>	Band Pass Filter
<b>Bpm</b>	Breath per minute
<b>bpm</b>	beat per minute
<b>CW</b>	Continuous Wave
<b>CWT</b>	Continuous Wavelet Transform
<b>DC</b>	Direct Current
<b>DFT</b>	Discrete Fourier Transform
<b>DWT</b>	Discrete Wavelet Transform
<b>ECG</b>	Electrocardiogram
<b>FCC</b>	Federal Communications Commission
<b>FDA</b>	Food and Drug Administration
<b>FFT</b>	Fast Fourier Transform
<b>FIR</b>	Finite Impulse Response
<b>FMCW</b>	Frequency Modulated Continuous Wave
<b>FSCW</b>	Frequency-Stepped Continuous-Wave
<b>FSK</b>	Frequency Shift-Keying
<b>HF</b>	High Frequency
<b>HPBW</b>	Half Power Beam Width
<b>HR</b>	Heart Rate
<b>ICNIRP</b>	International Commission on Non-Ionizing Radiation Protection
<b>IEEE</b>	Institute of Electrical and Electronics Engineers
<b>IIR</b>	Infinite Impulse Response

<b>ISM</b>	<b>Industrial, Scientific and Medical</b>
<b>LFM</b>	<b>Linear Frequency Modulation</b>
<b>LSB</b>	<b>Lower Side Band</b>
<b>PDM</b>	<b>Peak Detection Method</b>
<b>PSD</b>	<b>Power Spectral Density</b>
<b>PLO</b>	<b>Phase Locked Oscillator</b>
<b>RF</b>	<b>Radio Frequency</b>
<b>RMSE</b>	<b>Root Mean Square Error</b>
<b>SAC</b>	<b>Specific Absorption per phone Call</b>
<b>SAD</b>	<b>Specific Absorption per Day</b>
<b>SAR</b>	<b>Specific Absorption Rate</b>
<b>SNR</b>	<b>Signal to Noise Ratio</b>
<b>STFT</b>	<b>Short-Time Fourier Transform</b>
<b>UHF</b>	<b>Ultra High Frequency</b>
<b>USB</b>	<b>Upper Side Band</b>
<b>UWB</b>	<b>Ultra-Wide Band</b>
<b>VHF</b>	<b>Very High Frequency</b>
<b>VNA</b>	<b>Vector Network Analyzer</b>
<b>WLAN</b>	<b>Wireless Local Area Network</b>

# Résumé étendu

## Introduction générale

Récemment, la mesure des signaux vitaux sans contact a suscité un grand intérêt au niveau de la recherche. Ces recherches concernent plusieurs domaines d'application. On peut citer par exemple la détection des personnes sous les décombres suite à des tremblements de terre, ou la mesure des battements cardiaques à distance pour des personnes pour lesquelles les électrocardiographes traditionnels ne sont pas indiqués [2]. A cause de la grande sensibilité des micro-ondes aux petits mouvements, le radar Doppler a été utilisé comme un système de surveillance sans contact de l'activité cardio-pulmonaire [1].

Le but de cette thèse est de pouvoir proposer une solution fiable pour mesurer sans contact les battements de cœur d'une personne à l'intérieur de sa maison. Ceci présente un grand intérêt pour les personnes âgées, les personnes brûlées ou les bébés. Ainsi, la surveillance de leur activité cardiaque à distance leur permet de vivre leur propre vie normalement.

Cette thèse présente une étude comparative dans la détection des signaux de battements cardiaques, en considérant différentes fréquences et puissances d'émission. Cela permet de spécifier la fréquence opérationnelle optimale, qui donne un compromis entre la complexité du système de mesure, la précision ainsi que la puissance minimale émise.

De plus, une étude comparative entre plusieurs méthodes de traitement de signal est proposée pour extraire la meilleure méthode qui permet de mesurer le signal cardiaque et par suite extraire ses paramètres. Le paramètre extrait dans cette thèse est le taux des battements cardiaques *HR (Heart Rate)*.

Puisque la personne peut se déplacer d'une pièce à une autre à l'intérieur de son domicile, des mesures des quatre côtés de la personne et derrière un mur sont réalisées. Ajoutons une approche de modélisation fondée sur la mesure cardio-respiratoire pour une personne qui exerce une marche en avant.

Ce mémoire de thèse est divisé en 4 chapitres : Le chapitre 1 présente l'utilité du radar dans la surveillance cardio-pulmonaire. Dans le chapitre 2, nous utilisons le filtrage

classique comme outil de traitement de signal pour extraire le signal cardiaque. L'extraction du taux des battements est faite dans les domaines fréquentiel et temporel. Une étude comparative entre ces deux domaines et entre différentes puissances d'émission est présentée. Le chapitre 3 présente une étude réalisée de différents côtés de la personne sous test. Les mesures sont effectuées à des fréquences opérationnelles différentes afin de faire une comparaison entre elles. Des techniques de traitement basées sur des transformées en ondelettes ou le filtrage classique sont présentées et utilisées afin de faire une comparaison entre elles. Le chapitre 4 est focalisé sur des scénarios que la personne peut rencontrer à l'intérieur de sa maison ainsi que des études concernant un système utilisant une seule antenne. Enfin, une conclusion générale dresse un bilan de ces travaux et propose quelques perspectives pour la recherche.

## **Chapitre 1 Surveillance sans contact de l'activité cardio-pulmonaire**

De nos jours, la surveillance sans contact des signaux vitaux est nécessaire dans les applications de surveillance médicale et dans les soins de santé, en particulier pour les patients brûlés où l'utilisation des électrodes traditionnels pour mesurer les battements de cœur n'est pas envisageable. A cause de la sensibilité des micro-ondes aux petits mouvements, le radar Doppler peut être utilisé comme un système de surveillance sans contact de l'activité cardio-pulmonaire humaine. En outre, les signaux transmis peuvent, sous certaines conditions, pénétrer les murs et les obstacles, ce qui les rend utiles dans la détection de la vie sous les décombres en cas de tremblement de terre.

Le radar «Radio Detection And Ranging» désigne une technologie radioélectrique pour la détermination de la vitesse et les distances des objets stationnaires ou mobiles [35]. Le radar Doppler est utilisé dans beaucoup d'applications, comme la mesure de vitesse d'un véhicule ou le suivi des tempêtes. En outre, il peut être utilisé pour les petits mouvements, y compris la respiration et les battements cardiaques.

Un système radar est basé sur une paire d'antennes, l'une antenne émettrice, l'autre une antenne réceptrice, et enfin un processeur pour déterminer le mouvement de la cible [36]. Le radar émet une onde électromagnétique et observe l'écho retourné afin de détecter la présence de la cible. Seule une petite partie de l'énergie transmise est renvoyée vers le

radar, qui est ensuite traitée [38]. Si la cible est en mouvement, une fréquence de décalage apparaît à cause du mouvement de la cible : c'est l'effet Doppler [35].

Selon l'effet Doppler, le déplacement de la cible provoque une variation de phase du signal réfléchi [5]. Si le mouvement visé est celui de la cage thoracique d'une personne, la relation entre le déplacement thoracique  $\Delta x(t)$  et la variation de phase  $\Delta\theta(t)$  est la suivante :

$$\Delta\theta(t) = \frac{4\pi}{\lambda} \Delta x(t) \quad (1)$$

où  $\lambda$  est la longueur d'ondes du signal transmis. Le signal réfléchi contient le signal cardiaque et le signal respiratoire du patient.

Le mouvement de la poitrine causé par la respiration est entre 4 à 12 mm. Ce mouvement causé par le rythme cardiaque est généralement compris entre 0,2 et 0,5 mm [5]. Au repos, la fréquence de respiration pour un adulte varie entre 0,2 et 0,34 Hz. En outre, les changements de fréquence de battement dans l'intervalle 1 et 2 Hz pour un adulte. Par conséquent, le taux de respiration d'un adulte varie entre 12 et 20 respirations par minute (Bpm) [84] et le rythme cardiaque d'un adulte varie entre 60 et 120 battements par minute (bpm) [5].

Lors de l'utilisation d'un radar Doppler pour la détection de l'activité cardio-pulmonaire, l'onde est transmise vers la poitrine de la personne où elle subit une réflexion. L'onde réfléchie est ensuite détectée et les rythmes cardiaque et respiratoire peuvent alors être extraits.

Le traitement du signal est une étape importante pour l'extraction des paramètres vitaux du signal reçu. Il comprend la démodulation du signal en bande de base, l'élimination des mouvements indésirables du corps et finalement l'extraction du signal utile. Plusieurs méthodes de démodulation peuvent être utilisées comme l'approximation angulaire et la démodulation arc tangente [66]. En ce qui concerne le problème du mouvement indésirable du corps qui est considéré comme une source importante de bruit, il peut être résolu en utilisant plusieurs émetteurs-récepteurs qui détectent les signaux réfléchies de différents côtés du corps humain [67].

Selon la littérature, pour notre application, les radars peuvent généralement être classés en plusieurs catégories : radar à onde continue (CW), radar à onde continue modulée en fréquence (FMCW) et enfin radar impulsionnel ou ultra large bande (UWB). Chacun des systèmes utilisant ces technologies permet la mesure des signaux vitaux et a ses propres avantages et inconvénients.

Le radar UWB est capable de détecter la fréquence respiratoire ou cardiaque pour une ou plusieurs personnes ; il est également capable de détecter la distance entre le patient et les antennes du système [50]. En outre, il est relativement meilleur que les autres en termes de propagation à travers les obstacles [43]. Par contre, il n'est pas favorable pour les applications à courte portée. En effet, pour ces applications, un commutateur à très grande vitesse est nécessaire, d'où l'utilisation d'un convertisseur analogique/numérique à très grande vitesse qui consomme une grande puissance est indispensable [51], contrairement aux systèmes CW et FMCW qui permettent un niveau d'intégration plus élevé du système et une plus faible puissance. Le radar FMCW permet de mesurer l'éloignement de la cible [53]. Cependant, le radar CW est meilleur comparativement au radar FMCW en raison de sa meilleure précision à détecter le mouvement de la cible. De plus, son architecture est moins complexe et les techniques de traitement du signal associées sont plus simples [54]. Bien que la technique FMCW permet de déterminer la distance cible-antennes et facilite l'élimination des bruits stationnaires, elle reste inefficace lorsque ceux-ci deviennent proches de la cible [52]. CW a une bonne immunité contre l'interférence du bruit stationnaire [53]. Par conséquent, pour les applications qui ne nécessitent pas de connaître la distance système-cible, le radar CW est une meilleure option pour la détection des signaux vitaux [55].

La recherche des méthodes de détection de signes vitaux en utilisant des technologies hyperfréquences se développe rapidement. La première démonstration de la détection des signes vitaux sans contact a été rapportée en 1975 par J. C. Lin. Un système à 10 GHz a été utilisé en mesurant la respiration d'un lapin situé à 30 cm des antennes du système [3]. Après 2000, les avancées se sont accélérées à cause des progrès des technologies semi-conductrices et sans fil. Plusieurs architectures et algorithmes ont été proposés [4]. La plupart des systèmes utilisaient le radar CW. En 2008, un système utilisant un analyseur de réseau vectoriel a été utilisé [5]; ce système permet la sélection de la fréquence et la

puissance du signal émis pour déterminer la fréquence opérationnelle optimale et la puissance minimale permettant d'extraire les paramètres vitaux avec une bonne précision. Des mesures ont été effectuées pour une personne qui retient son souffle pendant les mesures aux différentes fréquences 2.4, 5.8, 10 et 60 GHz et avec des puissances rayonnées allant de -2 dBm à -27 dBm.

## **Chapitre 2 Détection de battements cardiaques d'une personne en utilisant le filtrage classique pour différentes puissances rayonnées**

Ce chapitre présente un système de mesure sans contact de l'activité cardio-pulmonaire. En utilisant un analyseur de réseau vectoriel, la phase du paramètre  $S_{21}$  est mesurée. La variation de phase de  $S_{21}$  contient le signal cardio-respiratoire. Pour déterminer la puissance minimale permettant de mesurer les paramètres vitaux avec une bonne précision après application des traitements de signal, plusieurs puissances rayonnées sont utilisées : 3, -2, -7, -12 et -17 dBm. Des travaux antérieurs [5] ont conduit à choisir des fréquences opérationnelles dans les bandes S (2,4 GHz), C (5,8 GHz) et X (10 GHz) pour l'extraction du rythme cardiaque. En outre, la fréquence de 60 GHz a été également étudiée. Dans ce travail, nous avons trouvé judicieux de travailler à une fréquence différente, les mesures ont été effectuées à 20 GHz. Cette fréquence est considérée comme un bon compromis entre le coût du système complet et la précision de mesure et d'extraction des paramètres vitaux. Par la suite, des techniques de traitement sont nécessaires pour extraire le signal cardiaque à partir du signal mesuré. Les travaux antérieurs avaient permis d'extraire le taux des battements cardiaques pour une personne qui retient son souffle. De plus, des techniques de traitement du signal ont été ensuite appliquées sur des modèles représentant l'activité cardio-respiratoire pour extraire le rythme cardiaque [5]. Plusieurs techniques de traitement du signal sont appliquées pour extraire le taux des battements cardiaques, soit dans le domaine fréquentiel, soit dans le domaine temporel, en utilisant différentes méthodes de filtrage. Dans notre travail, les mesures sont faites pour 2 cas : Pour une personne qui retient son souffle et ensuite pour une personne qui respire normalement. Ces essais sont réalisés pour montrer la possibilité d'extraire le signal cardiaque du signal cardio-respiratoire à une fréquence de 20 GHz. Cette personne était assise à 1 mètre des antennes du système. Par ailleurs, ces mesures



ont été effectuées simultanément avec un électrocardiographe (ECG) pour valider les techniques de détection du rythme cardiaque. La Figure 1 présente un signal ECG normalisé par rapport à son amplitude pour une personne qui respire normalement. 28 pics sont détectés pendant un intervalle de 21.93 sec, ce qui correspond à 74 battements / min.

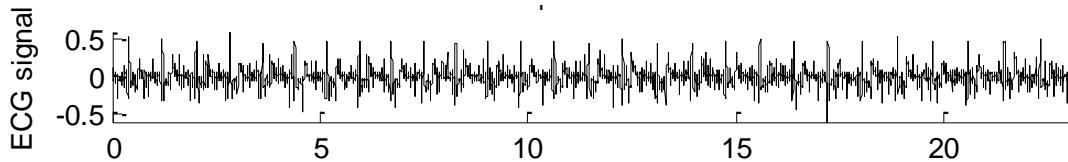


Figure 1. Le signal ECG normalisé

Outre le VNA, le système de mesure comprend deux antennes cornet une pour l'émission, et l'autre pour la réception. Ces composants rendent l'installation de l'expérience simple. La Figure 2 présente le système utilisé.

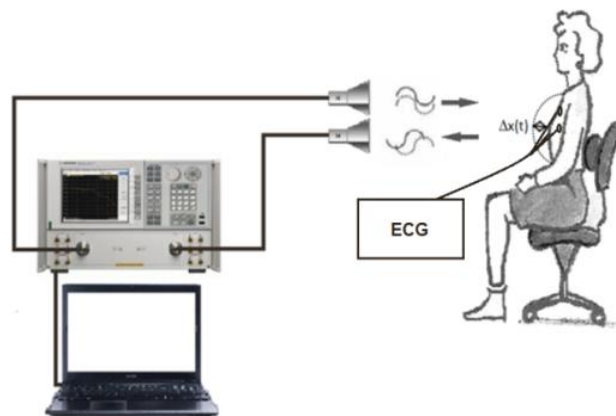


Figure 2. Système de mesure sans contact

Le système proposé présente des avantages par rapport aux autres de par sa capacité à faire varier la puissance et la fréquence du signal émis lors de la réalisation des mesures. Ainsi, la puissance d'émission minimale et la fréquence opérationnelle optimale peuvent être déterminées. La détermination de la puissance minimale est importante pour la sécurité du patient et minimise le risque d'exposition au rayonnement. De plus, la détermination de la fréquence opérationnelle optimale permet de faire un bon compromis entre la précision et le coût pour le système final.

Dans cette étude, le rythme cardiaque est extrait dans les deux domaines fréquentiel et temporel. Dans le domaine fréquentiel, lorsque la personne retient son souffle, la FFT est appliquée. La valeur maximale obtenue du signal dans la bande passante comprise entre 1 et 2 Hz correspond à la fréquence du battement cardiaque d'un adulte ; ces valeurs correspondent à un rythme cardiaque compris entre 60 et 120 battements/minute. Lorsque la personne respire normalement, la FFT est appliquée après l'utilisation du filtre Butterworth passe-haut d'ordre 4 ayant une fréquence de coupure 0.9 Hz pour éliminer le signal respiratoire. Ensuite, la valeur maximale obtenue dans la bande comprise entre 1 et 2 Hz est extraite.

Dans le domaine temporel, lorsque la personne retient son souffle, la méthode de lissage qui utilise la moyenne glissante est appliquée pour éliminer le bruit qui se trouve dans le signal. Lorsque la personne respire normalement, un filtrage est appliqué afin de séparer le signal respiratoire du signal cardiaque. Pour extraire la fréquence cardiaque, la détection des pics est utilisée après l'application du filtre passe-haut qui atténue le signal respiratoire puis du lissage qui réduit le bruit. Le filtre passe-haut utilisé est un filtre Butterworth d'ordre 4 avec une fréquence de coupure de 0.9 Hz. De plus, le filtre passe-bande Butterworth d'ordre 4 avec des fréquences de coupure de 0.9 et 2 Hz peut être utilisé. Ce filtre atténue le signal respiratoire et réduit le bruit.

Le rythme cardiaque est obtenu après application de la détection des pics. Il est calculé en utilisant la relation suivante:

$$HR = \frac{60(N - 1)}{d_1 + d_2 + \dots + d_{N-1}} \quad (2)$$

où  $N$  est le nombre de pics et  $d_k$  est la durée de l'intervalle déterminé entre 2 pics successifs exprimée en secondes.

La Figure 3 montre le module de la transformée FFT de la variation de phase de  $S_{21}$  d'une personne qui retient son souffle. Sur l'axe horizontal, à la place de la fréquence on indique le nombre de battements par minute. Ceci est obtenu en multipliant la fréquence par 60. La Figure 4 montre le module de la transformée de Fourier rapide (FFT) appliquée à la variation de phase de  $S_{21}$  après application d'un filtre passe-haut pour une

personne qui respire. Dans les deux cas, plusieurs puissances rayonnées sont considérées: 3, -2, -7, -12 et -17 dBm.

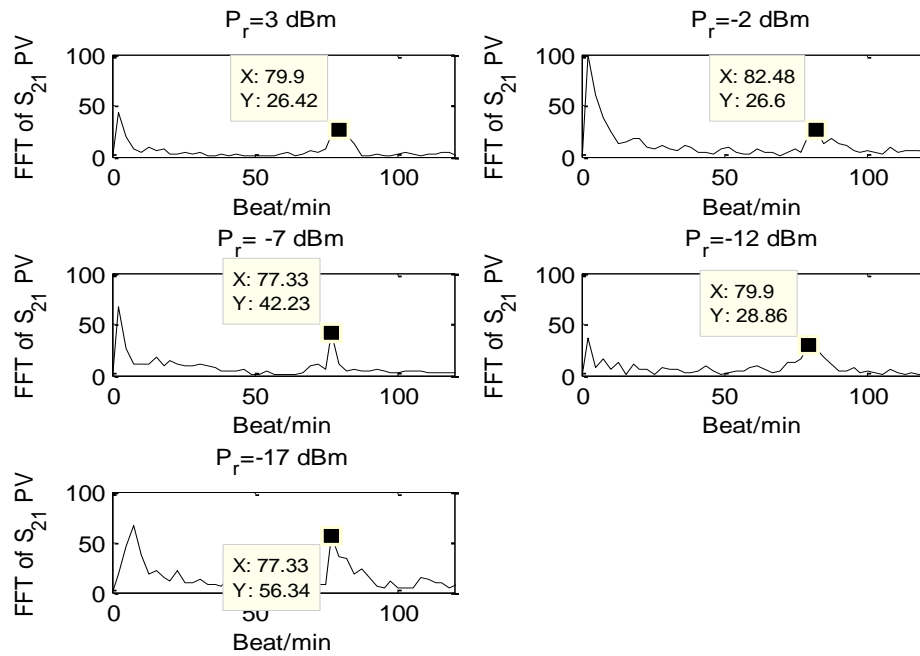


Figure 3. Module de la FFT de la variation de phase de  $S_{21}$  d'une personne qui retient son souffle

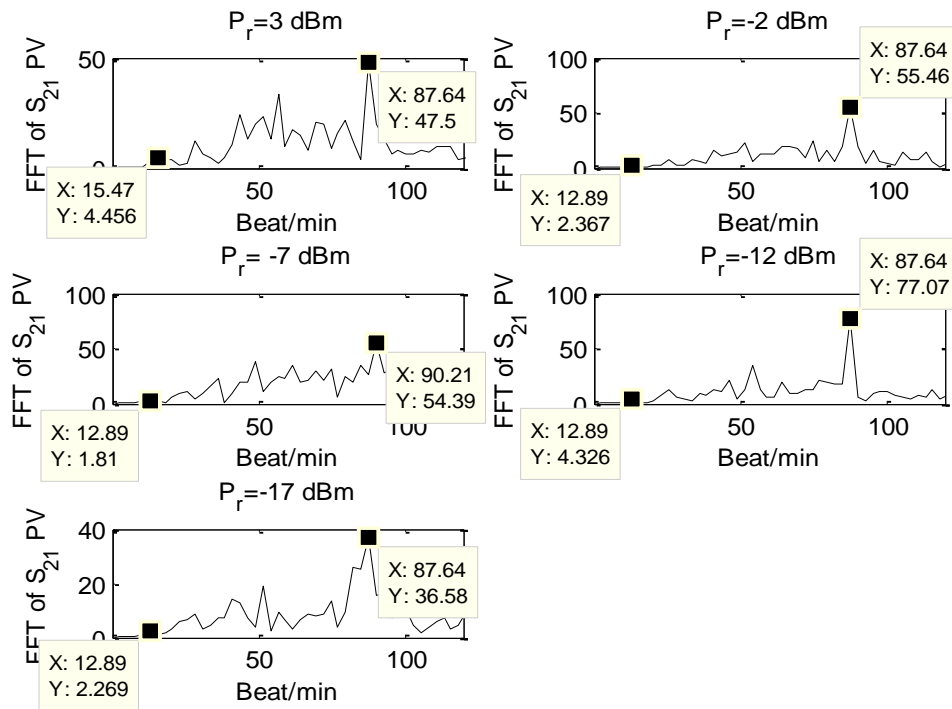


Figure 4. Module de la FFT de la variation de phase de  $S_{21}$  filtré d'une personne qui respire normalement

La Figure 5 présente la détection des pics à partir de la variation de phase de  $S_{21}$  lissé pour une personne qui retient son souffle. Le nombre d'échantillons total du signal est 12801. Le signal est lissé à l'aide d'une fonction 'Smooth' qui se trouve sur MATLAB. Cette fonction utilise une moyenne glissante de longueur  $n$ . La moyenne glissante prend la moyenne de chaque paquet de  $n$  échantillons consécutifs du signal qui doit être lissé. Après plusieurs essais, la longueur de la fenêtre  $n$  est choisie comme étant la valeur optimale correspondante à une détection avec la meilleure précision, la valeur obtenue est  $n = 199$ . Dans le cas de mesures avec respiration, le filtrage de la variation phase de  $S_{21}$  est appliqué, suivi d'une détection des pics. La Figure 6 présente la détection des pics après filtre passe-bande de la variation de phase de  $S_{21}$  pour une personne qui respire normalement. On utilise un filtre de type Butterworth d'ordre 4, ayant des fréquences de coupure de 0.9 Hz et 2 Hz. La Figure 7 présente la détection des pics après un filtrage passe-haut de la phase de  $S_{21}$  suivie par un lissage. On utilise un filtrage de Butterworth d'ordre 4 ayant une fréquence de coupure de 0,9 Hz. L'atténuation aux fréquences de coupures est de -3 dB.

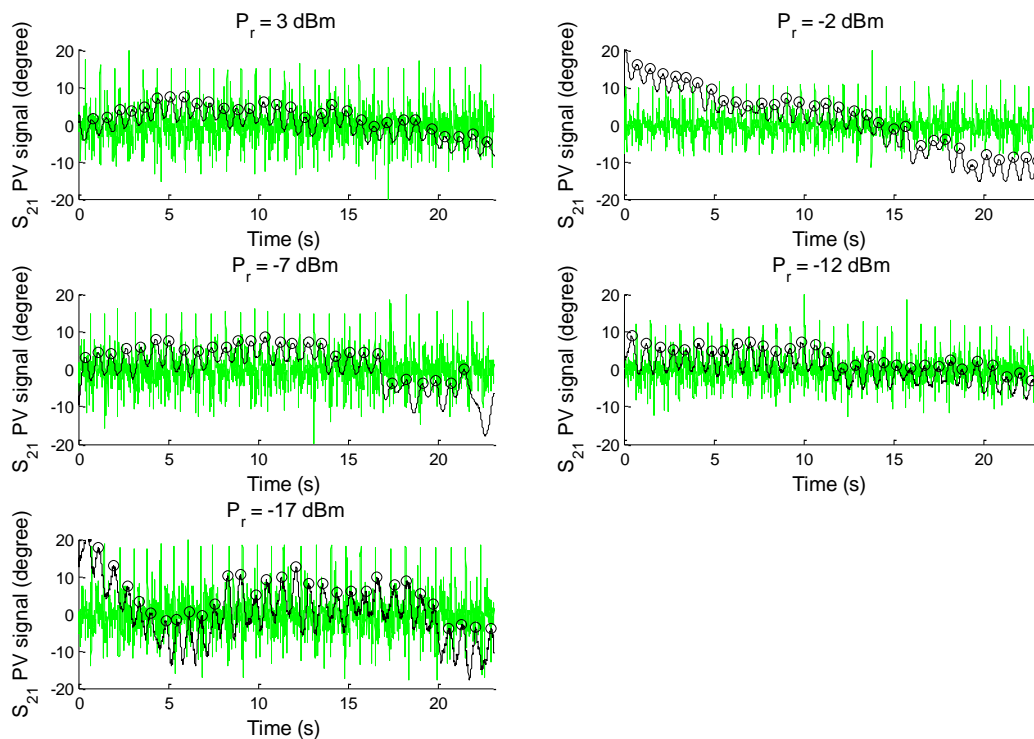


Figure 5. Détection des pics de la variation de phase de  $S_{21}$  lissée pour une personne qui retient son souffle à 20 GHz et à  $P_r = 3, -2, -7, -12$  and  $-17$  dBm (Noir), signal ECG (Vert)

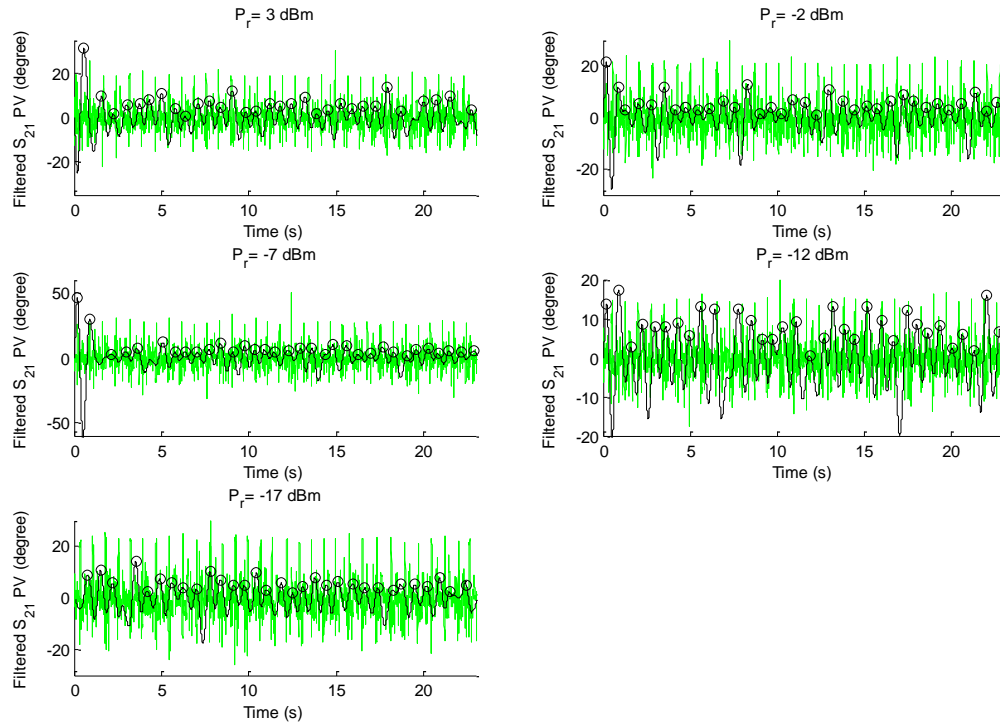


Figure 6. Détection des pics après application d'un filtre passe bande sur la variation de phase de  $S_{21}$  pour une personne qui respire normalement à 20 GHz et à  $P_r = 3, -2, -7, -12$  and  $-17$  dBm (Noir), signal ECG (Vert)

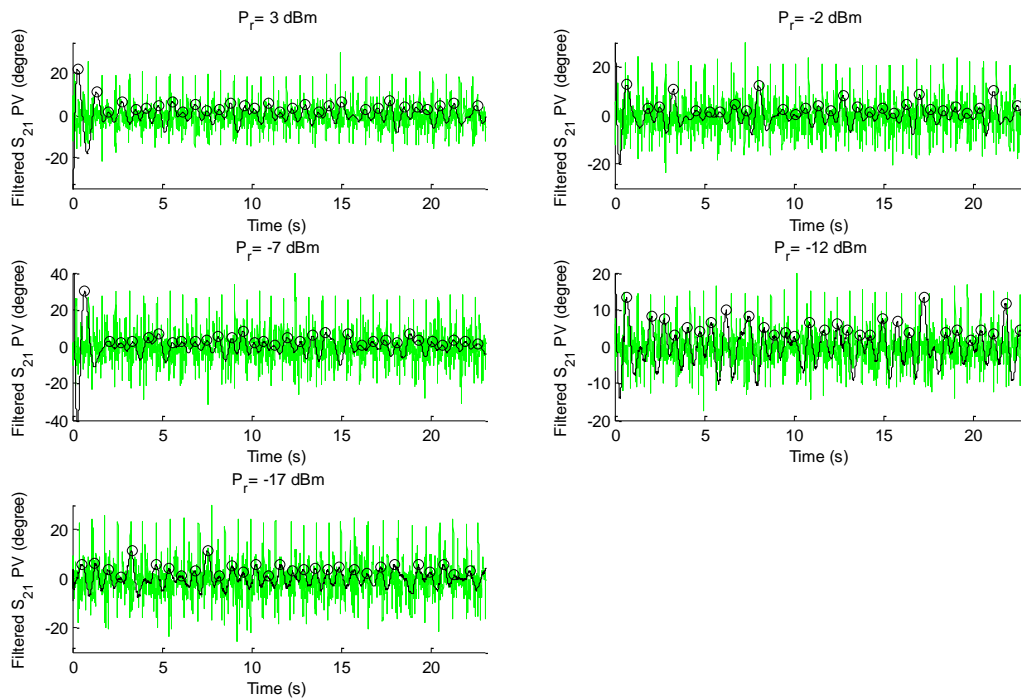


Figure 7. Détection des pics après application d'un filtre passe haut avec lissage de la variation de phase de  $S_{21}$  pour une personne qui respire normalement à 20 GHz et à  $P_r = 3, -2, -7, -12$  and  $-17$  dBm (Noir), signal ECG (Vert)

Ensuite, l'erreur relative entre le  $HR$  de l'ECG et le  $HR$  du système VNA est calculée en utilisant l'équation (3) :

$$Error (\%) = 100 \times \left| \frac{HR_{VNA} - HR_{ECG}}{HR_{ECG}} \right| \quad (3)$$

Il est à noter que selon la norme nationale américaine [90], les dispositifs médicaux mesurant le rythme cardiaque devraient avoir une erreur relative inférieure à 10% ou 5 bpm.

Etant donné que les résultats obtenus dans les domaines fréquentiel et temporel sont inférieurs à 10%, on peut déduire que l'extraction de la fréquence cardiaque est possible dans les deux domaines, avec ou sans respiration, à la fréquence de 20 GHz et pour plusieurs puissances d'émission allant de 3 à -17 dBm.

Il est à noter que la méthode utilisant la FFT ne peut donner une valeur  $HR$  précise que si la fréquence d'échantillonnage est très élevée. Des fois, celle-ci peut être limitée selon les caractéristiques et la capacité du VNA utilisé. C'est pourquoi la fréquence cardiaque est extraite en utilisant le domaine temporel.

Le domaine temporel donne des résultats meilleurs que ceux obtenus dans le domaine fréquentiel. En effet, dans le domaine temps, la méthode de lissage est suffisante pour extraire les propriétés cardiaques dans le cas où la personne retient son souffle. Par contre, avec respiration, deux types de filtres ont été utilisés afin de les comparer : un filtre passe-bande et un filtre passe-haut. Les résultats utilisant ces filtres sont considérés comme acceptables. De plus, les résultats obtenus à partir de la phase du  $S_{21}$  filtrée passe-haut puis lissée (moins de 5%) sont plus précis que les résultats obtenus à partir de la phase filtrée passe-bande et non lissée (moins que 9%). En outre, le rythme cardiaque est extrait avec une erreur relative inférieure à 5% lors de l'application du filtre passe haut et lissage, même avec une faible puissance (-17 dBm) et sur des mesures réelles réalisées sur une personne qui respire normalement. La fréquence opérationnelle de fonctionnement du système est de 20 GHz. Le Tableau 1 présente l'erreur relative dans les domaines de temps et fréquence entre le système et l'ECG en utilisant le filtre Butterworth d'ordre 4 passe-haut (PH) avec une fréquence de coupure de 0.9 Hz, pour

une personne qui respire. Lorsque celle-ci retient son souffle, un simple lissage est appliqué dans le domaine temporel.

Tableau 1. Erreur relative entre le système VNA et ECG

<b>Puissance rayonnée (dBm)</b>	<b>Respiration (Oui / Non)</b>	<b>Erreur relative au domaine temporel (PH + lissage) (%)</b>	<b>Erreur relative au domaine fréquentiel (PH) (%)</b>
3	Oui	1	9
-2	Oui	5	9
-7	Oui	1	7
-12	Oui	2	9
-17	Oui	1	9
3	Non	7	8
-2	Non	8	6
-7	Non	7	7
-12	Non	7	5
-17	Non	7	2

### **Chapitre 3 Extraction du signal cardiaque en utilisant les ondelettes pour plusieurs côtés et différentes fréquences opérationnelles**

Les travaux précédents sont effectués d'un seul côté de la personne : côté face. Cependant, l'un des objectifs de notre travail est de détecter le signal cardiaque pour une personne pouvant se déplacer dans une pièce, ainsi sa position par rapport au radar peut varier. C'est pourquoi dans ce chapitre, une étude est effectuée en considérant différents côtés : côté face, dos, gauche et finalement droit.

Dans ce chapitre, la personne respire normalement et se trouve à 1 mètre du système. Les mesures sont effectuées à différentes fréquences : 2.4, 5.8 et 10 GHz afin de faire une comparaison en fonction du paramètre fréquence et ceci pour différents côtés de la personne. Les fréquences opérationnelles devraient couvrir autant de bandes fréquentielles que possible, avec une préférence pour les bandes ISM. Les fréquences opérationnelles choisies sont : 2.4 GHz (bande S), 5.8 GHz (bande C) et 10 GHz (bande X). En outre, ces fréquences sont sélectionnées en tenant compte des limites du VNA car sa fréquence maximale est de 20 GHz. La puissance rayonnée est fixée à 0 dBm afin de limiter l'impact possible sur le patient.

Le système micro-ondes utilisé est le même que celui du chapitre précédent, mais avec différents types d'antennes puisque les fréquences opérationnelles sont différentes. Simultanément, un électrocardiographe (ECG) est utilisé pour déterminer la précision de l'extraction du rythme cardiaque.

Comme le signal détecté par le radar contient le signal respiratoire et celui du rythme cardiaque, des techniques de traitement du signal sont nécessaires pour pouvoir les séparer, surtout que l'amplitude du signal de respiration est beaucoup plus grande que celle du signal cardiaque. Dans ce contexte, des techniques de traitement basées sur les transformées d'ondelettes ou sur les filtres classiques peuvent être appliquées afin d'extraire le rythme cardiaque à partir d'un signal cardio-pulmonaire. L'utilisation de ces deux techniques est réalisée pour permettre de faire une comparaison entre elles.

La Figure 8 montre un exemple des mesures à 5.8 GHz de la variation de la phase de  $S_{21}$  résultante de l'activité cardio-pulmonaire à partir de différents côtés de la personne: côté face, côté dos, côté gauche et finalement côté droit.



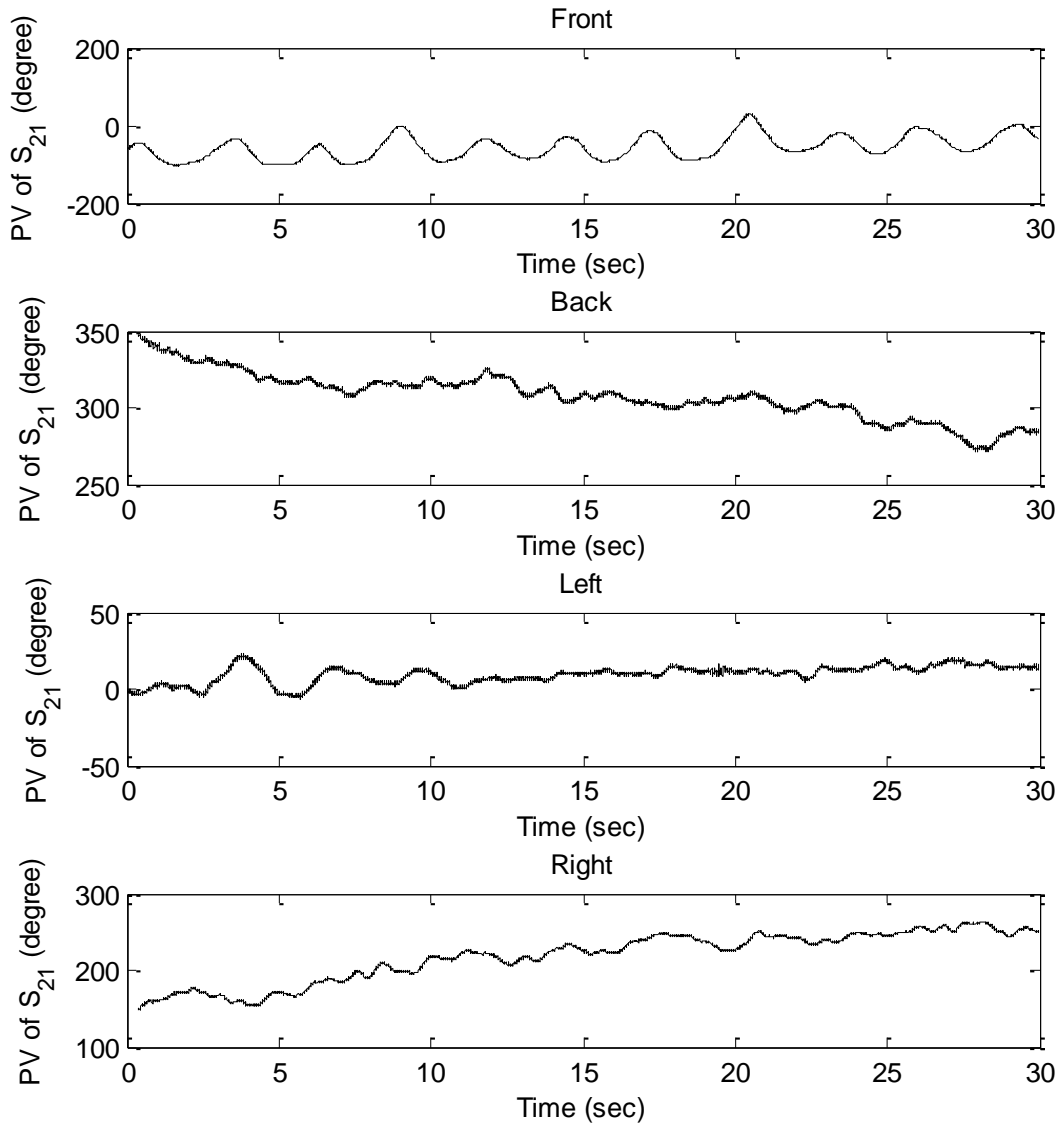


Figure 8. Variation de la phase de  $S_{21}$  pour les 4 côtés d'exposition ( $f_e = 5.8$  GHz)

On peut remarquer que le signal cardio-pulmonaire du côté face est moins bruité que les signaux obtenus pour les autres côtés. Toutefois, les techniques de traitement du signal montreront la possibilité d'extraire le signal cardiaque du signal cardio-pulmonaire dans les différentes positions.

Comme démontré dans ce chapitre, les filtres classiques sont capables d'extraire le signal cardiaque dans les domaines temporel et fréquentiel, l'erreur du taux des battements cardiaques par rapport à ECG augmente en raison de la distorsion obtenue lors de l'application des filtres classiques. La transformée de Fourier rapide réalise une

conversion du signal cardiaque du domaine temporel au domaine fréquentiel. La fréquence qui correspond à la fréquence des battements cardiaques est extraite en choisissant l'amplitude maximale comprise entre 1 et 2 Hz. La FFT est appliquée après l'utilisation de filtres classiques qui atténuent le signal respiratoire. La FFT donne de bons résultats, mais une erreur supplémentaire peut se produire si la fréquence réelle peut ne pas correspondre à  $n.\Delta f$  où  $\Delta f$  est le pas fréquentiel qui sépare deux échantillons successifs de la FFT. Par suite, la fréquence se propage aux fréquences adjacentes. Afin de suivre la variation du *HR* dans le temps, la Transformée de Fourier à Courte Durée est proposée (STFT). Cette technique est basée sur l'application de la transformée de Fourier sur des portions du signal (des fenêtres), au lieu de l'appliquer sur tout le signal. Cela permet d'analyser le signal dans les domaines temps et fréquence avec une résolution variable en fonction de la longueur sélectionnée de la fenêtre. Une fenêtre courte donne une bonne résolution dans le temps et une mauvaise résolution en fréquence, tandis qu'une grande fenêtre donne une faible résolution dans le temps, mais une bonne résolution en fréquence. L'inconvénient de la STFT est que la longueur de la fenêtre est fixe. Cet inconvénient a été éliminé par l'utilisation de la transformée d'ondelettes [97].

La transformée en ondelettes décompose le signal en approximations « $A_1, \dots, A_N$ » et en détails « $D_1, \dots, D_N$ ». Ils sont calculés par filtrages successifs passe-bas et passe-haut du signal. 'A' représente le signal filtré passe-bas et 'D' représente le signal filtré passe-haut [94]. En général,  $A_n$  contient les fréquences entre 0 et  $fs/2^{n+1}$  et  $D_n$  possède les fréquences entre  $fs/2^{n+1}$  et  $fs/2^n$ , où  $fs$  est la fréquence d'échantillonnage et  $n$  représente le niveau de la décomposition ( $n = 1, 2, \dots, N$ ).

Notons que le signal reconstruit possède l'équation suivante :

$$S_{reconstructed} = A_n + D_n + D_{n-1} + \dots + D_1 \quad (4)$$

Plusieurs familles d'ondelettes existent comme Daubechies, Coiflets, Symlets, etc... Le choix du type d'ondelettes est basé sur la reconstruction du signal. L'erreur entre le signal original et le signal reconstruit doit être la plus petite possible pour une reconstruction parfaite [99]. L'erreur quadratique moyenne (*RMSE*) est l'indicateur pour mesurer l'erreur entre le signal original  $x$  et le signal reconstruit  $\hat{x}$ . Elle est donnée par l'équation (5) :

$$RMSE = \sqrt{\frac{1}{N} \sum_{n=1}^N |x(n) - \hat{x}(n)|^2} \quad (5)$$

La moyenne des valeurs  $RMSE$  de tous les signaux obtenus pour les 4 côtés et les 3 fréquences est calculée pour chaque type d'ondelettes selon la relation (6):

$$RMSE \text{ mean}_{wavelet \text{ type}} = \frac{\sum_{p=1}^4 \sum_{q=1}^3 RMSE \text{ wavelet type } (p)(q)}{3 \times 4} \quad (6)$$

où  $p$  présente les positions et  $q$  présente les fréquences opérationnelles. Quatre positions sont considérées pour la mesure :  $p = 1$  pour le côté face,  $p = 2$  pour le côté dos,  $p = 3$  pour le côté droit et  $p = 4$  pour le côté gauche. Trois fréquences émises sont considérées lors des mesures :  $q = 1$  pour 2,4 GHz,  $q = 2$  pour 5,8 GHz et  $q = 3$  pour 10 GHz. La moyenne des valeurs  $RMSE$  est calculée pour chaque famille d'ondelettes considérée : Bior2.4, Rbio1.3, Sym5, Db5, Coif3, Dmey. On constate que Bior 2.4 possède la plus faible moyenne des valeurs  $RMSE$ .

Éliminer les fréquences inférieures à 1 Hz est nécessaire pour éliminer le signal respiratoire et garder seul le signal cardiaque, c'est pourquoi le ré-échantillonnage est appliqué pour convertir la fréquence d'échantillonnage de 666.7 Hz à 512 Hz. Après ré-échantillonnage, la décomposition en ondelettes est appliquée et arrêtée au niveau 8. L'approximation 8 qui contient les fréquences entre 0 et 1 Hz est éliminée du signal reconstruit, le signal  $S_{D18}$  obtenu contient toutes les fréquences supérieures à 1 Hz.  $S_{D18}$  est donné par la formule suivante :  $S_{D18} = S_{reconstruit} - A_8$ . Le signal est nommé  $S_{D18}$  parce qu'il possède toutes les décompositions allant de 1 à 8. La Figure 9 montre le signal  $S_{D18}$  pour les 4 côtés et à une fréquence opérationnelle de 5.8 GHz.

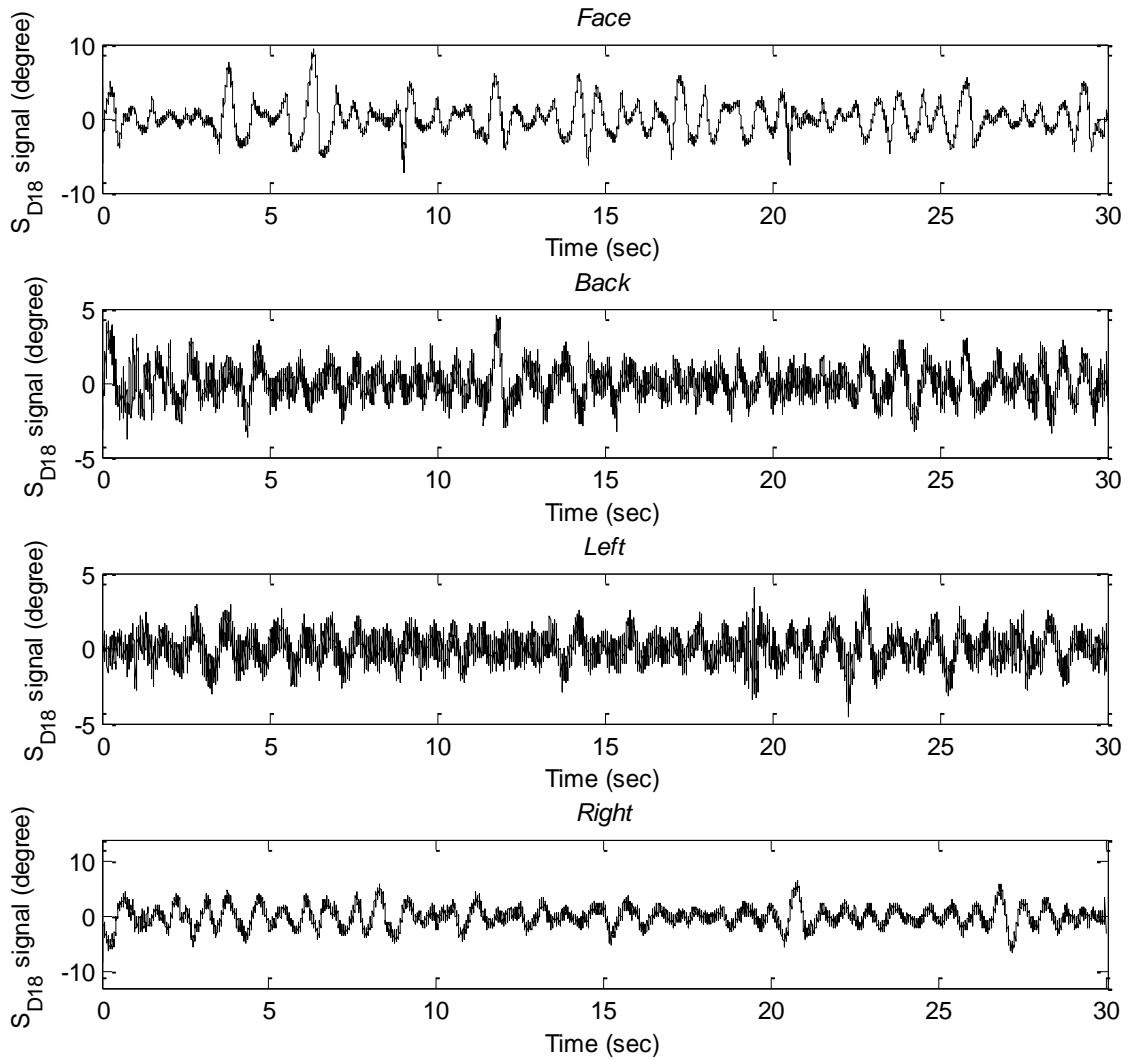


Figure 9. Signal  $S_{D18}$  pour les 4 côtés avec une fréquence opérationnelle 5.8 GHz

Parce que le signal  $S_{D18}$  est bruité, la détection des pics sera défectueuse. C'est pourquoi le lissage doit être appliqué pour éliminer le bruit. Le signal est lissé à l'aide d'une fonction 'Smooth' qui se trouve dans MATLAB qui utilise la moyenne glissante. Après plusieurs tentatives, le nombre d'échantillons se trouvant dans la fenêtre de lissage est choisi à 199. Ensuite, la technique de détection des pics est appliquée afin d'extraire la fréquence cardiaque à partir du signal  $S_{D18}$ . La Figure 10 présente de la détection des pics du signal  $S_{D18}$  lissé pour plusieurs types d'ondelettes appliquées au signal mesuré de face à 5.8 GHz pour une durée de 30 s.

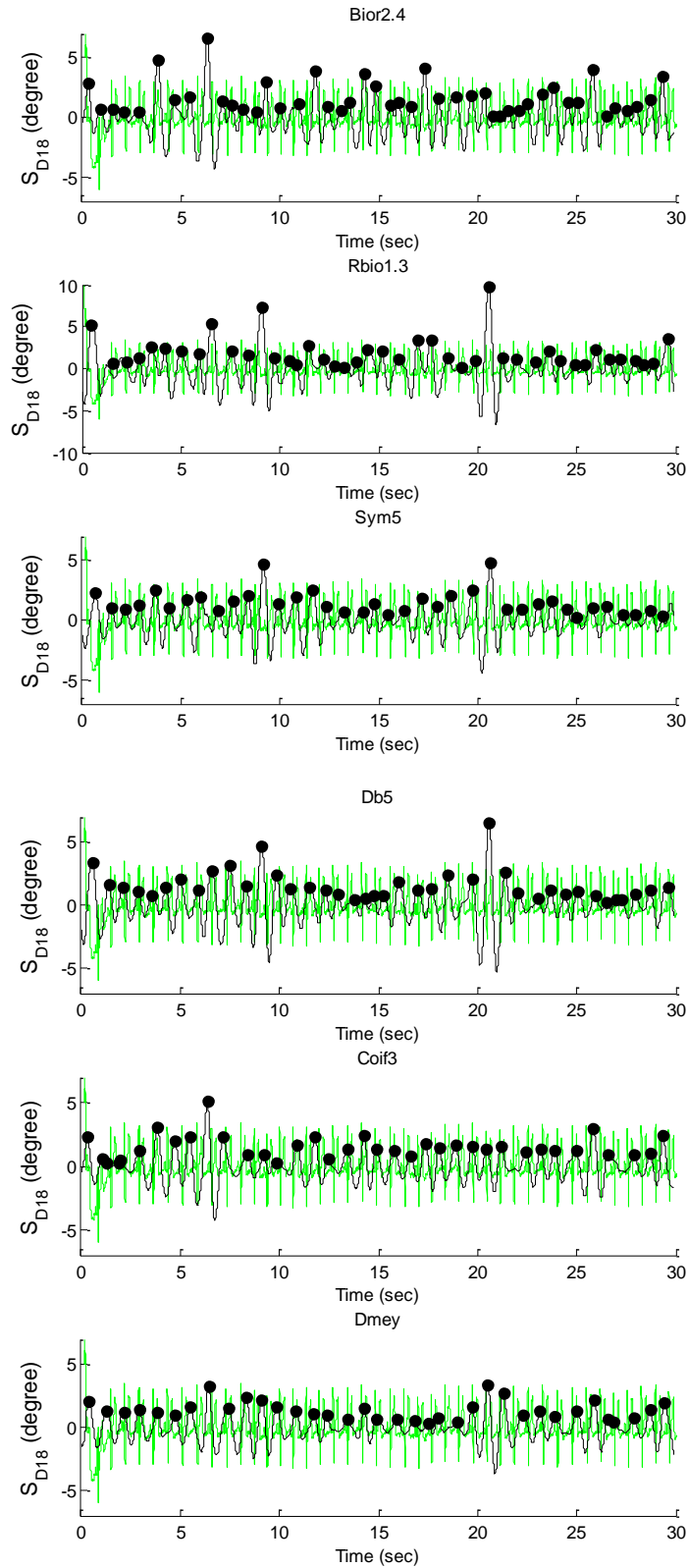


Figure 10. Signal  $S_{D18}$  lissé pris de face à 5.8 GHz et 0 dBm (Noir), Signal ECG (Vert)

Après la détection des pics du signal  $S_{D18}$  lissé, les taux des battements de cœur sont calculés pour chaque type d'ondelettes, chaque côté d'exposition et chaque fréquence d'émission. Ensuite, les erreurs relatives entre  $HR$  de  $S_{D18}$  et  $HR$  de l'ECG sont calculées.

La plupart des transformées d'ondelettes montrent la faisabilité d'extraire le signal cardiaque à partir du signal cardio-pulmonaire en utilisant différentes fréquences opérationnelles et ceci pour tous les côtés de la personne sous test et toujours avec la référence ECG utilisé simultanément. Le plus petit nombre d'erreurs relatives qui dépassent 10% est obtenu en utilisant Bior2.4. Rappelons que le type d'ondelettes ayant la plus faible  $RMSE$  est l'ondelette la plus appropriée. Donc ces résultats confirment que Bior 2.4 est l'ondelette qui donne les meilleurs résultats. En ce qui concerne les positions, le côté droit présente le plus grand nombre d'erreurs relatives qui dépassent 10%. En outre, ces résultats montrent que la position arrière correspond à l'erreur relative la plus faible (< 4%). Toutes les fréquences opérationnelles testées (2.4, 5.8 et 10 GHz) montrent la possibilité de suivre les signaux cardio-pulmonaires de tous les côtés. En ce qui concerne les fréquences, des mesures supplémentaires doivent être prises pour confirmer que l'erreur relative diminue avec l'augmentation de la fréquence de fonctionnement.

De plus, des filtres classiques sont appliqués pour faire une comparaison avec la transformée d'ondelettes. Un filtre passe-bas Butterworth d'ordre 4 avec une fréquence de coupure de 0,9 Hz est utilisé puis un lissage est appliqué ; le nombre d'échantillons trouvé dans la fenêtre de lissage est choisi à 199. Le choix de ce filtre est expliqué dans le chapitre 2. En outre, l'ondelette Bior 2.4 est choisie puisqu'elle possède le  $RMSE$  minimal entre les différents types de familles d'ondelettes. La fréquence cardiaque est calculée en utilisant ces deux techniques de traitement du signal, puis les erreurs relatives entre les résultats obtenus avec le VNA et les résultats de l'ECG sont calculées.

Comme conclusion, les ondelettes ont permis d'obtenir de meilleurs résultats par rapport aux filtres classiques. On peut attribuer cette différence entre autres à la présence de la distorsion en régime transitoire lors de l'utilisation du filtrage.

## Chapitre 4 Mesure du rythme cardiaque dans différents scénarios

La plupart des recherches jusque-là ont considéré la mesure du signal cardiaque d'une personne en face du système radar sans présence d'obstacles. Le but final de la recherche est de surveiller le signal cardiaque du patient à l'intérieur de son domicile, où il peut se déplacer d'une pièce à une autre. D'autre part, la plupart des recherches qui portent sur la mesure du signal de battement cardiaque derrière le mur utilisent l'UWB [101]. De plus, des mesures pour extraire le signal respiratoire pour une personne situé derrière un mur sont faites en utilisant le CW à 24 GHz à des distances inférieures à 1 m jusqu'à 2 m [101]. Dans ce chapitre, les mesures sont effectuées sur une personne fixe assise derrière un mur en utilisant le radar CW. Le but est de montrer la possibilité de mesurer le signal cardiaque pour une personne derrière un obstacle. Pour ces mesures, deux fréquences ont été considérées : 5.8 GHz et 10 GHz. L'obstacle est un mur en béton avec une épaisseur de 10 cm. La distance séparant le système de mesure et la personne sous test est de 1 m à laquelle il faut rajouter l'épaisseur du mur. L'onde transmise est dirigée vers la poitrine du patient. Les mesures ont été effectuées toutes les 30 secondes simultanément avec un électrocardiographe (ECG) utilisé comme système de référence. La transformée d'ondelettes discrète est utilisée comme technique de traitement pour séparer le signal cardiaque du signal respiratoire. Le signal de variation de phase de  $S_{21}$  a été ré-échantillonné de 666.7 à 512 Hz. Puisque Bior 2.4 possède le plus petit  $RMSE$  parmi les familles d'ondelettes, cette famille a été choisie pour l'appliquer sur le signal ré-échantillonné. Par la suite,  $A_8$  est retiré du signal reconstruit, et les signaux ayant des composantes inférieures à 1 Hz sont écartés. Par la suite, le signal  $S_{D18}$  qui ne comprend plus que le signal respiratoire est obtenu. Après, le lissage sur une fenêtre de 199 échantillons est appliqué pour éliminer le bruit et par la suite la détection des pics est effectuée. Finalement, l'erreur relative entre le taux des battements de cœur du système VNA et le taux des battements de cœur de l'ECG est calculés.

Les résultats obtenus sont acceptables sans mur (9 et 10% d'erreur relative), mais l'erreur augmente à 13 - 14% avec la présence du mur. Par conséquent, la surveillance d'une personne en présence d'un mur paraît difficile, puisque le mur provoque une atténuation qui augmente l'erreur relative dépassant 10%. D'autres mesures doivent être effectuées en

augmentant la puissance rayonnée. Le changement des valeurs de ces paramètres peut diminuer l'erreur obtenue.

Notons que la mesure du signal cardiaque pour une personne fixe en utilisant 2 antennes, une pour l'émission et une pour la réception, a été démontrée [5]. En outre, une étude a déjà démontré la faisabilité de faire cette mesure en utilisant une seule antenne, pour une personne qui retient son souffle [103]. Nous avons choisi de valider cette étude sans respiration avant de passer à des mesures avec respiration. Ainsi, dans ce chapitre, une comparaison entre le système micro-onde à une seule antenne et le système micro-onde à deux antennes est présentée pour une personne qui retient son souffle. Cette étude a été effectuée pour tester la précision du système à une seule antenne par rapport au système à deux antennes. Une durée de mesure de 23 s a été choisie pour éviter à la personne sous test de retenir sa respiration trop longtemps. La fréquence opérationnelle choisie est de 20 GHz avec plusieurs puissances rayonnées : -2, -7, -12 et -17 dBm. Notons que la distance entre la personne et le système est de 1 m. Lors de l'utilisation d'une seule antenne, la variation de phase de  $S_{11}$  est mesurée, tandis que lors de l'utilisation de deux antennes, la variation de phase de  $S_{21}$  est mesurée. Les Figure 11 et Figure 12 présentent la variation de phase de  $S_{11}$  et celle de  $S_{21}$  respectivement pour une personne qui retient son souffle pour différentes puissances rayonnées : -2, -7, -12 et -17 dBm.



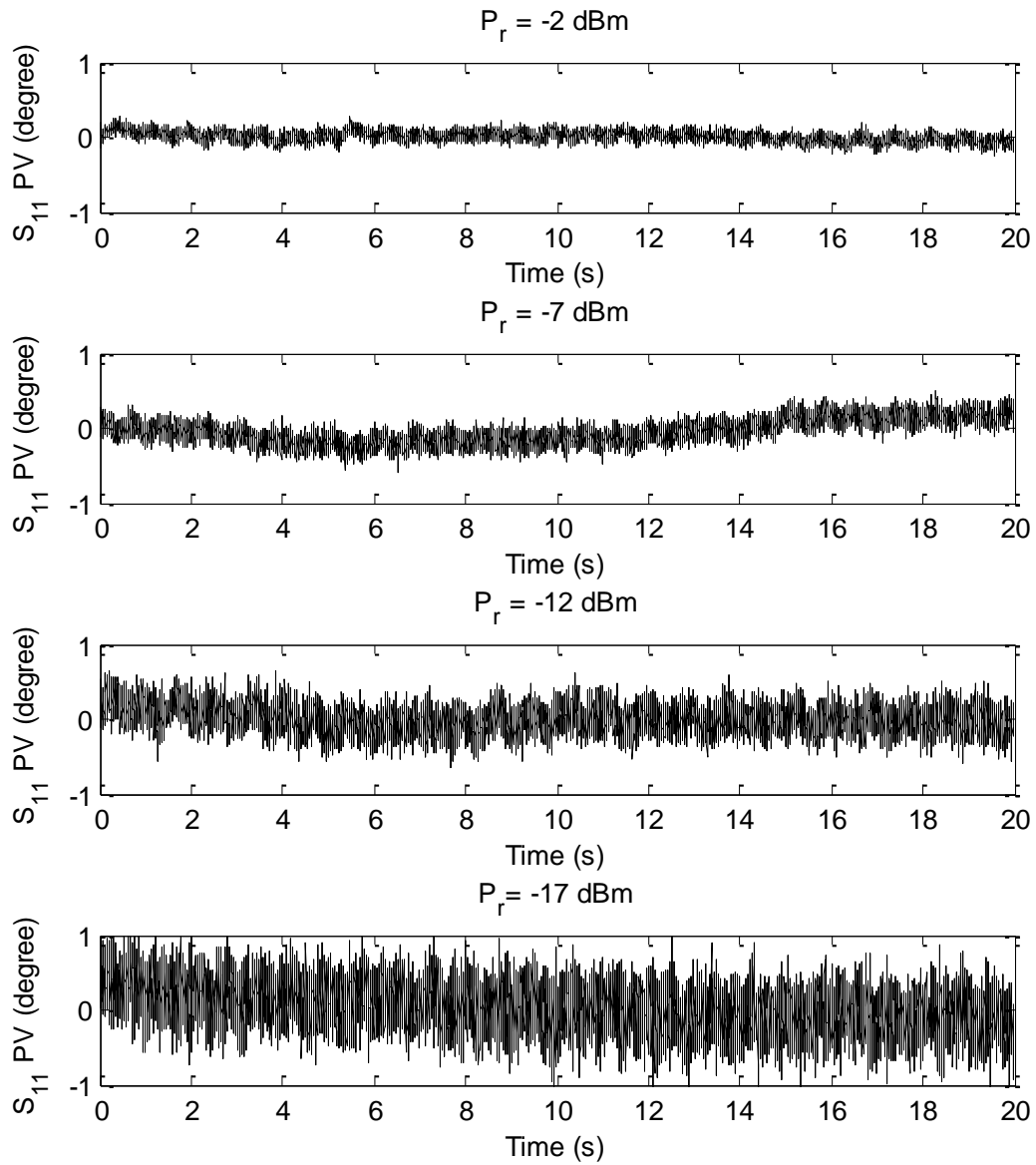


Figure 11. Variation de phase de  $S_{11}$  pour une personne qui retient son souffle à 20 GHz et  $P_r = -2, -7, -12$  and  $-17$  dBm

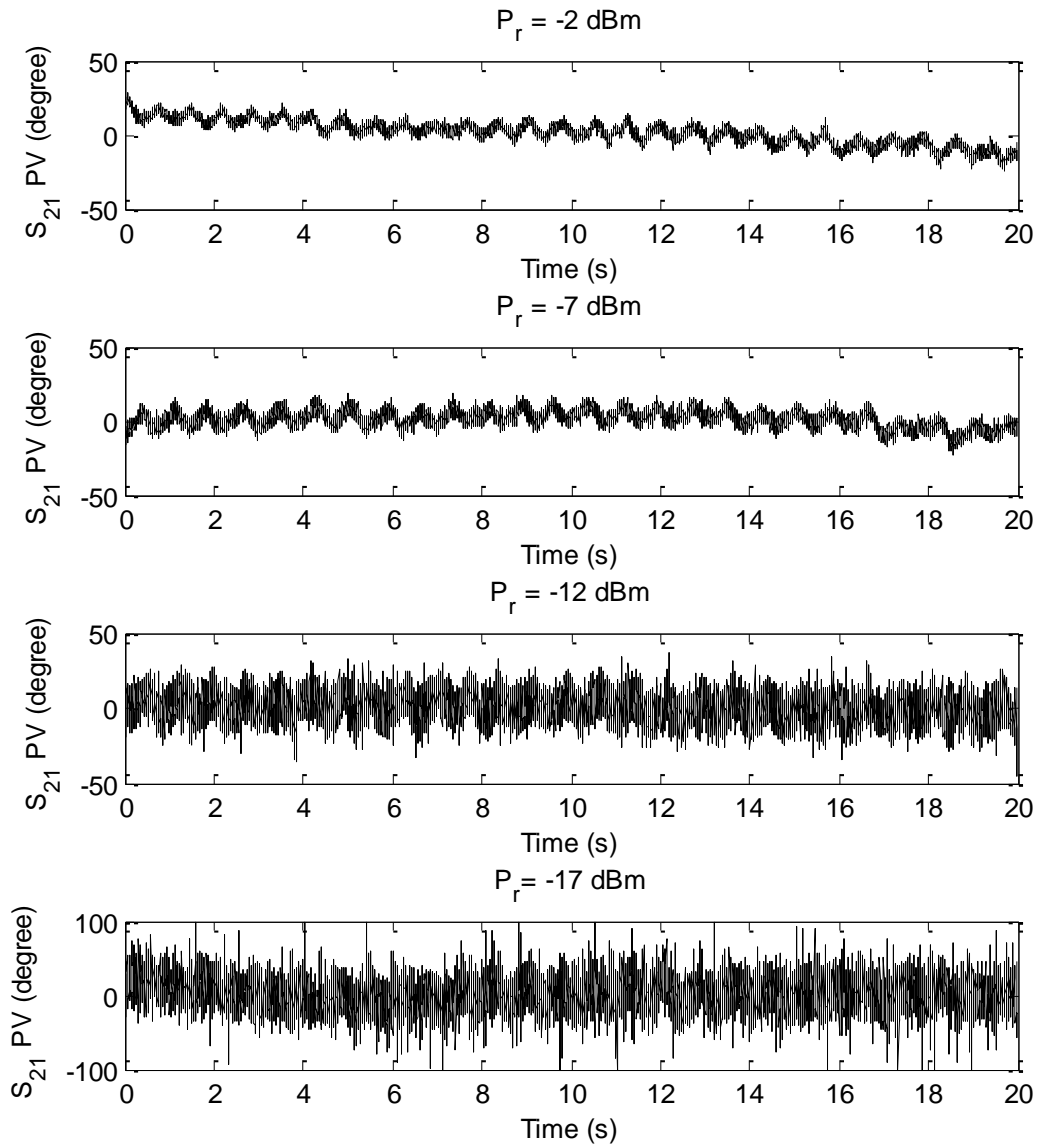


Figure 12. Variation de phase de  $S_{21}$  pour une personne qui retient son souffle à 20 GHz et  $P_r = -2, -7, -12$  and  $-17$  dBm

Il est remarquable que, pour une puissance donnée, la variation de phase du  $S_{11}$  est plus bruitée que celle du  $S_{21}$ . De plus, le bruit augmente lorsque la puissance rayonnée diminue dans les 2 phases. La méthode de lissage est utilisée pour éliminer le bruit et extraire le signal cardiaque. En conclusion, bien que les signaux du système micro-onde avec une seule antenne soient plus bruités que les signaux du système micro-onde à deux antennes, le système à une seule antenne est capable de mesurer le signal cardiaque avec une précision comparable à celle du système à deux antennes, pour toutes les puissances considérées avec un maximum d'erreur de 8%. Par suite, le système à une seule antenne a

été testé pour une personne qui respire normalement. Cette étude est faite pour montrer la faisabilité d'extraire les battements cardiaques avec ce type de système. Ce système fonctionne à une fréquence opérationnelle de 20 GHz et pour différentes puissances rayonnées : -2, -7, -12 et -17 dBm, la personne se trouve à 1 m du système. Les mesures sont effectuées toutes les 23 secondes simultanément avec un électrocardiographe (ECG). L'extraction du signal cardiaque a été faite en utilisant la technique des ondelettes.

Comme résultats, les fréquences cardiaques sont extraites même à faible puissance et les erreurs obtenues restent inférieures à 5%. Ainsi, on peut conclure que le radar CW Doppler à 20 GHz, avec une seule antenne émettrice et réceptrice, est un bon candidat pour extraire avec une bonne précision le taux du battement cardiaque pour une personne respirant normalement et ceci pour des faibles puissances rayonnées allant jusqu'à -17 dBm.

En outre, des scénarios avancés sont considérés pour tester la possibilité d'extraire le signal cardiaque d'un patient en mouvement à l'intérieur de sa maison. Ce scénario est réaliste pour les personnes âgées sous surveillance médicale dans leur domicile. Pour la modélisation, nous avons considéré le scénario d'une personne qui se déplace à une vitesse constante vers le radar, opérant à la fréquence de 20 GHz, avec une puissance d'émission de -19 dBm. Le gain de l'antenne est 24 dBm et la perte des câbles est 2 dBm, ce qui correspond à une puissance rayonnée de 3 dBm. La vitesse fixe est choisie faible pour modéliser le déplacement réel d'une personne âgée. Parce que la personne fait un mouvement vers le système, le déphasage de la variation de phase de  $S_{21}$  sera lié au déplacement relevé par le radar  $\Delta x(t)$ , qui est le résultat combiné de l'activité cardiaque, de l'activité respiratoire, et de l'activité due au mouvement de la personne se déplaçant à la vitesse  $v$ , auxquelles se rajoute le bruit. Ainsi,  $\Delta x(t)$  peut être exprimé par [107]:

$$\Delta x(t) = -vt + x_h(t) + x_r(t) + n(t) \quad (8)$$

où  $v$  est la vitesse de déplacement. Notons que le signe '-' est utilisé car la personne s'approche du système.  $x_h(t)$  représente la variation de phase de  $S_{21}$  résultante du rythme cardiaque,  $x_r(t)$  représente celui relatif à la respiration, et  $n(t)$  est le bruit additif. Pour

simplifier le modèle, nous avons considéré des mouvements respiratoire et cardiaque sinusoïdaux avec des fréquences et des amplitudes réalistes, basées sur des mesures.

Les techniques d'ondelettes sont appliquées à ce modèle. L'erreur relative obtenue est de 4 % ce qui est acceptable. Comme conclusion, la décomposition en ondelettes est capable d'extraire le signal cardiaque même en présence de ce type de mouvement.

## **Conclusion générale**

Dans cette thèse, le radar Doppler est proposé comme système sans contact pour la détection de signaux vitaux. Un système VNA émet un signal avec une fréquence constante, ce dernier est réfléchi par la poitrine de la personne sous test. La variation de phase du paramètre  $S_{21}$  contient les signaux respiratoire et cardiaque. Des techniques de traitement de signal sont alors nécessaires pour extraire le signal du rythme cardiaque. Toutes les mesures effectuées sont comparées simultanément à celles réalisées par l'ECG pris comme référence.

Une étude comparative des différentes puissances rayonnées a été réalisée : 3, -2, -7, -12 et -17 dBm à 20 GHz pour une personne assise à 1 m du système et respirant normalement. Les filtres classiques ont été appliqués pour atténuer le signal respiratoire du signal cardiorespiratoire. L'extraction du taux des battements du cœur a été faite dans les domaines temporel et fréquentiel. Pour passer au domaine fréquentiel, une FFT a été appliquée. Le problème du domaine fréquentiel est que la vraie fréquence peut ne pas être déterminée exactement si elle ne correspond pas à  $n.\Delta f$ . Dans le domaine temporel, 2 types de filtres ont été utilisés : passe-haut et passe-bande. L'utilisation d'un filtre passe-haut après lissage donne des résultats meilleurs qu'avec le filtre passe-bande. En outre, les résultats obtenus sont considérés comme satisfaisants même avec une puissance rayonnée de -17 dBm.

De plus, les mesures ont été effectuées sur une personne respirant normalement et assise à 1 m du système, en considérant différentes positions : avant, arrière, gauche, et droite. Différentes fréquences opérationnelles ont été utilisées (2.4, 5.8 et 10 GHz) à une puissance rayonnée de 0 dBm. La transformation en ondelettes a été appliquée. Entre toutes les familles d'ondelettes, Bior2.4 montre la plus haute performance pour extraire le taux des battements cardiaques. De plus, les résultats sont comparés avec ceux obtenus en

utilisant un filtre de type Butterworth. La transformation des ondelettes montre des résultats plus précis qu'avec le filtrage. Comme conclusion, le système et les techniques de traitement proposés montrent la possibilité de mesurer l'activité cardiaque dans les quatre positions et sans retenir la respiration.

Par ailleurs, des mesures ont été effectuées sur une personne assise derrière un mur en béton d'épaisseur de 10 cm à deux fréquences différentes: 5.8 et 10 GHz et à une puissance émise de 0 dBm. La distance séparant les antennes du système et la personne est de 1.1m. Les résultats montrent que l'erreur relative entre le rythme cardiaque obtenu par ECG et celle extraite à partir du système radar Doppler augmente et passe de 9 à 13-14% lorsque le mur existe.

Des modèles ont été développés pour une personne se déplaçant vers le système; pour une fréquence opérationnelle de 20 GHz et avec une puissance rayonnée de 3 dBm. La technique des ondelettes a permis d'extraire la fréquence cardiaque, même en présence de mouvements du corps avec une erreur de 4%.

D'autre part, des mesures en utilisant une seule antenne a été réalisée pour les comparer à celles obtenues à partir d'un système à deux antennes. Différentes puissances sont émises : -2, -7, -12 et -17 dBm. Bien que les signaux du système à une seule antenne soient plus bruités que les signaux du système à deux antennes, le premier reste capable de mesurer la fréquence cardiaque d'une personne qui retient son souffle, avec un maximum d'erreur de 8% ce qui comparable à celle avec deux antennes. En outre, les ondelettes sont capables d'extraire la fréquence cardiaque avec succès pour une personne respirant normalement en cas d'utilisation d'une seule antenne.

Comme perspectives, des mesures pour une personne qui exerce un mouvement aléatoire peuvent être réalisées pour des positions multiples et avec différentes fréquences et puissances avec toujours la présence d'un système de référence crédible tel que l'ECG. Puis, le traitement du signal le plus approprié pour les différentes possibilités sera élaboré. Ensuite, on pourra envisager l'intégration de l'algorithme correspondant sur un DSPIC avec une extraction de l'information souhaitée en temps réel.

## General introduction

Nowadays, contact-less monitoring patient's heartbeat using Doppler radar has attracted considerable interest of researchers, especially when the traditional electrocardiogram (ECG) measurements with fixed electrodes is not practical in some cases like infants at risk or sudden infant syndrome or burn victims [1]. Due to the microwave sensitivity toward tiny movements, radar has been employed as a noninvasive monitoring system of human cardiopulmonary activity [1].

According to Doppler Effect, a constant frequency signal reflected off an object having a varying displacement will result in a reflected signal, but with a time varying phase [84]. In our case, the object is the patient's chest; the reflected signal of the person's chest contains information about the heartbeat and respiration [5].

Using a vector network analyzer, the time varying phase of  $S_{21}$  is computed. The phase variation of  $S_{21}$  contains information about cardiopulmonary activity. Processing techniques are used to extract the heartbeat signal from the  $S_{21}$  phase variation.

The rest of this thesis is organized as follows: Chapter 1 presents background information about chest-wall displacement due to respiration and heartbeat motions. In addition, an overview of radar types and their fundamental equations are described. Finally, utility of radar in cardiopulmonary monitoring is presented.

Chapter 2 makes a comparison between several radiated powers: 3, -2, -7, -12 and -17 dBm in order to find the minimum power that is able to extract the heartbeat signal for a person set at a distance of 1 m far from the VNA system. The operating frequency chosen is 20 GHz because it is a good compromise between the hardware complexity and the precision. Then, several processing techniques are applied in order to extract the heartbeat rate either in frequency domain or in time domain using classical filters. The measurements are done for 2 cases: For a person holding his breath and for a person breathing normally. Holding the breath is applied to show the ability of extracting heartbeat rate for a non-breathing person at 20 GHz, while breathing normally assists in demonstrating the possibility of extracting heartbeat rate from the cardio-respiratory signal after using processing techniques. Measurements are performed simultaneously with a PC-based electrocardiograph to validate the heartbeat rate measurement.

Chapter 3 presents a study performed at different sides of a healthy subject: face, back, left and right sides, of a breathing person sitting at 1-meter distance from the system. The radiated power is fixed at 0 dBm in order to limit the possible impact on the health of the patient and the medical staff. Measurements are performed at different operating frequencies (2.4, 5.8 and 10 GHz) in order to make a comparison between them. Simultaneously with the microwave system, PC-based electrocardiograph is used in order to validate the accuracy of the heartbeat rate measurement. Processing techniques based on wavelet transforms or classical filtering are applied in order to extract the heartbeat from the cardiopulmonary signal. These two techniques are applied and the obtained results are compared.

Chapter 4 presents measurements performed with several scenarios: First scenario is for a fixed person sitting behind a wall using CW Doppler radar at 2 different frequencies: 5.8 GHz and 10 GHz. The wall is situated in the middle between the system and the person, the person is set at a distance of 1.1 m far from antenna system. The measurements are carried out every 30 seconds simultaneously with a PC based electrocardiograph (ECG) which is used as a reference signal to validate the information extracted from the measured signals. In addition, a comparison between single and two-antenna microwave system for a non-breathing person is performed to test the accuracy of the single-antenna system relatively to the two-antenna microwave system. After that, heartbeat rate is extracted from single-antenna microwave system for a breathing person using wavelet techniques. This system operates at an operating frequency of 20 GHz and for different powers, for a person sitting at 1-meter distance far from the system. Measurements are carried out every 23 seconds simultaneously with a PC based electrocardiogram (ECG). In addition, advanced scenarios are considered to test the ability of detecting heartbeat of a moving patient inside his home. The person is walking towards the radar with the operating frequency of 20 GHz and a radiated power of 3 dBm. This scenario is based on models. Wavelet-based techniques are applied to the measurement data for heartbeat detection.

## **Context**

The collaboration between the Lebanese university and the INSA of Rennes started with funding from LAsER (Lebanese Association for Scientific Research). In addition, another scholarship was acquired from Rennes Metropole as (mobilité entrante) for the year of 2014 and 2015. Noteworthy to mention that the INSA Rennes has cooperated in funding the months March and April of the year 2017.



<b>Chapter 1 Contactless cardiopulmonary monitoring ..</b>	<b>49</b>
<b>1.1. Introduction.....</b>	<b>49</b>
<b>1.2. Previous work.....</b>	<b>49</b>
<b>1.3. Chest motion.....</b>	<b>50</b>
1.3.1. Chest motion due to heartbeat.....	51
1.3.2. Chest motion due to respiration .....	54
<b>1.4. Doppler radar.....</b>	<b>55</b>
1.4.1. Doppler effect .....	55
1.4.2. Bistatic and monostatic radar architectures .....	57
1.4.3. Radar families .....	57
<b>1.5. Radar application for heartbeat detection.....</b>	<b>60</b>
1.5.1. Comparison of radar types for vital detection.....	61
1.5.2. Vital sign detection using CW.....	62
1.5.3. Operating frequency.....	68
1.5.4. Power considerations.....	68
<b>1.6. Conclusion .....</b>	<b>69</b>

# **Chapter 1 Contactless cardiopulmonary monitoring**

## **1.1. Introduction**

Nowadays, contactless monitoring of vital signs is needed in medical surveillance applications and in healthcare, especially for burn patients where the use of the traditional electrodes to measure vital signals like cardiopulmonary signals is not possible. Due to the microwave sensitivity toward tiny movements, radar has been employed as a noninvasive monitoring system of human cardiopulmonary activity [1]. Furthermore, signals transmitted by microwave sensors can penetrate walls and obstacles which make it helpful in life detection under rubble when earthquake occurs [2].

In this chapter, previous works are stated, after that, background information about chest-wall displacement due to respiration and heartbeat motions are presented. Then, general overview about radar types is presented. Finally, utility of radar in cardiopulmonary monitoring is described.

## **1.2. Previous work**

Research of methods for vital signs detection using microwave technologies grows rapidly in the recent years. The first demonstration of non-contact vital signs detection was reported at 1975 by J. C. Lin [3]. A 10 GHz system was used for measuring the respiration of a rabbit located at 30 cm away from the system antennas [4]. The work was done with heavy, bulky and expensive components [5]. The system was able to measure the respiration rate, but it was not sensitive enough to measure the heartbeat information. Human heartbeats were detected with the same system by replacing a vector voltmeter by a ratio meter [6]. A simultaneous detection of respiration and heartbeat system was performed by K. M. Chen in 1986 [7]. This system with operating frequency of 10 GHz was using a clutter cancellation to remove the reflection from other targets. It measured vital signs at 30 m away [7]. In 1990, systems operating at 2 and 10 GHz with radiated power varying between 10 and 20 mW were tested in detecting life signs for victims in clutter [8]. In addition, FMCW has been patented for vital sign detection [9]. In 1997, heartbeat and respiration signals were detected at a distance of 10 m using 24 GHz frequency system with 30 mW output power and 40 dB antenna gains [10]. In 2000,

systems operating at 450 MHz and 1150 MHz, with a radiated power around 300 mW, were used to detect life signs for victim under rubble [11]. In addition, the detection of vital signs using UWB systems was patented in 1996 by McEwan at the Lawrence Livermore National Laboratory. This radar was able to measure the breath and heartbeat signals at a distance of 0.3 m away from a subject thorax [11]. In 2001, a 1.2 GHz, 70 mW quadrature super heterodyne system was used to detect breathing for a subject under 1.5 m rubble [12]. Small vital sign radar transceiver operating at 2 GHz was reported in 2001. It is capable to measure both heartbeat and respiration rates of a human at a distance of 1 m. Direct-conversion Doppler radars have been integrated in 0.25  $\mu\text{m}$  CMOS and BiCMOS technologies [13]. The clutters are removed by using pass band filtering. After 2000, the progress in detecting vital signs is faster than before, due to the advances in semi-conductor and wireless technologies; hence many architectures and algorithms were proposed [4]. Most of the systems used CW signals. In 2005, researches were done to increase the signal-to-noise ratio by increasing the frequency. These experimentations were realized at frequencies above 26 GHz while the previous works used an operating frequency at 10 GHz and below [14]. The radar power is reduced to 16  $\mu\text{W}$  at 2 m away, unlike the previous researches that use for the transmitted signal a power ranged from 1 mW to 10 mW [14]. In 2006, measurements were reported for the detection of multiple heartbeats signals [15]. These measurements are operated at 2.4 GHz and 1 mW power. In 2007, a new study showed the possibility of detecting the presence of a person through a wall using UWB radar [16]. In 2008, a vector network analyzer system was reported, this system tuning both frequency and power to determine the optimum frequency and the minimum power able to extract heartbeat signal. The measurements were done for a non-breathing person at frequencies of 2.4, 5.8, 10 and 60 GHz and with radiated powers varying from -2 to -27 dBm. In 2012, researches demonstrated a chip of 60 GHz vital sign radar [17].

### **1.3. Chest motion**

When using microwave Doppler radar for cardiopulmonary activity detection, microwave is transmitted to hit the person's chest and the reflected wave is detected. The received signal contains information about the chest displacement due to the

activity of respiration and heartbeat. Based on this displacement, the heartbeat and respiration rates can be extracted. This section describes the mechanism of the chest motion due to heartbeat and respiration.

### 1.3.1. Chest motion due to heartbeat

When the heart beats, it pumps blood around body to carry oxygen and nourishment to whole body tissues and lungs. The cardiac cycle contains five events, as shown in Figure 1.1 [18]:

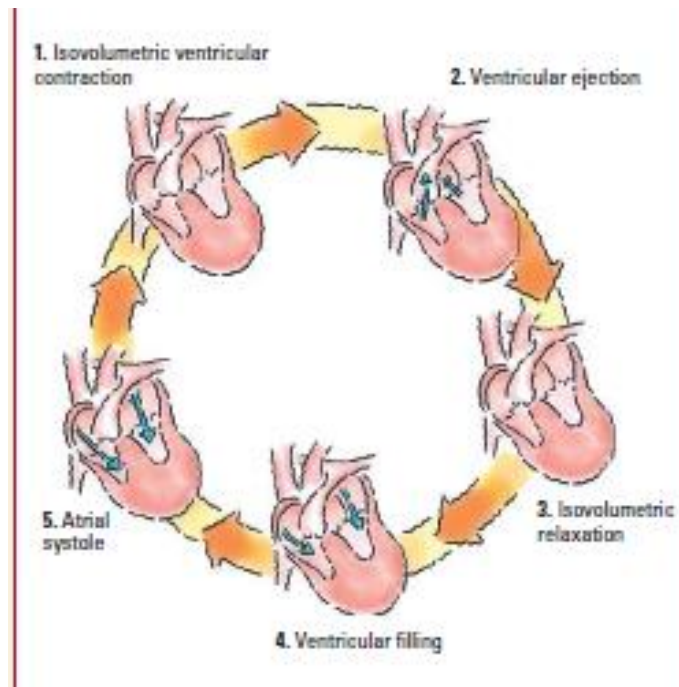


Figure 1.1. Five events of the cardiac cycle [18]

- The first event is the isovolumetric ventricular contraction. At this phase, the pulmonic and aortic valves are closed. The tension in ventricles increases, which lets the pressure rise. The rise in pressure within the ventricles leads to closure of the mitral and tricuspid valves.
- The second event is the ventricular ejection. At this phase, the aortic and pulmonic valves open and the ventricles eject blood when ventricular pressure exceeds aortic and pulmonary arterial pressure [18].

- The third event is the isovolumetric relaxation. In this phase, the aortic and pulmonic valves close because the ventricular pressure falls below the pressure in the aorta and pulmonary artery. Atrial diastole occurs as blood fills the atria [18].
- The fourth event is the ventricular filling. At this phase, atrial pressure exceeds ventricular pressure and the valves open. The blood flows passively into the ventricles. About 70% of ventricular filling takes place during this phase [18].
- The fifth and final event is when the atrial systole supplies the ventricles with the remaining 30% of the blood for each heartbeat. [18]

The contraction and the relaxation of the heart cause chest motion. Note that the left ventricle causes a larger chest motion since it carries out blood to all body parts. During the isovolumetric contraction, the lower front part of the ventricle hits the wall chest due to the partial rotation of the heart in a counterclockwise direction [19]. Furthermore, left ventricle shortens and shapes more spherical while contracting; hence its diameter increases to finally add a displacement in the surface of the chest-wall [20]. The peak outward motion of the left ventricle is happened just after the aortic valve opening. Then the left ventricular apex moves inward [19]. Some studies found an outward movement at the apex when the pre ejection beat [21]. The lowest point occurs on the chest-wall when the adjacent chest retracts during ventricular ejection [22]. It is above anatomical apex [23]. Several techniques are used for measuring the chest-wall displacement like the impulse cardiogram [23], single point laser displacement system [24], capacitance transducer [25], phonocardiograph microphone [26], magnetic displacement sensor [27] and laser speckle interferometry [28]. The skin motion values due to heartbeat changes because of several factors like age, fatness, body shape, etc. [29]. Note that when variation of arteries diameter decreases, the amplitude of the chest motion will decrease, hence the signal-to-noise ratio will also decrease. The peak-to-peak chest motion due to heartbeat is between 0.2 and 0.5 mm [30].

#### **1.3.1.1. ECG event of the heart**

Electrocardiography (ECG) is a trans-thoracic interpretation of the electrical activity of the heart over time captured by skin electrodes and externally recorded. The output of an

ECG is shown in Figure 1.2 [23] while Figure 1.3 presents the heart anatomy. The main peaks are labeled as P, QRS, and T:

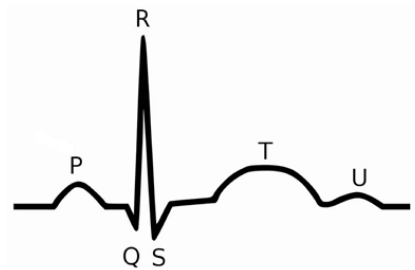


Figure 1.2. ECG output

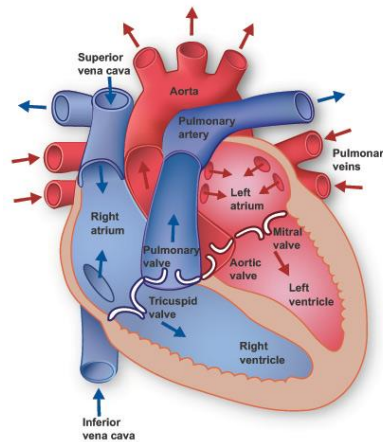


Figure 1.3. Heart anatomy (<http://www.texasheart.org>)

- P wave represents the depolarization of the atria. This wave precedes the QRS complex. A normal P wave has an amplitude between 2 and 3 mm and a duration between 0.06 to 0.12 second [18]
- P-R interval presents the delay between the beginning of activity in the atria and the ventricles. It is located from the beginning of the P wave to the beginning of the QRS complex, its duration is between 0.12 to 0.20 second [18].
- The QRS complex follows the P wave and represents depolarization of the right and left ventricles, hence it records the movement of electrical impulses through the lower heart chambers [31]. The ventricles have larger muscles than the atria, so that's why QRS complex has much larger amplitude compared to the P-wave. A normal QRS has duration between 0.06 to 0.10 second [18]. The duration is

- measured from the beginning of the Q wave to the end of the S wave or from the beginning of the R wave if the Q wave is absent [18].
- The ST segment represents the end depolarization of the ventricles and the beginning of ventricular repolarization. A normal ST is extended from the S wave to the beginning of the T wave [18].
  - T wave represents the repolarization of the ventricles. It is the period when the lower heart chambers are relaxing electrically and preparing to the next muscle contraction [31]
  - The QT measures ventricular depolarization and repolarization. It varies according to the heartbeat rate. A normal QT interval has duration between 0.36 and 0.44 seconds, it varies according to age, sex... It extends from the beginning of the QRS to the end of the T wave [31].
  - U wave is hypothesized to be caused by the repolarization of the interventricular septum. It has low amplitude, and it may be absent [31].

### **1.3.2. Chest motion due to respiration**

The respiratory system is involved in the intake and exchange of oxygen and carbon dioxide between an organism and the environment [32]. Breathing is a quasi-periodic activity in which each cycle has two parts: inhalation and exhalation. Note that exhalation takes double inhalation time [30].

Muscles contract to generate changes in the thorax volume during the gas exchange in the lungs. This contraction creates differences in air pressure between the thorax and the external environment. Hence, pushing the air to move from and to the lungs, from high pressure areas to low pressure areas, causes motions in the thorax, rib cage and abdomen. These motions cause significant displacements at the skin surface. The skin surface can be measured with Doppler radar. There is also a relation between the abdomen and the tidal volume [33]. Tidal volume is the total amount of air transferred during one period. Tidal volume is approximately 500 ml. The displacement of the abdomen is about 4 mm for 400 ml inspiration and 11 mm for 1100 ml inspiration. For a spontaneous breathing, an abdominal displacement is observed and it is about 12 mm. Comparing the motion in

all directions of the chest, the largest motion corresponds to the sternum and the navel. Sternum moves 4.3 mm in inspiration and the navel moves 4.03 mm in inspiration [34].

## **1.4. Doppler radar**

The radar (radio detection and ranging) designates a radio technology for the determination of velocity and distances to remote stationary or moving objects [35]. Doppler radar is widely used in many applications, including vehicle speed measurement and storm tracking. In addition, it can be used for tiny movement detection including breathing and heartbeat.

A radar system is based on a transmitter, an emitting antenna, a receiving antenna, and a processor to determine the target movement [36]. Radar transmits electromagnetic wave and observes the returned echo in order to detect the presence of objects [37]. Only a small portion of the transmitted energy is re-radiated back to the radar, which is then amplified, down-converted and processed [38].

### **1.4.1. Doppler effect**

The Doppler effect is the appearance of shift frequency resulted by a relative motion between the source of a radar signal and the observer of the signal [35]. The observer is the receiver that treats the received signal. In this case, the observer receives a wave with the following frequency:

$$f = \frac{c + v_r}{c - v_s} f_0 \quad (1.1)$$

where  $f_0$  is the operating frequency,  $c$  is the velocity of the wave in the medium,  $v_r$  and  $v_s$  are the velocity of the receiver and the radar source relative to the medium, respectively. The signs of  $v_r$  and  $v_s$  may be positive or negative. When  $v_s$  is positive, the source is moving toward the observer, otherwise it is moving away the observer. In addition, when  $v_r$  is positive, the observer is moving toward the source, otherwise it is moving away the source of radar. When the source is stationary, the relation between the observed frequency and the operating frequency is reduced to [35]:



$$f = \frac{c + v_r}{c} f_0 = \left(1 + \frac{v_r}{c}\right) f_0 \quad (1.2)$$

The Doppler shift is  $f_d = f - f_0$ , hence the relation between the operating frequency and Doppler frequency from the observer is the following:

$$f_d = \frac{v_r}{c} f_0 \quad (1.3)$$

If the source of the radar is considered as an observer, the Doppler frequency observed by the radar due to a target moving at relative velocity is twice that from the same target emitting a wave:

$$f_d = \frac{2v_r}{c} f_0 \quad (1.4)$$

The relative velocity  $v_r$  between a radar transmitter and a moving target has the following relation:

$$v_r = v_a \cos\theta \quad (1.5)$$

where  $v_a$  is the actual velocity of a target and  $\theta$  is the angle between the target trajectory and the line-of-sight. When  $|\theta| < 90^\circ$ ,  $v_r$  is positive hence the Doppler shift  $f_d$  is positive and corresponds to an approaching target. For an angle  $|\theta| > 90^\circ$ , the Doppler shift  $f_d$  is negative, hence the target moves away. When  $|\theta| = 90^\circ$ , the Doppler shift is zero. Thus, the velocity component perpendicular to the line-of-sight cannot be determined. Figure 1.4 presents the Doppler effect of a car approaching having a velocity  $v_a$  [35].

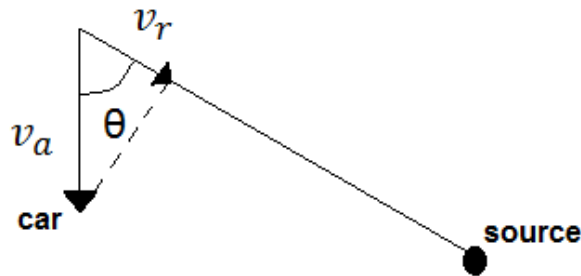


Figure 1.4. Doppler effect

### 1.4.2. Bistatic and monostatic radar architectures

Because antenna is one of the main components of the radar system, an overview about bistatic and monostatic radar architecture is described in this section. Bistatic radar contains separated antennas [39]. The first antenna is dedicated for the transmitted signal (Tx) and the second for the received signal (Rx). Figure 1.5.a shows bistatic radar architecture. In monostatic radar architecture, a single antenna performs both the transmission and reception of the radar signal. Signals generated in the transmitter are passed directly to the same antenna. The receiving signal is routed to the receiver part. The transmitted and received signals are separated through a circulator. Normally, the signal separation is usually realized using expensive circulator components [38]. In [40], a solution concerning the expensive component is founded by using a hybrid ring coupler. Note that an ideal circulator provides infinite isolation between the transmit and receive paths. Figure 1.5.b shows the monostatic radar diagram.

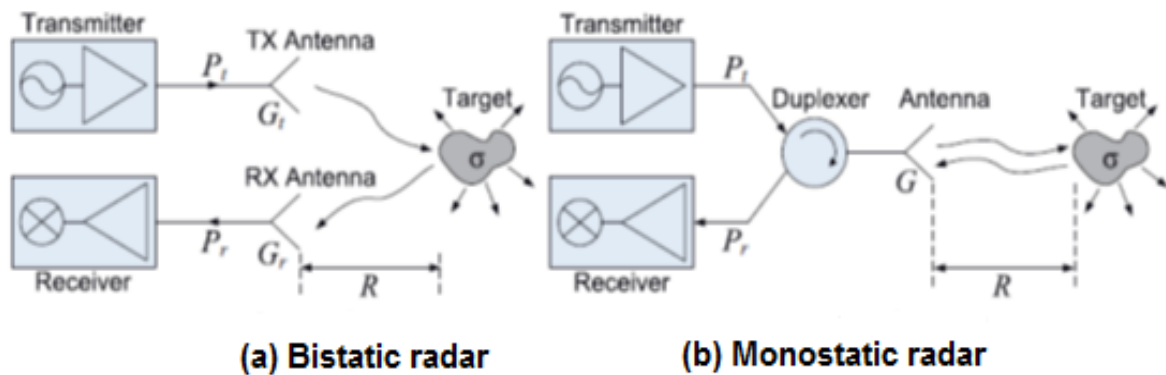


Figure 1.5. Monostatic and bistatic radar [38]

### 1.4.3. Radar families

According to the literature, radars can be generally classified into several categories: Continuous-Wave (CW) radar, Frequency-Modulated Continuous-Wave (FMCW) radar, and finally impulse or Ultra-Wide Band (UWB) radar. Figure 1.6 presents these radar types.

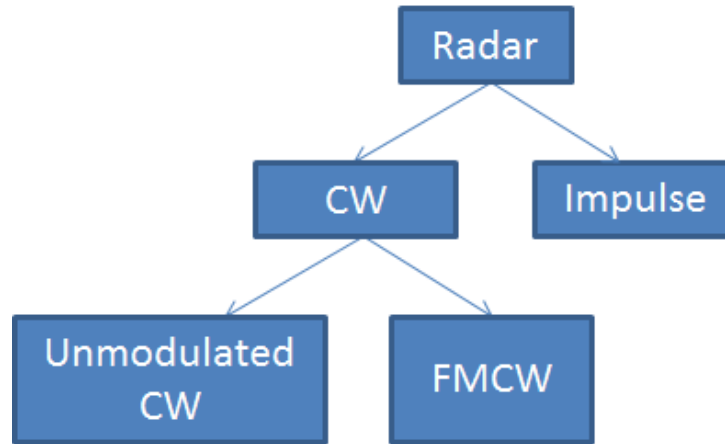


Figure 1.6. Radar types

#### 1.4.3.1. CW Doppler radar

Continuous Wave (CW) radars utilize CW waveforms, which are pure sine waves. When observing the spectra of the radar signal, the center will be shifted due to the echoes of the moving target. The shifted frequency is the Doppler frequency. CW radar can extract target radial velocity accurately. Because of the continuous nature of CW emission, range measurement is not possible since the strength of the received signal is dependent on many factors. Hence simple CW Doppler radar only allows the determination of target velocity, but not the distance to target. In order to have additional information about the range, frequency-modulated continuous-wave (FMCW) systems have been developed to resolve this drawback.

#### 1.4.3.2. FMCW radar

This type of radar transmits frequency modulated continuous wave. The advantage of FMCW is its ability to detect the range between the source and the target [41]. The transmitted signal has several modulation types, such as linear frequency modulation (LFM), frequency shift-keying (FSK), and frequency-stepped continuous-wave (FSCW) modulation. The most used FMCW modulation technique is the Linear Frequency Modulation (LFM) [42]. Figure 1.7 presents the emitted and received frequencies of the LFM. As seen, the frequency of the received signal is shifted by the Doppler shift  $f_d$ . From  $f_d$ , distance and the target velocity are extracted.

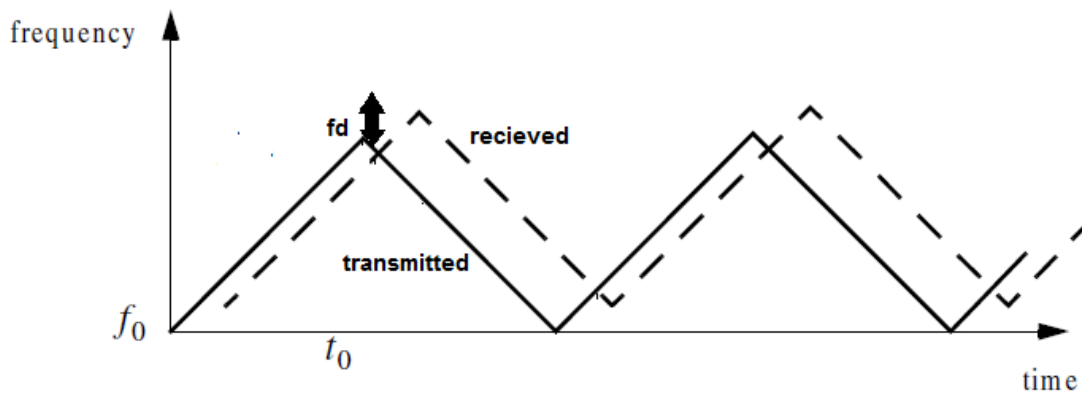


Figure 1.7. Emitted and received frequencies of LFM

### 1.4.3.3. Impulse or UWB radar

Impulse or Ultra-Wide Band (UWB) radar is a wireless technology that uses a large bandwidth (3.1 to 10.6 GHz) [43]. An UWB radar transmits large amounts of narrow digital pulses having duration of sub nanoseconds, then receives them [44]. Hence, it is the extremely short duration pulses instead of continuous waves which are used to transmit signals. Figure 1.8 presents the power spectral density (W/Hz) of UWB radar; the power of the signal is calculated by integrating the PSD.

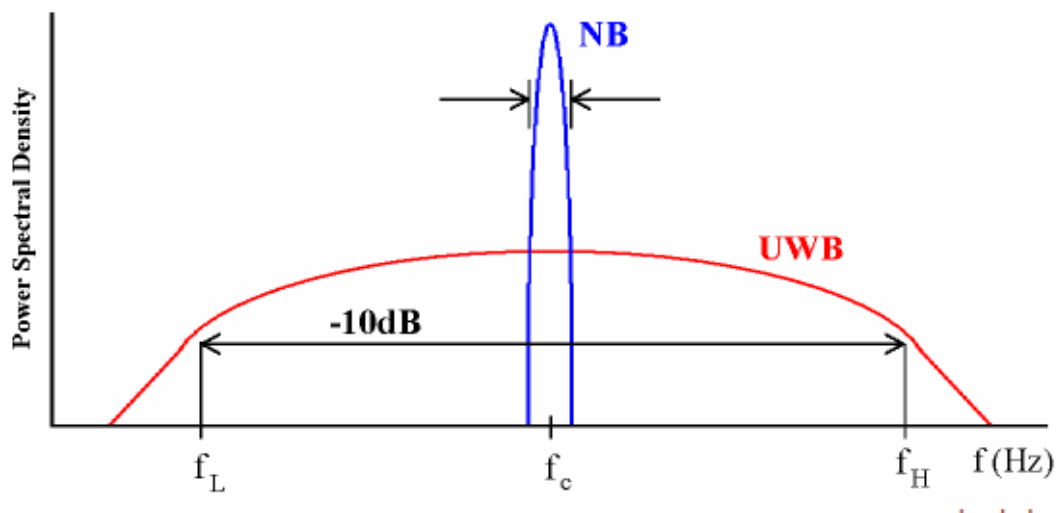


Figure 1.8. PSD of UWB radar [43]

Fractional bandwidth is defined as the ratio of the bandwidth occupied by the signal to the center frequency of the signal:

$$BW = \frac{2(f_h - f_l)}{(f_h + f_l)} \quad (1.6)$$

where  $f_l$  and  $f_h$  are the lower and upper frequency components in the signal measured at the -10 dB level, respectively. The FCC defined UWB systems as any system with fractional bandwidth exceeding 20%, or any system with a -10 dB bandwidth exceeding 500 MHz. The maximum PSD is limited to -42.25 dBm/MHz. Figure 1.9 presents the time evolution of a transmitted UWB signal.

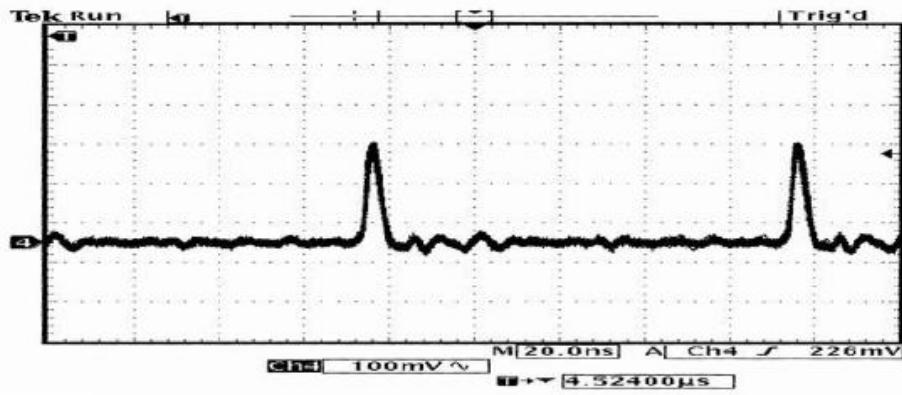


Figure 1.9. Time evolution of a transmitted UWB signal [43]

## 1.5. Radar application for heartbeat detection

Contactless monitoring of vital signs is needed in medical surveillance applications and in healthcare [45], especially for burn patients where the use of the traditional electrodes to measure vital signals like cardiopulmonary signals is not possible. Due to their sensitivity toward tiny movements, microwave radars have been employed as noninvasive monitoring systems of human cardiopulmonary activity [46]. Several works studied the vital sign detection through radar and use several types of radar like CW [47], FMCW [48] and impulse radar [49]. In this section, a comparison of different types of radar used for vital sign detection is proposed. Then, the theory, architectures, and signal processing techniques using CW signals for the vital signs detection are presented. After that, importance of operation frequency and power considerations are mentioned.

### **1.5.1. Comparison of radar types for vital detection**

Several radar types are used for vital signs detection like ultra-wideband (UWB) radars, frequency modulated continuous wave (FMCW) radars, and continuous wave (CW) Doppler radars. Each of these radar technologies can measure vital signs and has its own advantages and disadvantages.

The UWB radar has the ability to detect breathing rate for one or more persons; it is also capable to detect the distance between patient and system's antennas [50]. Furthermore, it is relatively better in terms of propagation through objects, hence, measurements through the wall can be achieved [43]. However, this is not feasible in terms of system integration and low-power operation, especially for short range applications. The short time delay requires an extremely high-speed switch, hence a very high speed analog to digital converter (ADC) which is a high power consumer [51], in contrast of CW and FMCW systems that allow higher level of system integration and lower power operation. CW continuous wave radars do not possess range resolution [41] like UWB and FMCW radars. Although FMCW radar allows measuring distance to the detected subject [52], the accuracy of FMCW systems is a critical issue. It requires a 1.5 GHz bandwidth to achieve 10 cm resolution; hence these systems cannot meet the requirement of vital sign monitoring or small gesture classification. Recently, a technique based on coherent phase detection of the FMCW signal has partially solved this problem [53]. However, the CW radar is superior to FMCW due to its higher measurement accuracy, less complex hardware architecture, and simpler signal processing techniques [54]. Although the range isolation property of FMCW is able to eliminate stationary clutters, it is still ineffective when the stationary clutters are close to target. In case of the cardio respiratory detection, the body acts like a large clutter, for example the shoulder, the arm [53]. CW radar has a good immunity to stationary clutters [53]. Therefore, for applications that only require displacement information regardless of the target range, CW radar is a better option for non-contact vital sign detection [55], sleep monitoring [56], mechanical vibration sensing [57], and health monitoring [58]. On the other hand, FMCW radar could be a better option for applications that need distance information because it relatively combines the ranging capabilities of UWB technology with sensitivity and robustness of Doppler

technology [59], for monitoring the versatile life activities [60, 61] and interactive gesture sensing [62]. Table 1.1 presents a comparison between radar types.

Table 1.1. Comparison between different types of radar

	CW	FMCW	UWB
Distance measurement	-	+	+
Through wall penetration	+	+	++
Low cost	+++	++	+
Low power consumer	+	+	-
Accuracy	+++	++	+
Low hardware complexity	++	+	-
Processing techniques simplicity	+++	++	+

## 1.5.2. Vital sign detection using CW

### 1.5.2.1. General equation of vital sign using CW

Figure 1.10 presents the block diagram of the bistatic CW radar sensor for noncontact vital sign detection. Note that the receiver structure shown in the figure is the direct-conversion homodyne.

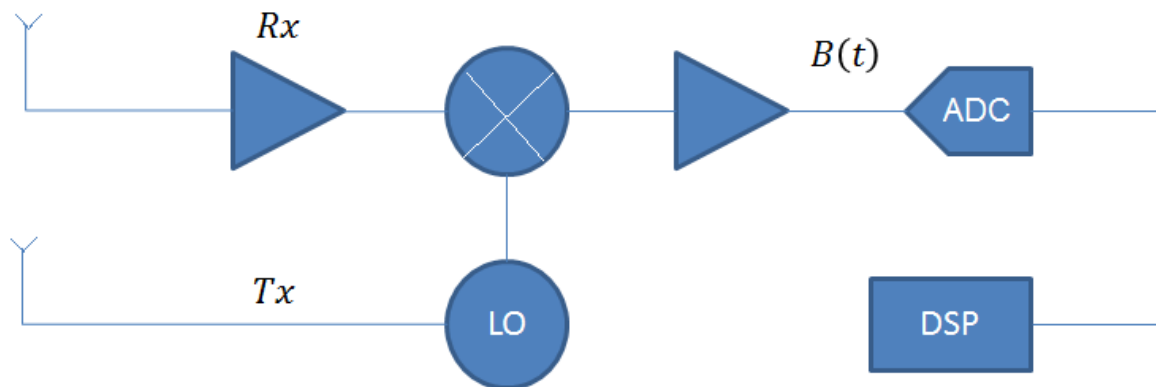


Figure 1.10. CW radar sensor [63]

A Doppler CW radar transmits RF signal to the target. It has the equation (1.7):

$$T(t) = A_T \cos(2\pi f_0 t + \theta(t)) \quad (1.7)$$

where  $f_0$  is the operating frequency,  $A_T$  is the amplitude and  $\theta(t)$  is the phase noise from the waveform generator. The transmitted signal is directed toward a human body and then received. The received signal can be expressed as [64]:

$$R(t) \approx A_R \cos\left(2\pi f_0 t - \frac{4\pi d_0}{\lambda} - \frac{4\pi x(t)}{\lambda} + \theta(t - 2d_0/c)\right) \quad (1.8)$$

where  $A_R$  is the received amplitude,  $d_0$  is the distance between the antennas and the target.  $\lambda$  is the wavelength of the carrier signal, and  $x(t)$  is the chest-wall movement including respiration and heartbeat and  $\theta(t - 2d_0/c)$  is the phase noise of a delay of  $2d_0/c$ .

The transmitter and receiver share the same signal source. Hence, the same Tx signal is used as local oscillator (LO) signal to down-convert  $R(t)$  to baseband signal  $B(t)$ :

$$B(t) = A_T \cos\left(\theta_0 + \frac{4\pi x(t)}{\lambda} + \Delta\theta(t)\right) \quad (1.9)$$

where  $\theta_0 = 4\pi d_0/\lambda + \sigma$  is the summation of phase shift from the nominal distance  $d_0$  and at the reflection surface;  $\sigma$  is measured from the delay introduced from the cables and antennas and  $\Delta\theta(t) = \theta(t) - \theta(t - 2d_0/c)$  is the residual phase noise.

### 1.5.2.2. Radar signal processing

Signal processing is an important stage for measuring vital signs. It includes the baseband signal demodulation, the removal of undesired body motion, and the isolation of the desired signal from multiple clutters. Several demodulation methods can be used like small angle approximation [65] and arc tangent demodulation [66]. Arc tangent demodulates the signal by calculating the Doppler phase shift. The Doppler phase shift can be computed as:

$$\varphi = \arctan \frac{Q(t)}{I(t)} \quad (1.10)$$



where I/Q are the outputs of the quadrature receiver. Figure 1.11 represents the homodyne quadrature receiver architecture.

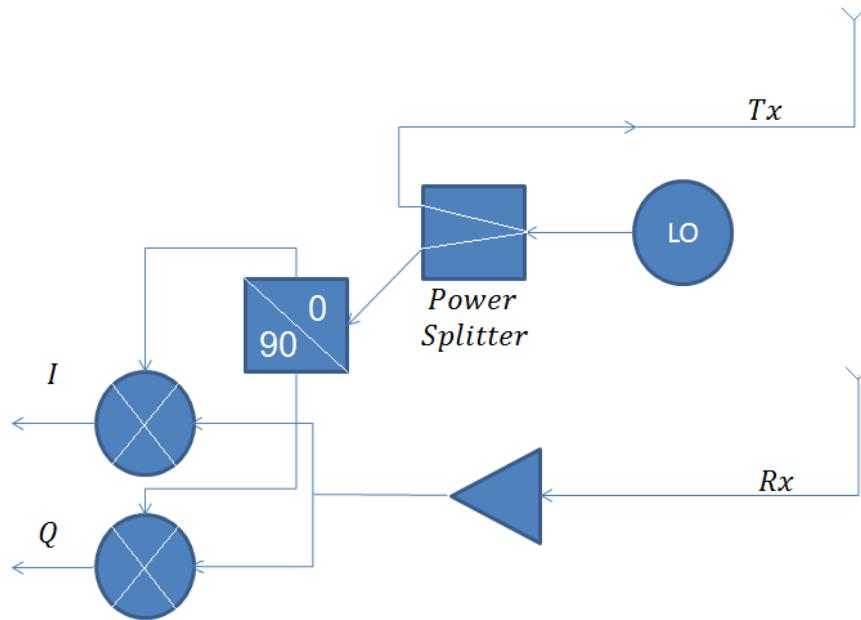


Figure 1.11. Homodyne quadrature receiver architecture [66]

Since  $\varphi$  is proportional to the movement, the movement this latter can be recovered. This is the ideal case. In reality, the system may suffer from the DC offset created by the circuit imperfection and the reflections from stationary objects [66] surrounding the body. Also, when the signal trajectory crosses the boundary of two adjacent quadrants,  $180^\circ$  phase discontinuity occurs in the arctangent function. The problem is solved by reformulating the equation of  $\varphi$  by:

$$F(t) = \arctan \frac{Q(t) - Q_{dc}}{I(t) - I_{dc}} + F = \frac{4\pi x(t)}{\lambda} \quad (1.11)$$

where  $F$  is a multiple of  $180^\circ$  dedicated for the discontinuity elimination caused when  $\varphi$  crosses the boundaries and  $Q_{dc}$  and  $I_{dc}$  are the desired dc offsets. Figure 1.12.a shows the constellation graph I/Q data dc information preserved. Figure 1.12.b presents the bloc diagram of the dc demodulation

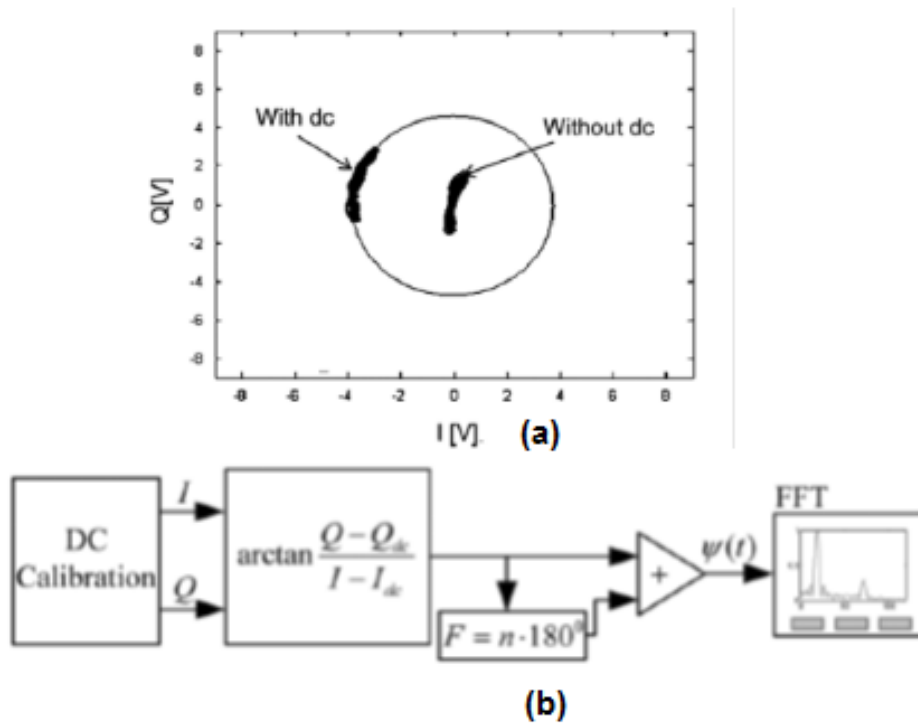


Figure 1.12. (a) Constellation graph I/Q data dc information preserved  
 (b) Bloc diagram of the DC demodulation [66]

Another technique is used for the baseband demodulation which is the small angle technique. Note that small angle is utilized for small displacement and arc tangent demodulation is widely used as a nonlinear demodulation to finally recover the phase information [66]. The small angle technique considers the respiration and heartbeat signals very small compared to the carrier wavelength. Hence the baseband signal  $B(t)$  is approximated as:

$$B(t) = \frac{4\pi x(t)}{\lambda} \quad (1.12)$$

The drawback of this technique is the presence of the null point issue that gives inaccurate measurement results, especially for short wavelengths. It appears when  $\theta_0$  of the equation (1.9) is an even multiple of  $\pi/2$ ; hence the baseband output is not proportional to  $x(t)$ .  $\theta_0$  depends from the target distance. Hence, this issue happens in

every  $\lambda/4$  from the radar. Techniques are reported to remove the null point like Quadrature Doppler radar receiver with  $I/Q$  channels or utilizing the double side band transmission [66]. Figure 1.13 presents the double side band architecture.

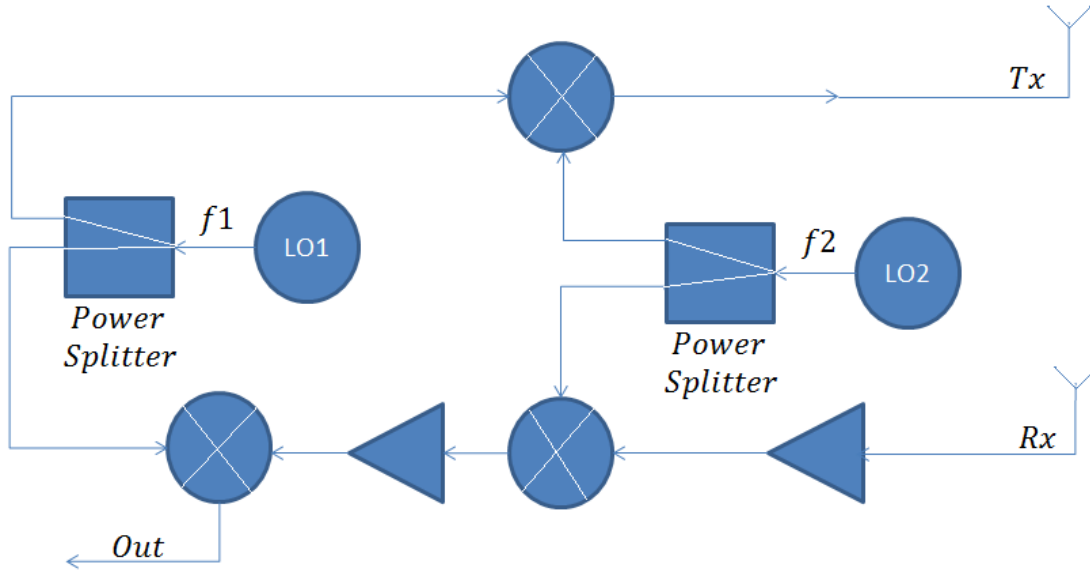


Figure 1.13. Double side band radar architecture for vital sign detection [66]

Double side band architecture mixes LO1 and LO2, and then both upper sideband (USB) and lower sideband (LSB) are transmitted. After receiving the signal from the target, the radar down-converts the reflected signals of both sidebands by mixing them with the same LO1 and LO2. Figure 1.14 presents the frequency tuning using double side band for the null point elimination.

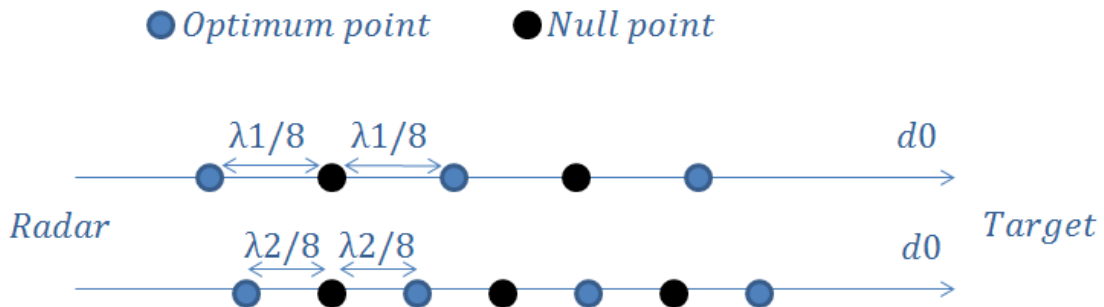


Figure 1.14. Frequency tuning using double side band for the null point elimination [63]

It works such a way that the null points from one sideband and the optimum points from the other sideband can overlap each other. Note that the frequency tuning technique needs hardware tuning to achieve good detection accuracy, which is not very convenient [63].

Concerning the problem of undesired body motion which is considered as a significant source of noise, it is resolved by using multiple transceivers detecting from different sides of the human body [67]. Figure 1.15 presents two radar systems for the body motion elimination.

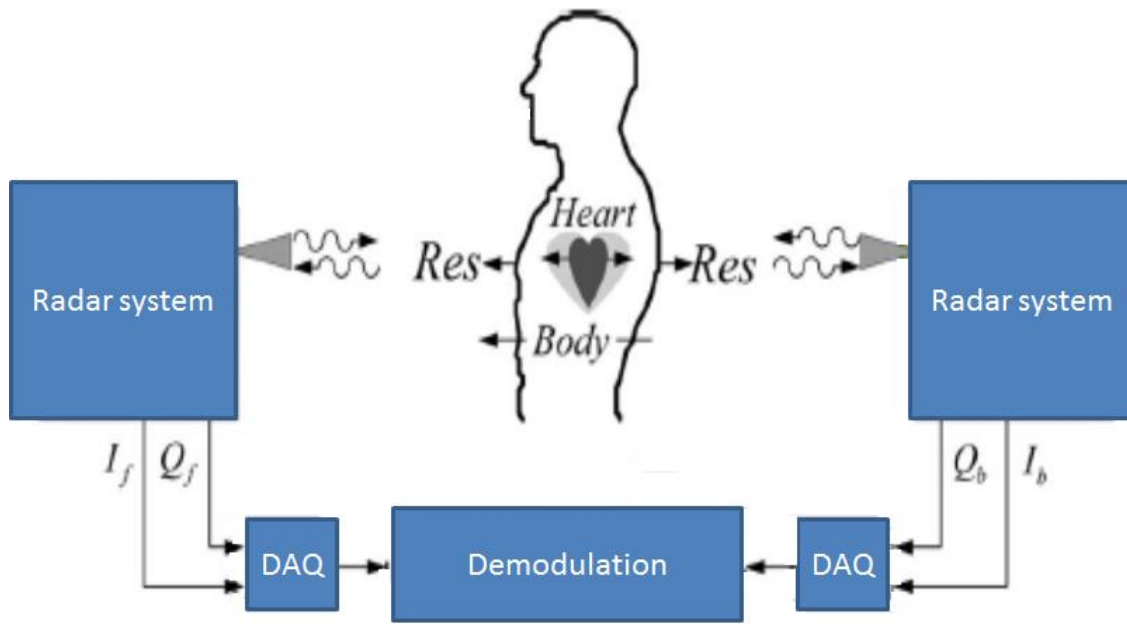


Figure 1.15. Two radar transceivers for the body motion elimination [66]

These two radars are identical and both use patch antennas with linear polarization. The person is set between the two radars. When the body moves toward one of these radars, it moves away from the other. That said, the distance change between the body and one radar is opposite as compared to that between the body and the other radar. Hence, when combining the two received signals, the body motion is canceled. Other solution made for the body movement cancellation by using differential front-end radar operating at 2 frequencies [68]. It uses dual helical antennas with 40 degrees half-power beam width (HPBW). The body movement is eliminated in two adjacent locations to perform a differential measurement. Also some researches use camera to remove body movement from the signal, like in [69, 70]. In addition, different approaches have been reported like multi-frequency interferometric radar [71].

### **1.5.3. Operating frequency**

Besides the signal processing, the choice of the operating frequency is also important in vital sign detection using CW. Operating frequencies ranging from hundreds of megahertz [72] to millimeter-wave frequency [73] have been tested for noncontact vital sign detection when using CW radar. At 2007, a work [74] has demonstrated that there is an optimal operating frequency for physiological movement detection for people. In addition, a direct relation exists between the variation of phase and the operating frequency. The variation of phase proportional to the carrier wavelength, hence higher is the operating frequency better is the detection sensitivity. But the hardware complexity and cost of the system should be taken into consideration; the cost increases when using higher operating frequencies. 2.4 GHz and 5.8 GHz are the most popular frequencies essentially due to the vast availability of low-cost RF/microwave components and integrated circuits (ICs) in the ISM bands. Several studies show that 2.4 GHz and 5.8 GHz Doppler radar are able to detect human vital signs [75]. To optimize the heartbeat detection, higher frequencies are proposed like 24 GHz [76], millimeter-wave 60 GHz/96 GHz [77], and 228 GHz [78].

### **1.5.4. Power considerations**

In general, increasing power leads to increase the SNR, hence the accuracy is increased. But the health of the person may be affected. Hence it is necessary to decrease the transmitted power in order to decrease the radiated energy to which the patient is exposed to during measurements. A parameter is taken into consideration for energy measurements: Specific absorption rate (SAR). SAR is expressed in Watt per kilogram of human body when it is exposed to a radio frequency (RF) electromagnetic field. It measures the dose of radio frequency fields having frequencies between 1 MHz and 10 GHz. In general, an SAR of at least 4 W/kg is needed to produce adverse health effects in people exposed to RF fields in this frequency range [79]. Many commissions limit the radiation exposure for the health of the human body like International Commission on Non-Ionizing Radiation Protection (ICNIRP) and U. S. Federal Communications Commission (FCC). For example, in case of mobile phones, the FCC limit for RF radiation exposure at a SAR of 1.6 W/Kg [80]. ICNIRP recommends that the

localized SAR in the head has to be limited to 2 W/kg averaged over any 10 g mass of tissues in the head [81]. According to ICNIRP, occupational exposure limits in microwave range are 10–50 W/m<sup>2</sup>. Public exposure limits for microwaves set to 2–10 W/m<sup>2</sup> [81]. Note that these ranges depend on frequency. In addition, the aspect of time is taken into consideration especially that sensation of fatigue is linked to exposure over a longer period of time. In case of using cellular, parameters as Specific Absorption per Day (SAD) and Specific Absorption per phone Call (SAC) are suggested. Both are expressed in W/kg [82].

## **1.6. Conclusion**

Detection of heartbeat wirelessly is a recent research subject. It can be used in a lot of applications like detection of life signs for victims under rubble, home monitoring for infants and old people. Doppler radar is proposed as contactless system for vital signs detection. This chapter gives an overview about Doppler radar and related previous works. The previous works lack determining the most appropriate parameters for these applications. These parameters are the operational frequency and the radiated power. In addition, several processing techniques have to be used to extract the heartbeat signal from the cardio-respiratory signal detected from the radar system and a comparative study between several processing techniques should be done. In addition, a reference signal will be used to determine the accuracy of the detected parameters which is the ECG.

<b>Chapter 2 Heartbeat detection of a person using filtering methods at different radiated powers.....</b>	<b>71</b>
<b>2.1. Introduction.....</b>	<b>71</b>
<b>2.2. System description .....</b>	<b>72</b>
<b>2.3. System advantages .....</b>	<b>74</b>
<b>2.4. The measurement setup .....</b>	<b>74</b>
<b>2.5. Characteristics of the measured signal.....</b>	<b>78</b>
<b>2.6. Signal processing techniques .....</b>	<b>79</b>
<b>2.6.1. Review of processing techniques .....</b>	<b>79</b>
<b>2.6.2. Separation of respiration and heartbeat signals.....</b>	<b>84</b>
<b>2.7. Conclusion .....</b>	<b>96</b>

## **Chapter 2 Heartbeat detection of a person using filtering methods at different radiated powers**

### **2.1. Introduction**

This chapter presents a wireless microwave measurement system for cardiopulmonary activity. Using a vector network analyzer, the phase variation of  $S_{21}$  is computed. This contains information about cardiopulmonary activity. In order to have a comparative approach for several radiated powers and to determine the minimum power at which the heartbeat signal can be extracted, several radiated powers have been used: 3, -2, -7, -12, and -17 dBm. Previous works [5] show the possibility of extracting the heartbeat signal at several frequencies and different bands: 2.4 GHz (S-band), 5.8 GHz (C-band), 10 GHz (X-band), and 60 GHz. In this work, the operating frequency is chosen to be 20 GHz. This frequency leads to a better precision than S, C and X bands since increasing the operating frequency gives higher SNR value. However, systems with high frequency are expensive; thus, the 20 GHz frequency is a good compromise between price and precision. Processing techniques are needed in order to determine the characteristics of the measured signal. Previous works extracted heartbeat signal from a non-breathing person [83] and applied processing techniques to simulation models to extract heartbeat and respiratory parameters from cardio-respiratory signal [5]. This chapter presents measurements of a cardiopulmonary activity. Then, several processing techniques are applied to extract heartbeat parameters either in the frequency domain or in the time domain using filtering techniques. The measurements are performed in two conditions: when holding the breath for showing the possibility of measuring heartbeat at 20 GHz, and when breathing normally for showing the possibility of extracting heartbeat signal from the cardio-respiratory signal. The person undergoing the test is sitting at a 1-meter distance away from the antennas. The measurements are performed simultaneously with a PC-based electrocardiogram to validate the heartbeat rate measurement. Then, the accuracy of the results obtained by the processing techniques used in this chapter has been discussed. This chapter is organized as follows: The proposed microwave system is presented in Section 2.2. Section 2.3 presents system advantages. Measurement setup is presented in section 2.4. Section 2.5 presents the characteristics of the measured signal.



Processing techniques background, application and results are described in Section 2.6. Finally, Section 2.6 concludes this part.

## 2.2. System description

The used system is based on a Vector Network Analyzer (VNA) and two horn antennas. These components make the installation easy and simple. Figure 2.1 presents the system used in the experiment.

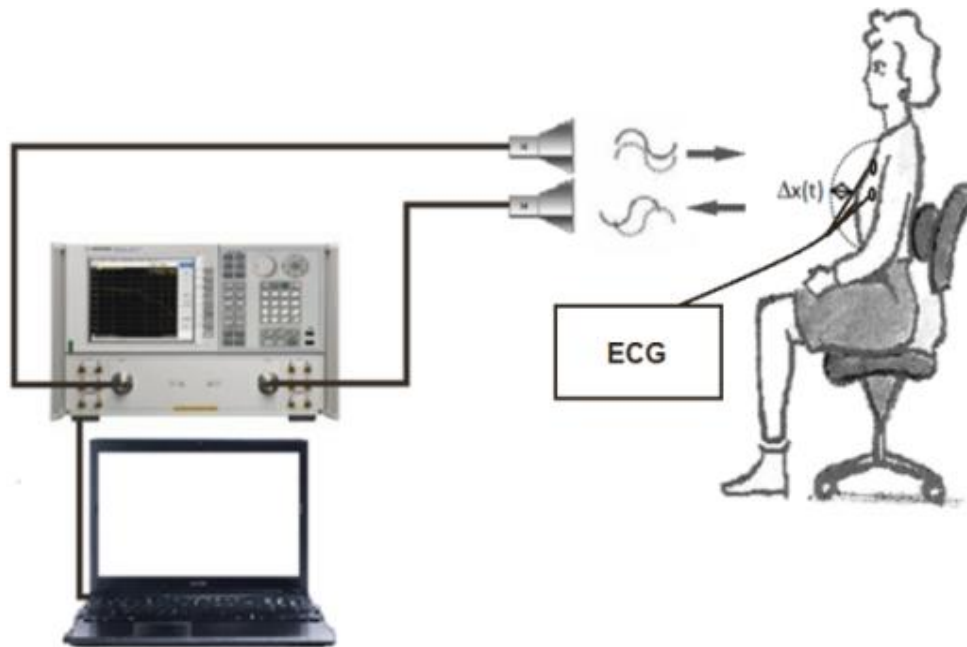


Figure 2.1. The measurement setup

The vector network analyzer used in our work is HP N5230A 4ports PNA-L. The VNA HP N5230A contains the following features and benefits:

- Full 4port  $S$  parameters and balanced measurements up to 20 GHz
- 120 dB dynamic range at 20 GHz
- < 0.006 dB of trace noise at 100 kHz IFBW
- < 4  $\mu$ sec/point measurement speed
- Automatic port extension automatically corrects for in fixture measurements
- Advanced connectivity with LAN, USB, and GPIB interfaces.

Several characteristics make the vector network analyzer attractive in the implementation, it is one of the main basic system used for microwave measurements and

RF applications. The vector network analyzer tunes both frequency and power. Furthermore, VNA allows controlling different parameters like sweep time and the number of sampling points. In addition, it measures the phase and amplitude of  $S$  parameters. The  $S$  parameters are a mathematical construct that quantifies how RF energy propagates through a multi-ports network. In particular, a VNA measures the time variation of the phase of the transmission coefficient  $S_{21}$ . This phase corresponds to the difference between the phase of the received and the transmitted signal.

The other components used in the microwave system are the two antennas; they are 2 identical horn antennas (LB-42-25-C2-SF) for the transmitted and received signals. The frequency range is between 18 and 26.5 GHz. The nominal gain of each antenna is 25 dBi and the nominal beam width at -3 dB is  $10^\circ$ . The dimensions of these antennas are 104\*85\*296 mm approximately with a SMA connector, the weight is 0.55 kg and they are composed of Cu material. Note that the cross polarization isolation at 20 GHz is -30 dB. The antenna gain depends on the frequency. Table 2.1 shows the antenna gain for different operating frequencies.

Table 2.1. Antenna gain

<b>Frequency (GHz)</b>	<b>Gain (dBi)</b>
18	23.6
19	23.9
20	24
21	24.5
22	24.9
23	24.8
24	24.9
25	25.4
26	25.4

The antenna's radiated power depends on the transmitted power of the VNA and the gain of the antenna, and has the following equation:

$$P_r(dBm) = P_t(dBm) + G(dB) \quad (2.1)$$

where  $P_r$  is the radiated power,  $P_t$  the transmitted power, and  $G$  the gain of the antenna.

It is noteworthy to mention that the distance between the Tx and Rx has a constant value because the position of the antennas is static and nothing moves around; this results in a constant phase shift, hence, the variables extracted from the phase variation are not affected.

### **2.3. System advantages**

Because the distance between the antenna's system and the person under test is not taken into consideration in this work, and as CW gives more accurate results than UWB radars and FMCW, CW radar is used. The proposed system has advantages over other systems by its ability of tuning the power and frequency of the transmitted signal. Thus, the minimal transmitted power and the optimal operating frequency can be determined. Determining the minimal power that processing technique is able to extract heartbeat's parameters is important for the safety of the patient and minimizes the risk of high radiation exposure. In addition, determining the optimal operating frequency helps obtaining the most accurate results with reasonable cost for the final system.

### **2.4. The measurement setup**

Several measurements have been performed for the heartbeat measurement. They are made in two conditions: when holding the breath, and when breathing normally. The experiments are performed for a 54 years old person who is sitting in front of the system at a distance of 1 m. The VNA generates a Continuous Wave (CW) 20 GHz signal. The reflected signal that carries chest movement information is received by the Rx antenna and detected by the VNA where the variation of phase of  $S_{21}$  is computed [5]. Different emitted powers have been used: -19, -24, -29, -34 and -39 dBm. At 20 GHz, the gain of the antenna is 24 dB. The cables losses are 2 dB; hence the radiated powers are 3, -2, -7, -12 and -17 dBm, respectively. The measurement duration is 23 seconds to avoid holding

the breath for too long. The number of samples is set by the VNA after choosing the time and the bandwidth. The bandwidth is chosen to be 500 Hz resulting from a compromise between the signal noise reduction and the sweep time. As the sweep time was 23 secs, the number of samples was set as 12801 samples by the VNA; hence the sampling frequency is 557 Hz. To validate the proposed system, ECG measurements were started simultaneously with the system measurements and a comparison was made. Figure 2.2 represents a picture of the experiment and Table 2.2 corresponds to the measurements setup for each of the experiments.

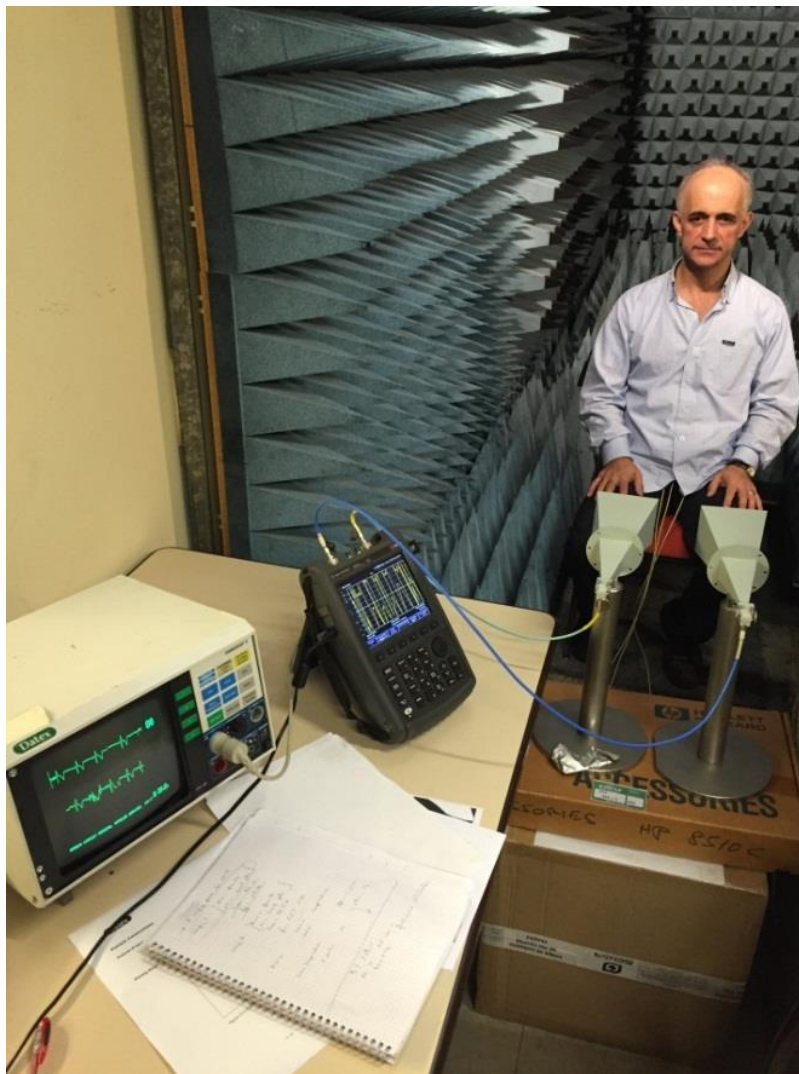


Figure 2.2. Photo of the experiment

Table 2.2. Measurement setup

System Specifications	
<b>Operating frequency (GHz)</b>	20
<b>Radiated power (dBm)</b>	3, -2, -7, -12, -17
<b>Number of points</b>	12801
<b>Time Window (sec)</b>	23
<b>Sampling frequency (Hz)</b>	557
Subject Information	
<b>Gender/ Age (y)</b>	M/ 54
<b>Position/ Side</b>	Setting/ Front
<b>Distance (m)</b>	1
<b>Breathing</b>	Y/ N

Figure 2.3 presents an example of an ECG signal. 28 peaks are obtained in 21.93 sec; hence it corresponds to 74 beat/min.

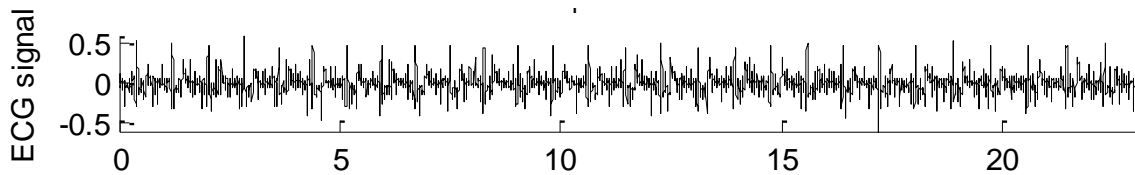


Figure 2.3. Normalized ECG

Figure 2.4 corresponds to the phase variation (PV) of  $S_{21}$  for a person holding the breath, and for different radiated powers (3, -2, -7, -12 and -17 dBm). Figure 2.5 presents the phase variation (PV) of  $S_{21}$  signal for a person who breathes and for the same radiated powers.

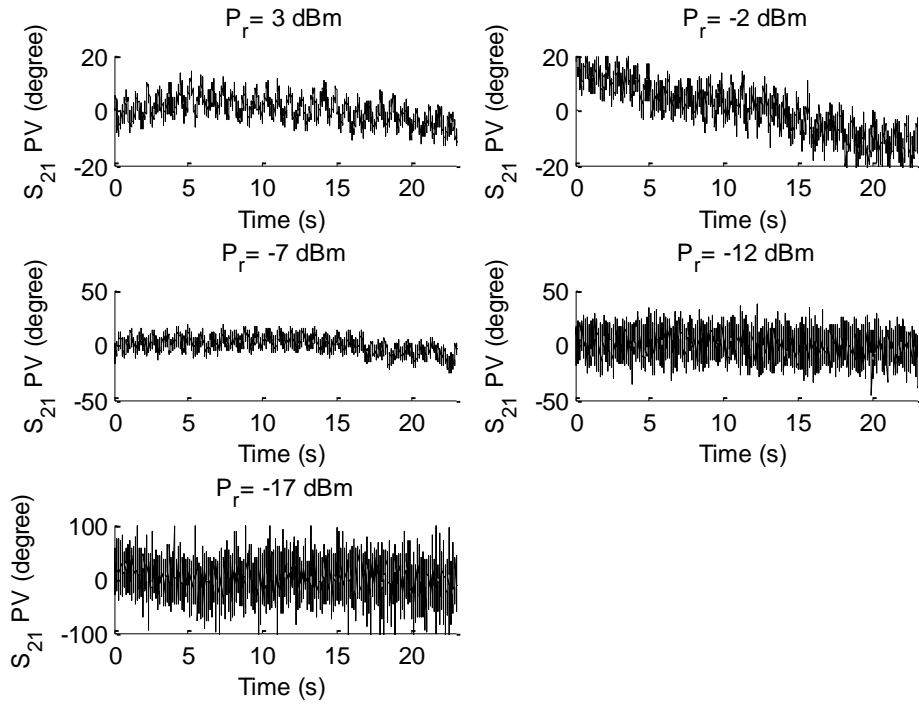


Figure 2.4.  $S_{21}$  phase variation for a non-breathing person at 20 GHz and  $P_r = 3, -2, -7, -12$  and  $-17$  dBm

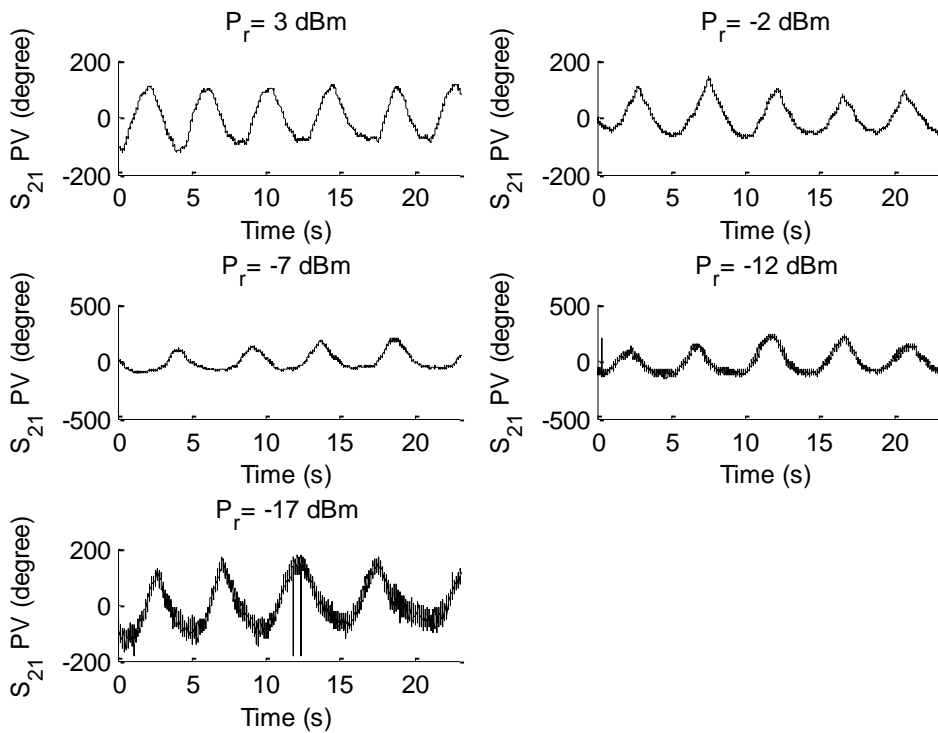


Figure 2.5. Phase variation of  $S_{21}$  for a breathing person at 20 GHz and  $P_r = 3, -2, -7, -12$  and  $-17$  dBm

In Figure 2.4, the *SNR* decreases when the radiated power decreases; hence processing techniques are required to eliminate noise in order to extract information with the lowest possible power. In addition, in Figure 2.5, Phase variation of  $S_{21}$  presents the respiratory signal that hides the heartbeat signal; hence, processing technique is required in order to eliminate the respiratory signal.

## 2.5. Characteristics of the measured signal

According to Doppler effect, the sinusoidal signal reflected off an object with a varying displacement will result in a reflected signal with a time varying phase [83]. The relation between the chest displacement  $\Delta x(t)$  and the phase variation  $\Delta\Theta(t)$  can be expressed by:

$$\Delta\Theta(t) = \frac{4\pi}{\lambda} \Delta x(t) \quad (2.2)$$

where  $\lambda$  is the wavelength of the transmitted signal. The reflected signal contains information about heartbeat and respiration of the patient [5]. The main information extracted from the received signal is the heartbeat rate (*HR*). The *HR* is measured as the number of heartbeats per unit time.

The average peak-to-peak chest motion due to respiration is between 4 and 12 mm, and due to the heartbeat alone is between 0.2 and 0.5 mm [83]. At rest, the respiration frequency of an adult varies between 0.2 and 0.34 Hz [84]. Moreover, the heartbeat frequency of an adult changes within the 1 and 2 Hz interval. Hence, the respiration rate of an adult varies between 12 and 20 Breath per minute (Bpm) [84] and the heartbeat rate varies between 60 and 120 beat per minute (bpm) [83]. Table 2.3 presents the frequencies and rates of respiration and heartbeat.

Table 2.3. Frequencies and rates of respiration and heartbeat

<b>Case</b>	<b>Frequency (Hz)</b>	<b>Rate (breathes or beats/min)</b>
<b>Babies Respiration (newborn to 6 months)</b>	0.5 to 1	30 to 60
<b>Children Respiration (1 to 5 years)</b>	0.34 to 0.5	20 to 30
<b>Adult Respiration</b>	0.2 to 0.34	12 to 20
<b>Adult Heartbeat</b>	1 to 2	60 to 120
<b>Babies Heartbeat</b>	2 to 3	120 to 180

## 2.6. Signal processing techniques

Because the detected signal from the cardiopulmonary activity contains respiratory and heartbeat information, signal processing is required for the separation of these 2 components. This section presents the background of signal processing used for signals. Then, the application of these processing techniques has allowed to extract the heartbeat characteristics.

### 2.6.1. Review of processing techniques

#### 2.6.1.1. Fast Fourier Transform

The Fast Fourier Transform (FFT) is one of the used methods for determining the average heartbeat frequency and the respiratory frequency. It is a faster version for calculating the Discrete Fourier Transform (DFT). DFT takes a discrete signal in the time domain and transforms that signal into its discrete frequency domain representation. Hence, it is able to determine characteristics of the signal in the frequency domain. Given  $n$  real or complex inputs  $x_0, \dots, x_{n-1}$ , the DFT is defined as [85]:

$$y_k = \sum_{0 \leq l < n-1} w_n^{kl} x_l \text{ where } 0 \leq k < n \quad (2.3)$$



with  $w_n = \exp(-2\pi i/n)$  and  $i = \sqrt{-1}$ . Stacking the  $x_l$  and  $y_k$  into vectors  $x = (x_0, \dots, x_{n-1})^T$  and  $y = (y_0, \dots, y_{n-1})^T$  yields the equivalent form of a matrix-vector product:

$$y = DFT_n x, \quad DFT_n = [w_n^{kl}] \quad 0 \leq k, l < n \quad (2.4)$$

Concerning the FFT, it is any method that compute the DFT in about  $\Theta(n \log n)$  time, instead of  $\Theta(n^2)$  time and gives the same result of the DFT; hence it utilizes some clever algorithms to do the same thing as the DFT but in much less time [86]

### 2.6.1.2. Filters

The aim of filters is to reduce the undesired range of frequencies from signals in order to extract the desired signal, which is the meaningful data of this work. There exist two types of filters: analog and digital filters. Analog filters are used in electronic circuits; they are made using electronic components such as resistors, capacitors and operational amplifiers to produce the required filtering effect for an analog signal [87]. Such filters are widely used in a lot of applications such as noise reduction, video signal enhancement, and many other areas. Digital filters perform mathematical operations on sampled signals. Because the received signal is a discrete-time signal, digital filters are used in this work.

A digital filter can be specified by a difference equation:

$$y(n) = \sum_{k=1}^N a_k y(n-k) + \sum_{k=0}^M b_k x(n-k) \quad (2.5)$$

or by a system function:

$$H(z) = \frac{Y(z)}{X(z)} = \frac{\sum_{k=0}^M b_k z^{-k}}{1 - \sum_{k=1}^N a_k z^{-k}} \quad (2.6)$$

where  $a_k$  and  $b_k$  are the coefficients of the filter,  $x$  is the input signal and  $y$  the output signal [88].

Two types of digital filters exist in the literature like finite impulse response (FIR) filters (non-recursive filters) and infinite impulse response (IIR) (recursive filters). FIR filters use current and past samples only. The impulse response is finite because there is no

feedback in the FIR. The system function and the difference equation of the FIR filter are the following:

System function:

$$H(z) = \sum_{k=0}^M b_k z^{-k} \quad (2.7)$$

Difference equation:

$$y(n) = \sum_{k=0}^M b_k x(n-k) \quad (2.8)$$

The output is the weighted sum of current and previous  $M$  inputs.  $M$  is the order of the filter if  $b_0 \neq 0$ . Concerning the system function, it is polynomial in  $z^{-1}$  of order  $M$ , it has a pole with order  $M$  at  $z = 0$  if  $b_M \neq 0$  and  $M$  zeros at positions in the  $z$ -plane determined by the coefficients  $b_k$ .

Infinite impulse response filters have feedback, having sets of coefficients for previous and current input samples and previous output samples. Since they depend on previous output samples, perturbations at the input can cause oscillations at the output. The IIR filter type has the difference equation (2.5) and the system function (2.6). The output signal is weighted sum of current and previous  $M$  inputs and previous  $N$  outputs. The  $H(z)$  has  $M$  zeros if  $b_0 \neq 0$  and  $M = N$ .  $M-N$  poles are added at  $z = 0$  if  $M > N$  and  $b_M \neq 0$ .  $N-M$  zeros are added if  $N > M$  and  $b_M \neq 0$ .

In general, the requirements of the filter design are the stability, causality, frequency response, phase shift and impulse response. In addition, the computational complexity and hardware or software implementation are taken into consideration. Filter properties are determined by the number and the values of its coefficients and the filter order. The properties of the frequency response of these filters include the cutoff frequency, the steepness of the transition between the pass-band and stop-band, and the amount or ripples in the pass-band and stop-band. Typical realistic magnitude response of a filter is shown in Figure 2.6 [89].

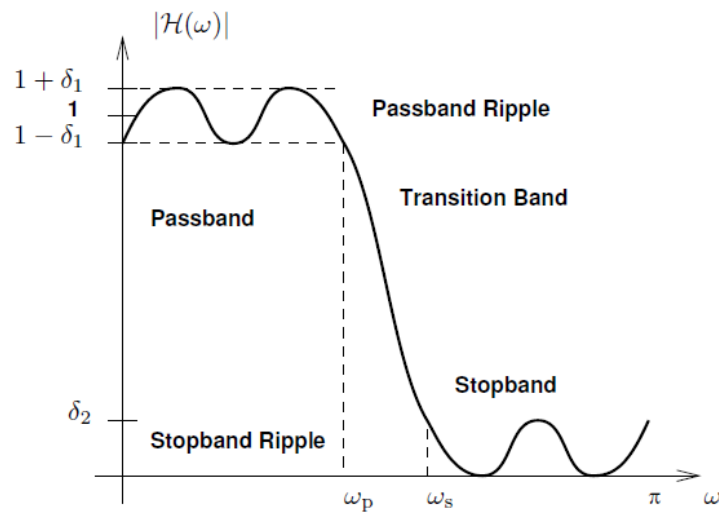


Figure 2.6. Realistic magnitude response of a filter

Each of FIR and IIR filters has its own advantages and disadvantages. The advantage of FIR filter is its stability for any choice of coefficients, while IIR filters must keep their poles inside the unit circle. Furthermore, FIR filter has a linear phase unlike IIR filters have nonlinear phase and unavoidable consequence of introducing poles. Recall that linear phase in the frequency domain corresponds to a simple delay in the time domain. Typically the phase distortion in case of IIR is greatest near the filter pass band edges. In the center of the pass band the phase is often nearly linear.

The advantage of IIR over FIR is by achieving a given filtering characteristic using less memory and calculations than a similar FIR filter, so in designing the similar filter, IIR requires a lower order than the FIR and can achieve all the desired specifications by low computational cost. In addition, it has shorter or no time delay compared to the FIR filter unlike the FIR that suffers from long delay between input and output [87].

The classical IIR filters are Butterworth, Chebyshev Types I and II, elliptic, and Bessel.

The design of filters is done using the MATLAB software. MATLAB is the one of the programming language which provides mathematical calculations, designing filters and many other tasks. It is very convenient in use and easy to perform. It has several tool boxes to design filters like FDA tool Box, GA, PSO, etc.

Because IIR filters have no time delay compared to FIR filters; IIR filter is implemented in this work. Because Butterworth is more linear phase response in the pass band than other IIR filters like Chebyshev or elliptic filters [87] and also a lower level of overshoot, Butterworth is chosen as a filter in this work. Linearity of the filter is taken into consideration to mitigate as possible the affection of the filter on the position of peaks, hence the heartbeat rate is not affected that much.

### 2.6.1.3. Smoothing method

A smoothing method is applied to reduce the noise of the heartbeat signal. It is based on a moving average filter. It replaces a given point by the average of its surrounding points. Considering a signal  $X$  with  $N$  samples,  $X = (X_0, \dots, X_{N-1})$ , the sample smoothed  $X_s(i)$  has the following equation:

$$X_s(i) = \frac{1}{n} \sum_{k=i-m}^{i+m} X(k) \quad (2.9)$$

where  $n = 2m+1$  is the length of the smoothing window,  $n$  is odd. Note that  $i$  should be between  $m$  and  $N-m-1$ . Otherwise, the length of the smoothing window is decreased.

### 2.6.1.4. Peak detection method

Peak detection method (PDM) is a method used for the heartbeat rate tracked in time domain. It is performed by detecting peaks having maximum amplitude every 0.5 s, this window corresponds to time when peaks must appear for a heart rate of 120 beats/min; this value presents the maximum heartbeat rate that an adult can achieve. This method of peak detection is performed to avoid detecting non meaningful peaks in the heartbeat signal. The rate is calculated by extracting the duration of each delay between 2 successive peaks. After peak detection of the heartbeat signal, heartbeat rate is calculated using the following relation:

$$HR = \frac{60(N - 1)}{d_1 + d_2 + \dots + d_{N-1}} \quad (2.10)$$

where  $N$  is the peaks number and  $d_k$  is the duration of the interval determined by 2 successive peaks expressed in seconds.

The PDM is used to extract the heartbeat rate and the heartbeat rate variability of the ECG. In general, it is utilized for the peak detection of electrocardiogram signals. These peaks are known by R-peaks. In this work, the R-peak could be extracted after applying filtering. Although they are not well defined like the R-peak of the ECG, still the peaks of the filtered signal are extracted.

### 2.6.2. Separation of respiration and heartbeat signals

In this study, heartbeat rate is extracted both in the time and frequency domains. The flowchart of heartbeat rate extraction applied in the time and frequency domains for a person who holds his breath is presented in Figure 2.7. Figure 2.8 presents the flowchart of heartbeat rate extraction applied in time and frequency domains for a person who breathes.

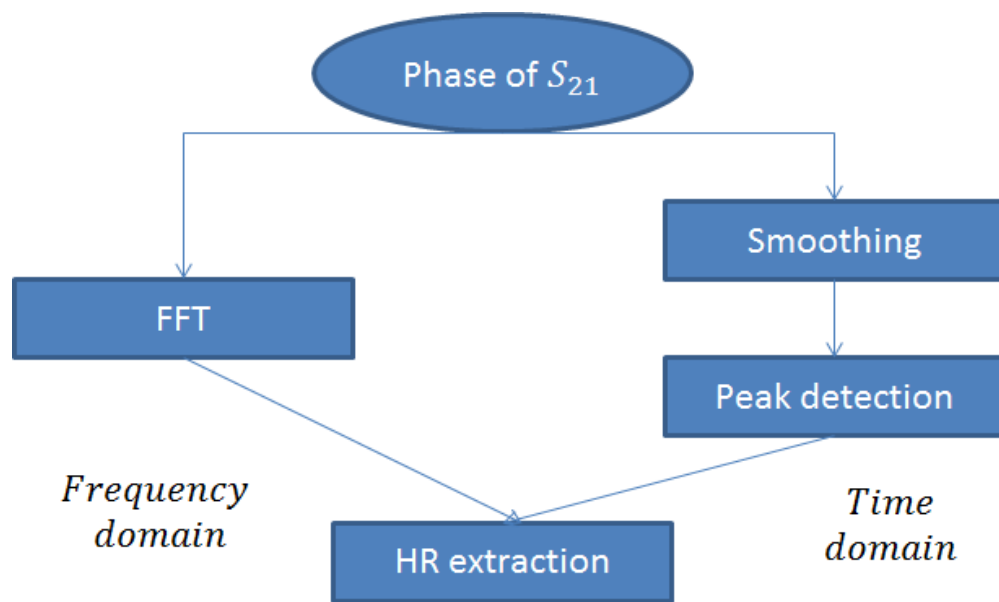


Figure 2.7. Flowchart of the processing techniques used in time and frequency domains for a person who holds his breath

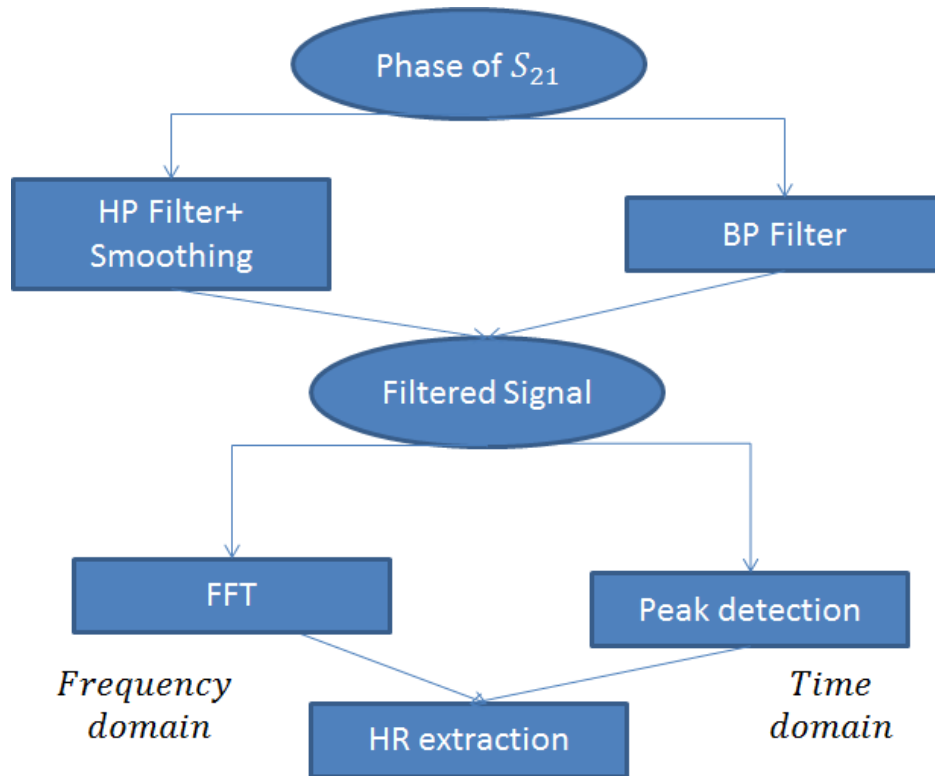


Figure 2.8. Flowchart of the processing techniques used in frequency and time domains for a person who breaths

When the person is holding his breath, smoothing method is used in order to reduce noise, then peak detection is applied in order to extract heartbeat rate by using (2.10). This technique represents the heartbeat rate extraction in time domain. In frequency domain, FFT is applied and then heartbeat rate is extracted by choosing the maximum value of the bandwidth between 1 and 2 Hz, these frequencies represent rates between 60 and 120 bpm which are the heartbeat rates of an adult. When breathing normally, filtering is applied in order to separate the respiratory signal from heartbeat signal. 2 types of filters could be used: High pass filter and band pass filter. The high pass filter is applied in order to attenuate the respiratory signal as it has the lower frequency components, while the smoothing is applied in order to reduce noise. Moreover, band-pass filter can be used. This filter is able to attenuate respiratory signal and reduce noise at the same time.

### 2.6.2.1. Heartbeat detection in frequency domain

Figure 2.9. shows the positive part of the absolute value of FFT transform of the phase for a person who holds his breath vs. beat per minute. The beat/min is obtained by multiplying the frequency by 60.

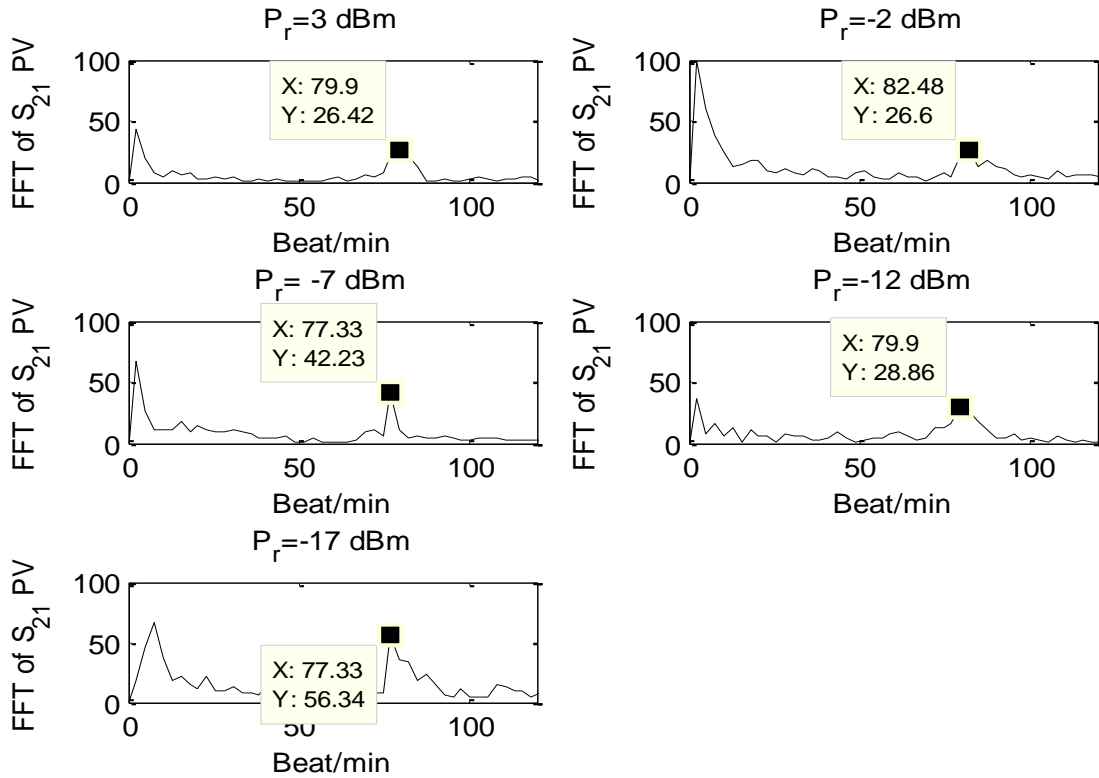


Figure 2.9. Positive part of absolute value of the FFT applied for the phase variation of  $S_{21}$  when measured at 20 GHz and  $P_r = 3, -2, -7, -12$  and  $-17$  dBm for a person who is holding the breath.

The maximum of peaks between 60 and 120 beat/min corresponds to the heartbeat rate. The heartbeat rate at radiated powers 3, -2, -7, -12 and -17 dBm for a person who holding his breath are 79.9, 82.48, 77.33, 79.9 and 77.33 bpm respectively. Figure 2.10 shows the results of the positive part of the absolute value of FFT applied to the received signals for the person who breathes normally.

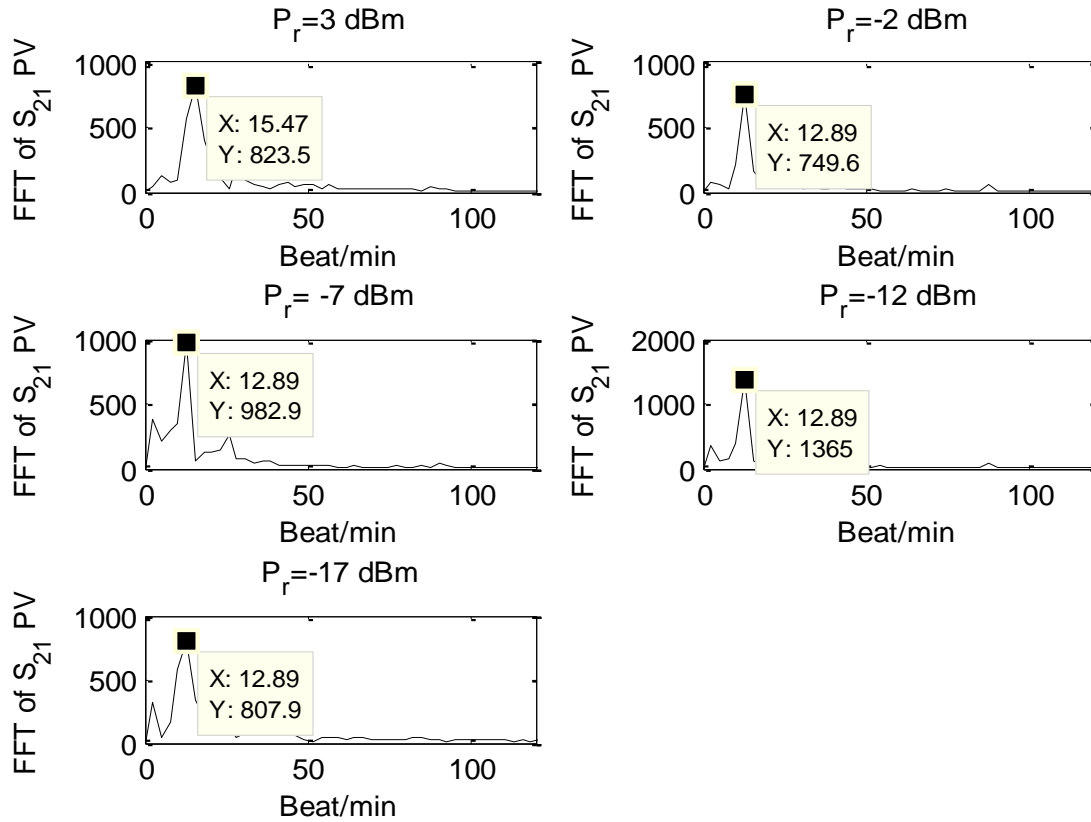


Figure 2.10. Positive part of the absolute value of FFT applied for the phase variation of  $S_{21}$  when measured at 20 GHz and  $P_r = 3, -2, -7, -12$  and  $-17$  dBm for a person who breathes

Note that the maximum peak between 12 and 20 breathes per minute corresponds to the respiratory rate; hence the respiratory rate for the person at radiated power 3 dBm is 15.45 Bpm. At -2, -7, -12 and -17 dBm, the respiration rates are 12.89 Bpm. However, the problem of heartbeat's low amplitude exists, and hence the extraction of the heartbeat frequency is quite difficult. To detect this frequency, high-pass filter (HPF) is applied with 0.9 Hz cut-off frequency. 0.9 Hz is chosen because it is able to reduce the respiratory frequency which is between 0.2 and 0.34 Hz and keep heartbeat signal located between 1 and 2 Hz. The high-pass filter is a Butterworth filter. When using Butterworth filter, the gain becomes more selective with higher order. For smaller order values, the cutoff will be less sharp.  $N = 4$  is chosen because it is sharp enough to attenuate the respiratory frequency. The attenuation at 0.9 Hz is -3dB. The attenuation at 0.2 Hz is -52 dB and -34 dB at 0.34 Hz. In addition, the attenuation caused by the filter at a rate of 12.89 is -50 dB and at 15.47 is -43.5 dB. Figure 2.11 shows the results of applying Fast



Fourier Transform (FFT) to the received signal after the high-pass filter for the person who breathes normally.

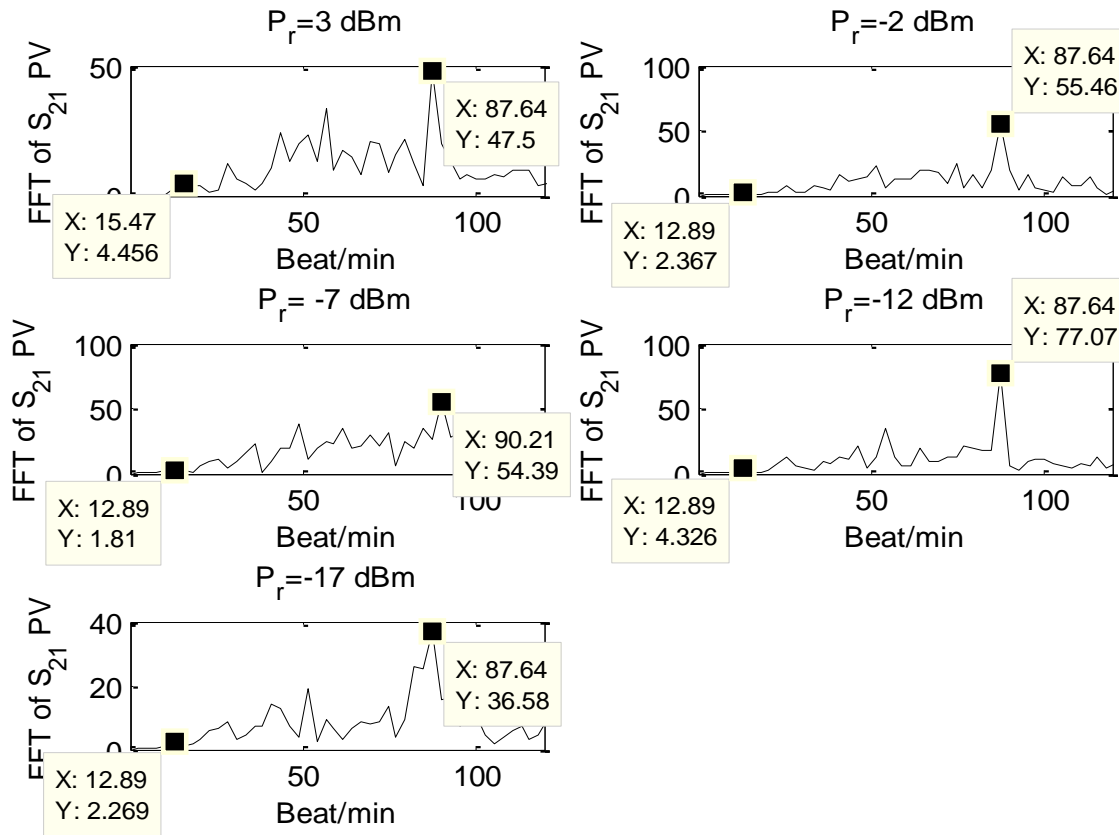


Figure 2.11. FFT applied for HP filtered  $S_{21}$  phase variation when measured at 20 GHz and  $P_r = 3, -2, -7, -12$  and  $-17$  dBm for a person who breathes

The amplitude of the respiratory rate is between 1.81 and 4.456 and the amplitude of heartbeat is between 36.58 and 77.07. At 3, -2, -7, -12 and -17 dBm, the respiratory amplitude is 10, 24, 27, 18 and 16 times smaller than heartbeat amplitude respectively; hence the respiratory peak is remarkably attenuated and becomes very small compared to the amplitude of the heartbeat peak. Simultaneously with the VNA, ECG signals are extracted in order to be used as reference signals for  $HR$  precision calculation. The sampling frequency of the ECG is 360 Hz. The measurements duration is 23 sec. The peak detection method is used to the ECG signal; and then the  $HR$  of ECG is calculated. Figure 2.12 presents the ECG signal taken simultaneously with the VNA system when taking measurements for a person who holds his breath at different radiated powers.

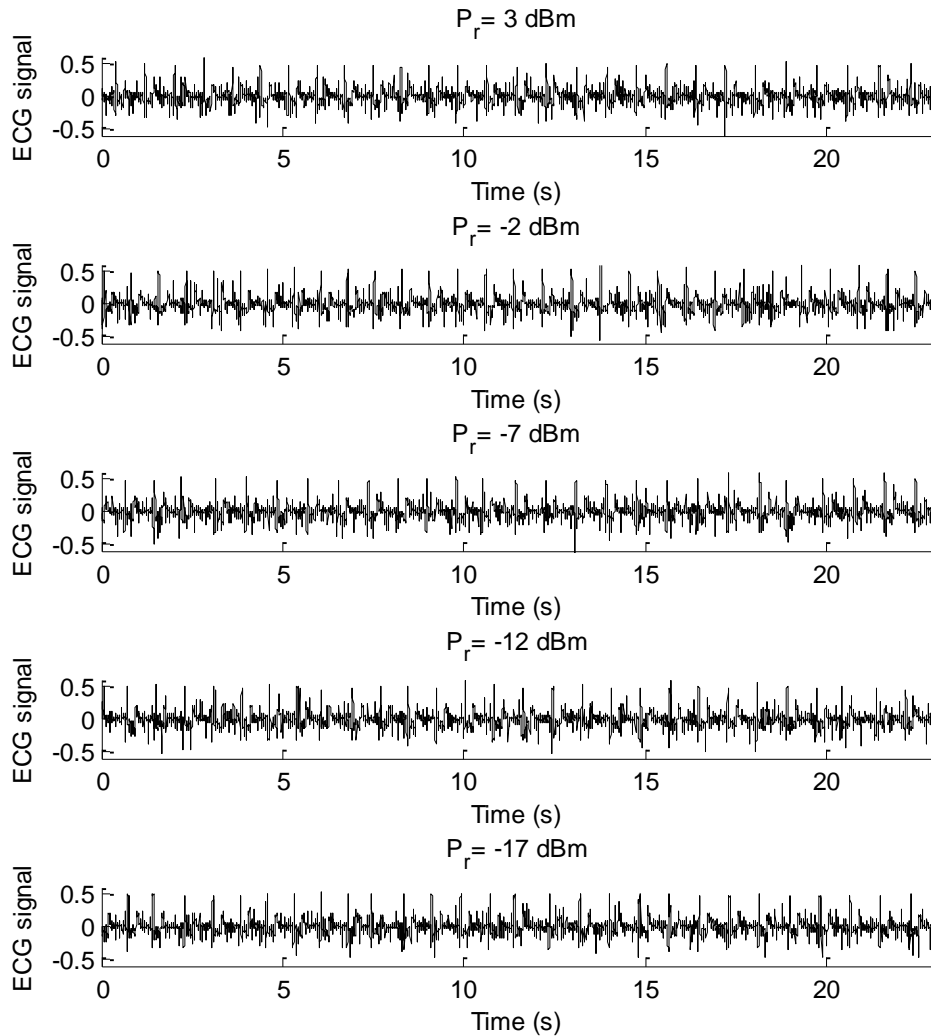


Figure 2.12. ECG signal taken simultaneously with VNA system when taking measurements for a person who holds his breath at 20 GHz and  $P_r = 3, -2, -7, -12$  and  $-17$  dBm

At radiated power 3 dB, 28 peaks are obtained in 21.93 sec. At -2 dB, 31 peaks are obtained in 22,95 sec. At -7 dB, 27 peaks are obtained in 21.7 sec. At -12 dB, 30 peaks are obtained in 23 sec and finally at -17dB, 28 peaks are obtained in 21.6 sec. Hence the ECG heartbeat rates for the person who is holding his breath at 3, -2, -7, -12 and -17 dB are 74, 78, 72, 76, 75 bpm respectively. Figure 2.13 presents the ECG signal obtained simultaneously with VNA system when taking measurements for a person who breathes normally at different radiated powers.

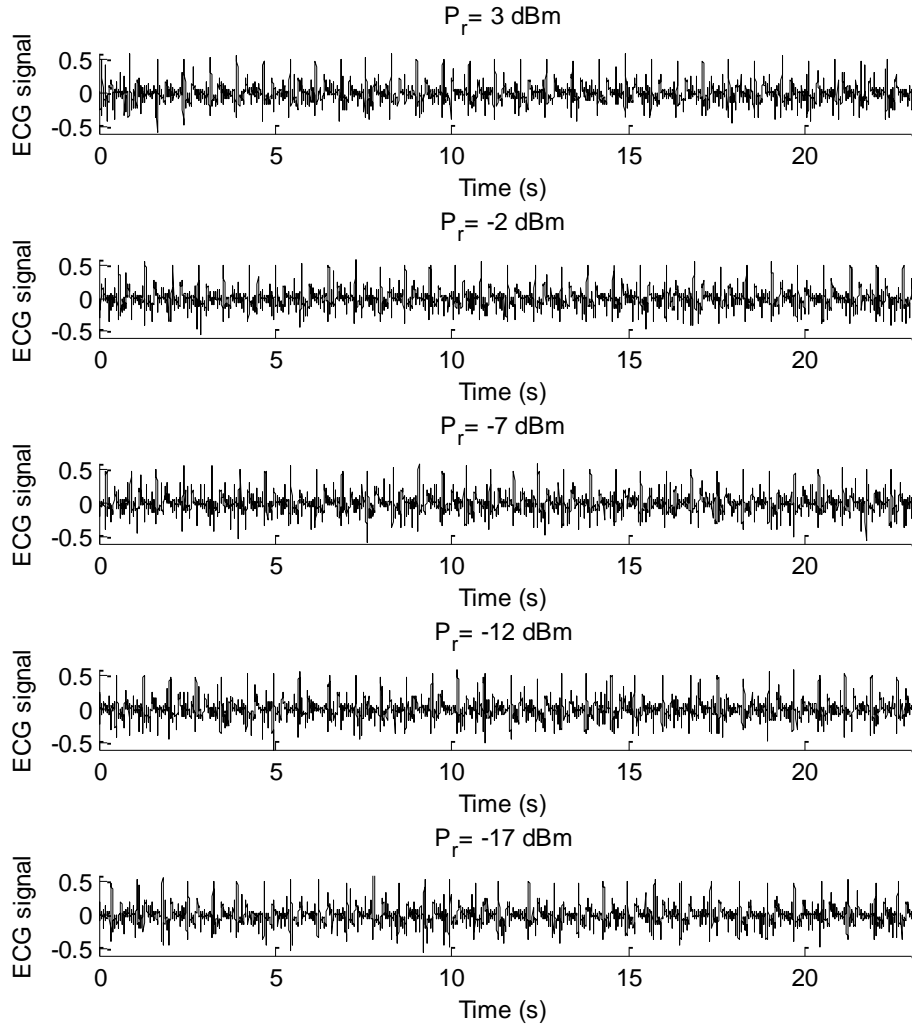


Figure 2.13. ECG signal taken simultaneously with VNA system when taking measurements for a person who breathes normally at 20 GHz and at 20 GHz and  $P_r = 3, -2, -7, -12$  and  $-17$  dBm

At radiated power 3 dB, 31 peaks are obtained in 22.32 sec. At -2 dB, 31 peaks are obtained in 22.21. At -7 dB, 32 peaks are obtained in 22.22 sec. At -12 dB, 31 peaks are obtained in 22.1 sec and finally at -17dB, 31 peaks are obtained in 22.28 sec. Hence the ECG heartbeat rates for the person who breathes normally at 3, -2, -7, -12 and -17 dB are 81, 81, 84, 81, 81 bpm respectively. The relative error between the *HR* of VNA and *HR* of ECG is calculated using the following equation:

$$Error = 100 \times \left| \frac{Filtered S_{21} \text{ heartbeat rate} - ECG \text{ heartbeat rate}}{ECG \text{ heartbeat rate}} \right| \quad (2.11)$$

Table 2.4 presents results in terms of *HR* relative error when using the frequency methods applied for signals at 20 GHz and for several radiated powers: 3, -2, -7, -12 and -17 dBm.

Table 2.4. Relative error of HR using FFT

<b>Radiated Power</b>	<b>Respiration (Y/N)</b>	<b>Respiration Rate (Bpm)</b>	<b>ECG HR (bpm)</b>	<b>VNA HR (bpm)</b>	<b>Relative Error (%)</b>
3	N	0	74	80	8.1
-2	N	0	78	83	6.4
-7	N	0	72	77	6.9
-12	N	0	76	80	5.2
-17	N	0	75	77	2.6
3	Y	15.5	81	88	8.6
-2	Y	13	81	88	8.6
-7	Y	13	84	90	7
-12	Y	13	81	88	8.6
-17	Y	13	81	88	9

According to the American National Standard [90], medical devices measuring the heartbeat rate should have a relative error lower than 10% or 5 bpm. Obtained results show the possibility of obtaining a *HR* with a maximum error of 8.1% for a person holding his breath and a maximum of 9% for a breathing person at 20 GHz. Although signals are noisier for low radiated power, heartbeat rates are detectable with a good accuracy.

It is noteworthy to mention that the time window is 23 sec, hence the resolution of the heartbeat signal after applying the FFT is 0.0435 Hz ( $\Delta f = 1/T = f_s/(N - 1) = 1/23 = 0.0435$  Hz). 0.0435 Hz corresponds to 2.6 beats/min, hence in each minute an error of 2.6 beats

may occur. Because the heartbeat rate of an adult varies between 60 and 120 beat/min, the relative error varies between 2.17%  $((120-122.6)/120)$  and 4.43%  $((60-62.6)/60)$ .

When using the Fast Fourier Transform to extract the heartbeat rate, the cardiac frequency cannot be found exactly because the precise value of the cardiac frequency may not match the FFT frequency step  $\Delta f$ , the power spectrum is spreading at the adjacent frequencies; hence errors between 2.17 and 4.43% may occur. Thus, next step is extracting the heartbeat rate in time domain to avoid this problem.

### 2.6.2.2. Heartbeat detection in time domain

Figure 2.14 presents the peak detection for a person who is holding his breath, after applying smoothing method. The signal is smoothed using a MATLAB function ‘Smooth’. This function uses moving average of length  $n$ . The length  $n$  is an odd. After trial and error, the length of the window ‘ $n$ ’ is chosen to be 199 as an optimal value for higher accuracy detection.

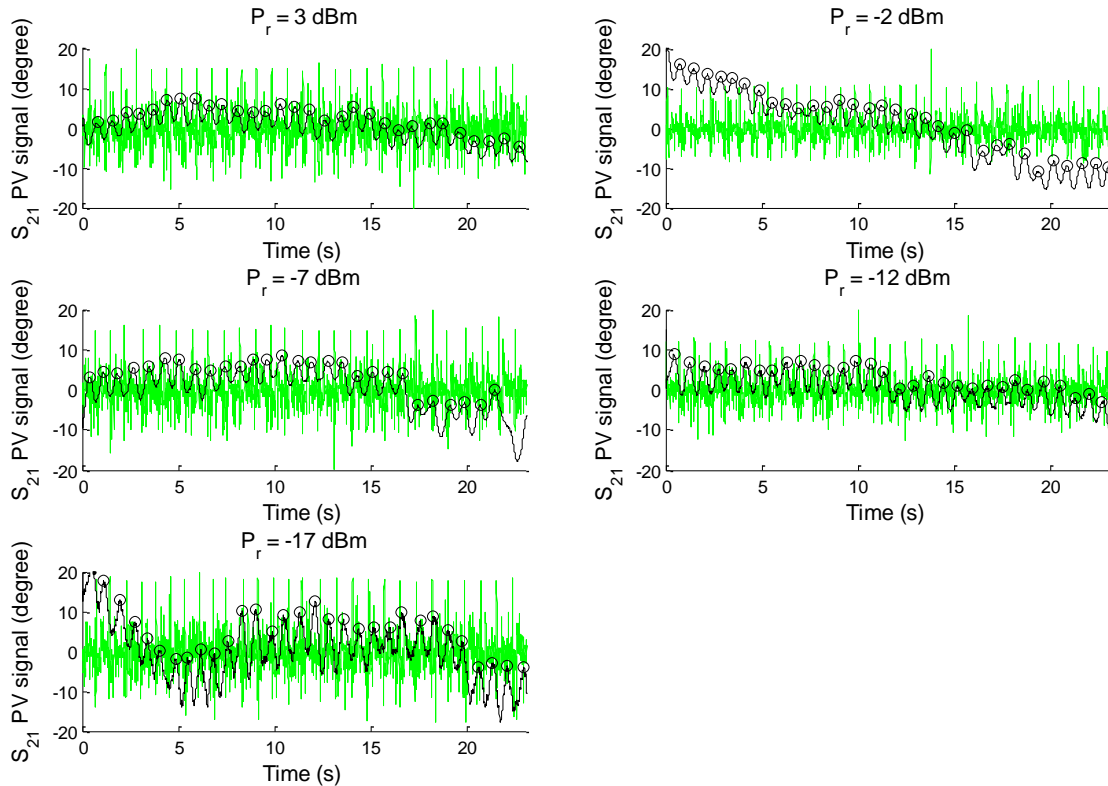


Figure 2.14. PDM applied to  $S_{21}$  phase variation for a non-breathing person after applying smoothing with  $n = 199$  at 20 GHz and at 20 GHz and  $P_r = 3, -2, -7, -12$  and  $-17$  dBm (Black), ECG signal (Green)

At radiated power 3 dB, 30 peaks are obtained in 21.89 sec. At -2 dB, 32 peaks are obtained in 22.12. At -7 dB, 28 peaks are obtained in 21.07 sec. At -12 dB, 31 peaks are obtained in 22.28 sec and finally at -17dB, 30 peaks are obtained in 21.86 sec. Hence the heartbeat rates for the person who holding is his breath at 3, -2, -7, -12 and -17 dB are 79, 84, 77, 81, 80 bpm respectively.

In the case of the presence of respiration, filtering of the phase variation of  $S_{21}$  is applied, followed by peak detection. Figure 2.15 presents the peak detection after applying a 4<sup>th</sup> order Butterworth band-pass filter, having 0.9 Hz and 2 Hz as cutoff frequencies: 0.9 Hz attenuates the respiratory frequencies and 2 Hz reduce high-frequency noise without attenuating the heartbeat signal. Thus, the heartbeat signal is obtained at its output. The attenuation at the cut-off frequency is -3 dB.

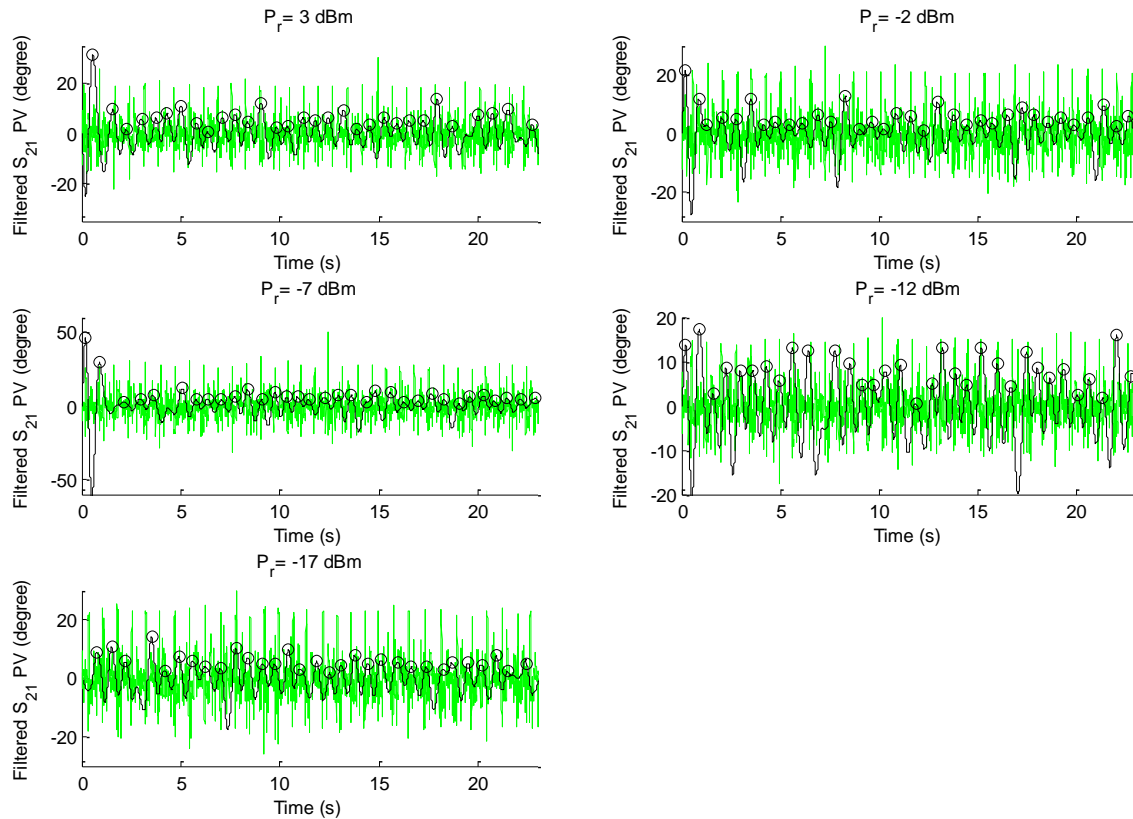


Figure 2.15. Peak detection applied to  $S_{21}$  phase variation after applying BP filter for a breathing person for different radiated powers at 20 GHz and  $P_r = 3, -2, -7, -12$  and  $-17$  dBm (Black), ECG signal (Green)

Although peaks are not easy to be detected like ECG signals, they are still detectable; then  $HR$  is extracted. At radiated power 3 dB, 31 peaks are obtained in 22.2 sec. At -2

dB, 34 peaks are obtained in 22.44 sec. At -7 dB, 33 peaks are obtained in 22.73 sec. At -12 dB, 33 peaks are obtained in 22.63 sec and finally at -17dB, 31 peaks are obtained in 21.61 sec. Hence the heartbeat rates when applying high pass filter and smoothing to  $S_{21}$  phase variation at 3, -2, -7, -12 and -17 dB are 81, 88, 84, 85 and 83 bpm respectively.

On the other side, high-pass filter is applied on  $S_{21}$  phase variation in order to reduce the respiratory signal, and then the high pass filtered signal is smoothed to reduce the noise. After that, peak detection is applied. Figure 2.16 presents the peak detection after smoothing method applied to the high-pass filtered phase variation of  $S_{21}$ . A 4<sup>th</sup> order Butterworth filter with cut-off frequency 0.9 Hz is used.

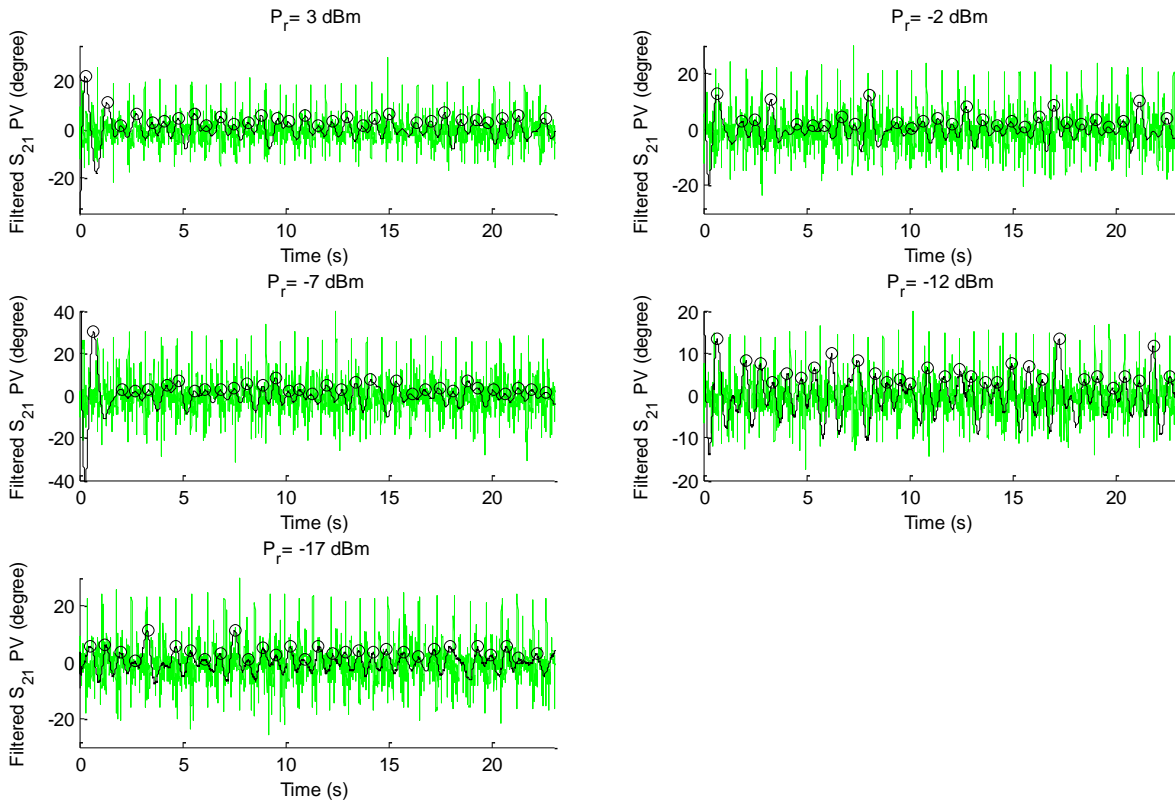


Figure 2.16. PDM applied to  $S_{21}$  phase variation after applying HP filter and smoothing for a breathing person at 20 GHz and  $P_r = 3, -2, -7, -12$  and  $-17$  dBm (Black), ECG signal (Green)

At radiated power 3 dB, 31 peaks are obtained in 22.07 sec. At -2 dB, 29 peaks are obtained in 21.71. At -7 dB, 32 peaks are obtained in 21.93 sec. At -12 dB, 30 peaks are obtained in 21.98 sec and finally at -17dB, 30 peaks are obtained in 21.69 sec. Hence the

heartbeat rates when applying high pass filter and smoothing to  $S_{21}$  phase variation at 3, -2, -7, -12 and -17 dB are 82, 77, 85, 79 and 80 bpm respectively.

Obtained  $HR$  is compared to that obtained from the ECG signal. Table 2.5 summarizes the relative error between VNA system and ECG for the non-breathing person.

Table 2.5. Relative error for a non-breathing person

<b>Radiated Power(dBm)</b>	<b>ECG HR (bpm)</b>	<b>VNA HR (bpm)</b>	<b>Relative Error (%)</b>
3	74	79	6.7
-2	78	84	7.7
-7	72	77	6.9
-12	76	81	6.6
-17	75	80	6.6

Obtained results show the possibility of obtaining a  $HR$  with a maximum error of 7.7% for a person holding his breath even in low radiated power. Table 2.6 presents the relative errors between VNA system and ECG of each filter type.

Table 2.6. Relative error for a breathing person

<b>Radiated Power (dBm)</b>	<b>Relative Error (%)</b>				
	<b>ECG HR (bpm)</b>	<b>BP Butterworth</b> $N = 4, f_{c1} = 0.9 \text{ Hz},$ $f_{c2} = 2 \text{ Hz}$		<b>HP Butterworth</b> $N = 4, f_{c1} = 0.9 \text{ Hz} +$ smoothing $n = 199$	
		<b>VNA HR (bpm)</b>	<b>RE (%)</b>	<b>VNA HR (bpm)</b>	<b>RE (%)</b>
3	81	81	0	83	2.4
-2	77	70	9	81	5.1
-7	84	84	0	85	1.2



-12	81	85	4.9	79	2.5
-17	81	83	2.5	82	1.2

Obtained results show the possibility of obtaining a *HR* with a maximum error of 9% for a breathing person when using BPF filter and with a maximum error 5.1% for a breathing person using HPF.

Obtained results show that extracting the *HR* is feasible in both frequency and time domains as the highest error is less than 9%. FFT cannot give real frequency; that's why heartbeat rate is extracted using time domain. Time domain gives better results than the frequency domain. In the time domain, two types of filters are used: Band pass filter (BPF) and high pass filter (HPF); the results using both filters types are considered as acceptable. Furthermore, the results obtained from the smoothed high-pass filtered phase variation of  $S_{21}$  (less than 5.1%) are more accurate than the results obtained from band-pass filtered phase variation of  $S_{21}$  (less than 9%), especially because smoothing reduce noise between 1 and 2 Hz. As result, the heartbeat is extracted with an error less than 10% even with low power (-17 dBm).

## 2.7. Conclusion

The measurement system used in this work generates a continuous wave toward a person's chest, and detects the reflected signal. Using a vector network analyzer, the phase variation of  $S_{21}$  that carries respiration and heartbeat signals is computed. The VNA has been used to determine the optimal frequency with minimum power before the implementation process. After measuring the received signal from the person's chest, processing techniques are required to extract the heartbeat signal. The measurement of the heartbeat rate can be applied both in the frequency and time domains. To make a transformation to the frequency domain, FFT has been applied; then heartbeat rate has been extracted by choosing the frequency between 1 and 2 Hz for which max |FFT| has been obtained. In the time domain, smoothing method has been sufficient to extract the heartbeat rate when the person holds his breath. When the person breathes, filtering method has been used to attenuate respiration signal from the phase variation of  $S_{21}$ , then peak detection has been applied to extract the heartbeat rate. Butterworth filter with order

4 and cut-off frequency 0.9 Hz has been used because it attenuates the respiratory signal enough and keeps the heartbeat signal. When using high pass filter, smoothing is required to reduce the noise, but in case of band pass filter the second cut off (2 Hz) reduces the noise. The signal processing methods used in this chapter have been applied to measurements and the obtained results have been compared to those given by the ECG. Relative errors in frequency domain are less than 9 %. In time domain, relative errors are less than 5.1% when applying high pass filter followed by smoothing and less than 9% when applying band pass filter. As a conclusion, the results are accurate even with a radiated power of -17 dBm; hence measurements for radiated power less than -17 dBm could be performed.

<b>Chapter 3 Heartbeat detection from different sides and at several operating frequencies using wavelets .....</b>	<b>99</b>
<b>3.1. Introduction.....</b>	<b>99</b>
<b>3.2. Choice of the operating frequency .....</b>	<b>100</b>
<b>3.3. Antennas .....</b>	<b>102</b>
<b>3.4. Measurement setup.....</b>	<b>102</b>
<b>3.5. Signal Processing techniques .....</b>	<b>108</b>
<b>3.5.1. Overview of the wavelet transform .....</b>	<b>108</b>
<b>3.5.2. Re-sampling method .....</b>	<b>113</b>
<b>3.5.3. Choice of the wavelet type.....</b>	<b>114</b>
<b>3.5.4. Application of wavelets.....</b>	<b>116</b>
<b>3.5.5. Application of smoothing .....</b>	<b>118</b>
<b>3.6. Results and discussion .....</b>	<b>126</b>
<b>3.7. <math>S_{DI8}</math> pass band reducing .....</b>	<b>129</b>
<b>3.8. Conclusion .....</b>	<b>129</b>

# **Chapter 3 Heartbeat detection from different sides and at several operating frequencies using wavelets**

## **3.1. Introduction**

The main objective of this work is to provide the ability of detecting the heartbeat activity for persons in motion. Previous work tends to provide measurements only from the front-side of the person under test. Accurate and reliable information is lacking when a person moves, this supposes that the position of the radar could be at any side of the person under test. Thus, the aim of this chapter is to provide the possibility of extracting the heartbeat activity of the person under test at different sides (front, back, left, and right) using advanced signal processing techniques.

In addition to the different sides of measurements, different scenarios are considered: the person under test is breathing normally and sitting at a 1-meter distance from the system. Measurements are performed at different operating frequencies: 2.4, 5.8, and 10 GHz. The radiated power is fixed at 0 dBm in order to limit the possible impact on the health of the patient and the medical staff.

The used microwave system is the same as described in the previous chapter but with different antennas depending on the operating frequencies. Simultaneously with the microwave system, a reference PC-based electrocardiograph is used in order to validate the accuracy of the heartbeat rate measurement.

As the signal received by the radar contains information on both the rhythm of respiration and that of the heartbeat, signal processing techniques are necessary in order to separate them, especially since the amplitude of the respiration signal is much greater than the amplitude of the heartbeat signal. In this context, processing techniques based on wavelet transforms can be applied in order to extract heartbeat from cardiopulmonary signal; then filtering technique is used in order to make a comparison between them. The choice of the operating frequencies and the antennas characteristics are studied in this chapter. Then the measurement setup and the processing techniques used in this work are described. The results of these measurements using processing techniques are presented.

### 3.2. Choice of the operating frequency

In order to provide a comparative study in terms of operating frequency, several frequencies were tested using the proposed system. In addition of using 20 GHz (K band) in the previous chapters, the operating frequencies should cover as much radar bands designations as possible, with preference for ISM bands. The operating frequencies chosen in this work are: 2.4 GHz (S band), 5.8 GHz (C band) and 10 GHz (X band). Besides, these frequencies are selected taking into account the operational limits of the available VNA frequency of 20 GHz and the antennas. According to IEEE standard letter band nomenclature [91], Table 3.1 presents the radar-frequency bands.

Table 3.1. Radar frequencies designation according to IEEE standard letter band nomenclature

Band designation	Frequency range
HF	0.003 to 0.03 GHz
VHF	0.03 to 0.3 GHz
UHF	0.3 to 1 GHz
L	1 to 2 GHz
S	2 to 4 GHz
C	4 to 8 GHz
X	8 to 12 GHz
K <sub>u</sub>	12 to 18 GHz
K	18 to 27 GHz
K <sub>a</sub>	27 to 40 GHz
V	40 to 75 GHz
W	75 to 110 GHz
mm or G	110 to 300 GHz

Note that when using the industrial, scientific and medical (ISM) bands, no license is required. These bands were approved by FCC in 1985. Table 3.2 presents the ISM bands list [92].

Table 3.2. ISM bands

Frequency Range	Center Frequency	Availability
6.765–6.795 MHz	6.780 MHz	Subject with local acceptance
13.553–13.567 MHz	13.560 MHz	
26.957–27.283 MHz	27.120 MHz	
40.66–40.70 MHz	40.68 MHz	
433.05–434.79 MHz	433.92 MHz	
902–928 MHz	915 MHz	Region 2 only (America)
2.400–2.500 GHz	2.450 GHz	
5.725–5.875 GHz	5.800 GHz	
24–24.25 GHz	24.125 GHz	
61–61.5 GHz	61.25 GHz	Subject with local acceptance
122–123 GHz	122.5 GHz	Subject with local acceptance
244–246 GHz	245 GHz	Subject with local acceptance

ISM bands must tolerate any interference generated by ISM applications. They are not entitled to interference protection which encouraged growth of the wireless industry

[93]. In several cases, some medical devices use technologies like frequency hopping that minimize the interference that leads to some errors. In addition, to reduce the electromagnetic interference to other devices, FDA recommends using the lowest power necessary [93].

### 3.3. Antennas

The same wide band horn antennas (Qpar Angus Ltd) were used for transmission and reception in experiments. The Qpar Angus Ltd (model number WBH218HN/ S) has a frequency range between 2 and 18 GHz, with a nominal gain between 10 and 22 dBi and a nominal beamwidth between 6 and 11 degrees. The voltage standing wave ratio (VSWR) of the antenna is less than 2.5:1 (typically < 2.0:1), and its cross polarization is less than 17 dB. The antenna dimensions are 622\*165\*165 mm<sup>3</sup> approximately with SMA or type N connector, it weighs 2.7 kg and operates for temperatures between – 40 and +70 °C. Table 3.3 presents the characteristics of the antenna.

Table 3.3. Antenna characteristics

Frequency (GHz)	Gain (dBi)	Half power beamwidth (deg)	
		H	E
2.4	11	22	18
5.8	16	10	8
10	19	8	7

### 3.4. Measurement setup

The person under test is a 54-years-old sitting at a distance of 1 m from the system and breathing normally. This distance was chosen as the measurement could be performed in the hospital room or in a medical office. The radiated power is fixed at 0 dBm. Therefore, the radiated power of the antenna depends on the transmitted power measured at the input of the transmitting antenna and the gain of the antenna. The power of the transmitted signal was set at: -11 dBm for 2.4 GHz, -16 dBm for 5.8 GHz and -19 dBm for 10 GHz.

Each measurement lasted for 30 seconds and was performed at four sides of the person under test: Front, Back, Left and Right sides. The number of samples was set by the VNA after choosing the time and the bandwidth. The bandwidth was chosen to be 500 Hz resulting from a compromise between the signal noise reduction and the sweep time. As the sweep time was 30 sec, the number of samples was set 20 000 samples by the VNA; hence the sampling frequency was 666.7 Hz. To validate the proposed system, radar measurements were performed simultaneously with ECG measurements. Table 3.4 summarizes the characteristics of the measurement setup and Figure 3.1 represents all measurement's positions.

Table 3.4. Characteristics of the measurement setup

System Specifications	
<b>Operating frequency (GHz)</b>	2.4, 5.8 and 10 GHz
<b>Radiated power (dBm)</b>	0 dBm
<b>Number of points</b>	20 000
<b>Time Window (sec)</b>	30
<b>Sampling frequency (Hz)</b>	666.7
Subject Information	
<b>Gender/ Age (y)</b>	M/54
<b>Position/ Side</b>	Setting/ Front, Back, Right, Left
<b>Distance (m)</b>	1
<b>Breathing</b>	Y

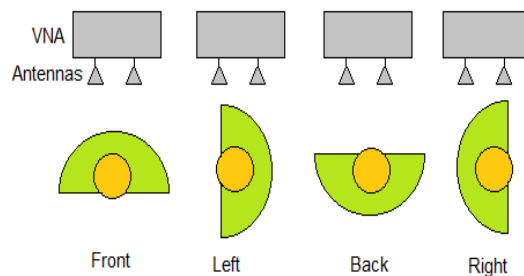


Figure 3.1. Measurement positions



Recall that the relation between the chest displacement  $\Delta x(t)$  and the phase variation  $\Delta\theta(t)$  is:

$$\Delta\theta(t) = \frac{4\pi}{\lambda} \Delta x(t) \quad (3.1)$$

where  $\lambda$  is the wavelength of the transmitted signal. The reflected signal contains information about heartbeat and respiration of the patient when breathing normally [83]. The displacement of the chest due to the heartbeat is between 0.2 and 0.5 mm. Hence, the theoretical values of the phase variation due to the chest displacement due to heartbeat at 2.4, 5.8 and 10 GHz are shown in Table 3.5.

Table 3.5. Theoretical values of the phase variation

Frequency	Wavelength ( $\lambda$ )	$\Delta\theta$ for $\Delta x = 0.2\text{mm}$	$\Delta\theta$ for $\Delta x = 0.5\text{mm}$
2.4 GHz	125 mm	1.15°	2.88°
5.8 GHz	51.72 mm	2.78°	6.69°
10 GHz	30 mm	4.8°	12°

It can be noticed that the phase variation due to heartbeat increases when the frequency increases. Thus, higher sensitivity to small displacements is obtained at higher frequencies. The use of higher frequencies will reduce the noise effect and increase the accuracy in detecting the peaks of the signal. Figure 3.2- 3.4 show the phase variation (PV) of  $S_{21}$  due to the cardiopulmonary activities measured at 2.4, 5.8 and 10 GHz respectively, for different sides of the subject: front side, back side, left side and right side.

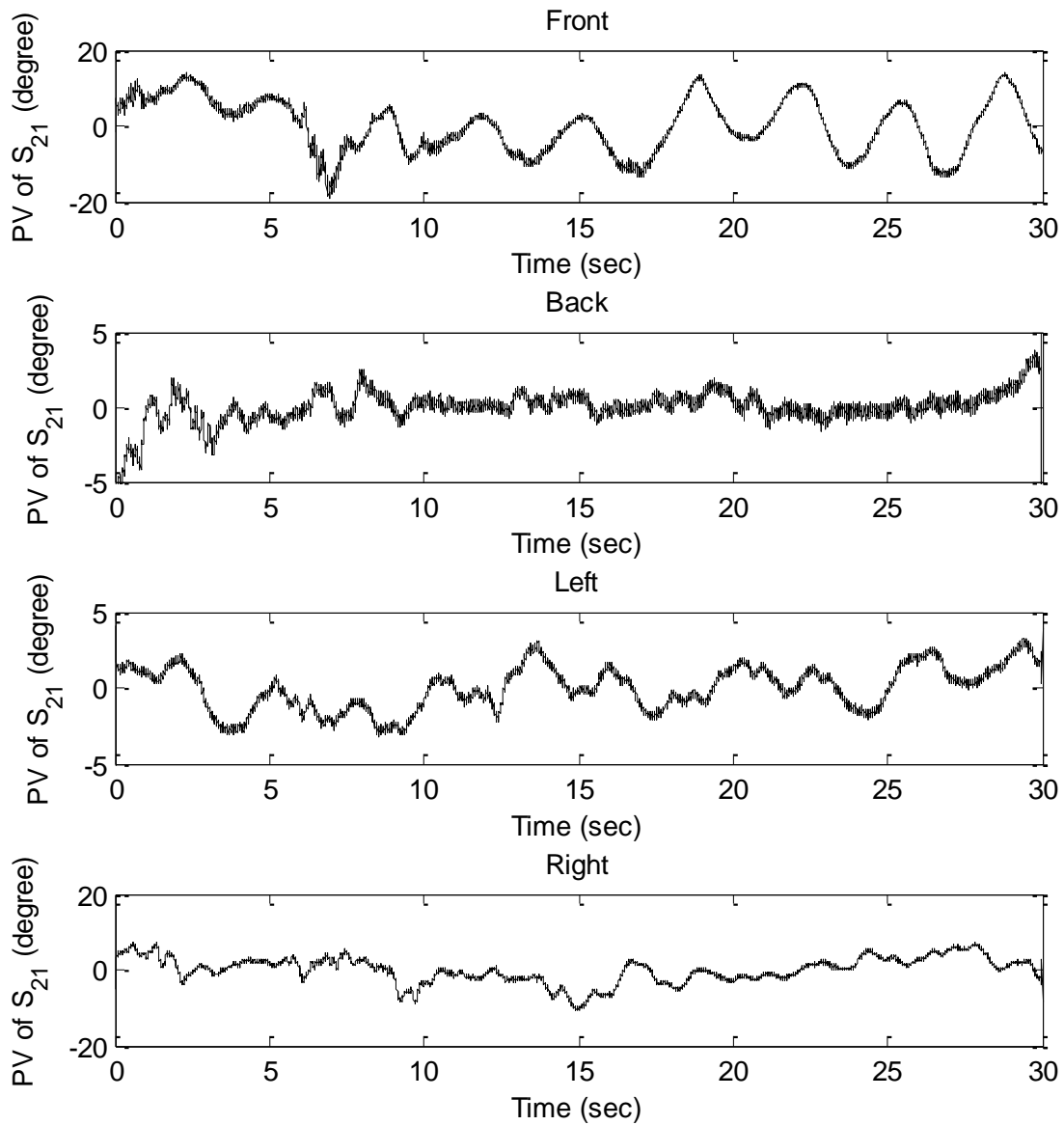


Figure 3.2. Phase variation of  $S_{21}$  due to the cardiopulmonary activities at different sides and at 2.4 GHz and 0 dBm

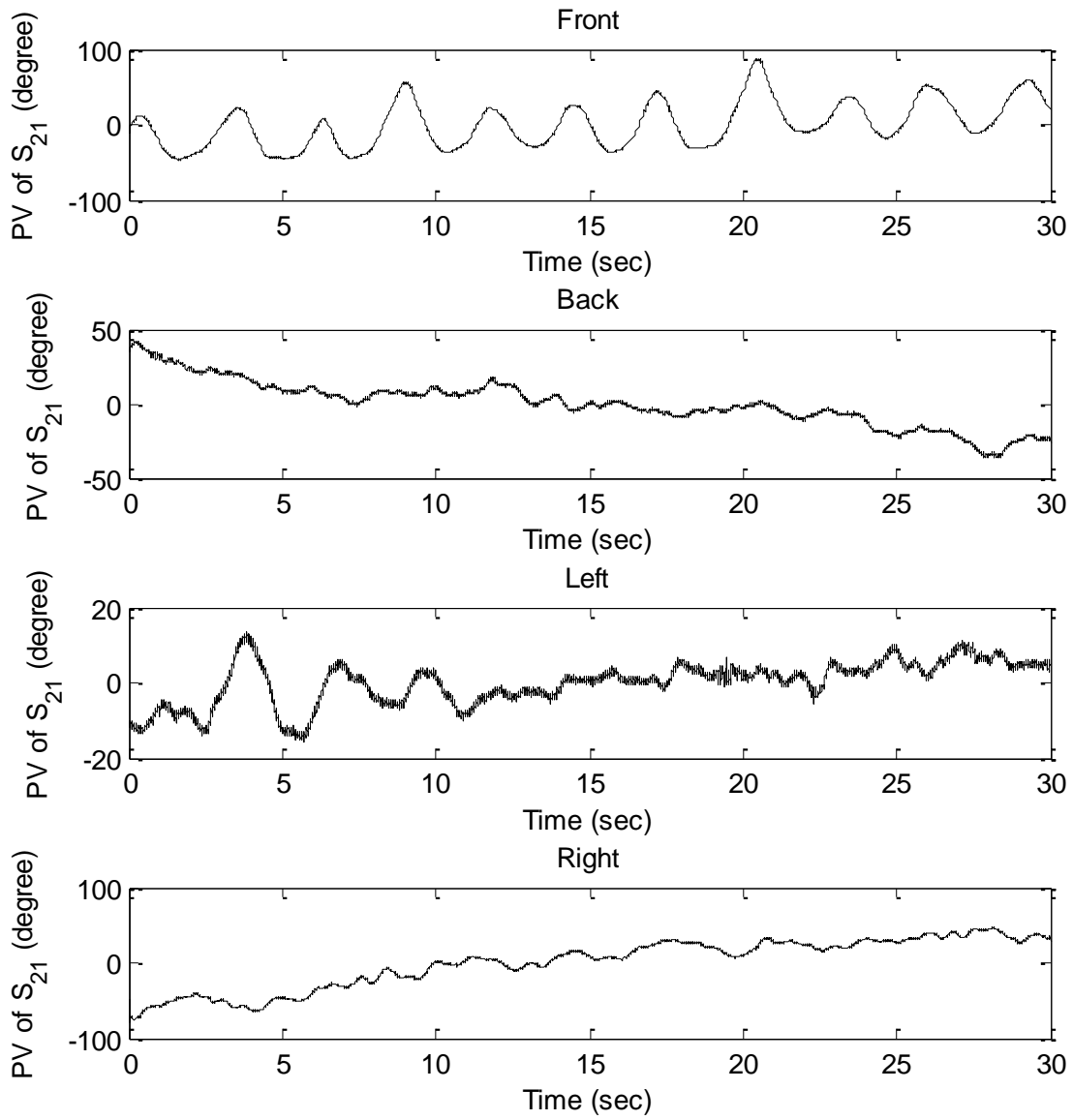


Figure 3.3. Phase variation of  $S_{21}$  due to the cardiopulmonary activities at different sides and at 5.8 GHz and 0 dBm

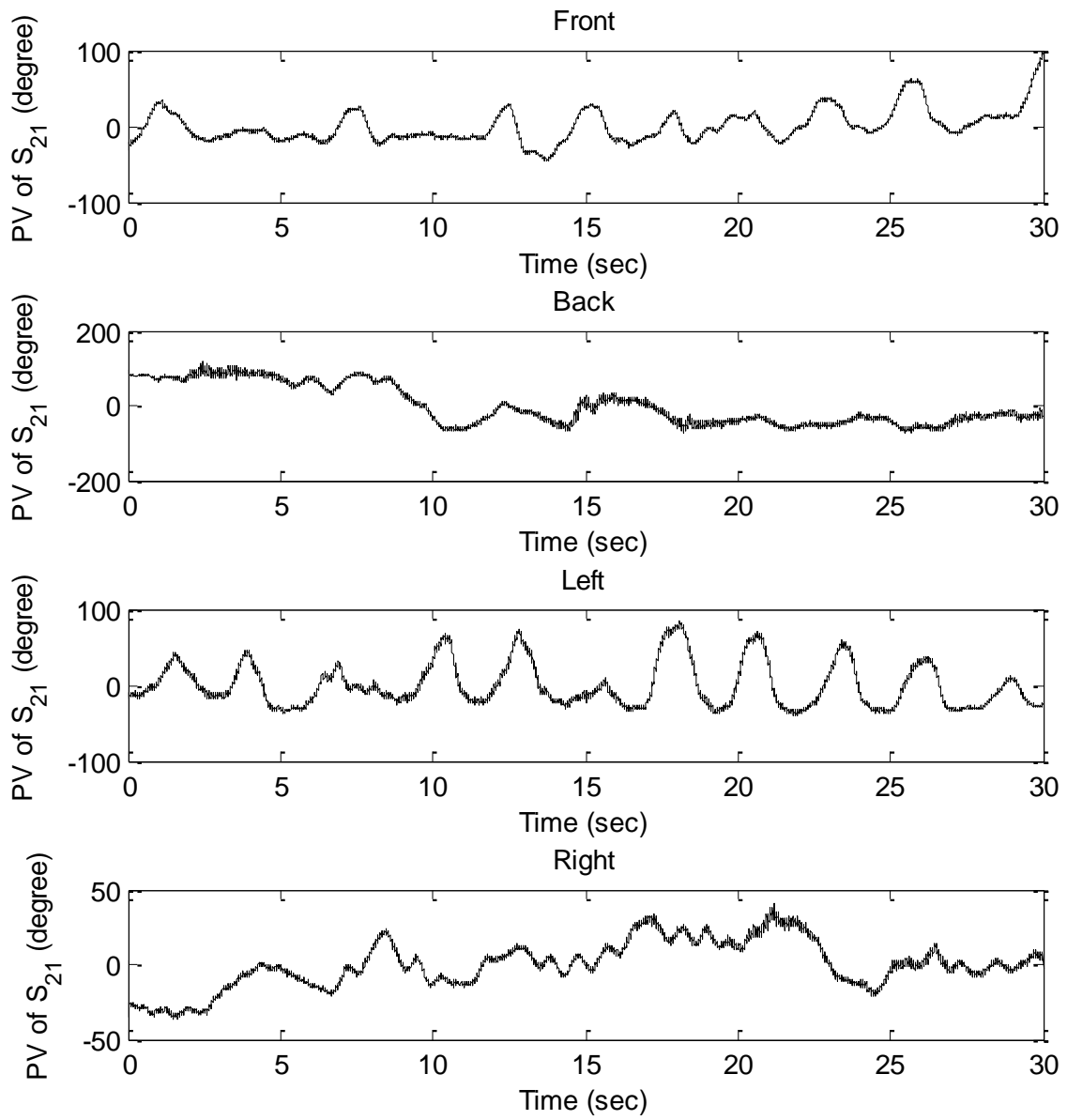


Figure 3.4. Phase variation of  $S_{21}$  due to the cardiopulmonary activities at different sides and at 10 GHz and 0 dBm

It can be noticed that the phase variation due to respiration increases with the increase of the operating frequency. In addition, respiration signal from the front side of the subject is clearer than at other sides in the time domain. The signal processing technique in the next subsection will show the possibility to extract the heartbeat signal from the cardiopulmonary signal over all sides.

### **3.5. Signal Processing techniques**

As breathing causes larger chest-wall motion than heartbeat, an advanced signal processing technique is required in order to extract the heartbeat signal from the cardiopulmonary signal. As seen in chapter 2, classical filters are able to extract the heartbeat signal, but error of variation of the heartbeat can be increased due to the distortion obtained when applying classical filters. Fast Fourier transform rapidly converts a signal from time domain to frequency domain. Hence, the heartbeat signal is converted to the frequency domain, and then the frequency corresponding to the rate of the heartbeats is extracted by choosing the maximum amplitude between 1 and 2 Hz. FFT gives accurate results but an extra error may occur because real frequency may not match the FFT frequency, the power spectrum is spreading at the adjacent frequencies. In order to track the variation of the *HR* over time, the Short-Time Fourier Transform is proposed (STFT). This technique is based on applying the Fourier transform over portions of the signal, namely windows, instead of applying the Fourier transform over the whole signal. This allows analyzing the signal in the time and frequency domain. Short time window results in high resolution in time, and poor resolution in frequency, while large window results in poor resolution in time, but high resolution in frequency. The drawback of the STFT having unchanged window length results in dilemma of resolution when the frequency becomes low; the drawback has been overcome with the wavelet transform [94].

#### **3.5.1. Overview of the wavelet transform**

The principles of wavelet transform consist of splitting the signal into many signals; each of them corresponds to an interval of frequencies. There are two types of wavelets: continuous wave transform (CWT) and discrete wavelet transform (DWT). DWT is interesting in the context of fast and non-redundant transforms [95]. The DWT is the

signal processing tool used in order to extract the heartbeat signal, hence, the heartbeat rate, from the cardiopulmonary signal. The DWT ( $W_{j,k}$ ) of a signal  $f(t)$  is given by the scalar product of  $f(t)$  with the scaling function (i.e. the wavelet basis function)  $\phi(t)$  which is scaled and shifted:

$$W_{j,k} = \langle f(t), \phi_{j,k}(t) \rangle = \int_{-\infty}^{+\infty} f(t) \phi_{j,k}(t) dt \quad (3.2)$$

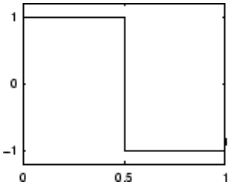
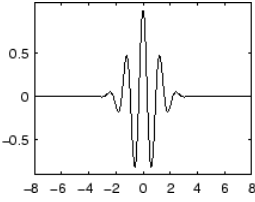
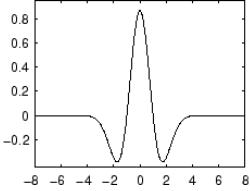
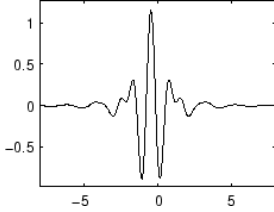
The basis function is given by:

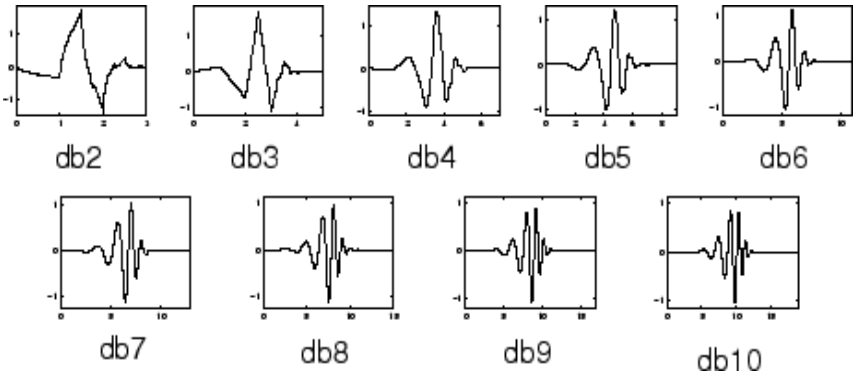
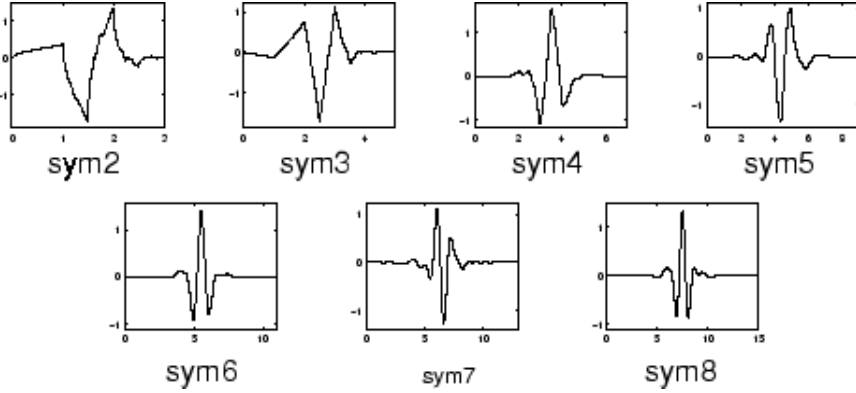
$$\phi_{j,k}(t) = 2^{-j/2} \phi(2^{-j}t - kT_s) \quad (3.3)$$

where  $j$  is the  $j^{th}$  decomposition level or step and  $k$  is the  $k^{th}$  wavelet coefficient at the  $j^{th}$  level [96]. Wavelet has several families like Daubechies, Coiflets, Symlets, etc. The difference between wavelet families makes compromise between how compactly they are localized in time and how smooth they are. Within each wavelet family, the number of coefficients and the iterations used in the wavelets are classified as subclasses [96]. The families vary according to several criteria like symmetry, orthogonality or bi-orthogonality, length of the support of the mother wavelet, number of vanishing moments and resulting analysis and existence of a corresponding scaling function [97]. Table 3.6 presents the different types of wavelet families.

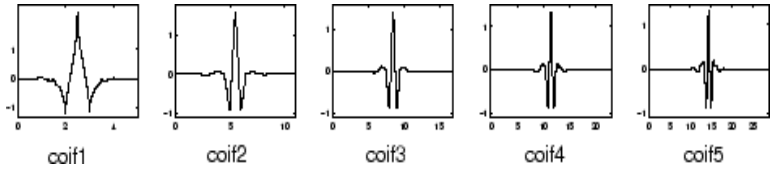
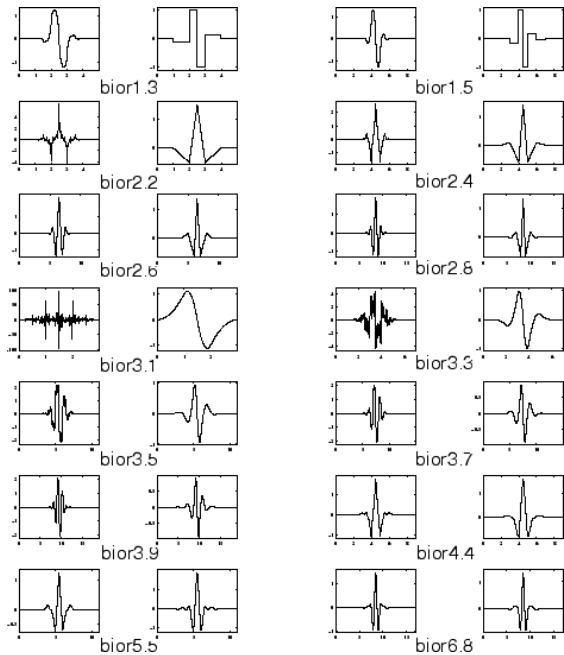
Table 3.6. Wavelet type description

Wavelet families	Description
Haar (haar)	<ul style="list-style-type: none"> <li>- First and simplest wavelet type proposed by Alfred Haar in 1909.</li> <li>- Has the shortest support among all orthogonal wavelets.</li> <li>- Resembles a step function.</li> <li>- Represents the Daubechies 1.</li> <li>- <u>Advantage:</u> 1) Memory efficient, computationally cheap and fast. 2) Good choice to detect time localized information.</li> <li>- <u>Disadvantage:</u> Is not well adapted to approximating smooth</li> </ul>

	<p>functions because it has only one vanishing moment.</p> 
<p>Morlet (morl)</p>	<ul style="list-style-type: none"> <li>- Suitable for continuous analysis.</li> <li>- No scaling function associated with it.</li> </ul> 
<p>Mexican Hat (mexh)</p>	<ul style="list-style-type: none"> <li>- No scaling function.</li> <li>- Derived from a function that is proportional to second derivative of Gaussian function.</li> </ul> 
<p>Myer (meyr)</p>	<ul style="list-style-type: none"> <li>- Scaling function is defined in the frequency domain.</li> </ul> 
<p>Daubechies (dbN)</p>	<ul style="list-style-type: none"> <li>- <math>N</math> refers to the number of vanishing moments. It is equal with half of the length of the support in the case of Daubechies family of mother wavelets.</li> <li>- It is a family of orthogonal wavelets characterized by a maximal number of vanishing moments for some given support's length.</li> <li>- Corresponding to each mother wavelets from this class, there is a</li> </ul>

	<p>scaling function (also called father wavelet) which generates an orthogonal Multi Resolution Analysis (MRA).</p> <p><u>Advantage:</u> 1) Most type used between wavelet types.</p> <p>2) Discrete wavelet analysis practicable.</p> 
Symlets (symN)	<ul style="list-style-type: none"> <li>- Modification of the Daubechies family and known as the Daubechies least asymmetric mother wavelets.</li> <li>- Compact, orthogonal, continuous, but only nearly symmetric mother wavelets.</li> <li>- Construction of symlets is very similar to the construction of Daubechies wavelets, but the symmetry of Symlets is stronger than the symmetry of Daubechies mother wavelets.</li> </ul> 
Coiflets (coifN)	<ul style="list-style-type: none"> <li>- Built by db that has <math>2N</math> moments.</li> <li>- Coiflets are designed by Ingrid Daubechies and named in the honor of Ronald Coifman to be more symmetrical than the Daubechies mother wavelet.</li> </ul>



	<ul style="list-style-type: none"> <li>- Support of size <math>3p - 1</math> instead of <math>2p - 1</math> like Daubechies.</li> </ul> 
<p style="text-align: center;">Splines biorthogonal wavelets (biorNr, Nd)</p>	<ul style="list-style-type: none"> <li>- Need two wavelets for signal reconstruction.</li> <li>- Needs two wavelets for the reconstruction: on the left side is for decomposition and the right side is for the reconstruction.</li> <li>- Wavelets exhibit the property of linear phase, which is needed for signal and image reconstruction.</li> <li>- Designing biorthogonal wavelets allows additional degrees of freedoms than orthogonal wavelets [96].</li> <li>- Reverse biorthogonal wavelets family is obtained from the biorthogonal wavelet pairs. Both biorthogonal and reverse biorthogonal wavelet families are compactly supported biorthogonal spline wavelets for which symmetry and exact reconstruction are possible with Finite Impulse Response (FIR) filters [97].</li> </ul> 

The choice of the suitable wavelet family depends on data. DWT decomposes the signal into approximation ‘A’ and detail information ‘D’. These are computed by successive low-pass and high-pass filtering of the discrete time-domain signal where ‘A’ represents the low-pass filtered signal and ‘D’ represents the high-pass filtered signal [96]. The decomposition is repeated to increase the frequency resolution. The DWT principle is resumed in Figure 3.5.

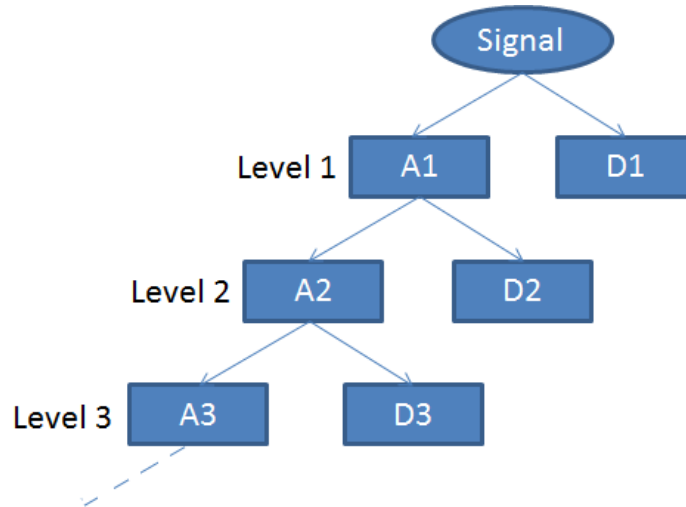


Figure 3.5. Wavelet decomposition

In general, if  $n$  is the decomposition number,  $A_n$  contains frequencies between 0 and  $f_s/2^{n+1}$  and  $D_n$  contains frequencies between  $f_s/2^{n+1}$  and  $f_s/2^n$ , where  $f_s$  is the sampling frequency and  $N$  is the decomposition level ( $n = 1, 2 \dots N$ ).

Recall that the decomposed signal can be reconstructed using the following relation:

$$S_{reconstructed} = A_N + D_N + D_{N-1} + \dots + D_1 \quad (3.4)$$

### 3.5.2. Re-sampling method

Re-sampling is required whenever it is necessary to convert sampled data from one sample rate to another. It is a calculation of a discrete set of points of a signal using another discrete set of known points of the signal. Signal re-sampling is generally implemented by two processes: It firstly applies the interpolation of the given discrete signal to a continuous and secondly sampling the interpolated signal at the new coordinate points [98]. The interpolation used in this thesis is linear. More the sampling

frequency increases will be heavier. If it decreases, the data will not be affected if the Shannon theorem is respected. The heartbeat rate for an adult is between 60 and 120 beats per minute, hence the frequency of the heartbeat is located between 1 and 2 Hz. A re-sampling method is necessary in order to obtain the decomposition of the signal in the appropriate frequency band. Thus, converting the sampling frequency from 666.7 Hz to 512 Hz results in obtaining frequencies between 0 and 1 Hz at the 8<sup>th</sup> approximation. The bandwidth of the 8<sup>th</sup> approximation is between 0 and  $f_s / 2^9$ . Eliminating the 8<sup>th</sup> approximation from the reconstructed signal results signal band between 1 to 256 Hz.

### 3.5.3. Choice of the wavelet type

Several wavelet families have been tested in MATLAB for the measurement performed at different sides of the person under test and for all the operating frequencies. As not all the wavelet families fulfill the properties of the desired signal, the wavelet family has to be chosen to be as close as possible to the analyzed signal to give a better reconstruction with fewer decomposition levels [99]. The choice of a suitable wavelet is based on the perfect reconstruction of the power system signal. The error between the original signal and the reconstructed signal should be the smallest for perfect reconstruction. The Root Mean Square Error (*RMSE*) is the indicator to measure the error between the original signal  $x(n)$  and the reconstructed signal  $\hat{x}(n)$ . It is given by the equation:

$$RMSE = \sqrt{\frac{\sum_{n=0}^{N-1} |x(n) - \hat{x}(n)|^2}{N}} \quad (3.5)$$

where  $N$  is the samples number of the signal  $x$ . The root mean square error is calculated in all available signals for different wavelet decompositions; then the mean of the *RMSE* of all available signals is calculated for each wavelet type according to the following equation:

$$RMSE \text{ mean}_{\text{wavelet type}} = \frac{\sum_{p=1}^4 \sum_{q=1}^3 RMSE \text{ of signal}_{pq} \text{ wavelet type}}{3 \times 4} \quad (3.6)$$

where  $p$  is the positions index and  $q$  is the index of the operating frequencies. Four positions are measured:  $p = 1$  for the front side position,  $p = 2$  for the back side position,

$p = 3$  for the right side position, and  $p = 4$  for the left side position. Three operating frequencies are considered during measurements:  $q = 1$  for operating frequency 2.4 GHz,  $q = 2$  for 5.8 GHz, and  $q = 3$  for 10 GHz. Mean *RMSE* of each wavelet are calculated. Smallest mean *RMSE* results for each wavelet family are chosen, hence Bior2.4, Rbio1.3, Sym5, Db5, Coif3, Dmey are chosen. Table 3.7 presents the mean of *RMSE* for each chosen wavelet. As shown, Bior 2.4 has the smallest mean *RMSE* value.

Table 3.7. Mean *RMSE*

Wavelet type	Mean <i>RMSE</i>
Bior 2.4	$6.08 \cdot 10^{-14}$
Rbio 1.3	$9.76 \cdot 10^{-14}$
Sym5	$6.67 \cdot 10^{-12}$
Coif3	$2.36 \cdot 10^{-11}$
Db5	$1.1 \cdot 10^{-10}$
Dmey	$3 \cdot 10^{-4}$

Figure 3.6 presents the flowchart of the proposed algorithm for finding the most suitable wavelet family.

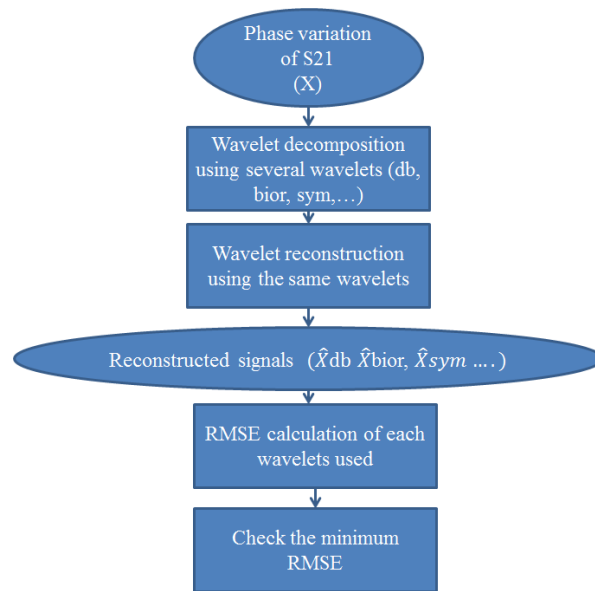


Figure 3.6. Flowchart of the proposed algorithm for finding the most suitable wavelet family

### 3.5.4. Application of wavelets

When applying the wavelet technique, the signal is decomposed to 8 decompositions, the  $n^{th}$  one has frequencies between  $f_s / 2^{n+1}$  and  $f_s / 2^n$ . Figure 3.7 presents the wavelet decompositions using Bior 2.4 to measurements taking from the face and at the operating frequency 5.8 GHz.

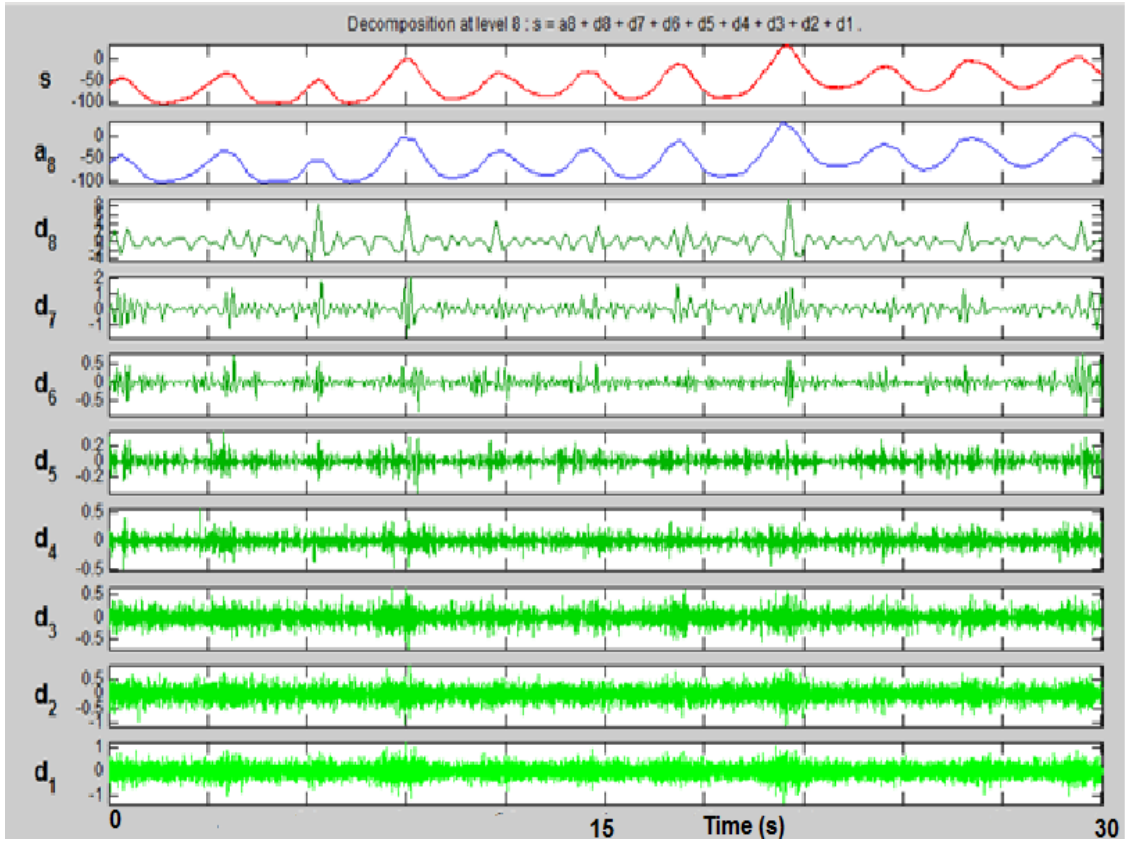


Figure 3.7. Wavelet decompositions using Bior 2.4

As said, respiratory amplitude is higher than heartbeat amplitude, hence the role of processing techniques is to eliminate respiratory signal from the cardio-respiratory signal. Respiratory frequency is between 0.2 and 0.34 Hz, hence  $A_8$  that contains this frequency band is excluded from  $S_{reconstructed}$ . Heartbeat frequency that has frequencies between 1 and 2 Hz is present.  $S_{D18}$  is given by:  $S_{D18} = S_{reconstructed} - A_8$ . It is named  $S_{D18}$  because it contains all decompositions between 1 and 8. Figure 3.8 presents the diagram of the signal  $S_{D18}$ .

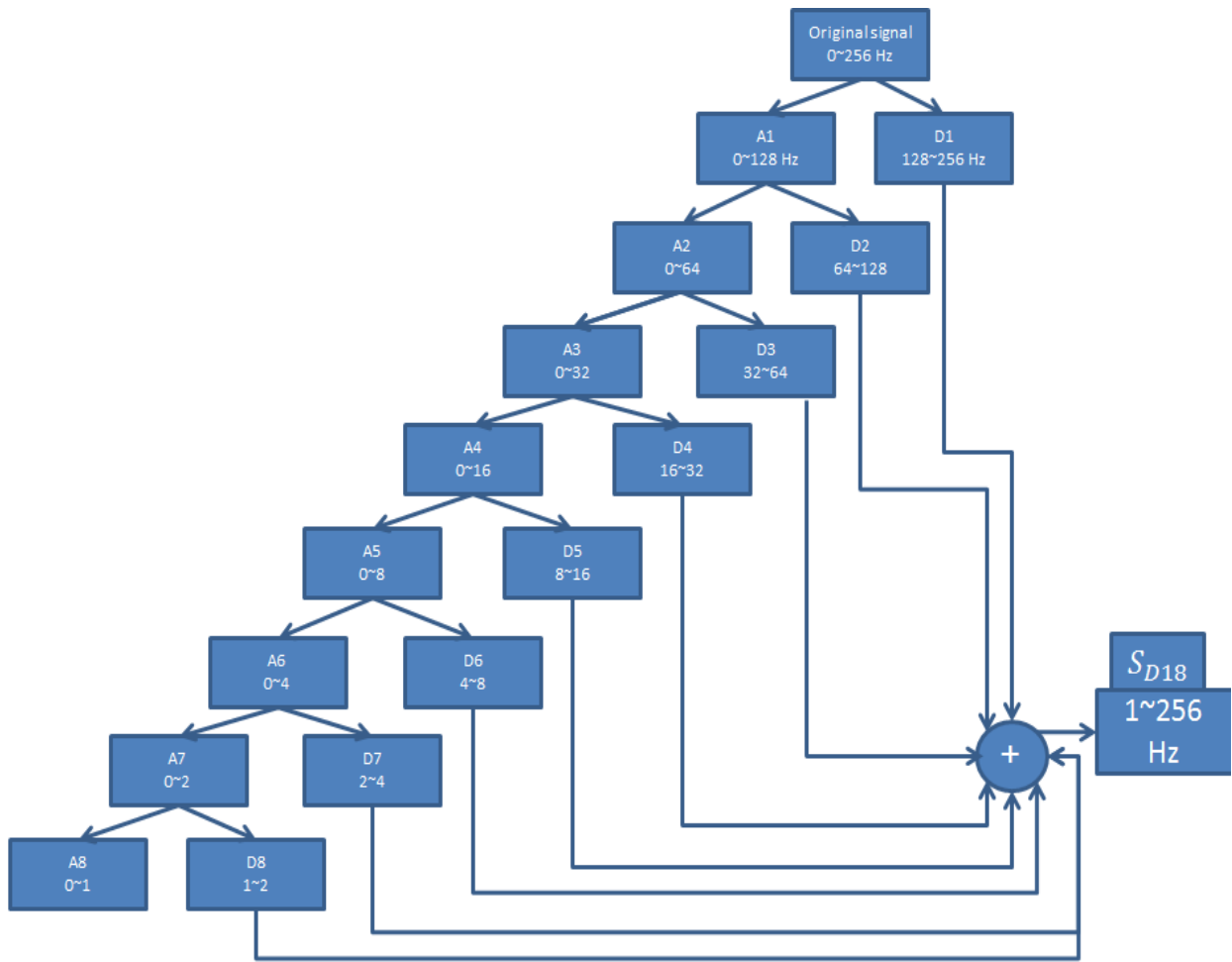


Figure 3.8. Addition of the decomposition 1 till 8

Figure 3.9 shows the  $S_{D18}$  signal at 4 sides and at operating frequency 5.8 GHz. As seen,  $S_{D18}$  contains heartbeat signal and noise; hence smoothing should be applied to  $S_{D18}$  in order to attenuate noise and extract heartbeat signal.

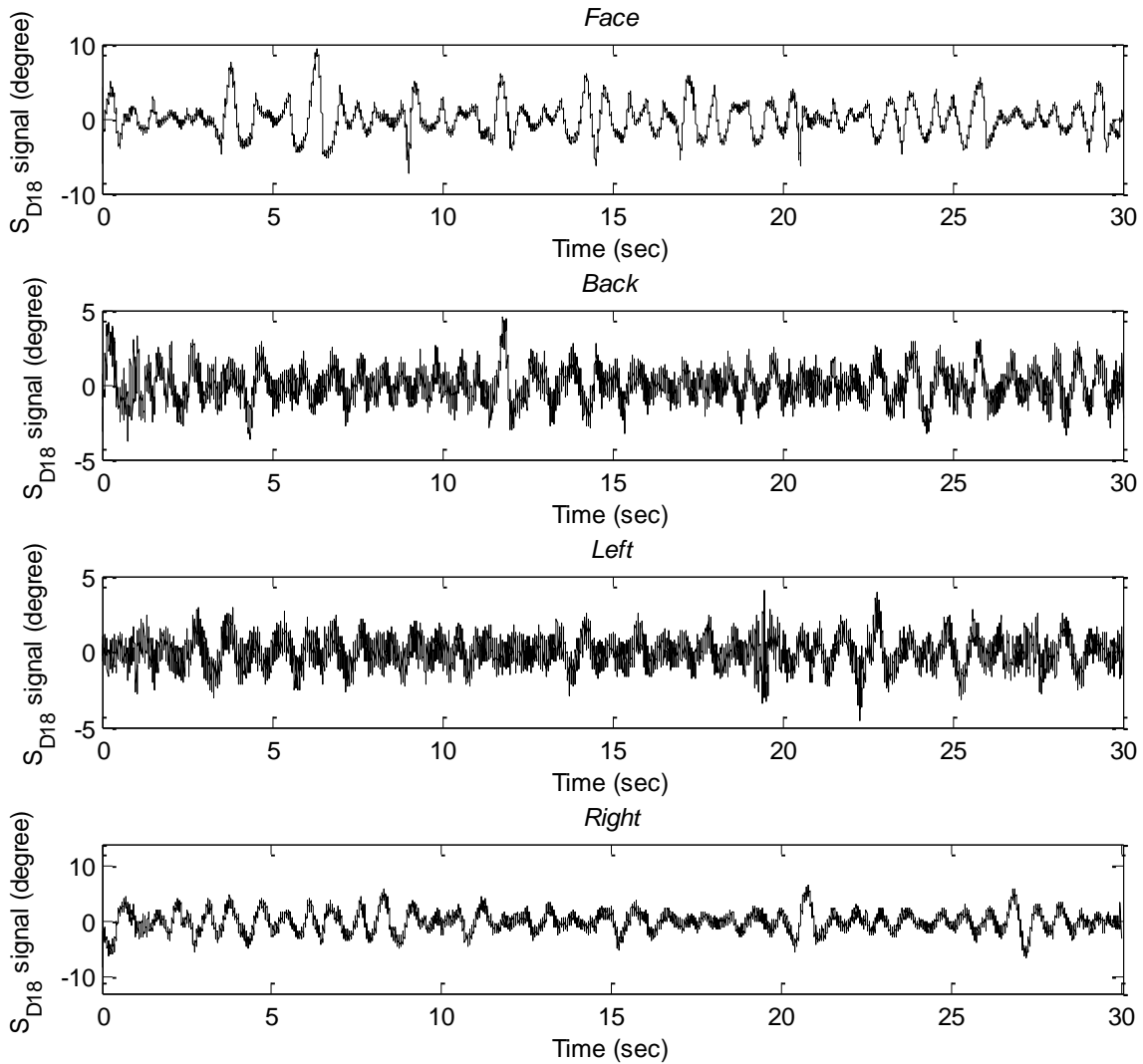


Figure 3.9.  $S_{D18}$  signal at different sides at 5.8 GHz

### 3.5.5. Application of smoothing

As seen, the phase of  $S_{D18}$  is noisy, hence peak detection will be faulty. Smoothing is applied to eliminate the noise. The signal is smoothed using a MATLAB function called “Smooth”, it is based on moving average filter.  $n$  is the smoothing window length and is

odd. When  $n$  is low, the noise does not totally disappear. For a high value of  $n$ , some peaks of the heartbeat signal may disappear. That's why a compromise should be taken into consideration between the disappearing of noise and the appearing of the heartbeat signal. Several values of  $n$  are tested to choose the better one:  $n = 99, 199$  and  $299$ . Figure 3.10 presents 10 s of  $S_{D18}$  signal using several smoothing numbers.  $n = 199$  gives better smoothing when comparing with the original signal. At 99, the 8<sup>th</sup> and 10<sup>th</sup> peaks are noisy; this may increase the error when applying peak detection. At 299, the 2<sup>nd</sup> and the 10<sup>th</sup> peaks are disappeared; hence  $n$  is considered as big. The length of the window ' $n$ ' is chosen to be 199 as an optimal value for higher accuracy detection.

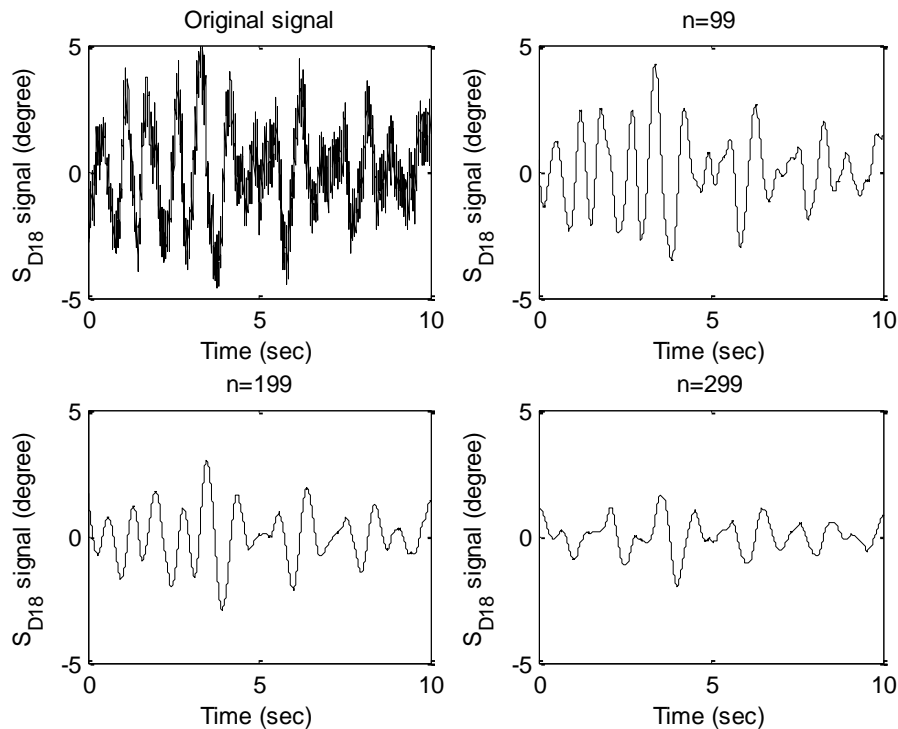


Figure 3.10.  $S_{D18}$  smoothing using  $n = 199, 299$  and  $399$

Then peak detection technique is applied in order to extract the heartbeat rate from  $S_{D18}$  signal. Figure 3.11 presents the flowchart of the proposed algorithm for extracting the heartbeat rate and heartbeat rate error using wavelets decomposition. Figure 3.12-15 present the smoothed  $S_{D18}$  signal issued from the front, back, left and right sides of the person respectively, at 5.8 GHz using several types of wavelets.



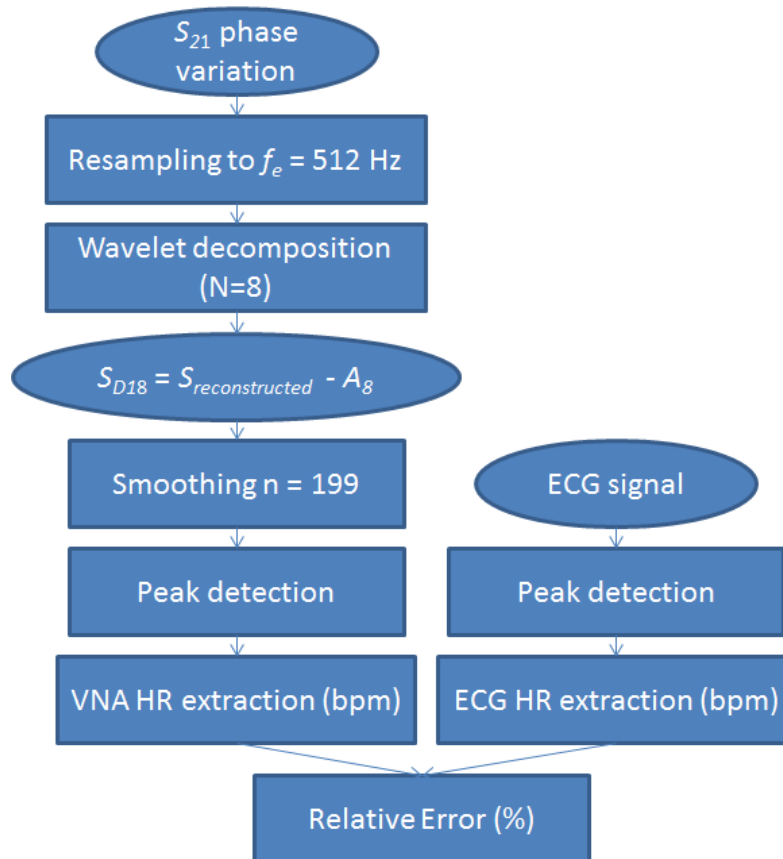


Figure 3.11. Flowchart of the proposed algorithm for extracting the heartbeat rate and heartbeat rate error using wavelets decomposition

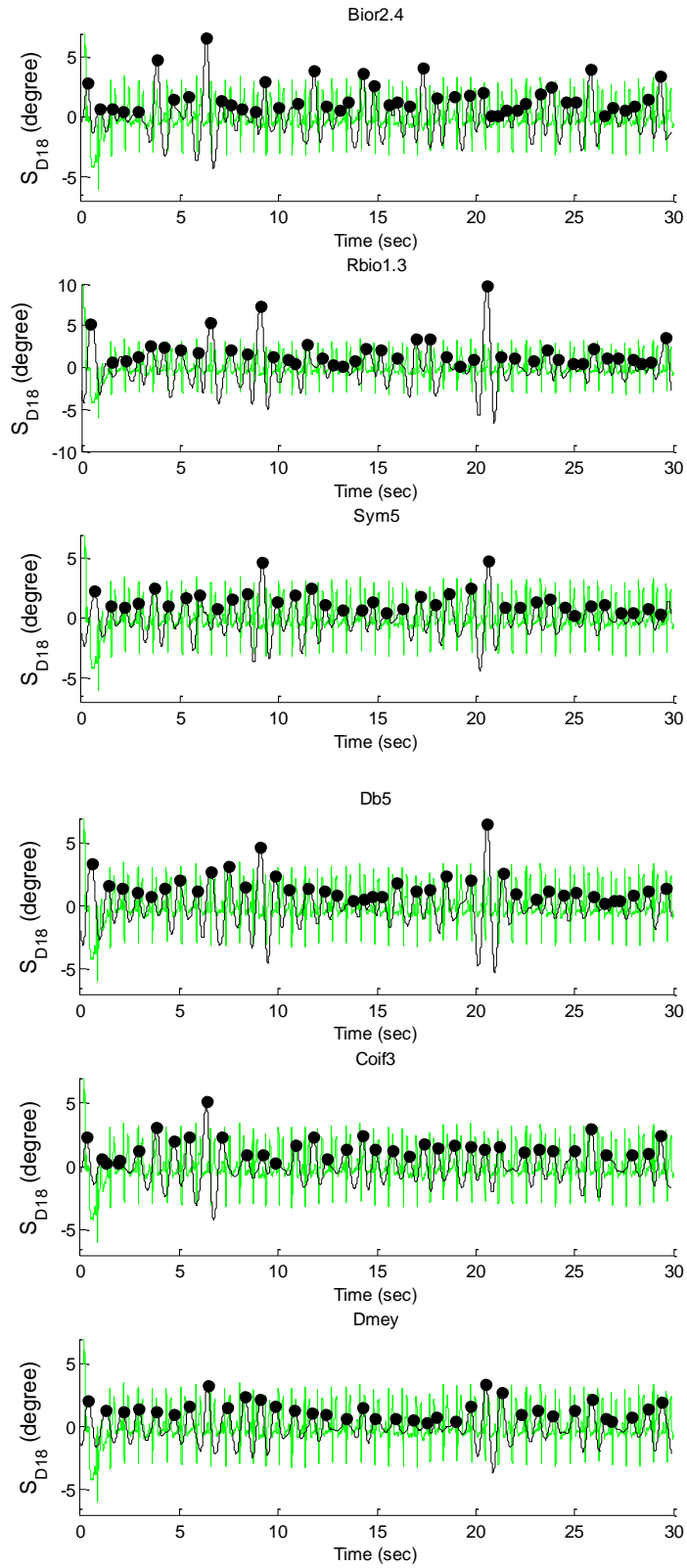


Figure 3.12. Smoothed  $S_{D18}$  taken from the front side using several wavelets at 5.8 GHz and 0 dBm (Black), ECG signal (Green)

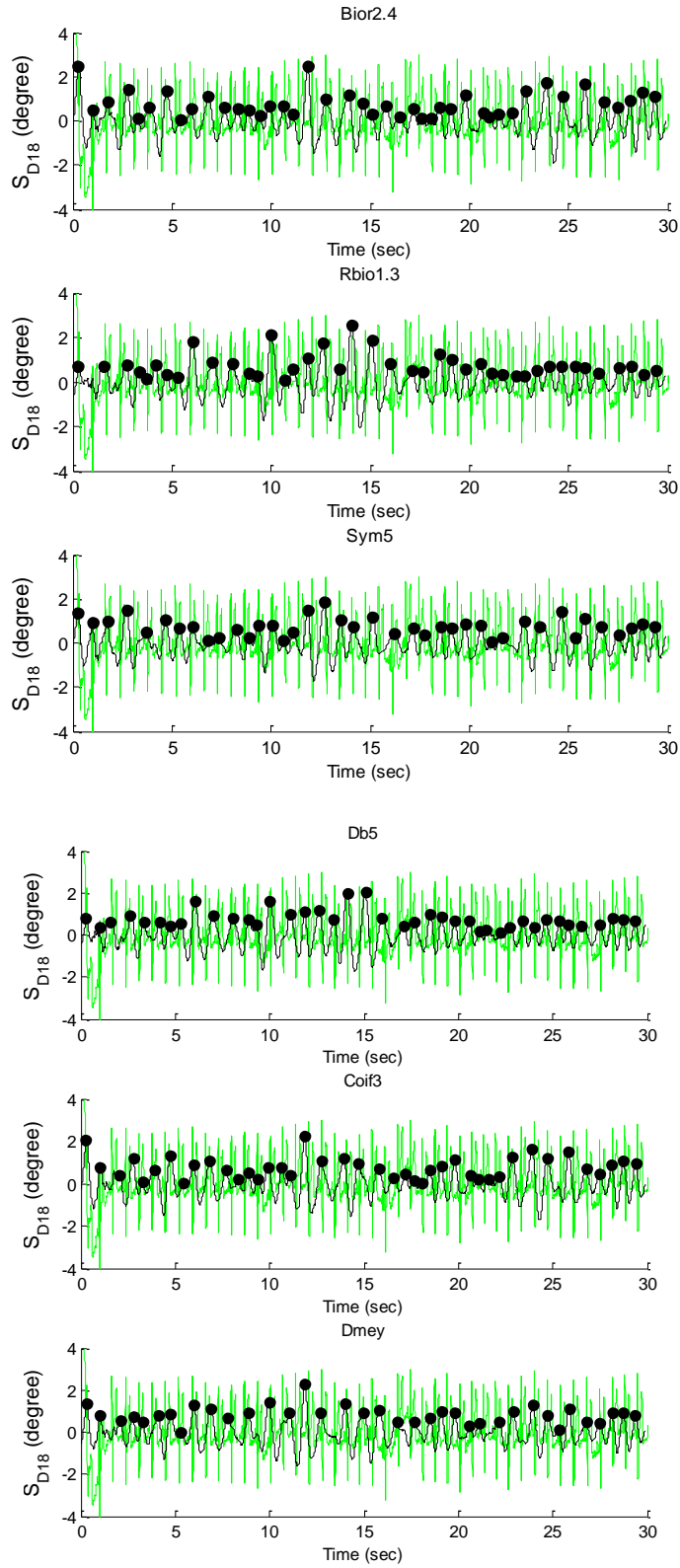


Figure 3.13. Smoothed  $S_{D18}$  taken from the back side using several wavelets at 5.8 GHz and 0 dBm (Black), ECG signal (Green)

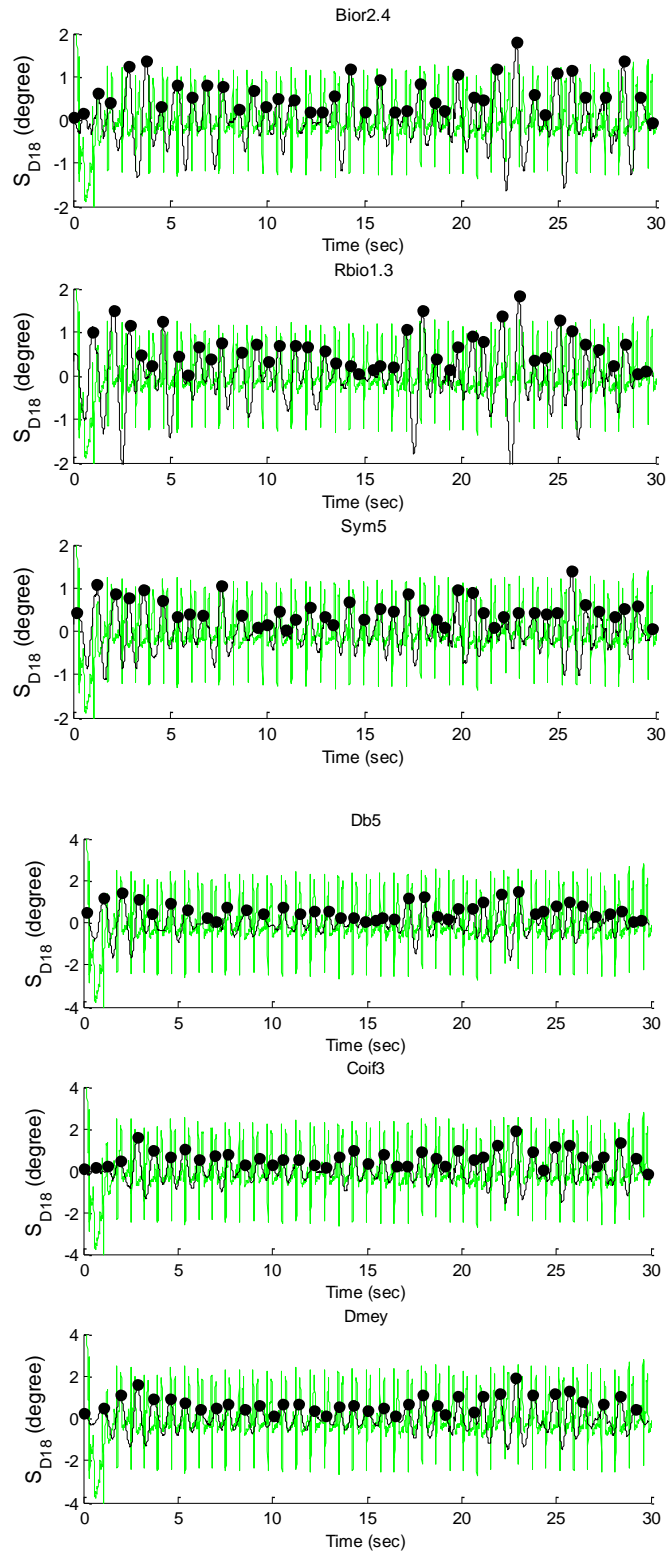


Figure 3.14. Smoothed  $S_{D18}$  taken from the left side using several wavelets at 5.8 GHz and 0 dBm (Black), ECG signal (Green)

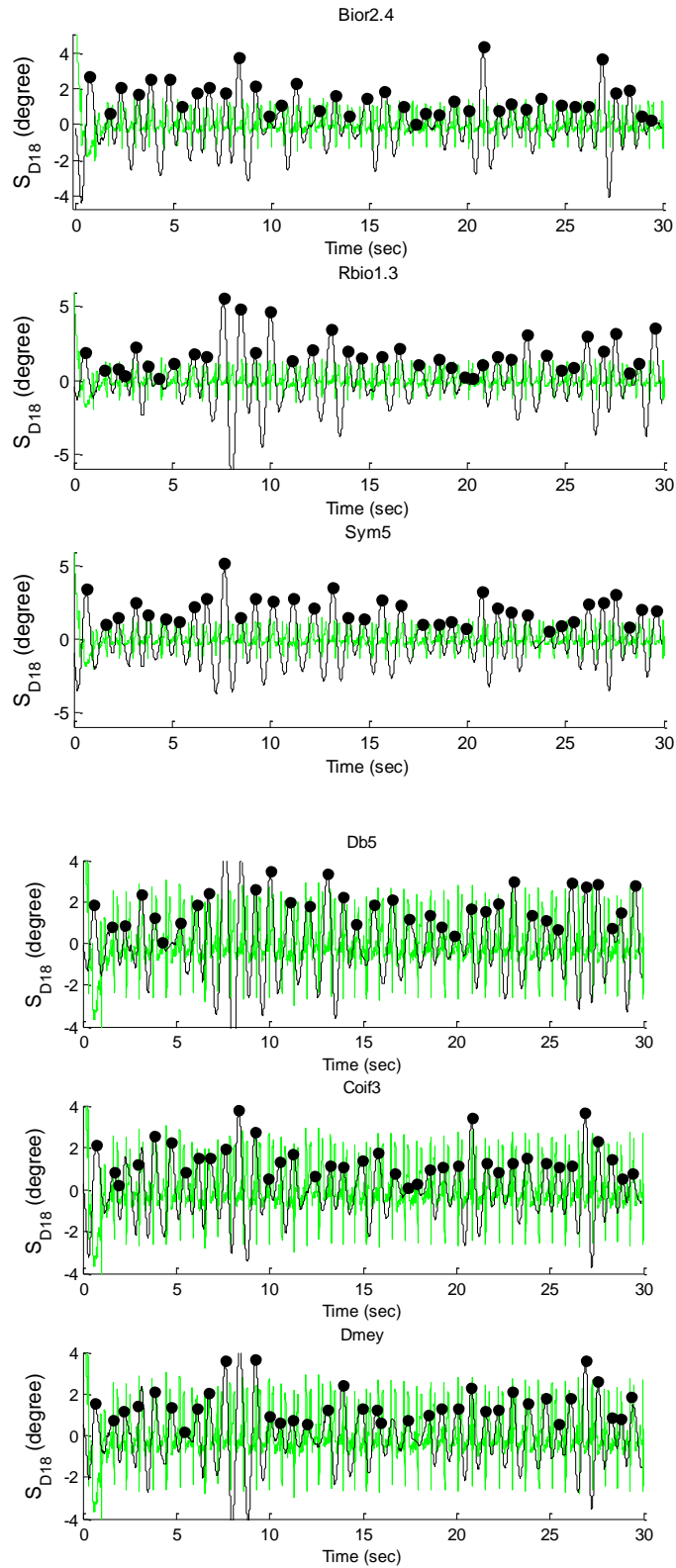


Figure 3.15. Smoothed  $S_{D18}$  taken from the right side using several wavelets at 5.8 GHz and 0 dBm (Black), ECG signal (Green)

The peaks of the smoothed  $S_{D18}$  are not clear like ECG peaks, but they are still detectable. In Figure 3.12, Bior 2.4 wavelet is applied on the  $S_{2l}$  phase variation taken from the front of the person at 5.8 GHz, 46 peaks are obtained in 29 sec. When applying Rbio1.3, 44 peaks are obtained in 29.11 sec. When applying Sym5, 39 peaks are obtained in 28.96 sec. When applying Db5, 39 peaks are obtained in 29.06 sec. When applying Coif3, 35 peaks are obtained in 28.81 sec. Finally when applying Dmey, 35 peaks are obtained in 29.52 sec. Hence the heartbeat rates obtained when applying Bior2.4, Rbio1.3, Sym5, Db5, Coif3 and Dmey for the signal taken from the front of the person are 93, 89, 79, 78, 71 and 69 bpm respectively.

In Figure 3.13, Bior 2.4 wavelet is applied on the  $S_{2l}$  phase variation taken from the back of the person at 5.8 GHz, 43 peaks are obtained in 29.1 sec. When applying Rbio1.3, 42 peaks are obtained in 29.1 sec. When applying Sym5, 40 peaks are obtained in 29.08 sec. When applying Db5, 41 peaks are obtained in 29.08 sec. When applying Coif3, 42 peaks are obtained in 29.1 sec. Finally when applying Dmey, 37 peaks are obtained in 29.02 sec. Hence the heartbeat rates obtained when applying Bior2.4, Rbio1.3, Sym5, Db5, Coif3 and Dmey for signal taken from the back of the person are 87, 85, 80, 83, 85 and 74 bpm respectively.

In Figure 3.14, Bior 2.4 wavelet is applied on the  $S_{2l}$  phase variation taken from the left of the person at 5.8 GHz, 39 peaks are obtained in 29.18 sec. When applying Rbio1.3, 43 peaks are obtained in 28.93 sec. When applying Sym5, 43 peaks are obtained in 29.62 sec. When applying Db5, 41 peaks are obtained in 29.27 sec. When applying Coif3, 40 peaks are obtained in 29.18 sec. Finally when applying Dmey, 37 peaks are obtained in 29.36 sec. Hence the heartbeat rates obtained when applying Bior2.4, Rbio1.3, Sym5, Db5, Coif3, Dmey for signal taken from the left of the person are 78, 87, 85, 82, 80 and 74 bpm respectively.

Finally, in Figure 3.15, Bior 2.4 wavelet is applied on the  $S_{2l}$  phase variation taken from the right of the person at 5.8 GHz, 39 peaks are obtained in 28.7 sec. When applying Rbio1.3, 39 peaks are obtained in 27.58 sec. When applying Sym5, 37 peaks are obtained in 29.03 sec. When applying Db5, 37 peaks are obtained in 28.94 sec. When applying Coif3, 39 peaks are obtained in 28.7 sec. Finally when applying Dmey, 38 peaks are

obtained in 28.76 sec. Hence the heartbeat rates obtained when applying Bior2.4, Rbio1.3, Sym5, Db5, Coif3, Dmey for signal taken from the right of the person are 79, 83, 74, 74, 75 and 77 bpm respectively. Same procedure of heartbeat rate extraction is applied at 2.4 and 5.8 GHz.

Concerning the ECG signal taken simultaneously with the VNA at 5.8 GHz, 42 peaks are obtained in 28.8 sec when the VNA measures are taken from the front of the person; hence the heartbeat rate of ECG is 85 bpm. 43 peaks are obtained in 28.51 sec when VNA measurements are taken from the back; hence the heartbeat rate of ECG is 88 bpm. 40 peaks are obtained in 28.57 sec where measurements are taken from the left; hence the heartbeat rate of ECG is 82 bpm. Finally, 44 peaks are obtained in 28.99 sec when measurements are taken from the right; hence the heartbeat rate of ECG is 89 bpm.

### 3.6. Results and discussion

This section presents the results obtained upon measuring the cardiopulmonary signals using a VNA and for different sides of the person under test. The separation of respiration and heartbeat signals is achieved upon applying several wavelet transforms families; then heartbeat rate of the person is calculated then compared to that extracted from the ECG. Recall that the relative error between the heartbeat rate of VNA system and heartbeat rate of ECG is calculated using the following equation:

$$Error = 100 \times \left| \frac{HR_{VNA} - HR_{ECG}}{HR_{ECG}} \right| \quad (3.7)$$

Hence the relative errors between the heartbeat rate of VNA system and heartbeat rate of ECG when applying Bior2.4, Rbio1.3, Sym5, Db5, Coif3, Dmey on VNA signal taken from a person setting in front of the system are 9, 5, 7, 8, 16 and 19 % respectively. The relative errors between the heartbeat rate of VNA system and heartbeat rate of ECG when applying Bior2.4, Rbio1.3, Sym5, Db5, Coif3, Dmey on VNA signal taken from the back at 5.8 GHz are 1, 3, 9, 6, 3 and 16 % respectively. The relative errors between the heartbeat rate of VNA system and heartbeat rates of ECG when applying Bior2.4, Rbio1.3, Sym5, Db5, Coif3, Dmey on VNA signals taken from the left of the person are 5, 6, 4, 0, 2 and 10 % respectively. Finally, The relative errors between the heartbeat rate

of VNA system and heartbeat rate of ECG when applying Bior2.4, Rbio1.3, Sym5, Db5, Coif3, Dmey on VNA signal taken from the right of the person are 13, 7, 17, 17, 16 and 13 % respectively. Same procedure is done at 2.4 GHz and 10 GHz. Table 3.8 shows the relative error calculated for the different wavelet transforms to each of the performed measurement.

Table 3.8. Relative error between  $HR_{VNA}$  and  $H_{RECG}$

Side	Frequency(Hz)	Bior2.4	Rbior1.3	Sym5	Db5	Coif3	Dmey
<b>Front</b>	2.4	12	21	8	13	7	3
	5.8	9	5	7	8	16	19
	10	9	4	6	6	11	10
<b>Back</b>	2.4	4	2	4	4	2	1
	5.8	1	3	9	6	3	16
	10	1	2	6	1	3	6
<b>Left</b>	2.4	2	2	1	4	1	6
	5.8	5	6	4	0	2	10
	10	2	5	13	3	7	7
<b>Right</b>	2.4	7	4	9	2	10	11
	5.8	11	7	17	17	16	13
	10	10	14	13	12	10	13

As shown in table, most of the wavelet transforms shows the ability to extract the heartbeat signal from the cardiopulmonary signal when using different operating frequencies and from all sides of the person under test. The lowest number of relative errors that exceeds the 10% is obtained when using the wavelet type Bior2.4. Recall that the type of wavelet having lowest *RMSE* is the most suitable wavelet; hence these results confirm that the Bior 2.4 is the wavelet that gives the best results. Concerning the positions, it can be noticed that the right position gives the highest relative error (> 10%).



This is due to the fact that the far side from the heart position is less affected by heart beating. In addition, these results show that back position has the lowest relative error. All tested operating frequencies (2.4, 5.8 and 10 GHz) show the possibility to track the cardiopulmonary signals from all sides. Concerning the frequencies, additional measures should be done to confirm that the relative error decreases with the increase of the operating frequency.

In addition, a comparison between classical filtering and wavelets is done. The filter, as described in chapter 2, is a Butterworth high pass filter with order 4 with cut-off frequency of 0.9 Hz, then smoothing with  $n = 199$  is used. Bior 2.4 wavelet is chosen because it is most suitable wavelet type for the current measures. The heartbeat rate is calculated using these two different signal processing techniques, and then relative errors are extracted. Figure 3.16 shows a comparison between relative errors after applying wavelets and classical filtering applied to signals obtained from the front, back, left and right sides of the person under test.

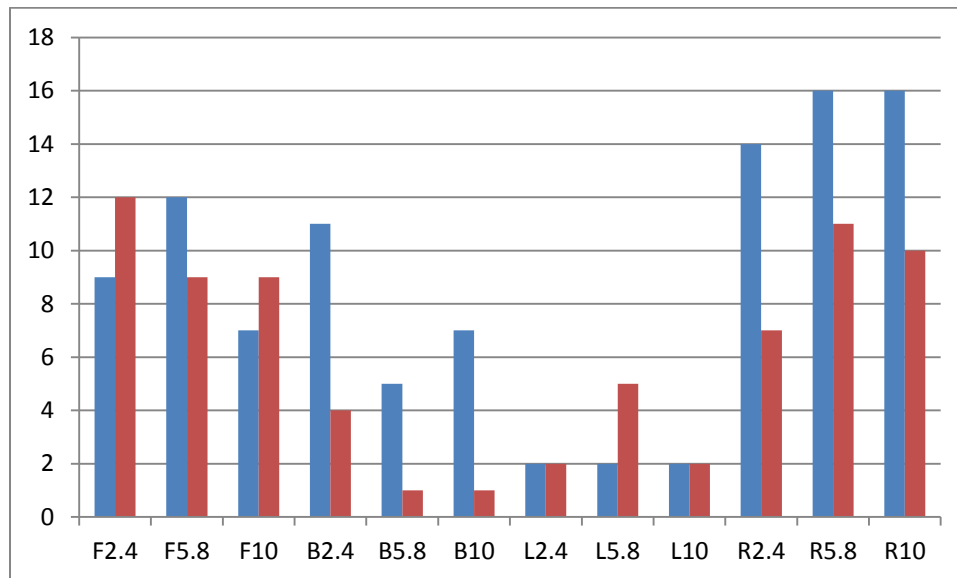


Figure 3.16. Comparison between relative errors after applying classical filtering (blue) and wavelets (red) taking from 4 sides

It is remarkable that, in general, wavelets have less relative errors than filtering. It can be explained by the presence of distortion at the transitional regime when using filtering, that is not present when using wavelet.

### 3.7. $S_{D18}$ pass band reducing

In this study, the  $A_8$  is subtracted from the reconstructed signal to eliminate the respiratory signal and keep all signals above 1 Hz including the heartbeat signal; hence all decompositions from 1 to 8 are kept. After that, smoothing method is applied to reduce the noise.

In fact, heartbeat signal is situated only in a small part of the bandwidth of the  $S_{D18}$  and not in all its bandwidth situated between 1 and 256 Hz. In this part, several decompositions are eliminated to reduce the bandwidth of the signal and keep the effective signal; hence  $D_8$ ,  $D_8+D_7$ ,  $D_8+D_7+D_6$ , ...  $D_8+D_7+D_6+D_5+D_4+D_3+D_2+D_1$  are extracted and smoothed, and then relative errors between the ECG and these signals are calculated.

As result,  $D_8+D_7$  gives results better than  $D_8$ ,  $D_8+D_7+D_6$  gives results better than  $D_8+D_7$ . Finally, from  $D_8+D_7+D_6$ , the relative errors are the same.

As conclusion, the band between 1 and 8 Hz is sufficient to extract the heartbeat rate successfully without adding frequencies above this marge. Also, a band a bit wider than [1 Hz 2 Hz] must be extracted to have a small error. In other words, the details in the higher bands help to better describe the heartbeat signal; hence the heartbeat signal is not a pure sinusoid.

### 3.8. Conclusion

This study presents the microwave system used in order to detect the chest motion, which contains information about respiration and heartbeat. The system has been tested at different operating frequencies (2.4, 5.8 and 10 GHz) with radiated power 0 dBm, on a person placed at 1 m from the system while breathing normally for 30 s, and in different sides for the subject: front, back, left, and right sides. The measurements have been performed on a 54 years old person. ECG signals have been measured simultaneously with the microwave system. After resampling, wavelet transform has been used for processing cardiopulmonary signals in order to extract the heartbeat signal. The elimination of the 8<sup>th</sup> approximation from the reconstructed signal having  $f_s=512$  Hz has been done in order to eliminate the respiratory signal. Smoothing method has been

applied to reduce noise followed by peak detection method. Bior2.4 showed the highest performance in providing the heartbeat signal in time domain where high accuracy has been obtained in terms of heartbeat rate; the relative error has been less than 4% when measures were taken from the back at 2.4, 5.8 and 10 GHz, less than 5 % when measures have been taken from the left at 2.4, 5.8 and 10 GHz, less than 9 % when measures have been taken from the front at 5.8 and 10 GHz and finally less than 10% when measures have been taken from the right at 2.4 and 10 GHz. The proposed system and signal processing technique showed the possibility of measuring the heartbeat rate of the subject at different positions with radiated power 0 dBm and different frequencies (2.4, 5.8 and 10 GHz). In addition, wavelet technique showed better results compared to classical filters. The next work will be about performing measurements behind a wall, as well as for a person in motion.

<b>Chapter 4 Heartbeat measurement based on several scenarios .....</b>	<b>132</b>
<b>4.1. Introduction.....</b>	<b>132</b>
<b>4.2. Measurements behind a wall .....</b>	<b>133</b>
4.2.1. Effect of barriers on wave propagation.....	134
4.2.2. Measurement setup.....	135
4.2.3. Signal processing and results.....	136
<b>4.3. Single antenna system .....</b>	<b>139</b>
4.3.1. Comparison between one and two antennas systems for a holding breath person .....	140
4.3.2. Results for a normally breathing person using single-antenna VNA system.....	149
<b>4.4. Models and processing of a moving person .....</b>	<b>151</b>
4.4.1. Modeling of a chest motion when moving forward .....	152
4.4.2. Phase variation of chest movement of a walking person at 20 GHz	161
4.4.3. Signal processing and results.....	162
<b>4.5. Conclusion .....</b>	<b>164</b>

## **Chapter 4 Heartbeat measurement based on several scenarios**

### **4.1. Introduction**

Previous researches have measured the heartbeat signal directly in front of the radar without the presence of a barrier or any possible movement of the patient. In fact, the main purpose of the research is to monitor the heartbeat signal inside a patient's home, where he may move from a room to another. On the other hand, most researches that measured the heartbeat signal behind a wall used UWB radar [100]. In addition, measurements using CW behind a wall were performed for respiratory signal extraction at 24 GHz and at distances below 2 m [101]. In Section 4.2, measurements have been performed on a person sitting behind a wall using CW Doppler radar to show the possibility of heartbeat measurement for a person sitting behind a wall at different frequencies: 5.8 GHz and 10 GHz. Furthermore, a comparative study between the presence and absence of a wall has been done. The transmitted signal has been directed toward the patient's chest situated at 1.1 m and then reflected. The measurements have been carried out during 30 seconds simultaneously with a PC based electrocardiograph (ECG) which has been used as a reference to validate the information extracted from the measured signals.

In previous studies, the measurement of the heartbeat rate for a fixed person using 2 antennas was demonstrated [102]. Furthermore, a study was performed to demonstrate the measurement feasibility using a single-antenna microwave system for a person who is holding his breath [103]. In addition, a study at 2.4 GHz was done using single-antenna system for a person who breathes normally without using a reference. In Section 4.3, a comparison between single and two-antennas microwave systems for a non-breathing person is performed to test the accuracy of the single-antenna microwave system relatively to the two-antenna microwave system. After that, a single-antenna microwave system has been tested using ECG as reference for a breathing person to show the feasibility of detecting heartbeat using one antenna for a breathing person. Heartbeat signal is extracted using the wavelet technique. This system has been operated at 20 GHz for different radiated powers, for a person sitting at a distance of 1 m far from the system.

Measurements are carried out during 23 seconds simultaneously with a PC based electrocardiograph (ECG). The duration of 23 s has been chosen because the person was not able to hold his breath longer than this duration.

In addition, in Section 4.4, advanced scenarios are considered to test the ability of detecting heartbeat of a moving patient inside his home. The person is walking toward the radar with an operating frequency of 20 GHz and emitted power of -19 dBm. This emitted power corresponds to a radiated power of 3 dBm. This scenario has been modeled and wavelet-based techniques have been applied for heartbeat rate extraction. Results have been analyzed and discussed.

## 4.2. Measurements behind a wall

This section presents measurements for the cardiopulmonary activity behind a wall. The importance of this study is to show the possibility of detecting heartbeat for a person sitting outside the room that contains the microwave system, especially that the patient may move from a room to another. Measurements are carried out during 30 seconds simultaneously with a PC based electrocardiograph (ECG); hence, the accuracy of measurements can be determined. The system generates a continuous wave and is used at 2 different frequencies: 5.8 and 10 GHz. This choice allows comparing the accuracy of the results obtained using these frequencies. The transmitted wave is directed toward the patient's chest situated at 1.1 m from the antennas and then reflected directly in front of the system and behind a wall. Discrete wavelet transform has been used as a processing technique to separate heartbeat signal from respiratory signal. Figure 4.1 presents measurement system behind the wall.

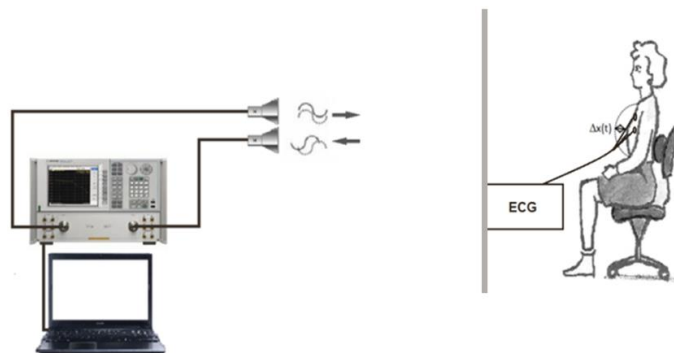


Figure 4.1. Measurement system behind a wall

### 4.2.1. Effect of barriers on wave propagation

This work presents the heartbeat detection in the presence of a barrier. The barrier is a concrete wall with 10 cm thickness. Barriers cause attenuation to the sinusoidal time varying electrical field vector  $\vec{E}$  that represents the propagated signal:  $\alpha$  is the attenuation parameter and  $\beta$  is the phase parameter [104]. They can be expressed in terms of the material properties and frequency as:

$$\alpha = \omega \sqrt{\frac{\mu\epsilon}{2}} [\sqrt{1 + \tan^2 \delta} - 1]^{1/2} \quad (4.1)$$

$$\beta = \omega \sqrt{\frac{\mu\epsilon}{2}} [\sqrt{1 + \tan^2 \delta} + 1]^{1/2} \quad (4.2)$$

where the loss tangent is:

$$\tan \delta = \frac{\frac{\sigma}{\epsilon_0} + \omega\epsilon_r''}{\omega\epsilon_r'} \quad (4.3)$$

$\omega$  is the angular frequency,  $\mu$  is the permeability,  $\epsilon = \epsilon' + j\epsilon''$  is the complex permittivity,  $\epsilon_r'$  is the real part of the relative dielectric permittivity,  $\epsilon_r''$  the imaginary part of the relative dielectric permittivity,  $\epsilon_0$  is the permittivity of the free space and finally  $\sigma$  is the conductivity of the medium. For an air dried concrete, loss tangent is 0.1 at 5.8 GHz and 0.2 and 10 GHz [105].

Note that the magnitude of the time-harmonic electrical field vector  $\vec{E}$  is written as:

$$E = \text{Re}[E_0 \cdot \exp(j\omega t)] \quad (4.4)$$

where  $E_0$  is the magnitude of the independent-time electrical field.

After attenuation,  $E$  is rewritten as:

$$E = \text{Re}[E_0 \cdot \exp(j\omega t - \gamma z)] \quad (4.5)$$

where  $\gamma = \alpha + j\beta$ , and  $z$  is the distance along the propagation which presents the thickness of the wall.

### 4.2.2. Measurement setup

The VNA system is the same as the one presented in chapter 3. These measurements are done inside the IETR building. The radiated power is set at 0 dBm. The bandwidth is 500 Hz. During 30 seconds, 20 000 points have been recorded. Hence, the sampling frequency is 666.7 Hz. A 54 years old person is sitting behind a concrete wall with 10 cm thickness. The distance between the antennas and the wall is 0.5 m and the distance between the wall and the person is 0.5 m. Adding the thickness of the wall, the total distance between the antennas and the patient is 1.1 m. The person is breathing normally. To validate the proposed system and its ability to detect heartbeat rate, the radar system measurements are performed simultaneously with ECG measurements. Table 4.1 presents the measurement setup.

Table 4.1. Measurement setup

<b>System Specifications</b>	
<b>Operating frequency (GHz)</b>	5.8 and 10
<b>Radiated power (dBm)</b>	0
<b>Number of points</b>	20 000
<b>Time Window (sec)</b>	30
<b>Sampling frequency (Hz)</b>	666.7
<b>Antennas number</b>	2
<b>Subject Information</b>	
<b>Gender/ Age (y)</b>	M/54
<b>Position/ Side</b>	Setting/ Front
<b>Distance (m)</b>	1.1
<b>Breathing</b>	Y
<b>Presence of wall</b>	Y/N
<b>Wall thickness (cm)/position</b>	10/middle



Figure 4.2 presents the phase variation (PV) (deg) of  $S_{21}$  for a person sitting in front of the system without and with a barrier (wall) for 2 different frequencies: 5.8 GHz and 10 GHz. These signals represent the cardio-respiratory signal.

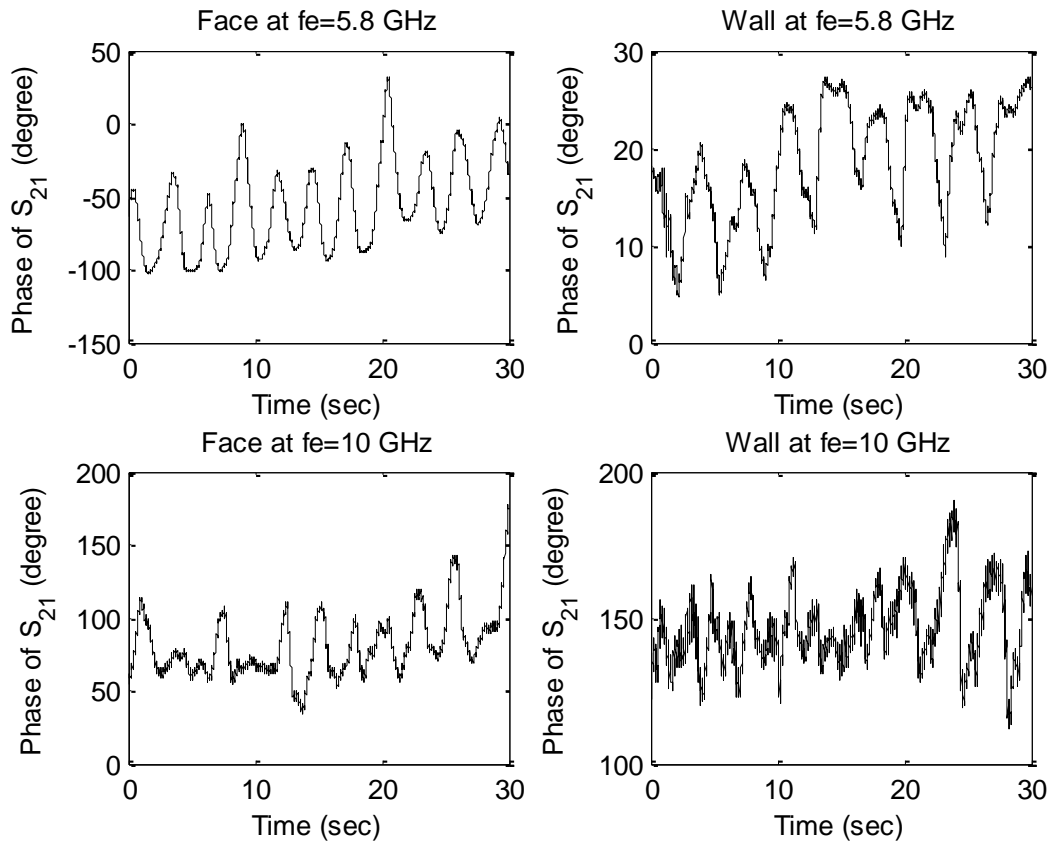


Figure 4.2. Phase variation of  $S_{21}$  at  $P_r = 0$  dBm and  $f_c = 5.8$  and 10 GHz with and without wall

The phase variation of  $S_{21}$  behind a wall is noisier than in the absence of wall. Indeed, the attenuation caused in the presence of wall decreases the SNR of the  $S_{21}$  phase variation. The role of signal processing is to reduce the perturbing signals (noise) and the respiration signal, in order to extract the heartbeat signal from the cardio-respiratory signal.

### 4.2.3. Signal processing and results

Because the heartbeat rate of an adult is between 60 and 120 bpm, which corresponds to a frequency between 1 and 2 Hz, resampling method is done before applying wavelet decomposition to obtain signal having frequencies above 1 Hz. In this work, the

resampling method uses linear interpolation to convert the sampling frequency from 666.7 Hz to 512 Hz. Hence after applying wavelet decomposition; the 8<sup>th</sup> approximation contains frequencies below 1 Hz. In conclusion,  $S_{D18} = S_{reconstructed} - A_8$  contains all frequencies above 1 Hz of the cardio-respiratory signal. Bior 2.4 is the family of wavelets chosen in this work because reconstructed signal of Bior 2.4 is nearest to the original signal compared to the other wavelets families for the current measurements. Figure 4.3 presents  $S_{D18}$  signal obtained at 5.8 and 10 GHz with and without wall.

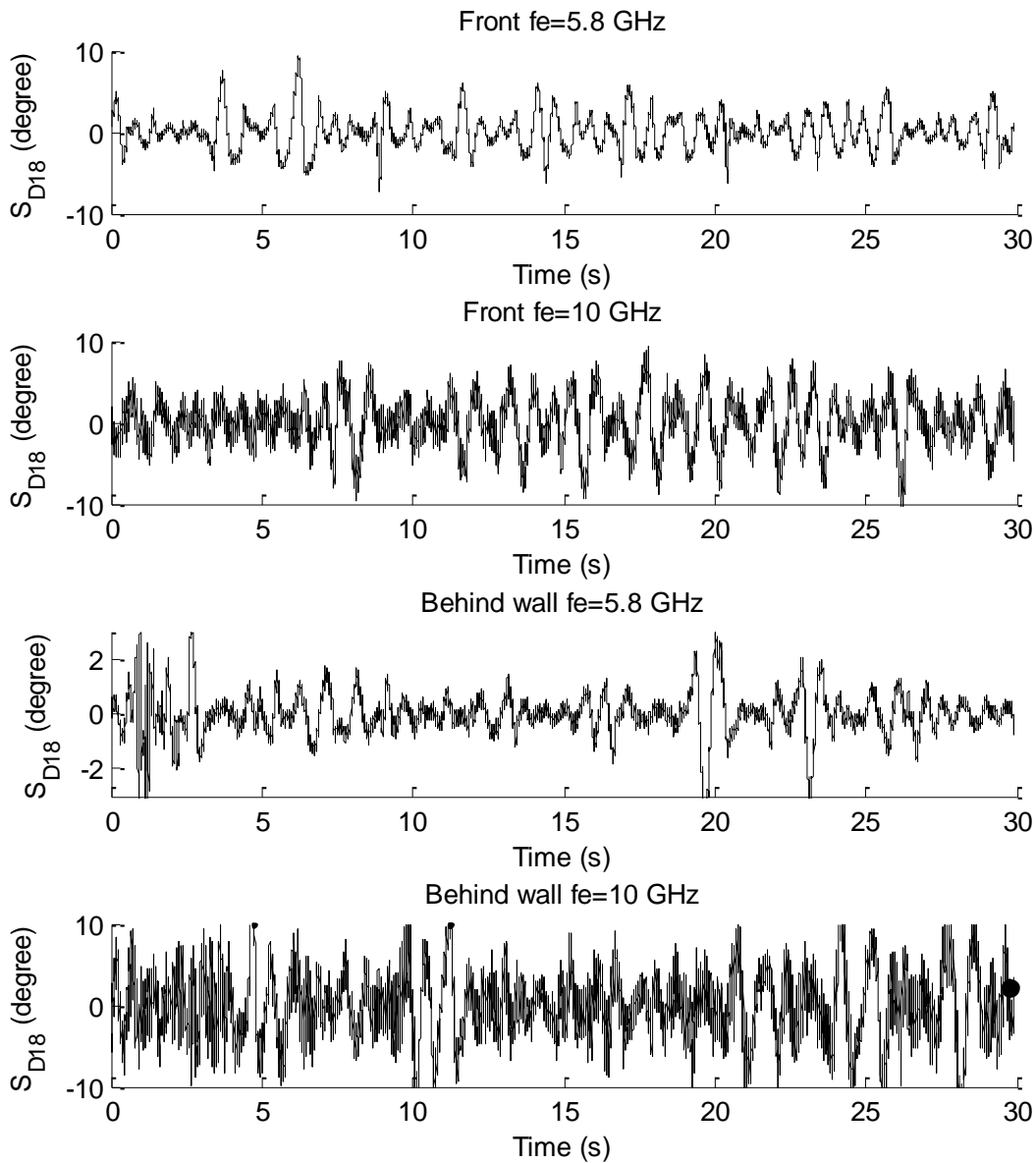


Figure 4.3.  $S_{D18}$  signal obtained at  $P_r = 0$  dBm and  $f_c = 5.8$  and 10 GHz with and without wall

Because  $S_{D18}$  is noisy, smoothing method using moving average is applied. After trial and errors,  $n$  is chosen to be 199. After that, peak detection is applied. Figure 4.4 presents the peak detection applied on smoothed  $S_{D18}$  for the results obtained at 5.8 GHz and 10 GHz, with presence and absence of wall.

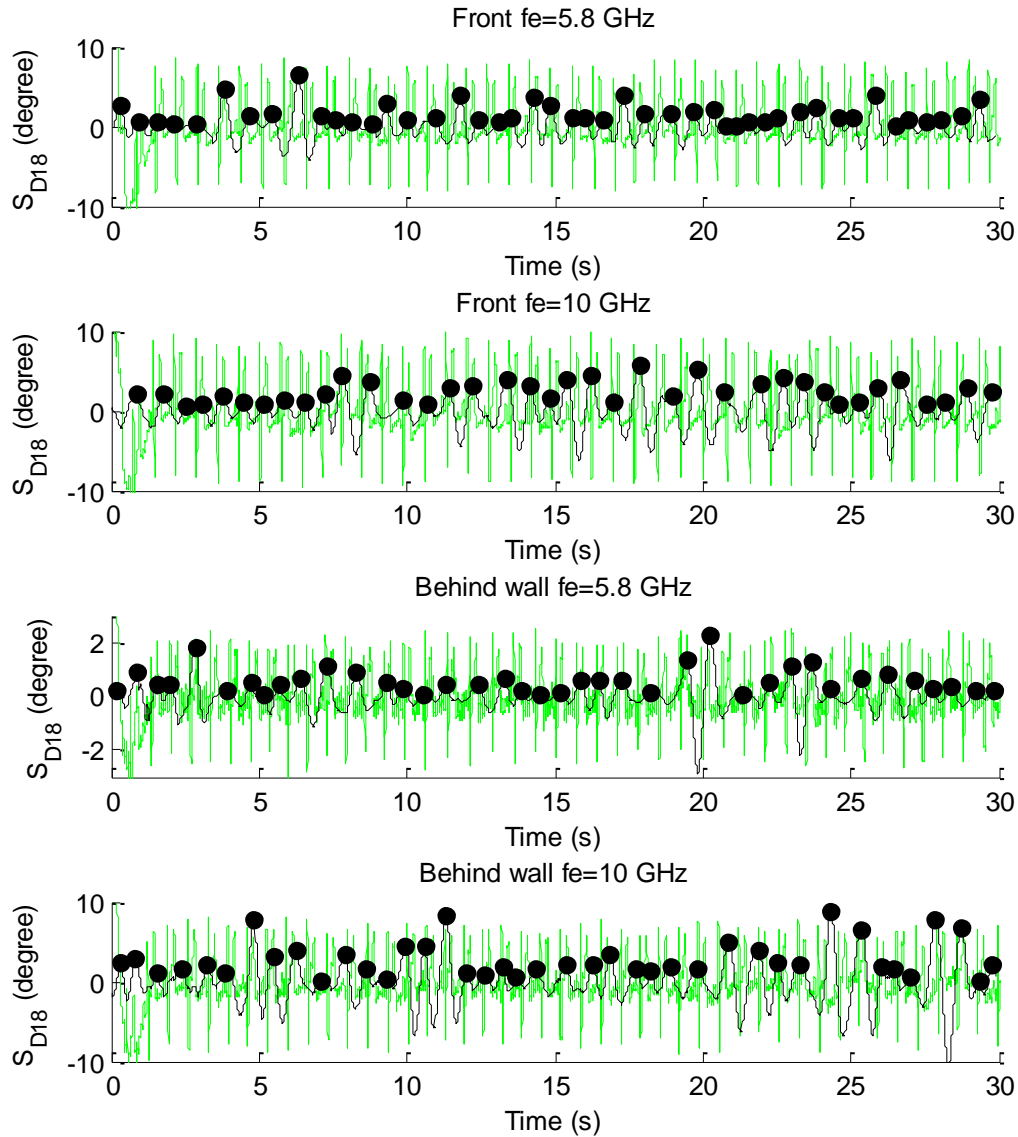


Figure 4.4. Peak detection of the smoothed  $S_{D18}$  obtained at  $P_r = 0$  dBm and  $f_e = 5.8$  and 10 GHz with and without wall (Black), ECG signal (Green)

For a person setting directly in front of the system, 46 peaks are obtained in 29.05 sec at 5.8 GHz and 38 peaks in 28.89 sec at 10 GHz, hence the heartbeat rates are 93 and 77 bpm at 5.8 and 10 GHz respectively. For a person setting behind the wall, 39 peaks are obtained in 29.63 sec at 5.8 GHz and 41 peaks in 29.46 sec at 10 GHz, hence the

heartbeat rates are 77 and 81 bpm at 5.8 and 10 GHz respectively. Then these heart rates are compared to those extracted from the ECG system. Table 4.2 presents heartbeat rates extracted from ECG ( $HR_{ECG}$ ) and VNA ( $HR_{VNA}$ ), as well as the relative error for each case and each operating frequency.

Table 4.2.  $HR_{VNA}$  and  $HR_{ECG}$  and their relative errors

Case	Frequency (GHz)	$HR_{VNA}$ (bpm)	$HR_{ECG}$ (bpm)	Relative Error (%)
Direct	5.8	93	85	9
Direct	10	77	85	9
Behind wall	5.8	77	90	14
Behind wall	10	80	92	13

Based on the American National Standard [90], the system is considered accurate when the relative error is lower than 10% or 5 bpm difference between  $HR_{VNA}$  and  $HR_{VNA}$ . In general, obtained results are acceptable without wall with maximum error 9%, but it increases up to 13-14 % with presence of the wall. Other measurements could be done by increasing the radiated power; the change of this parameter value may decrease the obtained error.

### 4.3. Single antenna system

Previous works have demonstrated the possibility of detecting the heartbeat activity with two-antenna microwave system, for different operating frequencies and several radiated powers [106]. In addition, a study of a single antenna system is done for a person who was holding his breath at 16 GHz [103]. Furthermore, a study at 2.4 GHz is done using single-antenna system for a person who breathes normally without a reference signal. In this section, a comparison between single-antenna microwave system and two-antenna microwave system for heartbeat measurement is proposed for a person who is holding his breath. Measurements are carried out simultaneously with a PC based electrocardiograph (ECG) and the relative error between system and ECG is presented. The importance of this work is to evaluate the accuracy of the single-antenna system relatively to the widely

used system which is the two-antenna system. The advantage of the single antenna system is to reduce the number of components used; hence reducing the cost. After that, the person breathes; hence the respiration signal is added. The single-antenna system is used at 20 GHz. Processing techniques are performed to extract the heartbeat signal. Note that the ECG is taken as reference. The scenario of holding breath is considered before doing measurements of a breathing person in order to perform measurements for the simplest case and validate the possibility of using one antenna even with low radiated powers. The simplest case is done by avoiding the presence of the respiration signal that could hide the heartbeat signal.

### **4.3.1. Comparison between one and two antennas systems for a holding breath person**

This section presents a comparison between single and two-antenna microwave systems for heartbeat detection. These measurements are performed at 20 GHz with different transmitted powers, for a person who is holding his breath. The single antenna system measures the heartbeat activity upon the measurement of the phase variation of parameter  $S_{11}$ . In the case of two antennas system,  $S_{21}$  is measured.  $S_{11}$  and  $S_{21}$  are respectively the reflection coefficient and the transmission coefficient.  $S_{ij}$  parameters describe the input-output relationship between ports; hence  $S_{21}$  represents the ratio of the received signal at the port 2 of the VNA to the emitted signal at the emitted antenna level, and  $S_{11}$  presents the ratio of the reflected signal to the emitted one from the same antenna. After detecting the 2 parameters  $S_{11}$  and  $S_{21}$ , smoothing is applied in order to reduce the noise. The proposed system is validated with an electrocardiogram (ECG) considered as reference.

#### **4.3.1.1. Measurement setup description**

The two-antenna system is identical to that presented in chapter 1. Concerning the single antenna system, it differs by using one antenna instead of two. In this case, the antenna plays the role of transmitter and receiver. The antenna used in this work is a horn antenna (LB-42-25-C2-SF). It has an operational frequency range of 18 – 26.5 GHz. In this work, the operating frequency is chosen to be at 20 GHz. The gain of this antenna at 20 GHz is 24 dB (see Table 2.1). The choice of this frequency is made according to two reasons: The first one is to obtain higher phase variation as it is directly proportional to the

frequency, and the second reason is due to the equipment's limitation (2 – 20 GHz of the VNA). Figure 4.5 presents the vital signs measurements using single antenna system.

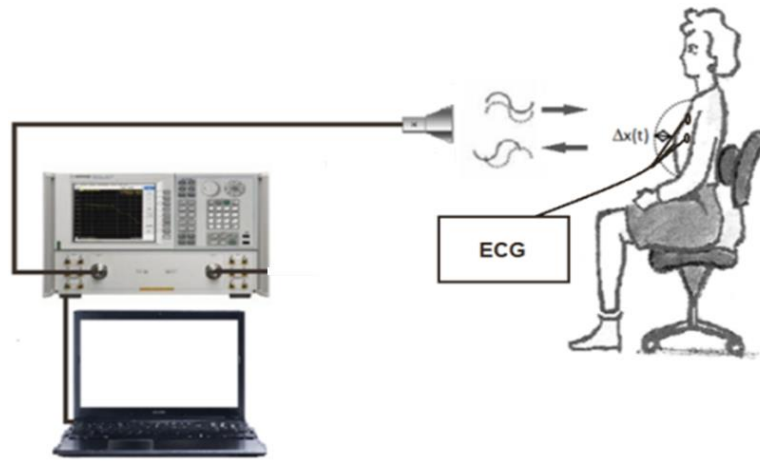


Figure 4.5. Measurement system with single antenna vs. electrocardiograph

The bandwidth is 500 Hz. The number of points taken for the signals measured with the VNA is 12801 points. The duration is 23 seconds; hence the sampling frequency is 557 Hz. The person was holding his breath. The 23 seconds is chosen to avoid stopping breathing too long. The measurements were performed for a 54 years person setting at 1 meter from the antenna. Considering the antenna gain (24 dB), cables loss (2 dB) and emitted power (-24, -29, -34 and -39 dBm), the radiated powers values are -2, -7, -12 and -17 dBm. Measurements with several values of the emission power allow us to determine the minimum power required to extract the heartbeat rate while limiting the risks of exposure to the waves by the patient and the medical staff.

Table 4.3 presents the measurement setup characteristics for this experiment.

Table 4.3. Measurement setup

<b>System Specifications</b>	
<b>Operating frequency (GHz)</b>	20
<b>Radiated power (dBm)</b>	-2, -7, -12, -17
<b>Number of points</b>	12801
<b>Time Window (sec)</b>	23
<b>Sampling frequency (Hz)</b>	557
<b>Antennas number</b>	1 or 2
<b>Subject Information</b>	
<b>Gender/ Age (y)</b>	M/54
<b>Position/ Side</b>	Setting/ Front
<b>Distance (m)</b>	1
<b>Breathing</b>	No
<b>Wall thickness (cm)/position</b>	Setting/ Front

#### **4.3.1.2. Signal processing and obtained results**

In this section, measurements were done for a person holding his breath using 2 systems: one-antenna system and two-antenna system. Figure 4.6 and Figure 4.7 present phase variation (PV) of  $S_{11}$  and  $S_{21}$  respectively, for a person holding his breath at different radiated powers: -2, -7, -12 and -17 dBm.



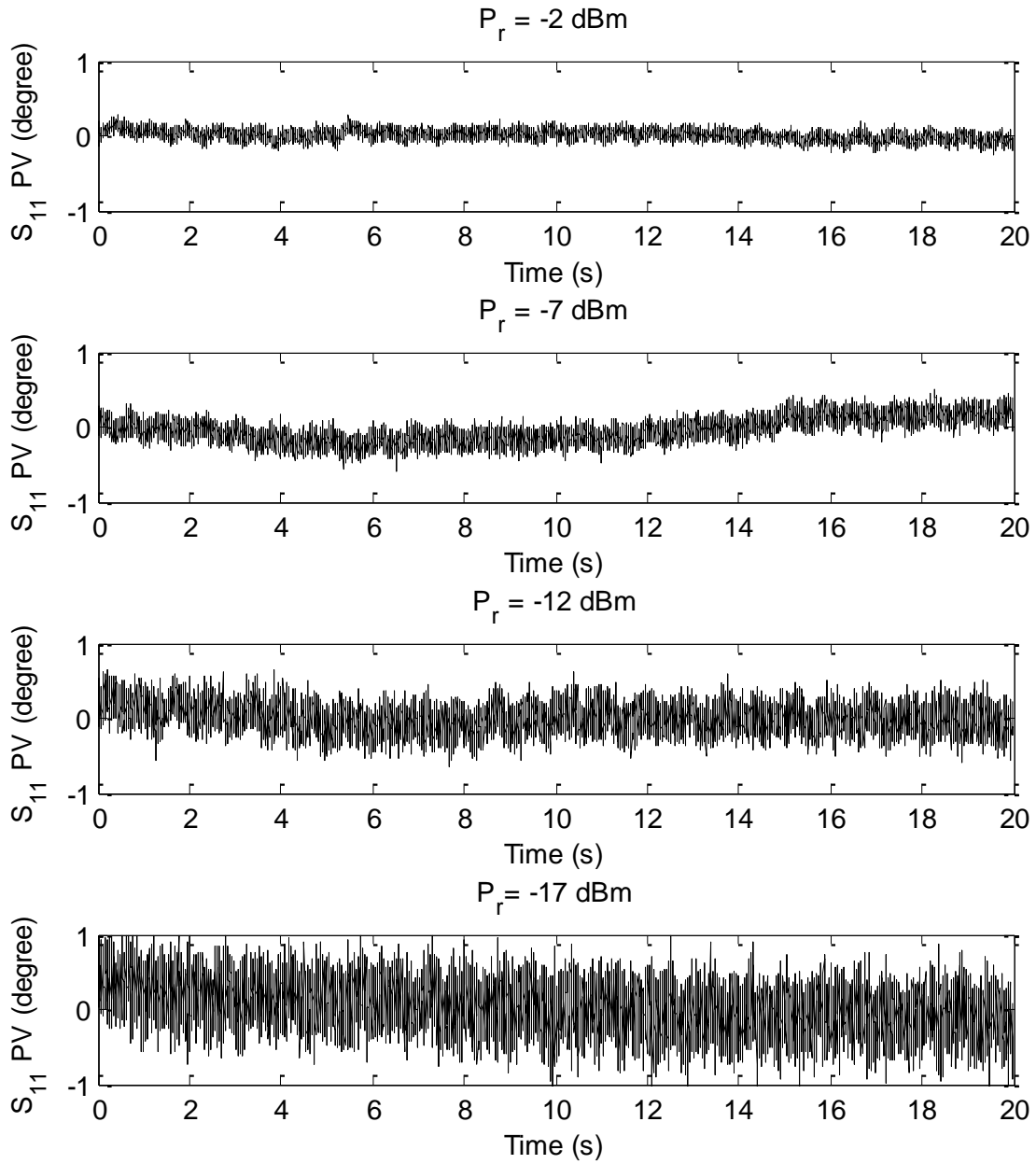


Figure 4.6. Phase variation of  $S_{11}$  of a person holding his breath at  $P_r = -2, -7, -12$  and  $-17$  dBm and  $f_e = 20$  GHz

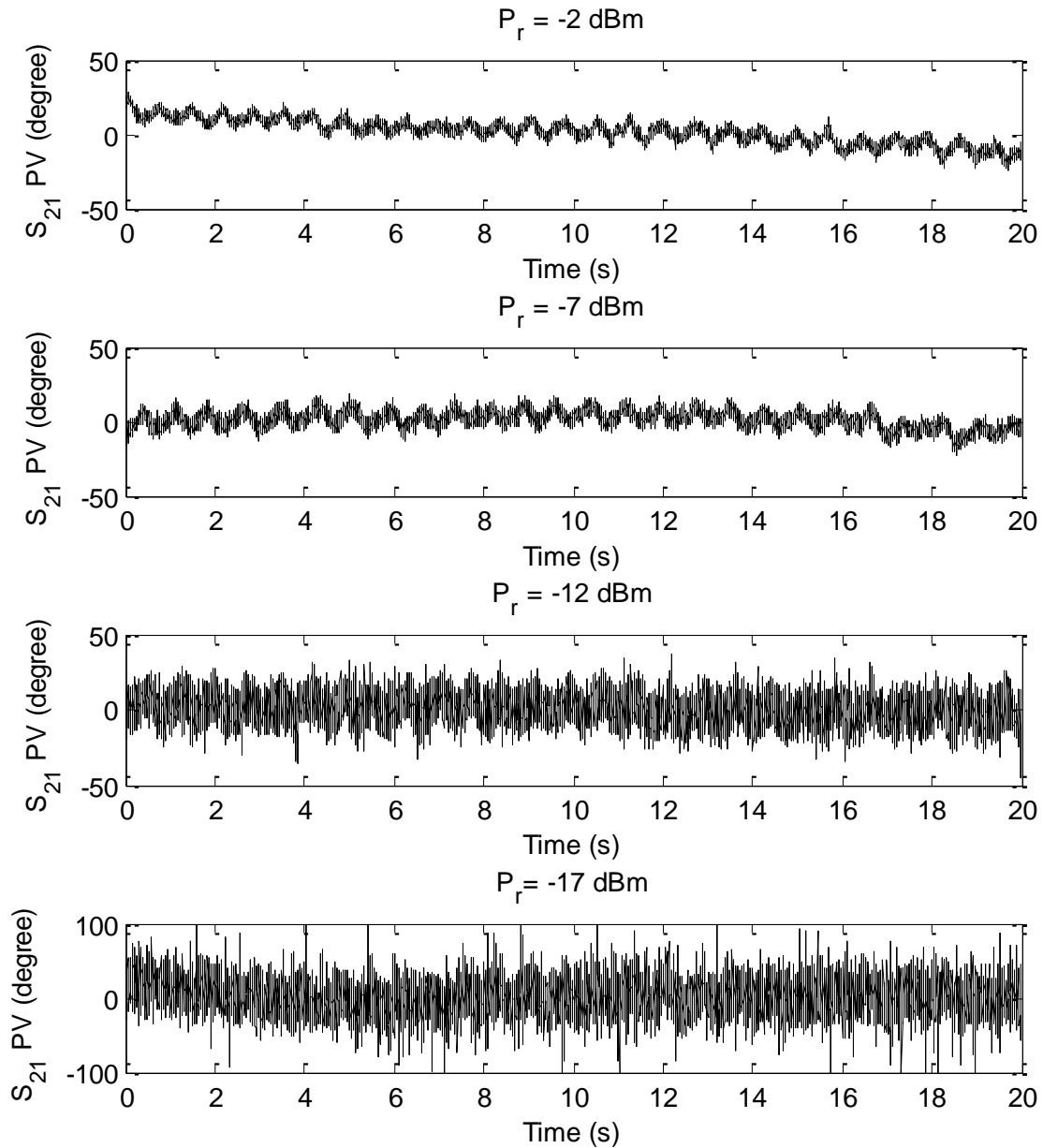


Figure 4.7. Phase variation of  $S_{21}$  of a person holding his breath at  $P_r = -2, -7, -12$  and  $-17$  dBm and  $f_e = 20$  GHz

It is remarkable that the phase variation of  $S_{11}$  is noisier and smaller than the phase variation of  $S_{21}$  and heartbeat signals is clearer in case  $S_{21}$  phase variation. In addition, the SNR of the signal decrease with the decrease of the radiated power in both cases. Because signals are noisy, especially at lower powers, extracting the heartbeat signal becomes more difficult. The smoothing method is used in order to eliminate noise and extract the heartbeat signal by using moving average that is applied on every  $n$

consecutive samples of the waveform. A compromise between the reduction of the noise and high lighting the heartbeat signal should be done: When  $n$  increases, the heartbeat signal may disappear. On the other hand, when  $n$  decreases, heartbeat signal could not be detected correctly due to the presence of noise. After trial and errors,  $n = 199$  was chosen because it presents a good compromise between the noise elimination and heartbeat signal keeping. Smoothing was applied for  $S_{11}$  and  $S_{21}$  and at different powers. After that, peak detection has been applied in order to extract the heartbeat rate. Figure 4.8 presents the peak detection of the phase variation (PV) of  $S_{11}$  when using the single-antenna microwave system, after applying smoothing with  $n = 199$ , and for different radiated powers: -2, -7, -12 and -17 dBm.

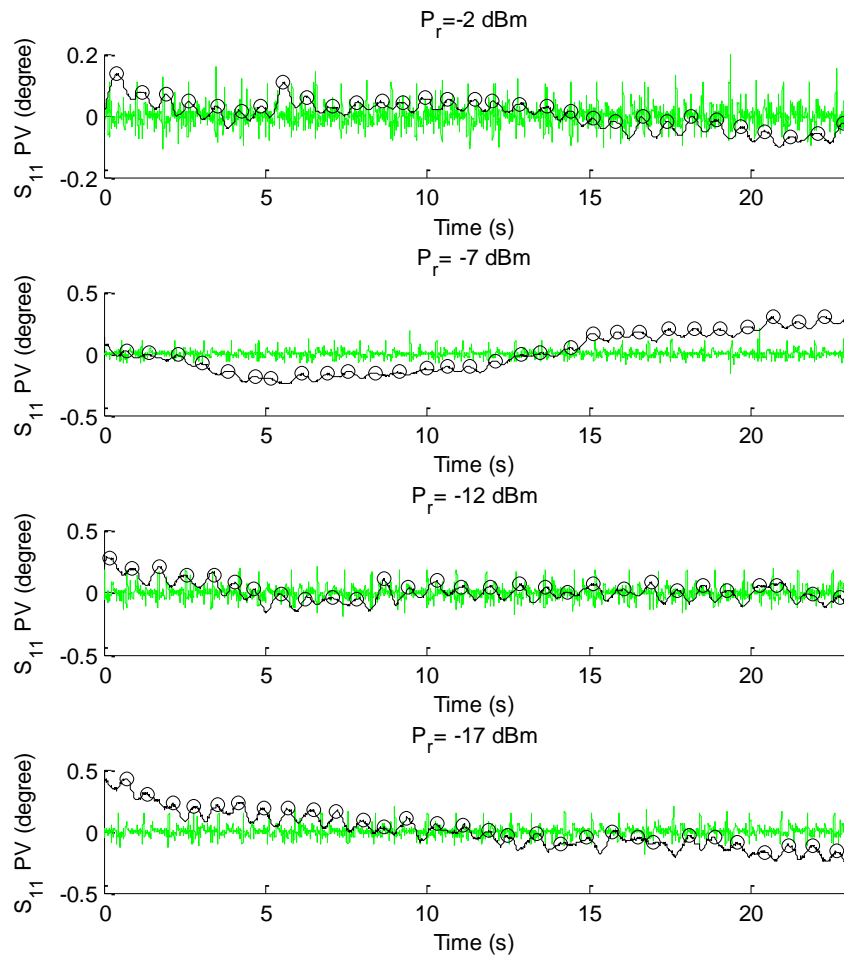


Figure 4.8. Peak detection for the phase variation of  $S_{11}$  after applying smoothing with  $n = 199$  at  $P_r = -2, -7, -12$  and  $-17$  dBm and  $f_e = 20$  GHz (Black), ECG signal (Green)

In the case of a single-antenna microwave system and at -2 dB, 31 peaks are obtained in 22.46 sec. At -7 dB, 29 peaks are obtained in 21.46 sec. At -12 dB, 29 peaks are obtained in 22.57 sec and finally at -17dB, 30 peaks are obtained in 21.91 sec. Hence the heartbeat rates for the person who holding his breath at -2, -7, -12 and -17 dB are 80, 78, 74, 79 bpm respectively. Figure 4.9 presents the peak detection of the phase variation (PV) of  $S_{21}$ , when using the two-antenna microwave system after applying smoothing with  $n = 199$ , and for different radiated powers: -2, -7, -12 and -17 dBm.

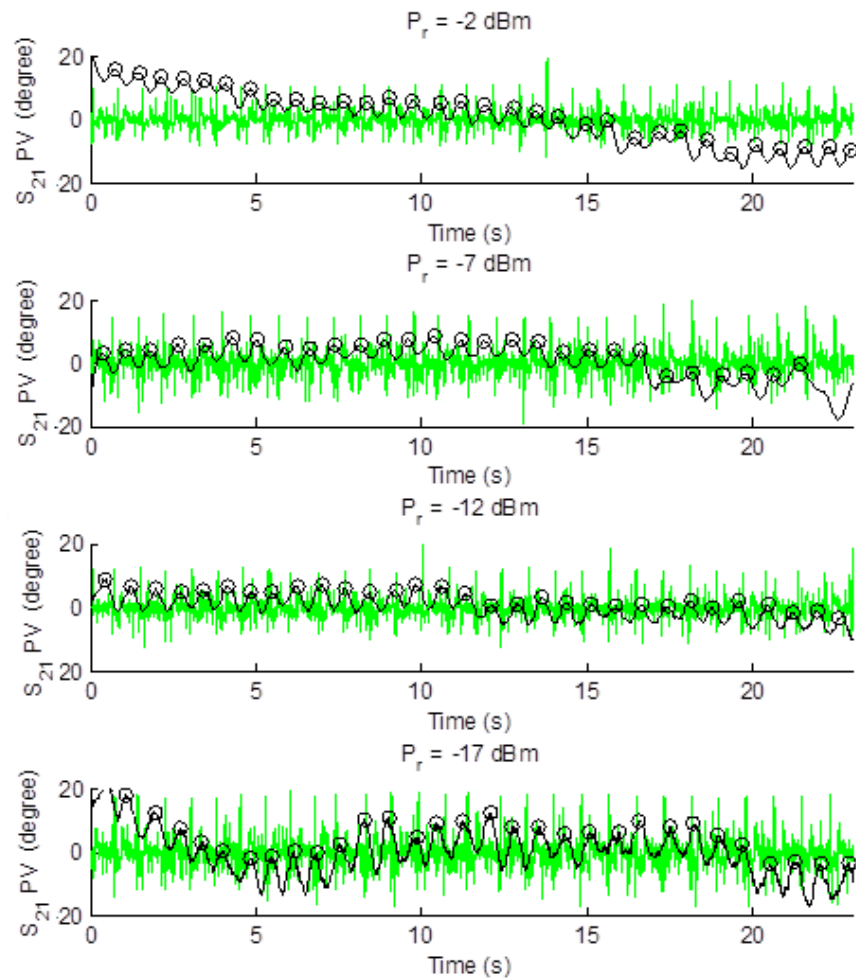


Figure 4.9. Peak detection of phase variation of  $S_{21}$  after applying smoothing with  $n = 199$  at  $P_r = -2, -7, -12$  and  $-17$  dBm and  $f_e = 20$  GHz (Black), ECG signal (Green)

In the case of the two-antenna microwave system and at -2 dB, 32 peaks are obtained in 22.12 sec. At -7 dB, 28 peaks are obtained in 21.07 sec. At -12 dB, 31 peaks are obtained in 22.28 sec and finally at -17dB, 30 peaks are obtained in 21.86 sec. Hence the heartbeat rates for the person who holding his breath at -2, -7, -12 and -17 dB are 84, 77, 81, 80

bpm respectively. Then the relative error between the  $HR$  of VNA system and  $HR$  of ECG system is calculated. Table 4.4 presents the heartbeat rate extracted from the single-antenna system ( $HR_{VNA-SA}$ ), the heartbeat rate extracted from the ECG ( $HR_{ECG}$ ) and finally the relative error between  $HR_{VNA}$  and  $HR_{ECG}$ .

Table 4.5 presents the heartbeat rate extracted from the two-antenna system ( $HR_{VNA-TA}$ ), the heartbeat rate extracted from the ECG ( $HR_{ECG}$ ) and the relative error between  $HR_{VNA}$  and  $HR_{ECG}$ .

Table 4.4. Heartbeat rate comparison between  $HR_{VNA-SA}$  and  $HR_{ECG}$

<b>Radiated power (dBm)</b>	<b><math>HR_{VNA-SA}</math> (bpm)</b>	<b><math>HR_{ECG}</math> (bpm)</b>	<b>Relative Error (%)</b>
-2	80	75	7
-7	78	72	8
-12	74	79	7
-17	79	73	8

Table 4.5. Heartbeat rate comparison between  $HR_{VNA-TA}$  and  $HR_{ECG}$

<b>Radiated power (dBm)</b>	<b><math>HR_{VNA-TA}</math> (bpm)</b>	<b><math>HR_{ECG}</math> (bpm)</b>	<b>Relative Error (%)</b>
-2	84	78	8
-7	77	72	7
-12	81	76	7
-17	80	75	7

Recall that the relative error is acceptable when it is less than 10%; hence the obtained results are acceptable for both systems with maximum error of 8% in both systems. As conclusion, although signals of single-antenna microwave system are noisier than signals of two-antenna microwave system, it is still able to measure heartbeat rate and its relative errors are comparable to relative errors of two-antenna microwave system. After holding

breath, the next step is making measures using single-antenna microwave system for a breathing person.

### 4.3.2. Results for a normally breathing person using single-antenna VNA system

Similar measurements are performed with the same system for the same person at 20 GHz using single-antenna system only. In this case, the person was breathing normally and sitting at 1 m from the system with always the ECG system used as reference. Figure 4.10 presents the phase variation (PV) of  $S_{11}$  for a breathing person at different radiated powers: -2, -7, -12 and -17 dBm.

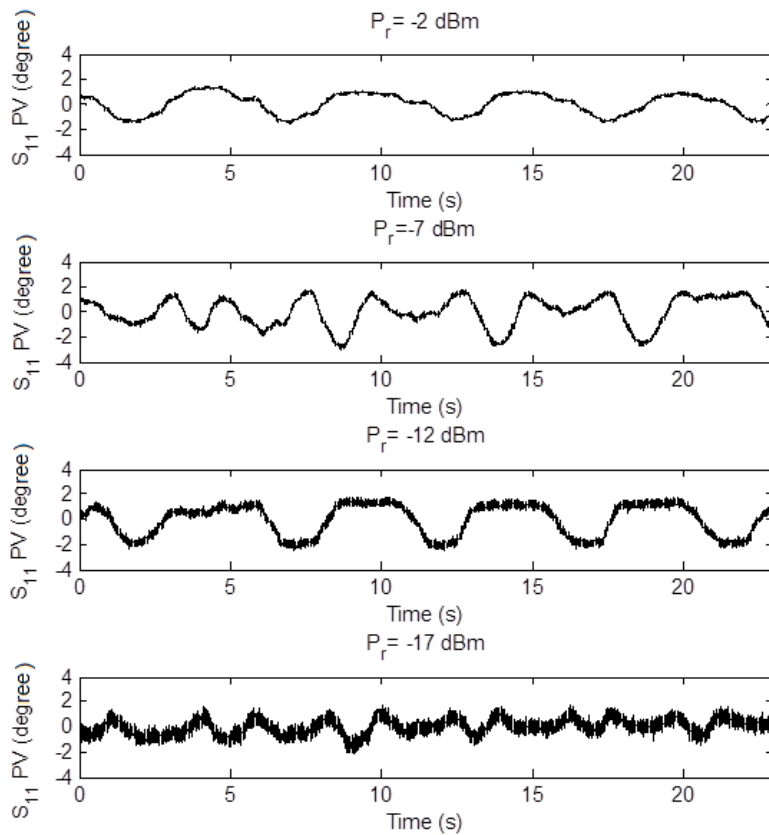


Figure 4.10. Phase variation of  $S_{11}$  for a breathing person at  $P_r = -2, -7, -12$  and  $-17$  dBm and  $f_e = 20$  GHz

These measurements are performed to confirm that the single-antenna system is able to extract the heartbeat rate when the person is breathing. The SNR decreases with the decrease of the radiated power. Wavelet decomposition is applied to extract the heartbeat signal. Bior 2.4 is chosen because its reconstructed signal is the closest to the original one

compared to the other wavelets families. The resampling using linear interpolation is applied to change the sampling frequency to 512 Hz, then  $S_{D18} = S_{reconstructed} - A_8$  is extracted; hence  $S_{D18}$  contains frequencies higher than 1 Hz. Smoothing method using moving average with  $n = 199$  is applied to  $S_{D18}$ , and then peak detection is applied to the smoothed  $S_{D18}$ . Figure 4.11 presents the peak detection of the extracted heartbeat signal for radiated powers of -2, -7, -12 and -17 dBm respectively.

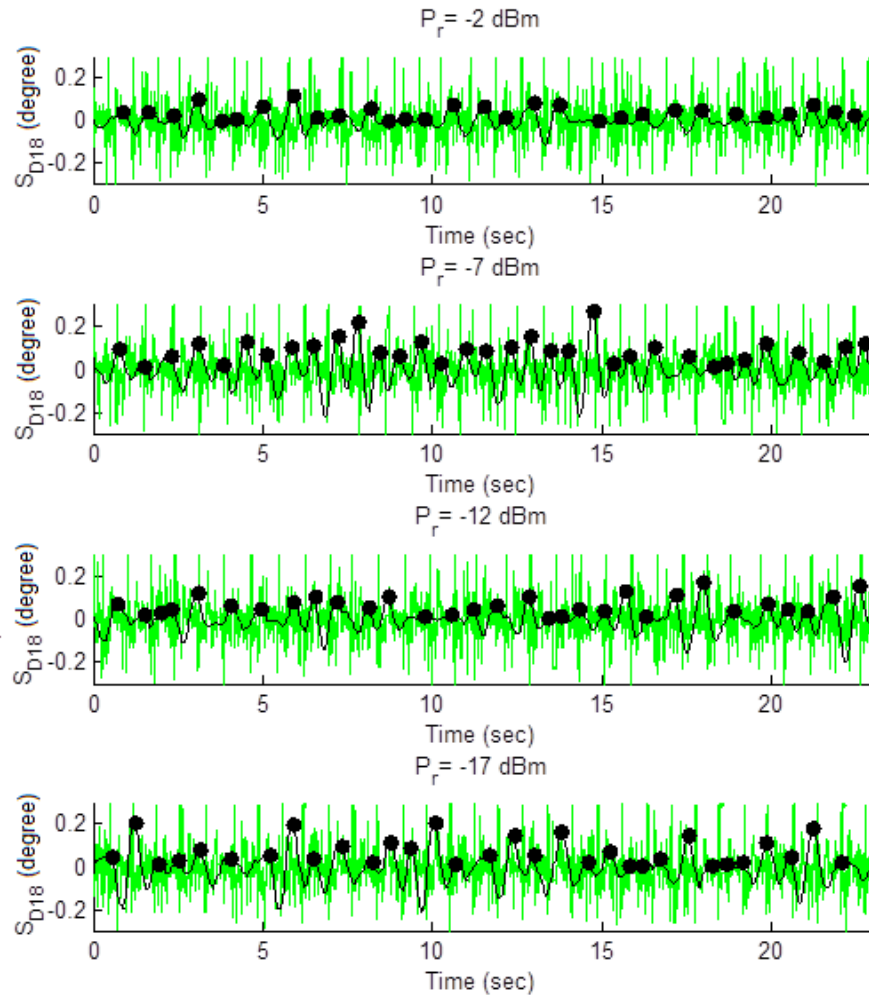


Figure 4.11. Peak detection of the extracted heartbeat signal at  $P_r = -2, -7, -12$  and  $-17$  dBm and  $f_e = 20$  GHz (Black), ECG signal (Green)

At -2 dB, 31 peaks are obtained in 21.55 sec. At -7 dB, 34 peaks are obtained in 21.98 sec. At -12 dB, 31 peaks are obtained in 21.89 sec and finally at -17dB, 32 peaks are obtained in 21.53 sec. Hence the heartbeat rates for the person who holding his breath at -2, -7, -12 and -17 dB are 81, 90, 82 and 86 bpm respectively. Table 4.6 presents the heartbeat rate

extracted from the single-antenna microwave system ( $HR_{VNA-SA}$ ), the heartbeat rate extracted from the ECG signal ( $HR_{ECG}$ ) and finally the relative errors between  $HR_{VNA-SA}$  and  $HR_{ECG}$  for a breathing person and with different radiated powers.

Table 4.6. Heartbeat rate comparison between  $HR_{VNA-SA}$  and  $HR_{ECG}$  for a breathing person with different radiated powers

<b>Radiated power (dBm)</b>	<b><math>HR_{VNA-SA}</math> (bpm)</b>	<b><math>HR_{ECG}</math> (bpm)</b>	<b>Relative Error (%)</b>
-2	81	80	1
-7	90	77	17
-12	82	80	3
-17	86	83	4

Heart-rates are extracted even at low power and are less than 4%; hence, the obtained results are acceptable. However, at -7 dBm, the relative error is 17%, hence new measurements should be done at -7 dBm to ensure the results and lead into a good interpretation. As a conclusion, after applying wavelets, one antenna microwave system is able to extract heart rate successfully like two-antenna microwave system.

#### **4.4. Models and processing of a moving person**

Previous researches worked on the non-contact detection of the heartbeat using wireless systems under different conditions. Most of these researches are applied to fixed subjects. However, the subject can move with a Random Body Movement (RBM). RBM is considered as a significant source of noise and the most challenging issue for the vital signs detection using touch less radar systems. RBM is mostly bigger than the chest movements due to tiny vital signs that have several millimeters to centimeters; hence the RBM signal is able to hide the signal of interest. Some studies resolved the problem of RBM by using multiple transceivers detecting from different sides of the human body [72]. In general, when the person moves between two radars, from one to the other, the body moves toward one of them and moves away from the other radar. When combining



the two signals, the body motion can be canceled. Other methods studied the RBM elimination using either two-frequency radar [73] or multi-frequency interferometric radar [62]. However, these studies have some drawbacks. Firstly, the use of multiple radar systems to cancel RBM increases the system complexity. Secondly, the alignment of different systems could be a potential bottleneck for accurate detection. In this section, models of chest motion with the presence of 1-D body motion are performed. A case of an old person that performs a uniform movement in his room is taken into consideration. One radar system is used to emit and then detect the vital signs. After that, wavelet method is used to extract the heartbeat signal. Figure 4.12 presents the detection setup for a moving person.

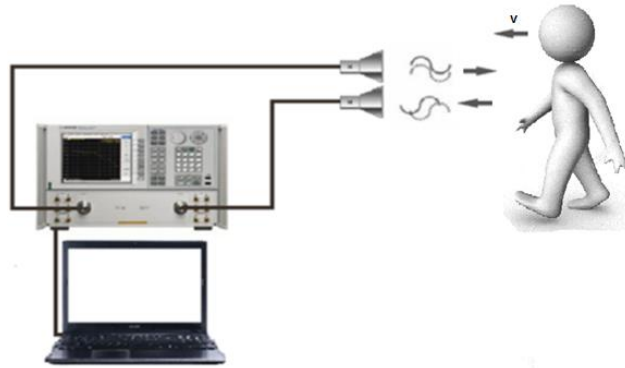


Figure 4.12. Detection setup for a moving person ( $v$  is the velocity of the person)

#### 4.4.1. Modeling of a chest motion when moving forward

As shown previously, according to Doppler effect, a constant frequency signal reflected off an object having a varying displacement will result in a reflected signal with a time varying phase [88]. The relation between the chest displacement  $\Delta x(t)$  and the phase variation  $\Delta\theta(t)$  is:

$$\Delta\theta(t) = \frac{4\pi}{\lambda} \Delta x(t) \quad (4.6)$$

where  $\lambda$  is the wavelength of the transmitted signal. The reflected signal contains information about heartbeat, respiration and body movement of the patient [5].

Because the person is making a move towards the system,  $\Delta x(t)$  is result of movement of the old person with speed, heartbeat motion and finally respiratory motion; hence  $\Delta x(t)$  can be computed as [107]:

$$\Delta x(t) = -vt + x_h(t) + x_r(t) + n(t) \quad (4.7)$$

where  $v$  is the velocity of the old person. Note that the ‘-’ sign is due to the movement forward.  $x_h(t)$  is the heartbeat motion,  $x_r(t)$  is the respiratory motion and  $n(t)$  is the added noise.

#### 4.4.1.1. Phase variation due to the body motion

Considering that the old person walks toward the radar. This person is starting with a distance of 3 m far away from the antennas and walks forward with a constant velocity of 0.25 m/s. This value is chosen to represent the traveling speed of an elderly person; hence the equation of the walking forward is  $-0.25 t$ . The person stopped at a distance of 1 m far from the system; hence the person is walking for a time of 8 s. The operating frequency chosen for this work is 20 GHz and the phase is  $0^\circ$  at  $t = 0$  s, the  $0^\circ$  is an arbitrary value. In fact, the maximum variation of the phase ranges between  $-180^\circ$  and  $+180^\circ$ , hence each time the phase reaches the  $-180^\circ$ , it permutes to  $+180^\circ$  and vice versa.

#### 4.4.1.2. Phase variation due to the heartbeat

By assuming that the heartbeat signal can be represented by a sine wave [5]; it can be expressed by  $x_h = A_h \sin(2\pi f_h t + \emptyset_{oh})$ , where  $A_h$  is the amplitude of chest movement due to heartbeat,  $f_h$  is the heartbeat frequency and  $\emptyset_{oh}$  is the heartbeat sine wave phase at  $t = 0$ . The amplitude of the chest’s displacement due to heartbeat is between 0.2 and 0.5 mm and the heartbeat frequency  $f_h$  of an adult is between 1 and 2 Hz [83]. Because the heartbeat signal is not a pure sinusoid, hence variability in duration between 2 successive peaks exists expressed in sec; an example of 2 successive peaks duration is taken from an experiment done for a holding breath person. The duration between 2 successive peaks are distributed in this way: 0.9953s 0.7271s 0.8529s 0.8473s 0.9639s 0.7215s 0.9787s 0.6993s 0.8566s; hence the heartbeat rate obtained from this signal is 70.73 beats/min. According to the relation (4.6), the phase variation due to heartbeat is

presented in Figure 4.13 (a) with operating frequency 20 GHz, the displacement of the chest due to heartbeat is 0.5 mm.  $\emptyset_{oh}$  is an arbitrary value and chosen to be  $90^\circ$ .

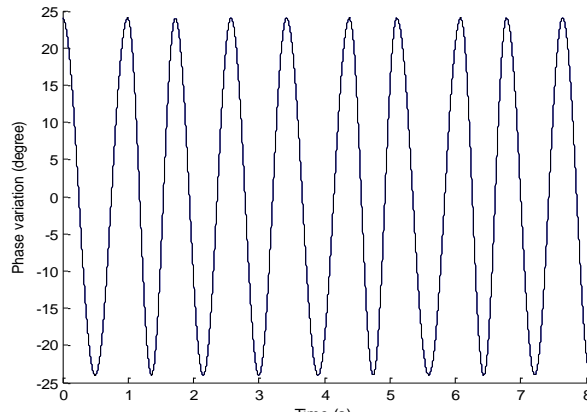


Figure 4.13. (a) Model of phase variation due to heartbeat at 20 GHz

#### 4.4.1.3. Phase variation due to the respiration

Respiration is modeled also as a sine wave; hence  $x_r = A_r \sin(2\pi f_r t + \emptyset_{or})$ , where  $A_r$  is the amplitude of the chest movement due to respiration,  $f_r$  is the respiratory frequency and  $\emptyset_{or}$  is the phase at  $t = 0$  s. The amplitude of the respiration is between 4 and 12 mm and the rate is between 12 and 20 breaths per minute, hence the respiration frequency is between 0.2 and 0.34 Hz. According to the relation (4.6), 8 s of a model of phase variation due to respiration is presented in Figure 4.13 (b). The operating frequency 20 GHz, the displacement of the chest due to respiration is 12 mm, the respiration frequency is 0.2 Hz and  $\emptyset_{or} = 90^\circ$ .  $\emptyset_{or}$  is an arbitrary value.

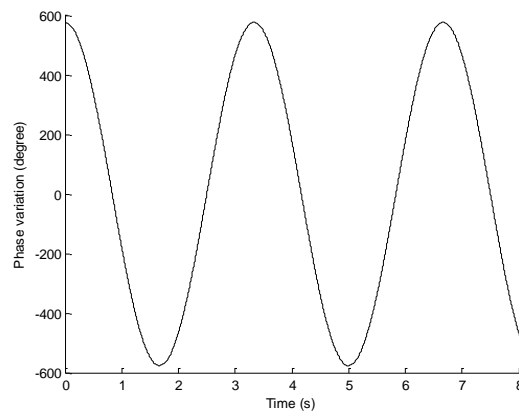


Figure 4.13. (b) Model of the phase variation due to respiration at 20 GHz

#### 4.4.1.4. Phase noise model

Eliminating noise that affects the signal quality is considered as one of the biggest challenges. Equations (4.8) and (4.9) present the signal power at the input of VNA system and the signal to noise ratio (SNR) of VNA input respectively:

$$P_S(dBm) = P_e(dBm) + G_e(dB) + G_r(dB) - A_1(dB) - Refl(dB) - A_2(dB) \quad (4.8)$$

$$\begin{aligned} SNR_{VNA\ input}(dB) &= P_S(dBm) - P_b(dBm) \\ &= P_e(dBm) + G_e(dB) + G_r(dB) - A_1(dB) - Refl(dB) \\ &\quad - A_2(dB) - P_b(dBm) \end{aligned} \quad (4.9)$$

where  $P_e$  is the emitted power,  $G_e$  is the antenna gain at the emission,  $G_r$  is the antenna gain at the reception,  $A_1(dB) + A_2(dB)$  are the round trip free space losses,  $Refl$  is the reflection loss on the human body and  $P_b$  is the noise power at the VNA input.

Note that global free space losses have the following equation:

$$\begin{aligned} A(dB) &= A_1(dB) + A_2(dB) = 2A_1(dB) \\ &= 40 \log(4 \pi d / \lambda) \end{aligned} \quad (4.10)$$

Because this study presents the case of a person moving toward the VNA system, the distance ‘ $d$ ’ between the person and the VNA system decreases; hence, based on (4.9), the  $SNR$  of the input signal increases when the person is getting closer to the Doppler radar.  $SNR$  of the phase variation is certainly related to the signal  $SNR$ ; but no direct equation between  $SNR$  of the signal and  $SNR$  of the phase is presented nor between phase noise and distance between the person and the radar. Measurements are used to find a relation between signal noise and distance. As seen in (4.8), for each emitted power  $P_e$  of a fixed person (distance is fixed), signal power at the VNA input is fixed. In addition, for each emitted power taken used for fixed person, the variance of phase noise is assumed to be constant. From  $S_{21}$  phase measurements, the variance of the phase noise is extracted for several values of the emitted power, hence a relation between the emitted power and

the variance of the phase noise is found from these measurements; hence a relation between the signal power at the VNA input and the phase noise variance is found from the relation extracted from measurements and (4.8). Figure 4.14 presents  $S_{21}$  phase is extracted at different emitted powers: -19, -24, -29, -34, -39 and -44 dBm for a person holding his breath. These values correspond to radiated powers: 3, -2, -7, -12, -17 and -22 dBm. The operating frequency is 20 GHz and the sampling frequency is 20 kHz. The person is fixed at a distance of 1 m far from the antennas system. Gain of each antenna at 20 GHz is 24 dB.

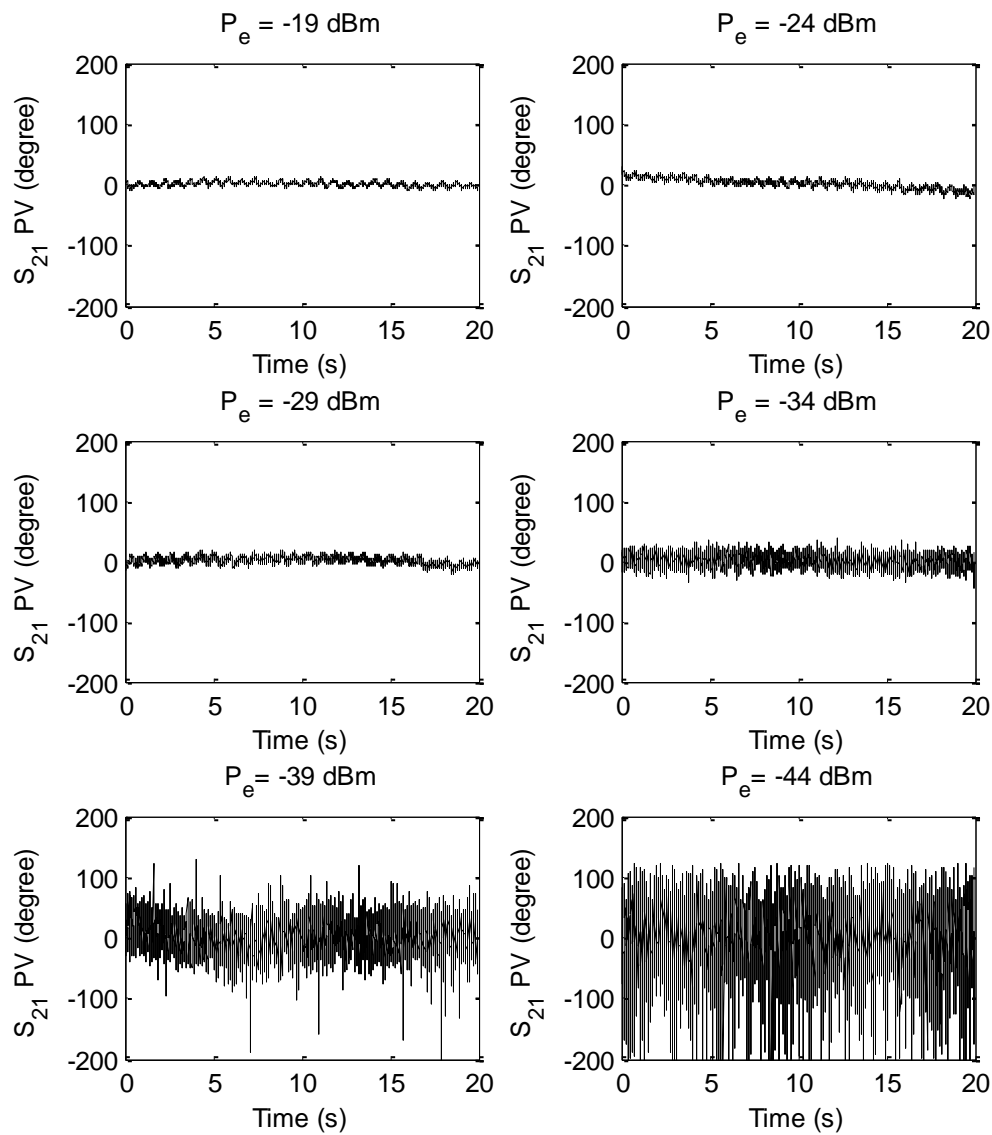


Figure 4.14. Phase variation of  $S_{21}$  at  $P_e = -19, -24, -29, -34, -39$  and  $-44$  dBm and  $f_e = 20$  GHz

The variation of the  $S_{21}$  phase contains heartbeat signal and noise; hence heartbeat signal should be eliminated to extract the variance of the phase noise. The heartbeat signal is extracted by using moving average with  $n = 199$ . When subtracting the original  $S_{21}$  phase with heartbeat signal, noise is obtained. Figure 4.15 presents the phase noise for different emitted powers.  $Refl$  depends on the material construction and the geometrical surface of the target [108].

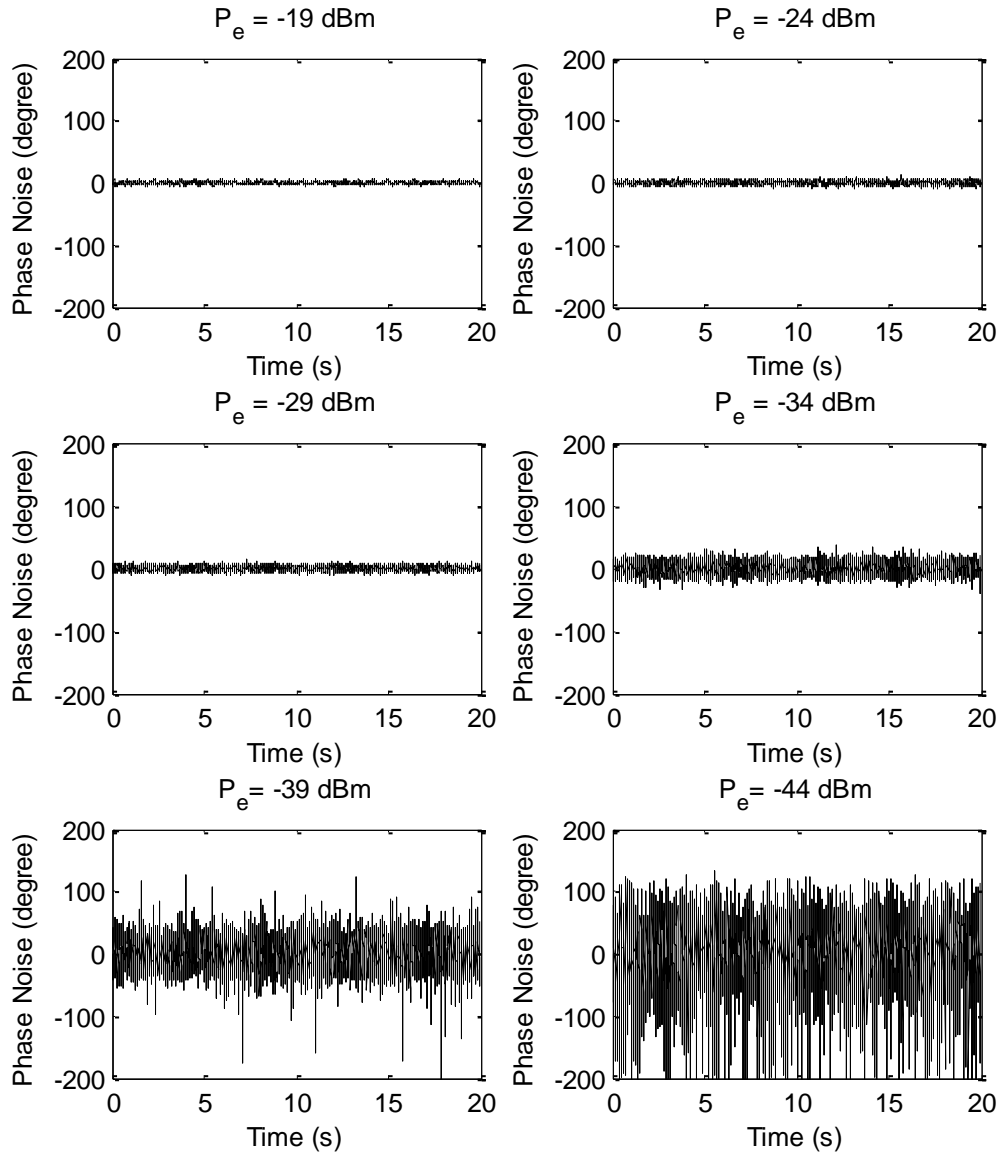


Figure 4.15. Phase noise at  $P_e = -19, -24, -29, -34, -39$  and  $-44$  dBm and  $f_e = 20$  GHz

After extracting the noise of  $S_{21}$  phase variation, the variance of the phase noise ( $\text{deg}^2$ ) is calculated using the following equation:

$$\sigma^2 = \frac{1}{N} \sum_0^{N-1} (\text{phase noise } (i))^2 \quad (4.11)$$

where  $N$  is the samples number. Table 4.7 presents the variance of the noise for each emitted power. Figure 4.16 presents the variation of phase noise variance in function of the emitted power. Finally, Figure 4.17 presents the noise variance as a function of the power of the signal at the input of the VNA at distance 1 m subtracted by the reflection loss.

Table 4.7. Variance of the phase noise at  $P_e = -19, -24, -29, -34, -39$  and  $-44$  dBm and  $f_e = 20$  GHz

<b>Emitted Power <math>P_e</math> (dBm)</b>	<b>Variance <math>\sigma^2</math> (<math>\text{deg}^2</math>)</b>
-19	3.9
-24	7.5
-29	11.8
-34	75.7
-39	470.9
-44	1776.8

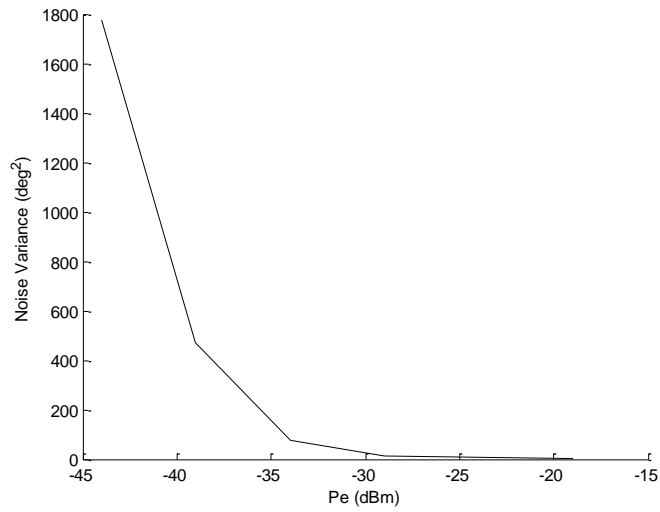


Figure 4.16. Phase noise variance vs. emitted power at 20 GHz

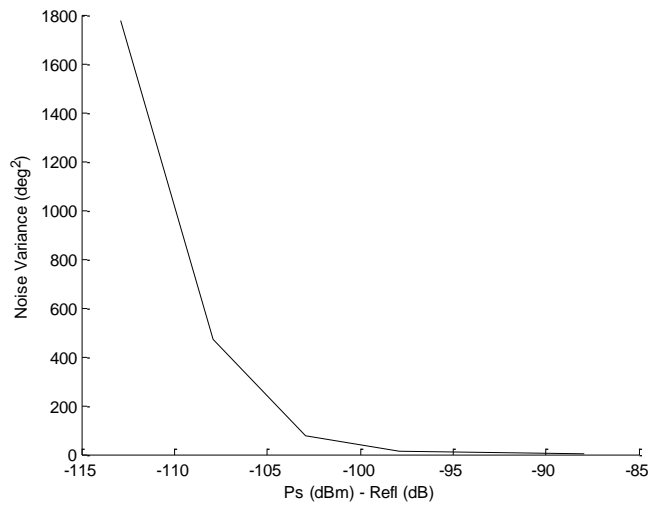


Figure 4.17. Phase noise variation vs. signal power at VNA input at  $d = 1$  and  $f_e = 20$  GHz

On the other hand, signal power at the VNA input is calculated in function of the distance for a certain emitted power  $P_e$ . The person is walking for distance between 1 and 3 m far from the system. Figure 4.18 presents the signal power at VNA input subtracted by the reflection loss for distance between 1 and 3 m at  $P_e = -19$  dBm.



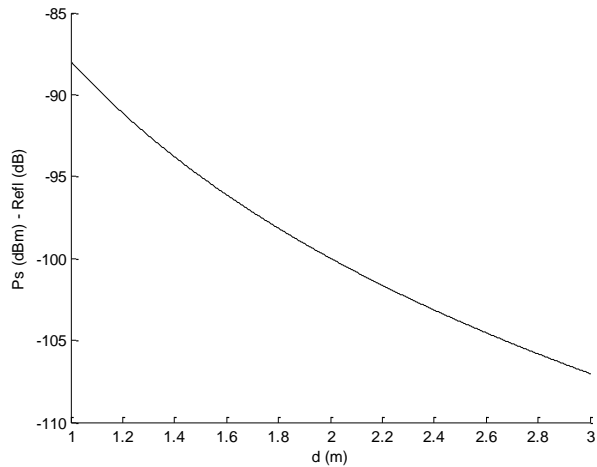


Figure 4.18. Signal power at VNA input vs. distance at  $P_e = -19$  dBm and  $f_e = 20$  GHz

After that, the phase noise variance as a function of the distance is presented. Signal power at VNA input subtracted by reflection loss is between -87,88 and -112,88 dBm for a fixed person set at 1 m far from the system at emitted power varied from -19 dBm to -44 dBm; and the interval of variation of signal power at VNA input subtracted by reflection loss for distance between 1 and 3 m at -19 dBm is between -87.88 and -107 dBm; hence measurements for extracting the noise variance are enough. Figure 4.19 presents phase noise model vs. time for a person moving toward the system at 20 GHz and at emitted power -19 dBm starting from  $d = 3$  m till  $d = 1$  m, this walk takes 8 s.

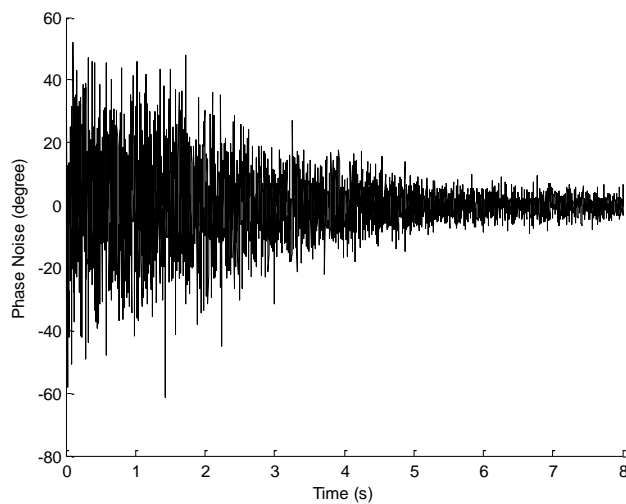


Figure 4.19. Phase noise model for a person moving toward the VNA system at  $f_e = 20$  GHz and  $P_e = -19$  dBm walking from  $d = 3$  m to  $d = 1$  m at a velocity  $v = 0.25$  m/s

#### 4.4.2. Phase variation of chest movement of a walking person at 20 GHz

Figure 4.20 presents the phase variation for a person chest movement, due to his walking toward the system with a constant velocity of 0.25 m/s, starting at a distance of 3 m far from the system and stopping at a distance of 1 m, without taking into consideration the phase permutation between  $-180^\circ$  and  $180^\circ$  degrees.

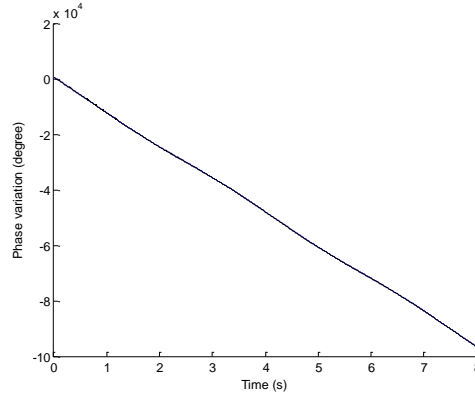


Figure 4.20. Phase variation due to a person chest moving toward the VNA system at 20 GHz

Because phase variation is between  $-180^\circ$  and  $180^\circ$ , permutations from  $-180^\circ$  to  $180^\circ$  and from  $180^\circ$  to  $-180^\circ$  are done each time the phase variation reaches the  $-180^\circ$  and  $180^\circ$  respectively. Figure 4.21 and Figure 4.22 present the phase variation of a walking person chest at the first 0.5 s and the last 0.5 s, respectively.

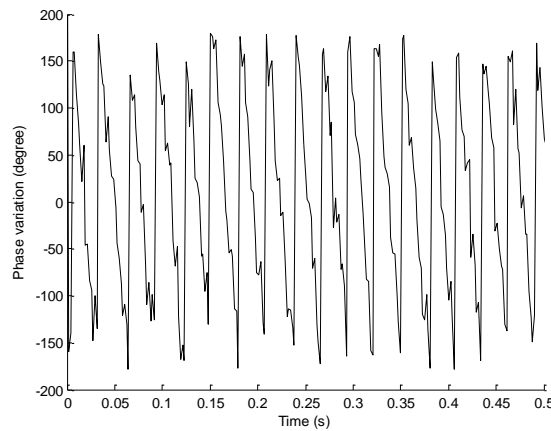


Figure 4.21. Phase variation of a moving person at first 0.5 s with presence of respiration, heartbeat and noise at 20 GHz

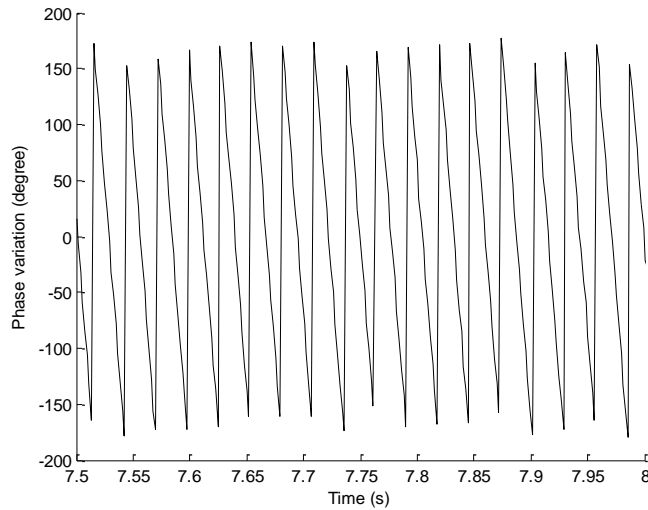


Figure 4.22. Phase variation of a moving person at last 0.5 s with presence of respiration, heartbeat and noise at 20 GHz

Because the distance at first 0.5 s is higher than last 0.5 s, the variation of the phase at the first 0.5 s is noisier than last 0.5 s.

#### 4.4.3. Signal processing and results

Before applying signal processing, all permutations between the  $-180^\circ$  and  $180^\circ$  are eliminated because permutations affect cardiopulmonary signal. Permutations elimination is done each time the phase difference between the current sample and the previous sample is equal or slightly less than  $360^\circ$ .

Note that the respiratory and heartbeat signals are hidden because of the presence of the movement; hence signal processing is required to extract the heartbeat signal from the phase variation. Wavelet decomposition is used as the signal processing technique for the heartbeat extraction. The sampling frequency is 512 Hz, it is chosen to avoid resampling; hence  $S_{D18}$  decomposition contains frequencies higher than 1 Hz which contains the heartbeat frequency. Bior 2.4 is the wavelet chosen for this signal because it has the smallest *RMSE* compared to the other wavelet families. Figure 4.23 presents  $S_{D18}$  applied on model for the heartbeat extraction.

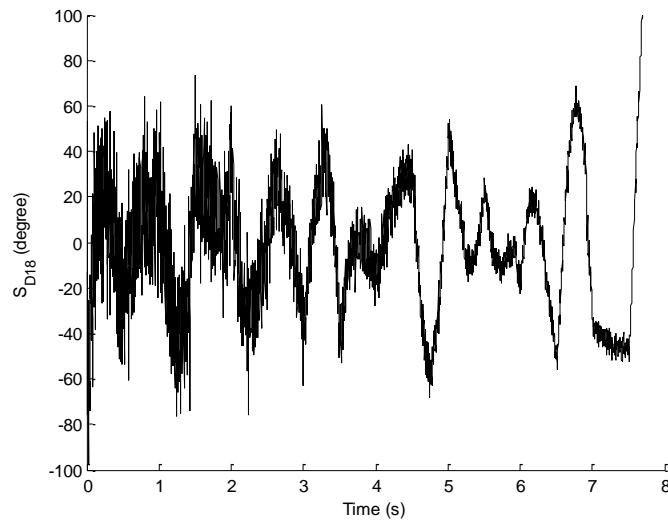


Figure 4.23.  $S_{D18}$  applied on model for heartbeat extraction at  $P_e = -19$  dBm and  $f_e = 20$  GHz

Because signal is noisy, especially between  $t = 0$  and 2 sec, a smoothing using moving average with  $n = 199$  is used to eliminate noise before applying peak detection. Figure 4.24 presents the peak detection of  $S_{D18}$  signal and the heartbeat model.

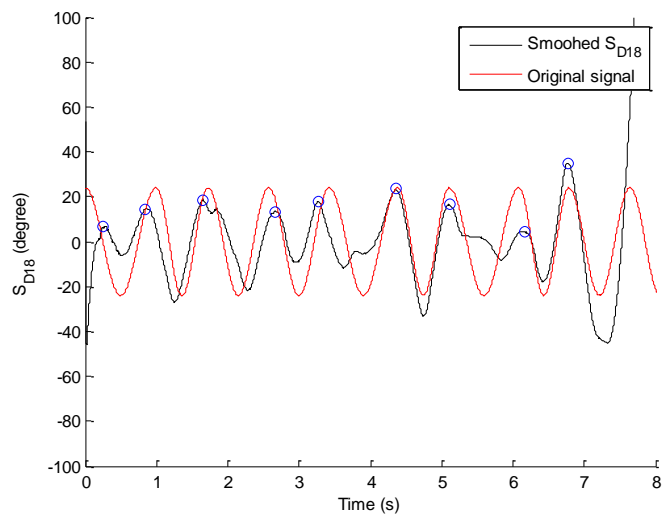


Figure 4.24. Peak detection of  $S_{D18}$  signal and heartbeat model at  $P_e = -19$  dBm and  $f_e = 20$  GHz

After peak detection, the heartbeat rate extracted from  $S_{D18}$  is equal to 73.65 bpm, while the heartbeat rate of the signal model is 70.73 bpm, hence the relative error is equal to 4% that is acceptable. As a conclusion, wavelet decomposition is able to extract heartbeat

signal even in the presence of a walking forward movement. As a future work, measurement could be performed in the presence of random movement with distance higher than 3 m to validate that heartbeat signal can be extracted in such cases.

## **4.5. Conclusion**

Previous researches have studied heartbeat for a person sitting behind a wall using UWB. In addition, a research has measured the respiration rate using CW with different distances [101]; the error of respiration rate was 6.2 % when the distance between the patient and the radar system was below 1 m and increased to 7.3 % when the distance was 2 m [101]. In this chapter, CW is used for a person set with the presence and absence of a wall at two frequencies: 5.8 and 10 GHz and for an emitted power of 0 dBm. Results show that the relative error between the heartbeat rate obtained by ECG and the one extracted from the Doppler radar system increases to 13 % when wall exists. Other measurements could be done by increasing the radiated power; the change of the value of this parameter may decrease the obtained error. Note that previous researches were measuring heartbeat using two antennas: one for emission and the other for reception. In this chapter, measurements using single antenna microwave system have been performed for a non-breathing person and then compared to the two-antenna microwave system. After that, the person is breathing and the heartbeat rate is calculated and compared with heartbeat rate of ECG signal. Different emitted powers have been considered to reach the minimum power possible that would be safe enough for both patient and medical staff. As a result, detected signals with single-antenna microwave system are noisier than those obtained with two-antenna microwave system. However, after using smoothing method, single-antenna microwave system becomes able to measure the heartbeat rate in the case of a holding breath person with comparable results to two-antenna microwave system with maximum error 8%. In addition, the one-antenna system is able to detect heartbeat rate for a breathing person using wavelets.

The last scenario was performed for a person moving toward the system; this scenario is based on models for an emitted frequency 20 GHz and emitted power -19 dBm that corresponds to a radiated power 3 dBm. The wavelet technique was able to extract the heartbeat rate even with presence of body movement. Other measurements could be

performed with presence of random to show the ability of extracting heartbeat for distances bigger than 3 m and for movements different than walking forward.

## **Future work**

Doppler radar monitoring is considered as an effective tool for measuring life signs in order to determine the heartbeat and respiration rates.

The final goal of this project is the monitoring of heartbeat and respiration signals for a person setting in his home; this person may move from a room to another; hence additional scenarios could be considered, in more realistic environment and at different distances.

After making measurements and applying signal processing techniques to signal of a person staying behind the wall at a distance 1 m with radiated power 0 dBm; the relative error between the results obtained with the microwave system and the ECG exceeds the limit; hence measurements with radiated power higher than 0 dBm could be performed in order to show the feasibility of heartbeat rate extraction for a person setting behind a wall.

As shown, this thesis presented model for a person moving toward the system with radiated power 3 dBm and frequency 20 GHz. This scenario could be applied to real measurements. Same measurements could be performed for a person doing a random body movement or moving at different directions of the room with different radiated powers and different operational frequencies.

In addition, future work should take into consideration statistical measurements aspects. This includes measurements performed on persons with different age, sex, weight, etc.

Note that after applying processing techniques, the less radiated power taken into consideration (-17 dBm) gives good results, powers less than this value could be performed to reach the minimum power that is able to extract heartbeat rate successfully.

Furthermore, advanced processing techniques for diseases diagnosis and prediction of the heartbeat and the respiration could be applied.

Next, the integration of the corresponding algorithm is envisaged on a DSPIC with a retrieval of the desired information in real time.





## General conclusion

Recently, wireless heartbeat measurement is used in lot of applications like detection of life signs for victims under rubble, home monitoring for infants and old people. In this thesis, Doppler radar is proposed as a contactless system for vital signs detection. A VNA system emits a signal with fixed operating frequency. This signal is then reflected from the person's chest. The phase variation of the parameter  $S_{21}$  measured by the VNA contains information about chest displacement. The chest displacement contains respiration and heartbeat signals. Because the amplitude of the respiration signal is much higher than the amplitude of the heartbeat signal, processing techniques are required in order to extract the heartbeat signal. The results of all measurements are compared to those measured by the ECG taken as reference.

First, a comparative study for different radiated powers have been performed (2, -3, -7, -12 and -17 dBm) at 20 GHz for a person holding his breath and for a breathing person sitting at a distance of 1 m far from the system. In the frequency domain, after eliminating the respiration frequency by using Butterworth high pass filter, FFT has been applied. The problem of the frequency domain is that real frequency cannot be found exactly because real frequency may not match the FFT frequency step  $\Delta f$ , especially if the sampling frequency wasn't sufficiently large. The problem has been solved by extracting heartbeat rate in the time domain. In the time domain, and for a non-breathing person, a smoothing method has been sufficient to extract the heart properties. When the person breathes, classical filtering has been used to separate the heartbeat signal from the phase of  $S_{21}$ , and then peak detection has been applied to extract the heartbeat rate. Two types of filters have been used: high pass and band pass filters. Butterworth filter has been performed as a type of filtering. 0.9 Hz is a reasonable cut off frequency that could be used because it is able to attenuate the respiratory frequencies and keep the heartbeat frequency. When using high pass filter, smoothing is required because it reduce the noise. Maximum error when using high pass filter is 5%. In case of band pass filter, the second cut off frequency (2Hz) reduces the noise. Maximum error when using band pass filter is 8%. Smoothed high-pass filtered phase variation of  $S_{21}$  gives results better than band-pass filtered phase variation of  $S_{21}$ , but they are still acceptable. In addition, results are considered accurate even with a radiated power of -17 dBm.

Secondly, measurements have been performed on a breathing person set at different sides: front, back, left, and right sides. The person was placed at 1 m far from the system. The radiated power was 0 dBm. Different operating frequencies were used (2.4, 5.8 and 10 GHz). After resampling, wavelet transform has been applied. Approximation 8 has been eliminated from the reconstructed signal in order to eliminate respiration; and then smoothing method has been applied in order to reduce noise, then heartbeat rate has been extracted. Between all wavelet families, Bior2.4 shows the highest performance in providing the heartbeat signal where high accuracy is obtained in terms of heartbeat rate. In parallel to using wavelets as processing technique, Butterworth filter was used in order to make a comparison between them. Wavelets technique shows more accurate results than classical filtering. This difference could be explained by the presence of distortion at the transitional regime when using filtering, which is not present when using wavelet. As a conclusion, the proposed system and signal processing technique show the possibility of measuring the cardiopulmonary activities of the subject at four different positions with high accuracy.

In addition, measurements have been done on a person setting behind a wall at different frequencies: 5.8 and 10 GHz and at emitted power of 0 dBm. Results show that the relative error between the heartbeat rate obtained by ECG and the one extracted from the Doppler radar system increases up to 14% when a wall exists.

Also, measurements using single antenna radar has been performed for a non-breathing person and compared to the two-antenna VNA system. After that, measurements have been performed to a breathing person. Different emitted powers (-2, -7, -12 and -17 dBm) have been considered to reach the minimum power possible that would be safer for both patient and medical staff. As result, signals of single-antenna VNA system are more noisy than signals of two-antenna VNA system but after using smoothing method, single-antenna VNA system becomes able to measure heartbeat rate like two antenna VNA system in case of holding breath person with maximum error of 8%. Furthermore, wavelets are able to extract heartbeat rate successfully for a breathing person when using single-antenna VNA system.

Finally, models have been developed for a person moving toward the system; for an operating frequency 20 GHz and radiated power 3 dBm. The wavelet technique has been able to extract heartbeat rate successfully even with the presence of body movement.

## **Research publications**

### **International Journals**

- S. El-Samad, D. Obeid, G. Zaharia, S. Sadek, G. El Zein, “Remote Heartbeat Detection Using Microwave System from Four Positions of a Normally Breathing Patient”, International Journal on Communications Antenna and Propagation (IRECAP 2016).
- D. Obeid, S. El-Samad, G. Zaharia, S. Sadek, G. El Zein, “Advanced signal processing techniques for microwave cardiopulmonary signals separation”, International Journal on Biology and Biomedical Engineering, Vol. 10, ISSN: 1998-4510, November 2016, Rome.

### **Book Chapter**

- D. Obeid, S. El-Samad, G. Zaharia, S. Sadek, G. El Zein, “Position-free vital sign monitoring: Measurements and processing”, Chapter 2 in book “Advanced Biosignal Processing and Diagnostic Methods”, InTech, pp. 31-53, July 2016, ISBN 978-953-51-2520-4, Print ISBN 978-953-51-2519-8.

### **International Conferences**

- S. El-Samad, D. Obeid, G. Zaharia, S. Sadek, G. El Zein, “Contact-Less measurement system or cardiopulmonary activity”, Proc. of 2014 Mediterranean Microwave Symposium (MMS), 2014, December 2014, Marrakech.
- S. El-Samad, D. Obeid, G. Zaharia, S. Sadek, G. El Zein, “Measurements of cardiac and cardiopulmonary activities using contactless Doppler radar “, Advances in Biomedical Engineering (ICABME), 2015, September 2015, Beirut.
- S. El-Samad, D. Obeid, G. Zaharia, S. Sadek, G. El Zein, “Feasibility of heartbeat detection behind a wall using CW Doppler radar”, Antennas and Propagation (MECAP), 2016, September 2016, Beirut.



## Bibliography

- [1] D. Obeid, G. Zaharia, S. Sadek, G. El Zein, “Doppler radar for heartbeat rate and heart rate variability extraction”, E-Health and Bioengineering Conference (EHB), 2011.
- [2] H.-R. Chuang, Y. Chen, K.-M. Chen, “Automatic clutter-canceler for microwave life-detection systems”, IEEE Transactions on Instrumentation and Measurement, Vol. 40, No. 4, pp. 747 –750, August 1991.
- [3] J. C. Lin and J. Salinger, “Microwave measurement of respiration”, Microwave Symposium, pp.285-287, May 1975.
- [4] J. Lin, W. Wu, “Vital sign radars: Past, present, and future”, IEEE 15th Annual Wireless and Microwave Technology Conference (WAMICON), June 2014.
- [5] D. Obeid, “Touchless cardiopulmonary monitoring: Measurements, processing, and modeling” Thesis, September 2010.
- [6] J. C. Lin, J. Kiernicki, M. Kiernichi, P. B. Wollschnaeger “Microwave apexcardiography”, IEEE Transactions on Microwave and Techniques, Vol. 27, No.6, pp.618-620, June 1979.
- [7] K. M. Chen, D. Misra, H. Wang, H. R. Chuang, E. Postow, “A X-band microwave life detection system”, IEEE Transactions on Biomedical Engineering , Vol. 33, No. 7, pp.697-702, July 1986.
- [8] H. R. Chuang, Y. F. Chen, K. M. Chen, “Microprocessor-controlled automatic clutter-cancellation circuits for microwave systems to sense physiological movements remotely through the rubble”, Instrumentation and Measurement Technology Conference, pp. 177–181, 1990.
- [9] K. Mostov, R. Boutchko, “Medical applications of shortwave FM radar: Remote monitoring of cardiac and respiratory motion”, Medical physics, Vol. 37, No. 3, March 2010.
- [10] E. F. Greneker, “Radar sensing of heartbeat and respiration at a distance with applications of the technology”, Radar Conference, pp. 150– 154, 1997.
- [11] S. Pisa, E. Pittella, “barrier survey of radar systems for medical applications”, IEEE Aerospace and Electronic Systems Magazine, November 2016.
- [12] I. Arai, “Survivor search radar system for persons trapped under earthquake rubble”, Asia Pacific Microwave Conference, pp. 663–668, 2001.

- [13] A. D. Droitcour, O. B. Lubecke, V. M. Lubecke, J. Lin, “0.25m cmos and bicmos single chip direct conversion Doppler radars for remote sensing of vital signs”, IEEE Int. Solid-State Circuits Conf. Tech. Dig., February 2002, pp. 348–349.
- [14] Y. Xiao, J. Lin, O. Boric Lubecke, V. Lubkecke, “A ka band low power Doppler radar system for remote detection of cardiopulmonary motion”, IEEE Engineering in Medicine and Biology, pp. 7151-7154, September 2005.
- [15] Q. Zhou, J. Liu, A. H. Madsen, O. B. Lubecke, V. Lubecke, “Detection of multiple heartbeats using Doppler radar”, International Conference on Acoustics, Speech, and Signal Processing, Vol. 2, pp. 1160–116, 2006.
- [16] V. M. Lubecke, O. B. Lubecke, A. H. Madsen, A. E. Fathy, “Through the wall radar life detection and monitoring”, IEEE International Microwave Symposium, pp. 769–772, 2007.
- [17] T.-Y.J. Kao, A. Y.-K. Chen, Y. Yan, T.-M. Shen, J. Lin, “A flip-chip packaged and fully integrated 60 GHz CMOS micro radar sensor for heartbeat and mechanical vibration detections”, IEEE Radio Frequency Integrated Circuits symposium (RFIC), pp.443-446, June 2012.
- [18] W. Kluwer, “Ecg Interpretation”, Lippincott Williams and Wilkins.
- [19] J. K. Perlkoff, “Physical examination of the heart and circulation”, Heart disease center, UCLA school of medicine, Los angeles, California.
- [20] W. Dressler, “Pulsations of the chest-wall”, 1937.
- [21] A. A. Deliyannis, P. M. S. Gillam, J. P. D. Mounsey, R. E. Steiner, “The cardiac impulse and the motion of the heart”, Br Heart J, 1964.
- [22] P. M. S. Gillam, A. A. Deliyannis, J. P. D. Mounsey, “The left parasternal impulse”, Br Heart J, 1964.
- [23] E. H. Awtry, J. Loscalzo, “Evaluation of the patient with cardiovascular disease”, Cecil Essentials of Medicine. Editor 6, 2004, Philadelphia.
- [24] A. E. Aubert, L. Welkenhuysen, J. Montald, L. de Wolf, H. Geivers, J. Minten, H. Kesteloot, H. Geest, “Laser method for recording displacement of the heart and chest-wall”, Journal of Biomedical Engineering, Vol. 6, No. 2, pp.134 – 140, April 1984.
- [25] G. Ramachandran, S. Swarnamani, M. Singh, “Reconstruction of out-of-plane cardiac displacement patterns as observed on the chest-wall during various phases of ecg by capacitance transducer”, IEEE Transactions on Biomedical Engineering, Vol. 38, No. 4, pp.383-385, April 1991.
- [26] K. Ikegaya, N. Suzumura, T. Funada, “Absolute calibration of phonocardiographic microphones and measurements of chest-wall vibration”,

- Medical and biological engineering, Vol. 9, No. 6, pp. 683–692, November 1971.
- [27] K. Mohri, T. Jinnouchi, K. Kawano, “Accurate mechanocardiogram sensors using amorphous star-shaped core multivibrator combined with amagnet”, IEEE Transactions on Magnetics, Vol. 23, No. 5, pp. 2212 - 2214, September 1987.
- [28] G. Ramachandran, M. Singh, “Three-dimensional reconstruction of cardiac displacement patterns on the chest-wall during the p, qrs, and t-segments of the ECG by laser speckleInterferometry”, Medical and Biological Engineering and Computing, Vol, 27, No. 5, pp. 525–530, September 1989.
- [29] G. W. Yip, Y. Zhang, P. Y. Tan, M. Wang, P. Y. Ho, L. A. Brodin, J. E.Sanderson, “Left ventricular long-axis changes in early diastole: Impact of systolic function on diastole”, 2002.
- [30] H. David Coulter, “Anatomy of Hatha Yoga: A manual for students, teachers, and practitioners”, January 2010.
- [31] E.M. Tamil, N.H.Kamarudin, R. Salleh, A.M. Tamil, “A review on feature extraction and classification techniques for biosignal processing (Part 1: Electrocardiogram)”, International conference on biomedical engineering, Kuala lumpur, June 2008.
- [32] J. Tu, K. Inthavong, G. Ahmadi, “The human respiratory system”, In Book “Computational fluids and particle dynamics in the human respiratory system” Chap. 2, Springer, XVIII, Hardcover ISBN: 978-94-007-4487-5, p. 374, 2013.
- [33] T. Kondo, T. Uhlig, P. Pemberton, P. D. Sly, “Laser monitoring of chest-wall displacement”, European Respiratory Journal, Vol. 10, No. 8, pp. 1865-1869, August 1997.
- [34] A. DeGroot, M. Wantier, G. Cheron, M. Estenne, M. Pavia, “Chest-wall motion during tidal breathing”, Journal of Applied Physiology, Vol. 7, pp. 1531-1537, November 1997.
- [35] J-F. Recoche, “Radar et effet doppler”, Dossier thématique n°5.
- [36] Y.K. Tan, P.R.P. Hoole, “Chirp-signal based processor for radar antennas”, IEEE Antennas and Propagation Society International Symposium, 1-26 June 1998.
- [37] D. Ghose, “Continuous wave and frequency modulation radar”, Chapter 3 in book “Navigation, guidance and control”, NPTEL Course, March 2012.
- [38] V. Issakov, “Microwave circuits for 24 GHz automotive radar in silicon-based technologies”, Springer Book, August 2010.



- [39] N. J. Willis, H. D. Griffiths, “Advances in bistatic radar”, Scitech Pub, p. 493, 2007.
- [40] B. Dehlink, “Integrated millimeter wave front-end design in siGe bipolar technology”, Dissertation, Institut für Nachrichten- und Hochfrequenztechnik der TU Wien, 2007.
- [41] M. He, Y. Nian, Y. Gong, “Novel signal processing method for vital sign monitoring using FMCW radar”, Journal in Biomedical Signal Processing and Control, Vol. 33, pp. 335-345, March 2017.
- [42] A. G. Stove, “Linear FMCW radar techniques”, IEEE Proceedings F, Radar and Signal Processing, Vol. 139, pp. 343-350, October 1992.
- [43] A. Lazaro, D. Girbau, R. Villarino, “Analysis of vital signs monitoring using an IR-UWB Radar”, Progress in Electromagnetic Research, PIER 100, pp. 265-284, 2010.
- [44] G. Wang, J-M munaz-ferreras, C Gu, C. Li, R. Gomez Gracia, “Application of linear-frequency- modulated continuous wave (LFMCW) radars for tracking of vital signs”, IEEE transactions on microwave theory and techniques, Vol. 62, No. 6, June 2014.
- [45] J. Kuutti, M. Paukkunen, M. Aalto, P. Eskelinen, R. E. Sepponen, “Evaluation of a Doppler radar sensor system for vital signs detection and activity monitoring in a radio frequency shielded room”, Measurement, Vol. 68, pp. 135-142, May 2015.
- [46] G. Wang, C. Gu, T. Inoue, C. Li, “A hybrid FMCW- Interferometry radar for indoor precise positioning and versatile life activity monitoring”, Microwave Theory and Techniques, IEEE Transactions, Vol. 62, No. 11, pp. 2812-2822, November 2014.
- [47] S. Kim, C. Nguyen, “On the development of a multifunction millimeter-wave sensor for displacement sensing and low-velocity measurement”, IEEE Transactions on Microwave Theory and Techniques, Vol. 52, No. 11, pp. 2503–2512, November 2014.
- [48] D. Vivet, P. Checchin, R. Chapuis, “Localization and mapping using only a rotating FMCW radar sensor”, Sensors, pp. 4527–4552, 2013.
- [49] C. Zhang, M-J. Kuhn, B-C. Merkl, A-E. Fathy, M-R. Mahfouz, “Real-time noncoherent UWB positioning radar with millimeter range accuracy: Theory and experiment”. IEEE Transactions on Microwave Theory and Techniques, Vol. 58, No.1, January 2010.

- [50] Y. S. Koo, L. Ren, Y. Wang, A.E. Fathy, “UWB Micro Doppler Radar for human Gait analysis, tracking more than one person, and vital sign detection of moving persons”, IEEE International Microwave Symposium Digital (IMS), June 2013.
- [51] Y. Wang, Y. Yang, A.E. Fathy, “Reconfigurable ultra-wide band see-through-wall imaging radar system”, IEEE Antennas and Propagation Society International Symposium, pp. 1-4, June 2009, North Charleston, SC, USA.
- [52] L. Crocco, V. Ferrara, “A review on ground penetrating radar technology for the detection of buried or trapped victims”, IEEE International conference on Collaboration Technologies and Systems (CTS), pp. 535–540, May 2014, Minneapolis.
- [53] G. Wang, J.-M. Munoz-Ferreras, R. Gomez-Garcia, C. Li, “Clutter interference reduction in coherent FMCW radar for weak physiological signal detection”, IEEE International conference on Microwave Symposium (IMS), pp. 1-4, June, 2014, Tampa.
- [54] L. Lu, C. Li, J.A. Rice, “A software-defined multifunctional radar sensor for linear and reciprocal displacement measurement. In Wireless Sensors and Sensor Networks (WiSNet)”, IEEE Topical Conference, 2011, Phoenix, AZ, USA.
- [55] C. Gu, R. Li, C. Li, S-B. Jiang, “Doppler radar respiration measurement for gated lung cancer radiotherapy”, In Biomedical Wireless Technologies, Networks, and Sensing Systems (BioWireless), pp. 91-94, January 2011, Phoenix, AZ, USA.
- [56] M-C. Huang, J. Liu, W. Xu, C. Gu, C. Li, M.A. Sarrafzadeh, “A self-calibrating radar sensor system design for measuring vital signs”, IEEE Transactions on Biomedical Circuits and Systems, Vol. 10, No. 2, April 2016.
- [57] Y. Yan, L. Cattafesta, C. Li, J. Lin, “Analysis of detection methods and realization of a real-time monitoring RF vibrometer”, IEEE Transactions on Microwave and Techniques, pp. 3556-3566, 2011.
- [58] C. Gu, G. Wang, J.A. Rice, C. Li, “Interferometric radar sensor with active transponders for signal boosting and clutter rejection in structural health monitoring”, In Microwave Symposium Digest (MTT), pp. 1–3, June 2012, Montreal, QC, Canada.
- [59] K. Mostov, R. Boutchko, “Medical applications of shortwave FM radar: Remote monitoring of cardiac and respiratory motion”, Medical physics, Vol. 37, No. 3, March 2010.
- [60] G. Wang, C. Gu, T. Inoue, C. Li, “Hybrid FMCW-interferometry radar system in the 5.8 GHz ISM band for indoor precise position and motion detection”, In Microwave Symposium Digest (IMS), pp. 1-4, June 2013, Seattle, WA, USA.

- [61] F.-K. Wang, M.-C. Tang, Y.-C. Chiu, T.-S. Horng, "Gesture sensing using retransmitted wireless communication signals based on Doppler radar technology", *IEEE Transactions on Microwave and Techniques*, pp. 4592–4602, 2015.
- [62] I. Nasr, E. Karagozler, I. Poupyrev, S. Trotta, "A highly integrated 60-GHz 6-Channel transceiver chip in 0.35  $\mu\text{m}$  SiGe technology for smart sensing and short-range communications", *IEEE Compound Semiconductor Integrated Circuit Symposium (CSICS)*, pp. 1-4, October 2015, New Orleans, LA, USA.
- [63] C. Gu, "Short-Range noncontact sensors for healthcare and other emerging applications: A Review", *MDPI, Sensors*, July 2016.
- [64] A.D. Droitcour, O. Boric-Lubecke, V.M. Lubecke, J. Lin, G.T. Kovac, "Range correlation and I/Q performance benefits in single-chip silicon Doppler radars for noncontact cardiopulmonary monitoring", *IEEE Transactions on Microwave and Techniques*, pp. 838-848, 2004.
- [65] W. Massagram, V. Lubecke, A. Host-Madsen, O. Boric-Lubecke, "Assessment of heart rate variability and respiratory sinus arrhythmia via Doppler radar" . *IEEE Transactions on Microwave Theory and Techniques*, Vol. 57, pp. 2542–2549, 2009.
- [66] C. Li, V. Lubecke, O. Boric-Lubecke, J. Lin, "A review on recent advances in doppler radar sensors for noncontact healthcare monitoring", *IEEE Transactions on Microwave and Techniques*, pp. 2046-2060, 2013.
- [67] C. Li, J. Lin, "Complex signal demodulation and random body movement cancellation techniques for non-contact vital sign detection", *Microwave Symposium Digest*, pp. 567-570, June 2008.
- [68] R. Fletcher, H. Jing, "Low-cost differential front-end for Doppler radar vital sign monitoring", *Microwave Symposium Digest*, pp.1325-1328, June 2009.
- [69] C. Gu, G. Wang, T. Inoue, C. Li, "Doppler radar vital sign detection with random body movement cancellation based on adaptive phase compensation", *Microwave Symposium Digest (IMS)*, pp.2-7, June 2013, Seattle, WA, USA.
- [70] C. Gu, G. Wang, T. Inoue, C. Li, "A hybrid Radar-camera sensing system with phase compensation for random body movement cancellation in Doppler vital sign detection", *IEEE Transactions on Microwave and Techniques*, pp. 4678-4688, 2013.
- [71] A.Wiesner, "A multifrequency interferometric CW radar for vital signs detection," *IEEE Radar Conference*, pp.-14, 2009.

- [72] K.-M. Chen, Y. Huang, J. Zhang, and A. Norman, “Microwave life-detection systems for searching human subjects under earthquake rubble or behind barrier”, IEEE Transaction in Biomedical Engineering, Vol. 27, No. 1, pp. 105–114, January 2000.
- [73] D. T. Petkie, C. Benton, E. Bryan, “Millimeter wave radar for remote measurement of vital signs”, IEEE Radar Conference, pp. 1-3, 2009.
- [74] C. Li and J. Lin, “Optimal carrier frequency of non-contact vital sign detectors”, IEEE Radio Wireless Symposium, pp. 281–284, 2007.
- [75] C. Gu, C. Li, “From tumor targeting to speech monitoring: Accurate respiratory monitoring using medical continuous-wave radar sensors”, IEEE Microwave Magazine, Vol. 15, No. 4, pp. 66-76, June 2014.
- [76] C. Gu, T. Inoue, C. Li, “Analysis and experiment on the modulation sensitivity of Doppler radar vibration measurement”, IEEE Microwave and Wireless Components Letters, Vol. 23, No. 10, October 2013.
- [77] T. Kao, Y. Yan, T. Shen, A. Chen, J. Lin, “Design and analysis of a 60-GHz CMOS Doppler micro-radar system-in-package for vital-sign and vibration detection”, IEEE Transactions on Microwave and Techniques, pp. 1649–1659, 2013.
- [78] A.J. Gatesman, A. Danylov, T.M. Goyette, J.C. Dickinson, R.H. Giles, W. Goodhue, J. Waldman, W.E. Nixon, W. Hoen, “Terahertz behavior of optical components and common materials”, Terahertz Military Security Appl, 2006.
- [79] T. J. Rundquist, “Millionaire and healthy -Millionaire from being Poor : A Reasonable Way for Average People to Become Wealthy and Become Healthy until Your 90's”, Nova Media Inc, 2004.
- [80] <https://www.fcc.gov/general/radio-frequency-safety-0>
- [81] I. Yakymenko, E. Sidorik , S. Kyrlylenko , V. Chekhun, “Long- term exposure to microwave radiation provokes cancer growth: Evidences from radars and mobile communication systems”, Experimental Oncology, pp. 62-70, June 2011.
- [82] R. Habash, “Bioeffects and Therapeutic Applications of Electromagnetic Energy”, CRC Press, p. 400, November 2007.
- [83] D. Obeid, G. Zaharia, S. Sadek, G. El Zein, “Microwave Doppler radar for heartbeat detection vs. electrocardiogram”, Microwave and Optical Technology Letters, Vol. 54, No. 11, pp. 2610-2617, 2012.
- [84] <http://www.webmd.com/lung/counting-respiration-rate>

- [85] K.R.Rao, P.C.Yip, "The transform and data compression handbook", The electrical engineering and signal processing series, Boca Raton, CRC Press LLC, 2001.
- [86] "FFT Tutorial", University of Rhode Island Department of Electrical and Computer Engineering ELE 436: Communication Systems.
- [87] S. Dwivedi, "Comparison and implementation of different types of IIR filters for lower order & economic rate", International journal of engineering studies and technical approach, Vol. 01, No. 10, October 2015.
- [88] S.W.Smith, "The scientist and engineer's guide to digital signal processing", 1997.
- [89] J. Fessler, "Digital signal processing and analysis lecture notes", EECS 451
- [90] American National Standard, "Cardiac monitors, heart rate meters, and alarms", ANSI/ AAMI EC1.
- [91] IEEE aerospace and electronic systems society, "IEEE standard letter designations for radar-frequency bands", IEEE Std 521<sup>TM</sup>-2002 (revision of Std 521-1984).
- [92] S.C Mukhopadhyay, "Intelligent sensing, instrumentation and measurements", Smart Sensors, Measurement and instrumentation 5, Springer.
- [93] U.S. Department of Health and Human Services, Food and Drug Administration Center for Devices and Radiological Health, "Radio frequency wireless technology in medical devices guidance for industry and food and drug administration staff", August 2013.
- [94] R. Motard, B.Joseph, "Wavelet application in chemical engineering", Washington University in St. Louis, springer science + business media.
- [95] <http://users.rowan.edu/~polikar/WAVELETS/WTpart4.html>
- [96] G. A. Blackburn, J. Garke Ferwerda, "Retrieval of chlorophyll concentration from leaf reflectance spectra using wavelet analysis", Remote Sensing of Environment, Vol. 112, No. 4, pp. 1614-1632, April 2008.
- [97] C. Stolojescu, I. Railean, S. Moga , A. Isar , "Comparison of wavelet families with application to WiMAX traffic forecasting", International Conference on Optimization of Electrical and Electronic Equipment, 2010.
- [98] P. Hao, "Reversible resampling of integer signals", IEEE Transactions on signal processing, Vol. 57, No. 2, pp. 516-525, February 2009.
- [99] S. Z. Mohd Tumari, R. Sudirman, A. H. Ahmad, "Selection of a suitable wavelet for cognitive memory using electroencephalograph signal", Scientific Research, , May 2013.

- [100] S. Shirodkar, P. Barua, D Anuradha, "Heart-beat detection and ranging through a wall using ultra wide band radar", International conference in Communications and Signal Processing (ICCSP), February 2011.
- [101] A. Üncü, "A 24- GHz Doppler sensor system for cardiorespiratory monitoring", Industrial Electronics Society (IECON), December 2016.
- [102] D. Obeid, S. Sadek, G. Zaharia, G. El-Zein, "Feasibility study for non-contact heartbeat detection at 2.4 GHz and 60 GHz", URSI GA 2008, August 2008, Chicago.
- [103] D. Obeid, G. Zaharia, S. Sadek, G. El Zein, "ECG vs. single-antenna system for heartbeat activity detection", 4th International Symposium on Applied Sciences in Biomedical and Communication Technologies (ISABEL), October 2011, Barcelona, Spain.
- [104] A. H. Muqaibel, M. A. Alsunaidi, N. M. Iya, A. Safaai-Jazi, "Wall attenuation and dispersion", In book "Through the wall: Radar and imaging", CRC Press, Ch. 1, pp. 1-32, 2010.
- [105] H. C. Rhim, O. Buyukozturk, "Electromagnetic properties of concrete at microwave frequency range", Materials Journal, Vol. 95, No. 3, pp. 262-271, January 1998.
- [106] D. Obeid, S. Sadek, G. Zaharia, G. El Zein, "NonContact heartbeat detection at 2.4, 5.8 and 60 GHz: A comparative study", Microwave and Optical Technology Letter, Vol. 51, No. 3, pp. 666-669, March 2009.
- [107] J. Tu, T. Hwang, Member, J. Lin, Fellow, "Respiration rate measurement under 1-D body motion using single continuous-wave Doppler radar vital sign detection system", IEEE Transactions on Microwave Theory and Techniques, Vol. 64, No. 6, pp. 1937-1946, June 2016.
- [108] P. Singh, V. K. Babbar, A. Razdan, T. C. Goel, S. L. Srivastava, "Magnetic, dielectric and microwave absorption studies of Ba-CoTi hexaferrite-epoxy composites", Indian Journal of Pure and Applied Physics, Vol. 42, pp. 221-228, March 2004.

## AVIS DU JURY SUR LA REPRODUCTION DE LA THESE SOUTENUE

**Titre de la thèse:**

Détection sans contact de l'activité cardio-pulmonaire d'une personne dans différents scénarios

**Nom Prénom de l'auteur : SAMAD SARAH**

**Membres du jury :**

- Monsieur EL ZEIN Ghais
- Monsieur ZAHARIA Gheorghe
- Madame SADEK Sawsan
- Monsieur VAUZELLE Rodolphe
- Madame SAGNARD Florence
- Monsieur DAWY Zaher
- Monsieur TCHOFFO TALOM Friedman
- Monsieur OBEID Dany

Président du jury : *Rodolphe VAUZELLE*

Date de la soutenance : 24 Mai 2017


Reproduction de la these soutenue

Thèse pouvant être reproduite en l'état

~~Thèse pouvant être reproduite après corrections suggérées~~

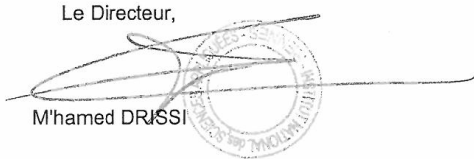
Fait à Rennes, le 24 Mai 2017

Signature du président de jury



Le Directeur,

M'hamed DRÏSSI



## Résumé

De nos jours, les mesures sans contact du signal cardiaque du patient en utilisant le radar Doppler a suscité un intérêt considérable chez les chercheurs, surtout que les électrocardiographes traditionnels avec des électrodes fixes ne sont pas pratiques dans certains cas comme les nourrissons ou les victimes de brûlure. En raison de la sensibilité des micro-ondes à de petits mouvements, le radar a été utilisé comme système de surveillance de l'activité cardio-pulmonaire humaine.

Selon l'effet Doppler, un signal de fréquence constante est transmis vers la cible ayant un déplacement variable puis réfléchi. Le signal réfléchi possède une variation de phase par rapport au temps. Dans notre cas, la cible est la poitrine du patient; Le signal réfléchi de la poitrine de la personne contient le signal cardiorespiratoire. Le système est basé sur un analyseur de réseau vectoriel et deux antennes cornet. Le  $S_{21}$  est calculé en utilisant un analyseur de réseau. La variation de phase de  $S_{21}$  contient des informations de l'activité cardio-pulmonaire. Des techniques de traitement sont utilisées pour extraire le signal cardiaque de la variation de la phase de  $S_{21}$ .

Cette thèse présente une étude comparative dans la détection des signaux de battements cardiaques au niveau de la puissance rayonnée et de la fréquence opérationnelle. Les puissances rayonnées sont comprises entre 3 et -17 dBm et les fréquences opérationnelles utilisées sont 2.4, 5.8, 10 et 20 GHz. Cela permet de spécifier la fréquence opérationnelle optimale, qui donne un compromis entre la puissance minimale émise ainsi que la complexité du système de mesure. De plus, une étude comparative entre plusieurs méthodes de traitement de signal est proposée pour extraire la meilleure méthode qui permet de mesurer le signal cardiaque et par suite extraire ses paramètres. Des techniques de traitement basées sur des transformées en ondelettes ou le filtrage classique sont présentées et utilisées afin de faire une comparaison entre elles. Le paramètre extrait dans cette thèse est le taux des battements cardiaques. Les mesures ont été effectuées simultanément avec un électrocardiographe afin de valider les mesures du signal cardiaque.

Puisque la personne peut se déplacer d'une pièce à une autre à l'intérieur de son domicile, des mesures des quatre côtés de la personne et derrière un mur sont réalisées. Ajoutons une approche de modélisation fondée sur la mesure cardio-respiratoire pour une personne qui exerce une marche en avant. De plus, une comparaison entre un système à micro-ondes à simple et deux antennes pour une personne qui prend son souffle est effectuée afin de tester la précision du système à antenne unique par rapport au a la deuxième. Par suite, des mesures sont effectuées pour une personne qui respire en utilisant un système à une seule antenne.

## Abstract

Nowadays, contact-less monitoring patient's heartbeat using Doppler radar has attracted considerable interest of researchers, especially when the traditional electrocardiogram (ECG) measurements with fixed electrodes is not practical in some cases like infants at risk or sudden infant syndrome or burn victims. Due to the microwave sensitivity toward tiny movements, radar has been employed as a noninvasive monitoring system of human cardiopulmonary activity.

According to Doppler effect, a constant frequency signal reflected off an object having a varying displacement will result in a reflected signal, but with a time varying phase. In our case, the object is the patient's chest; the reflected signal of the person's chest contains information about the heartbeat and respiration. The system is based on a vector network analyzer and 2 horn antennas. The  $S_{21}$  is computed using a vector network analyzer. The phase variation of  $S_{21}$  contains information about cardiopulmonary activity. Processing techniques are used to extract the heartbeat signal from the  $S_{21}$  phase.

This thesis presents a comparative study in heartbeat detection, considering different radiated powers and frequencies. The radiated powers used are between 3 and -17 dBm and the operational frequencies used are 2.4, 5.8, 10 and 20 GHz. This helps to make a compromise between the minimum power emitted and the complexity of the measurement system.

In addition, a comparative study of several signal processing methods is proposed to extract the best technique for heartbeat measurement and thus to extract its parameters. Processing techniques are based on wavelet transforms and conventional filtering in order to make a comparison between them. The parameter extracted in this thesis is the heartbeat rate HR. Measurements were performed simultaneously with a PC-based electrocardiograph to validate the heartbeat rate measurement.

Since the person can move from a room to another inside his home, measurements from the four sides of the person and behind a wall are performed. In addition, a modeling approach based on cardio-respiratory measurement for a person who is walking forward is presented. Furthermore, a comparison between single and two-antenna microwave systems for a non-breathing person is carried out to test the accuracy of the single-antenna system relative to the two-antenna microwave system. After that, measurements are performed using one antenna microwave system for a person who breathes normally.